Applications of artificial neural networks (ANNs) in several different materials research fields

Zhang, Yiming

Applications of Artificial Neural Networks (ANNs) in Several Different Materials Research Fields

Yiming Zhang

School of Engineering and Materials Science

Queen Mary, University of London

A thesis submitted for the degree of Doctor of Philosophy at University of London

March 2010

Declaration:

"I certify that this thesis, and the research to which it refers, are the product of my own work, and that any words or ideas and the figures from the work of other people, published in books and papers or otherwise, are fully acknowledged in accordance with the standard referencing."

Y. Zhang

09/03/2010

Signature:_____

Date:_____

Abstract

In materials science, the traditional methodological framework is the identification of the *composition-processing-structure-property* causal pathways that link hierarchical structure to properties. However, all the properties of materials can be derived ultimately from structure and bonding, and so the properties of a material are interrelated to varying degrees.

The work presented in this thesis, employed artificial neural networks (ANNs) to explore the correlations of different material properties with several examples in different fields. Those including 1) to verify and quantify ***known*** correlations between physical parameters and solid solubility of alloy systems, which were first discovered by Hume-Rothery in the 1930s. 2) To explore ***unknown*** cross-property correlations without investigating complicated structure-property relationships, which is exemplified by i) predicting structural stability of perovskites from bond-valence based tolerance factors t_{BV}, and predicting formability of perovskites by using A-O and B-O bond distances; ii) correlating polarizability with other properties, such as first ionization potential, melting point, heat of vaporization and specific heat capacity. 3) In the process of discovering unanticipated relationships between combination of properties of materials, ANNs were also found to be useful for highlighting unusual data points in handbooks, tables and databases that deserve to have their veracity inspected. By applying this method, massive errors in handbooks were found, and a systematic, intelligent and potentially automatic method to detect errors in handbooks is thus developed.

Through presenting these four distinct examples from three aspects of ANN capability, different ways that ANNs can contribute to progress in materials science has been explored. These approaches are novel and deserve to be pursued as part of the newer methodologies that are beginning to underpin material research.

Publications within the PhD Period

Peer Reviewed Journals

1. **Zhang Y. M., Yang S., Evans J. R. G.** Revisiting Hume-Rothery's rules with artificial neural networks. *Acta Materialia*. 2008, **56**, 1094-1105.

2. **Zhang Y. M., Evans J. R. G., Yang S.** The prediction of solid solubility of alloys: developments and applications of Hume-Rothery's Rules. *The Journal of Crystallization Physics and Chemistry, Invited review. Accepted, In press.*

3. **Zhang Y. M., Yang S., Evans J. R. G.** A method to police and correct handbooks and databases by artificial neural networks. *Journal of Chemical Information and Modelling. Submitted.*

4. **Zhang Y. M., Yang S., Evans J. R. G.** Corrected values for boiling points and enthalpies of vaporization of elements in handbooks. *Journal of Physical and Chemical Reference Data*. *Submitted*.

5. **Zhang Y. M., Qiu T., Evans J. R. G., Yang S.** Solubility prediction of metallic systems using artificial neural network from Hume-Rothery rules and melting temperatures. *To be submitted.*

6. **Zhang Y. M., Yang S., Evans J. R. G.** Exploring Cross-Properties Multiple Correlations using Artificial Neural Networks. *To be submitted.*

7. **Zhang Y. M., Ubic R., Xue D., Yang S.** Predicting the Structural Stability and Formability of ABO_3-type Perovskite Compounds Using Artificial Neural Networks. *Journal of Physics: Condensed Matter*. Submitted

Book Chapter

1. **Li N., Zhang Y. M., Yang S., Xue D**. Chemical bonding characteristics and structural formability of perovskite compounds. *In*: **Xue D. (Ed.)** *Perovskites: Structure, Properties and Uses*. *To be published.*

Conference Presentation

Zhang Y. M. Application of data mining method in solid solubility prediction. *International Conference on Advances in Functional Materials*. Jiu Zhai Gou, China, 9-13 June, 2009.

Prize and Honour

2006-2009 Queen Mary, University of London Research Studentships.

2008-2009 Central Research Fund (Ref. AR/CRF/B): *£2,650 awarded by the Academic Trust Funds Committee to support the research into exploring materials property relationships using artificial neural networks.*

2009 Advances in Functional Materials Conference Young Researcher Award.

Public Engagement

2nd-5th Jul. 2007 Royal Society Summer Science Exhibition Exhibitor: *From Music to Sand Painting*.

(In this work, I responsible for the robot motion control programming of the solid freeforming machine (use LABVIEW software). In the exhibition I showed visitors the and explain the mechanism of the processing method).

Acknowledgement

Firstly, I would like to thank Dr. Shoufeng Yang, my first supervisor, for his generous and persistent helps throughout my PhD work. He continuously keeps my thinking sharp and my standards for evidence high, and has embedded what I learned within doing this work preceded what I was attempting to do. I also thank Prof. Julian R. G. Evans, my second supervisor, for his insightful and selfless help within the discussions about the problems encountered from the work. I will be forever grateful for what they have taught me during the past days. The guidance received from them not only has helped me to finish the degree, but also lightens the road of my future career. In the film of the *Star Wars*, Luke Skywalker, in order to become a Jedi Knight, seeks the help from Yoda, who is a powerful and sapiential Jedi master. Every Luke needs a Yoda, and they are the ones of mine!!

My deepest gratitude is to my parents – my Dad Junle Zhang and my Mum Jingru Lu. With their unhesitating faith, they supported me for my studying and researching in UK from year 2003 to now, not only materially, but also spiritual. During this period, they tolerated the loneliness that their only son was not with them for most of the time; and gave me the encouragements when I met the frustrations from study, research and living. I am forever grateful for their love and support, and I dedicate this work to them.

I also take this opportunity to express my appreciations to my girlfriend Xiaoyan Jiang and her family for their caring, loving and understanding. The callings with Xiaoyan at every weekend during the past year relieved my lonely feeling that I did have before I knew her. Other friends in London also need to be appreciated, from whom the specially appreciations are given to Ms. Audrey Costin, Ms. Helen Xue, Mr. Zhiqiang Dong and his wife Ms. Shujie Ding.

Finally I am grateful to School of Engineering and Materials Science of Queen Mary, University of London and Central Research Fund from University of London (Ref: AR/CRF/B) for providing research studentship and research fund to me.

Contents

List of Figures

List of Tables

1.0 Introduction

1.1 Aims and Objectives

Artificial neural networks (ANNs) represent one type of data mining procedure and they have found acceptance in many subjects for modelling complex problems. They have been applied in materials science for more than one decade for finding the correlations between different materials parameters. The general aim of this work is to explore correlations that might exist between different properties in materials using ANN. Four distinct examples of their applications are presented.

The objectives of this work are as follows:

1. To test whether it is feasible to predict solid solubility limits by using Hume-Rothery's Rules. If the result is positive, then to find what is the relative importance of each rule, or to find the relative weighting and to assess how well the weighted rules work for a) copper and silver alloys; b) a wider range of alloys. If not, to find what other parameters are needed.

2. To discover a systematic, intelligent and potentially automatic method to detect errors in handbooks and stop their transmission by using unrecognised relationships between materials properties.

3. To make predictions of global instability index (GII) from bond-valence based tolerance factors t_{BV} for perovskites and to make the predictions of the formability of perovskites by using A-O and B-O bond distance.

4. To explore the correlations that might exist between different properties without knowing the direct structure-property relationships, and it is exemplified by analyzing the correlation between polarizability and other properties in detail.

1.2 Approaches to Materials Science

In materials science it is important to establish the general composition-processing-structure-property-performance relationships (**Flemings, 1999**), and then allow the optimization of the processing parameters and compositions in order to achieve the desired combination of properties for any particular application (**Malinov and Sha, 2003**). These relationships can be obtained in the following ways:

1) ***By experimental characterisation***. The execution of well designed experiments make it possible to get precise results which help to establish structure-property relationship, but this is a time consuming and financially costly procedure. Recently, experimental characterisation has been accelerated by a method called combinatorial and high throughput materials development and the details of these methods are discussed in part 1.2.1. These developments result from a concern about the slow pace of conventional laboratory procedure.

2) ***By physical and empirical models***. As set out by Bhadeshia (**1999**), a theory can be judged by at least two criteria: 1) it must be able to describe a large number of observations with few arbitrary parameters; 2) it must be able to make predictions which can be verified or disproved. During the past decades, the developments of theory on materials have helped greatly in understanding the underlying phenomena. The further details are discussed in part 1.2.2.

3) ***By mathematical modelling***. In terms of functionality, these approaches can be classified into four categories: a) those which lead to unexpected outcomes that can be verified; b) those which are created or used in hindsight to explain diverse observations; c) existing models which are adapted or grouped to design materials or processes; d) models used to express data, reveal patterns, or for implementation in control algorithms (**Bhadeshia, 2008; 2009**). In terms of the tools, they can be further subdivided into two classes: i) physical modelling and ii) statistical modelling. Further details for physical modelling are discussed in part 1.2.3 and statistical modelling is discussed in part 1.2.4.

1.2.1 Combinatorial and High Throughput Methods

At the early stages of "science", that is, before relationships between chemical composition, crystal structure and material properties had been established, artificial materials (artefacts) was produced by trial and error, known as pure empiricism (**Steurer, 1996**). At present, the discovery of most new materials is still solidly based in experimentation, although some progress has been made in the ability to design or predict the properties of new materials. However, these experimental approaches for materials development are being to be automated by "high throughput" or "combinatorial" methods, which emerged as a response to the challenges of materials development in increasingly complex experimental spaces, i.e. the enormous number of possible combinations of composition, host structure, dopants, defects, interfaces, processing conditions and so on, in an attempt to increase the pace of materials development (**Cawse, 2003**). This kind of methods are based on the construction of a library which may be thick or thin film, continuous gradient, randomised or discrete (**Dagani, 1999; Amis *et al.*, 2002; Zhao, 2006**). Once a library has been created, it can be regarded as a capital asset upon which a multitude of properties can be measured. It not only make impressive successes in materials discovery, but also provide a new paradigm for advancing a central scientific goal – the fundamental understanding of structure-property relations of materials behaviour (**Amis *et al.*, 2002**). Further, the information obtained from such experiments can be used for converting the data from high-throughput experimentation to high-throughput knowledge discovery (**Evans *et al.*, 2001; Rajan, 2008**).

The principle of this method can be traced to the 1960s when the groundbreaking experiments in the field were first published. Kennedy *et al.* (**1965**) used a ternary-alloy phase "library" produced by electron-beam co-evaporation techniques and analyzed by electron diffraction, to successfully demonstrate qualitative agreement between the phase diagram produced by combinatorial techniques and that determined by conventional methods. In 1967, Miller and Shirn (**1967**) analyzed the Au-SiO_2 system by using a co-sputtering technique in which a film exhibiting a controlled composition gradient of Au/SiO_2 was deposited on the substrate by aligning Au and SiO_2 targets carefully. They then used this gradient library to measure the electrical resistivity of the system over

the full range of composition. In the following years, this "composition-spread" method was used to study transition-metal-alloy superconductors (**Hanak *et al.*, 1969; Sawatzky and Kay, 1969; Hanak, 1970**).

Modern combinatorial chemistry appeared first in the 1980s in the pharmaceutical industry (**Borman, 1997**). Geysen *et al.* (**1984**) helped jump-start the field when his group developed a technique for synthesizing peptides on pin-shaped solid supports; Richard (**1985**) developed a technique in which tiny mesh packets act as reaction chambers and filtration devices for solid-phase parallel peptide synthesis. After pioneering work done by Xiang *et al.* in 1995 (**Xiang *et al.*, 1995**), the interest in combinatorial materials sciences resurged. The work after that included the search of superconductors (**Xiang *et al.*, 1995; Xiang, 1999; Amis *et al.*, 2002**), ferroelectrics (**Schultz and Xiang, 1998; Murakami *et al.*, 2004**), catalysts (**Senkan, 1998; Jandeleit *et al.*, 1999**), dielectric materials (**Pullar *et al.*, 2007a and 2007b**) and for studying of phase diagrams and composition-structure-property relationships (**Zhao, 2006**). At present, it can be said that combinatorial methods not only make impressive successes in materials discovery but also provide a new paradigm for advancing a central scientific goal – the fundamental understanding of structure and property relationships of materials behaviour (**Amis *et al.*, 2002)**.

However, it is also needs to be mentioned that this method is based on the philosophy of Baconian science. It is important to notice that the words from Francis Bacon (**Bacon *et al.*, 1905**) were supposed to establish a philosophy of science but William Harvey, who was one of the greatest experimental scientists of that time, said that Bacon spoke of making observation, but omitted the vital factor of judgment about what to observe and what to pay attention to (**Feynman, 1969**). As a result, essential analysis and judgments are needed after using the high throughput data mining method.

1.2.2 Traditional Methodological Framework for Materials Science

In materials science, after the most simple binary and ternary alloys have been studied, it becomes progressively more difficult, time consuming, and costly to create useful new materials by using only experimental studies, so people have

ambitions to predict material properties theoretically without experimentation (**Kawazoe, 1999**). The traditional methodological framework for materials science is the identification of the causal pathways that link composition and structure to properties. The historical success of this approach is unquestioned.

The chemical composition is identifiable as the bulk elemental constituents as determined to within a few molar percent by a range of analytical methods. For some properties, 'impurity' or 'dopant' constituents which may be present at the parts per million level have an effect on properties that is far out of proportion to their concentrations. For example, in semiconductors and colorants, bulk properties are strongly influenced by dopants; in ceramics, 'impurities' have a pronounced effect on semiconduction and diffusion; conducting polymers can be obtained by doping; and conducting polymer-matrix composites can be obtained by the use of conducing fillers.

The structure of a material usually relates to the arrangement of its internal components. Subatomic structure involves electrons within the individual atoms and interactions with their nuclei; then, on atomic level, structure encompasses the organization of atoms or molecules relative to one another; the next largest structural realm, which contains large groups of atoms that are normally agglomerated together is termed microscopic, which associated with grain boundaries and stacking faults, also include point, line and planar defects such as vacancies, substitutional and interstitial defects, dislocations, stacking faults, twin and grain boundaries; finally, structural elements that may be viewed with the naked eye are termed macroscopic, which includes pore size and fraction (**Callister, 2003**).

Different levels of structures determine different kinds of properties:

1. The subatomic structure determines the chemical characteristics of elemental materials (**Mangonon, 1999**).
2. Atomic structure influences the deformability of crystalline materials, like metals and alloys.
3. Comparing with others, microstructure has strong effects on a large number of material properties, such as I) Body centre cubic (BCC) structure is assumed

to be more stable at higher temperature than the face centre cubic (FCC) or hexagonal close packed (HCP) structure owing to its higher vibrational entropy (**Steurer, 1996**); II) Incipient melting of metals occurs first at the grain boundaries, which decreases the melting point; and grain boundaries also enhance the creep deformation at high temperatures; III) At low temperatures, the smaller the grain size of the material, the higher are its yield strength, fracture strength, and toughness; IV) Two basic diffusion mechanisms by which an atom moves in the structure are *interstitial diffusion* which results from the interstitial defects, and *vacancy diffusion* which results from substitutional defects or vacancies. Also, dislocations, grain boundaries can enhance atomic movement; V) Dislocations allow crystalline materials to be deformed into shapes, and make them more ductile compared with materials that do not have dislocations or have sites that block dislocations.

4. Macroscopic structure, such as inclusions and cracks could influence transport properties; and the overall component shape and size determine strengths.

The study of causation within the sequence composition-processing-structure-properties is the traditional basis of the subject. Many of the successes in materials science have emerged from its careful implementation. Many examples of explaining properties from the structure are listed in textbooks. By using fundamental principles of physics and chemistry that govern the states and properties of condensed matter, as well as materials theory, it is possible to model the structure and functional properties of real materials quantitatively, and consequently to design and predict novel materials and devices with improved performance (**Elsässer *et al.*, 2001**).

1.2.3 Physical Modelling of Materials

Although it can be admitted that the scientific community at present is closer to the realization of designing any material with given properties on the basis of improved understanding of structure-property relationships (**Steurer, 1996**), the development and processing of materials is complex, existing theories still lack predictive power, i.e. the current level of theoretical and empirical understanding of materials does not allow people to predict structures and hence the resulting properties of the materials completely (**Disalvo, 1990**). As mentioned by

Bhadeshia (**1999**), there remain many problems where quantitative treatments are dismally lacking; and this incapability specially happens in the prediction of mechanical properties, due to their dependence on large number of variables. Examples are elastic modulus, yield strength, tensile strength, toughness, creep strength, hardness and so on.

It is possible to predict properties by physical modelling. This method has been characterized by multiscale; linking the simulation models and techniques across the micro-to-macro length and time scales with the goal of analyzing and controlling the outcome of critical materials processes. By combining different modelling methods, such as quantum mechanical calculations, Monte Carlo simulations, finite element analysis (FEA), the complex problems can be dealt with in a much more comprehensive manner than when the methods are used individually (**Yip, 2005**). These kinds of method are based on recognizing the relationships between a structure and its properties: if a structure can be calculated and optimized from given stoichiometries and connectivities, its properties can be calculated as well (**Fey, 1999**).

Ab initio, or 'first principles' electronic structure calculations, is one typical method; and are based solely upon 1) the laws of quantum mechanics, 2) the masses and charges of electrons and atomic nuclei, and 3) the values of fundamental physical constants, such as the speed of light or Planck's constant (**Dorsett and White, 2000**). The first *ab initio* calculation on a material was done by Wigner and Seitz in 1934 (**Wigner and Seitz, 1934**) following their previous paper, which is the first to apply the Schrödinger equation to the problem of bonding in metals (**Wigner and Seitz, 1933**). At present, there is a large number of commercial *ab initio* software packages available, such as *GAMESS*, *Dalton*, *Gaussian*, *Spartan*, *Chem3D*, *Material Studio*, *VASP*, *WIEN*, *PWSCF*, *SIESTA*, *ADF*, *ABINIT*, *CPMD* and *Octopus*. With these tools, the number of diverse problems to which *ab initio* calculations have been directed is very large (**Cargnoni *et al.*, 1998; Harrison *et al.*, 1998; Milman *et al.*, 2000; Li, 2004; Van de Walle and Neugebauer, 2004; Music *et al.*, 2007**).

Although *ab initio* calculations are theoretically the most rigorous, the techniques that have been developed for solving these equations are extremely computationally intensive (**Yip, 2005**). When large number of atoms (10^{23}) and the many-body interactions to be treated, this method would place a considerable demand on computer resources (**Kawazoe, 1999**); and even when only a small number of atoms are of interest, each step of the calculation may take several hours on a multiprocessor machine (**Chin *et al.*, 2003**). As mentioned by Pettifor (**2003**), even with the largest parallel computer, only about 1000 non-equivalent atoms can be simulated from first principles, which corresponds to a 3-D cell size of about 1nm; and assuming the atoms are held together by some valence force field or interatomic potential in order to simulate larger systems, only 1000 million atoms can be treated using the largest parallel computer, which corresponds to a cell size of 0.1 μm. From comparing the highest computing power recorded for year 2003 and at present from TOP500 (**TOP500 website**), it is found that, even today, the cell size that can be treated is about 4 μm. However, for nanomaterials, the reduction in size towards nanometric scales together with the ever increasing computational power begin to allow direct application of *ab initio* calculations to realistic systems (**Lannoo, 2001**), such as the work done by Ordejón (**2000**).

At present, accompanying increasing computing power, several other techniques have been developed for enhancing the resource efficiency and time for computation such as 1) coarsening most of the details of the atomic or molecular but retaining enough information for the essential physics to describe the phenomena of interest, 2) employing multiprocessor computers and efficient code parallelisation and 3) incorporating computational steering (**Chin *et al.*, 2003**). These make the simulation of systems that having length-scales of several million atoms and timescales of up to milliseconds possible (**Klein and Shinoda, 2008**). Other examples for application of large-scale simulations that are free from finite size effects can be found for layered materials (**Suter *et al.*, 2007; Thyveetil *et al.*, 2007; Suter *et al.*, 2009**). However, these simulations have the capability to study a system of large number of atoms, but are not as reliable as *ab initio* calculations (**Dorsett and White, 2000**; **Yip, 2005**).

1.2.4 Statistical Modelling of Materials

When dealing with difficult problems where the physical models are not available or tedious to apply, it is helpful to correlate the results with chosen parameters by applying regression analysis, in which the data are best-fitted to a specified relationship that is usually linear. The result of linear regression is an equation, in which each of input x_i is multiplied by a parameter a_i; and the sum of all such products and a constant C then gives an estimate of the output $y = \sum_i a_i x_i + C$ (**Bhadeshia, 1999**).

There are examples of applying linear regression method in materials sciences of the type (**Bhadeshia, 1999; 2009**):

1) $$y = a_1 x_1 + a_2 x_2 + \ldots + a_i x_i + C$$ Equation 1.2.1

This is a typical linear function and the idea is to predefined the function, then correlate the empirically determined results against chosen variables using regression analysis. One example for this kind of linear regression is the bainite reaction start temperature (B_S) in steel which can be written as:

$$B_S(°C) = 830 - 270 \times C_C - 90 \times C_{Mn} - 37 \times C_{Ni} - 70 \times C_{Cr} - 83 \times C_{Mo}$$

where C_C, C_{Mn}, C_{Ni}, C_{Cr} and C_{Mo} are the compositions of elements in wt.%, typically C, Mn, Ni, Cr and Mo (**Stevens and Haynes, 1956**). However, in this case, it needs to be pointed out that the physical model for B_S has been found later and the dependence on concentration of added elements is not linear (**Bhadeshia, 1981**).

2) $$y = a_1 x + a_2 x^2 + \ldots + a_i x^i + C$$ Equation 1.2.2

Or the function can be like this, which is a pseudo-linear polynomial. The example in material science is the basic thermodynamic parameter – heat capacity at constant pressure (C_P), which is expressed empirically as a function of the absolute temperature T as follows:

$$C_P = a_1 + a_2 T + a_3 T^2 + \frac{a_4}{T^2}$$

As stated by Reid and Sherwood (**1958**), the prediction is usually based on correlations of known information. These correlations can be classified as three different types: purely empirical, partly empirical but based on some theoretical concept, and purely theoretical. Within these, the first is often unreliable and may not be worthy, the third is seldom adequately developed. The most widely used correlations are of a form suggested in part by theory, with empirical constants based on experimental data. Both of above two examples belong to the second kind of correlations.

However, as mentioned by Specht (**1991**) and Bhadeshia (**1999**), there are several difficulties associated with these general linear regression analysis: i) A predefined relationship has to be chosen before analysis; ii) the chosen relationship tends to be linear, or pseudo-linear with non-linear terms added together and iii) when the regression equation once derived, it applied across the entire span of the input space. However, it may not be a reasonable case; and so the accuracy of predictions for unseen data would be low, as has been examined in several people's work (**Bratchell *et al.*, 1990; Barayani and Roberts, 1995; Sofu and Ekinci, 2007; Moghtased-Azar and Zaletnyik, 2009**).

Neural network, which falls in the statistical modelling category, can avoid the difficulties that regression methods have. The details are discussed in what follows.

1.3 Artificial Neural Networks (ANNs)

1.3.1 Introduction to ANNs

The human brain is able to process information rapidly and efficiently through a system of neural networks consisting of vast numbers of neurons. It has evolved to enable a greater awareness of itself and its actions within its environment (**Amari, 2007**). Compared with the programmed computing, in which (usually procedural) algorithms are designed and subsequently implemented using the currently dominant architecture, computation in the human brain is different in that I) the computation is massively distributed and parallel, i.e. the basis of biological computation is a small number of serial steps, each occurring on a massively parallel scale; II) learning replaces *a priori* program development (**Schalkoff, 1997**).

Taking these cues from nature, the biologically motivated computing paradigm of artificial neural networks (ANNs) has arisen. Its appearance was determined by two factors: one is the principal stages of the development of modern elemental base technology that mainly determines the development of computer architecture, and the second is the practical requirement to solve specific problems in a faster and more economical manner. The main reason for the development of neural computing since the 1950s appeared as a development of the threshold logic which is in direct contrast to the classical development of the elemental base on the basis of AND, OR, NOT and so on (**Galushkin, 2007**).

The ability to learn is a peculiar feature of intelligent systems. In artificial systems, learning is viewed as the process of updating the internal representation of the system in response to external stimuli so that it can perform a specific task. ANN learning includes modifying the network architecture, which involves incrementally adjusting the magnitude of the weights or, as it is known ‘synapse’ strength. This process is performed repetitively as the network is presented with training examples, which is similar to the way that people learn from experience. Then the ANN can generalize from the tasks it has learned to unknown cases (**Basheer and Hajmeer, 2000**).

Active research projects in the ANN field have been conducted by psychologists, mathematicians, computer scientists, engineers, and others. It is considered that if ANNs are to become a mature technology, the interfaces between existing technologies and application areas such as modelling and simulation, optimization theory, artificial intelligence, pattern recognition, and nonlinear systems must be identified and unified. Like many engineering and scientific disciplines, ANN system design often involves "trade-offs between exact solutions to approximate models and approximate solutions to exact models" (**Schalkoff, 1997**).

1.3.2 Comparison with General Regression Analysis

The comparison with general linear regression analysis can be illustrated by Figure 1.3.1. The neural network also can represent linear regression, as shown in Figure 1.3.1 (a). Here, each input x_i is multiplied by a random weight a_i and the products are summed together with a constant C to give the output y. The summation operates at the hidden node. Since initially, the weights a_i and the constant C are chosen at random, the output generally is not a match with experimental data and so the weights are systematically changed, known as training, until a best-fit description of the output is obtained as a function of the inputs.

In comparison with that, the non-linear representation of neural networks is shown in Figure 1.3.1 (b). In this case, the input data x_i are multiplied by weights $a_i^{(1)}$, and the sum of all these products forms the argument of a hyperbolic tangent: $h = \tanh\left(\sum_i a_i^{(1)} x_i + C^{(1)}\right)$, then $y = w^{(2)} h + C^{(2)}$. The choice of the hyperbolic tangent function is due to its flexibility. The combination of more than one hyperbolic tangent transfer function permits the ANN to capture almost arbitrarily non-linear relationships; and the availability of a sufficiently complex and flexible function means that the analysis is not as restricted as in linear regression where the form of the equation has to be specified before the analysis. The change of the exact shape of the hyperbolic tangent can be reached by altering the weights, that is, hyperbolic function varies with position in the input

space. Also, the neural network can capture interactions between the inputs because the hidden units are nonlinear (**Bhadeshia, 1999**).

As a result, artificial neural networks are currently one of the most powerful modelling techniques based on statistical approaches and can be used to solve problems that are not amenable to conventional statistical methods (**Malinov and Sha, 2003**). The attractiveness of ANNs comes from the remarkable information processing characteristics of these methods which mimic biological systems such as nonlinearity, high parallelism, robustness, fault and failure tolerance, learning ability to handle imprecise and fuzzy information, and their capability to generalize (**Jain *et al.*, 1996**).

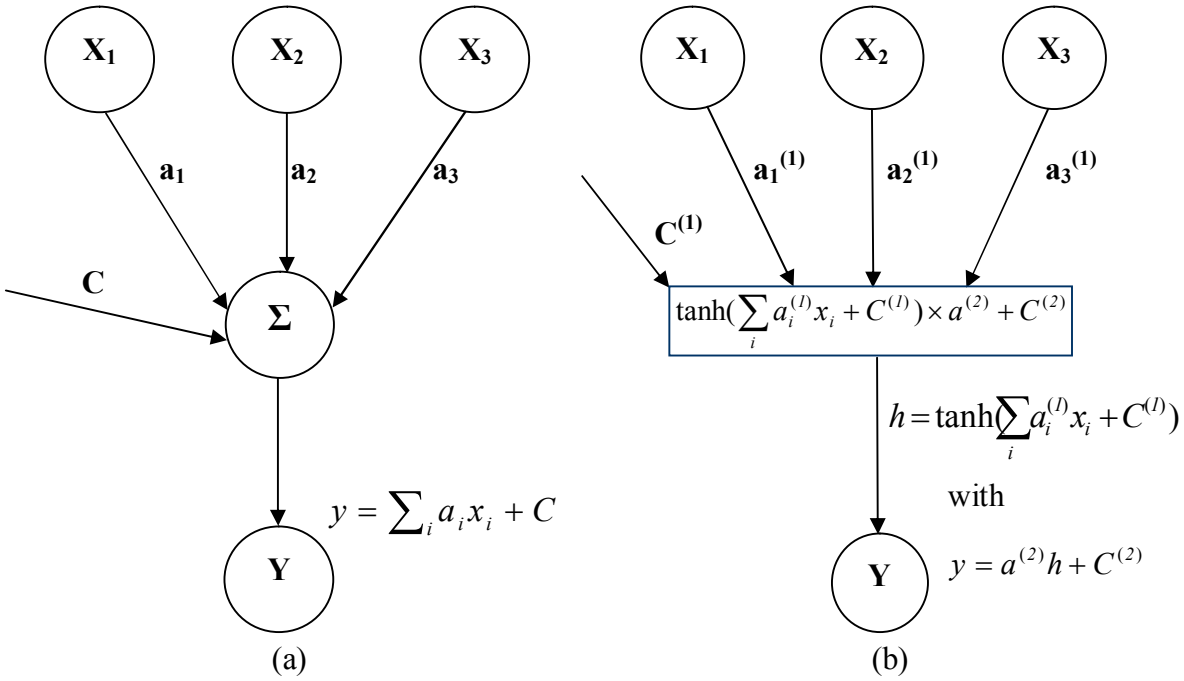

Figure 1.3.1 (a) A neural network representation of linear regression. (b) A non-linear network representation (Redrawn from **Bhadeshia, 1999**).

Sometimes, artificial neural networks are described as a non-algorithmic, black-box computational strategy, in which the internal computation is irrelevant, not understood, or defies quantification, but trainable. The intention is to train the black box to "learn" the correct response or output for each of the training examples, with the minimum required amount of a priori knowledge and detailed understanding of the internal system operation (**Schalkoff, 1997**). On the

contrary, some people think neural network is transparent, consisting of an equation and associated coefficients (the weights) and both the equation and the weights can be studied to reveal the relationships and interactions. Due to the nature of the interactions is implicit in the values of the weights and in some cases there exist more than just pairwise interactions, the problems are difficult to visualize from the examination of the weights. As a result, it is suggested that a better method is to actually use the network to make predictions and to see how these depend on various combinations of inputs (**Bhadeshia, 1999**).

At present, neural networks have been treated as wonderful tools that permit the availability of quantitative expressions without compromising the known complexity of the problem (**Bhadeshia, 2009**).

1.3.3 Types and Selection of ANNs

There are some frequently used ANNs from which to select. They have their own characteristics and special applications:

1. ***Backpropagation Networks (BPANNs):*** This kind of network is versatile and can be used in many fields such as data modelling, classification, forecasting, control, data and image compression and pattern recognition (**Hassoun, 1995**).
2. ***Hopfield Network:*** This kind of network is a symmetrical fully connected two-layer recurrent network, which acts as a nonlinear associative memory and is especially efficient in solving optimization problems (**Hopfield, 1984; Hopfield and Tank, 1986**).
3. ***Adaptive Resonance Theory (ART) Networks:*** ART networks consist of two fully interconnected layers, a layer that receives the inputs and a layer consisting of output neurons. Like Hopfield networks, ART networks can be used for pattern recognition, completion, and classification (**Basheer and Hajmeer, 2000**).
4. ***Kohonen Networks:*** These networks are two-layer networks, which transform n-dimensional input patterns into lower-ordered data where similar patterns project onto points in close proximity to one another (**Kohonen, 1989**). In addition to pattern recognition and classification, Kohonen networks also can be used for data compression, i.e. high-

dimensional data are mapped into a lower dimensional space while preserving their content. (**Zupan and Gasteiger, 1991**).

5. ***Counterpropagation Networks:*** These networks, which are developed by Hecht-Nielsen (**1988, 1990**), are trained by hybrid learning to create a self-organizing look-up table useful for function approximation and classification (**Zupan and Gasteiger, 1993**).
6. ***Radial Basis Function (RBF) Networks:*** These networks are a special case of a multiplayer feedforward error-backpropagation network with three-layers (**Schalkoff, 1997**). The choice between the RBF networks and the BPANNs is problem dependent (**Pal and Srimani, 1996**). RBF networks train faster than BPANNs but are not as versatile and are comparatively slower in use (**Attoh-Okine *et al.*, 1999**).

Within the vast number of networks that currently have been developed, the backpropagation networks (BPANNs) are the most widely used type of network and are considered as the work-horse of ANNs (**Rumelhart *et al.*, 1986**). In BPANNs, the data are fed forward into the network without feedback, i.e., all links are unidirectional and there are no same layer neuron-to-neuron connections (**Basheer and Hajmeer, 2000**).

The model is shown schematically in Figure 1.3.2

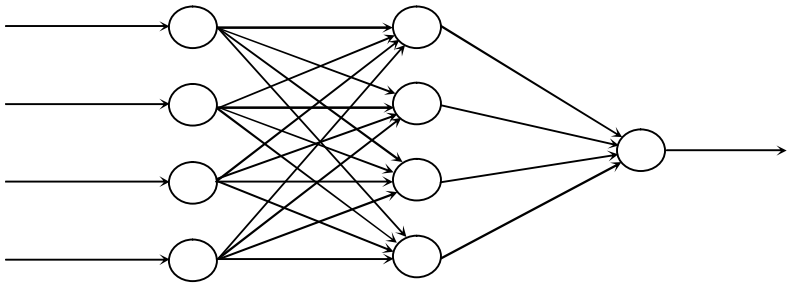

Figure 1.3.2 A model of a feed-forward hierarchical artificial neural network.

The reasons for selecting a particular ANN are now explained. As Basheer and Hajmeer (**2000**) mentioned, the decision depends strictly on the problem logistics. The Kohonen network is required by a clustering problem, BP or RBF networks can model mapping problems; but Hopfield networks can only solve some optimization problems. ANN selection also depends on the type of input

(Boolean, continuous or a mixture of these) and the speed of the network once it is trained. In the initial problem of simulating the process that Hume-Rothery used to derive his rules (in object 1) the output is 'soluble/insoluble', and in the prediction of the formation of perovskites (in object 3) the output is perovskite formable/not, they are a kind of classification problems, and so the probabilistic neural network (**Specht, 1990; Vicino, 1998**) is designed for use. This is a type of radial basis network suitable for classification problems. In other works, the problems all are mapping problems so backpropagation artificial neural networks (BPANNs) are used.

1.3.4 Applications of ANNs in Materials Science

The application of neural networks in materials science at present is wide and it has had a liberating effect on materials science by studying the diverse phenomena which are not yet accessible to physical modelling. As afore cited, the development and processing of materials is very complex and although scientific investigations on materials have reached greater understanding of the underlying phenomena, there still remain many problems where quantitative treatments are dismally lacking. The lack of progress in predicting some properties is because of their dependence on a large numbers of variables. Neural networks are extremely useful in circumstances where the complexity of the problem is overwhelming from a fundamental perspective and where simplification is unacceptable (**Bhadeshia, 1999**).

There are some applications of neural networks in materials, and these applications can be classified into two categories: 1) process control problems; 2) materials properties prediction.

(1) Use of ANNs for process control

In Arkadan *et al.*'s work (**1995**), the location and shape of a crack were deduced from measured magnetic field values as input. Raj *et al.* (**2000**) used ANNs in metalworking to predict forging load in hot upsetting, cutting forces in machining and loads in hot extrusion. Guessasma and Coddet (**2004**) used an ANN to quantify the relationship between Automated Plasma Spraying process parameters and microstructural features of aluminium-titanium coatings. Nam

and Oh (**1999**) used a trained network to interpreted the output from sensors for tracking the weld seam, and then to control a welding robot.

(2) Use of ANNs for materials properties prediction

It is the potential uses for prediction of properties of matter that is interesting for materials scientists. The impact toughness of ferritic steel welds has been predicted from the welding process, chemical composition, test temperature and microstructure using neural networks (**Bhadeshia *et al.*, 1995**). Homer *et al.* (**1999**) used physical properties such as molecular weight, number of bonds and temperature as input factors to predict the viscosity, density, enthalpy of vaporization, boiling point and acentric factors for pure, organic, liquid hydrocarbons over a wide range of temperatures ($T_{reduced}$≈0.45-0.7). Huang *et al.* (**2002**) predicted the mechanical properties of a ceramic tool based on materials properties. Malinov and Sha (**2004**) used ANNs for correlation between processing parameters and properties in titanium alloys such as fatigue life and corrosion resistance. A three-layer backpropagation network ANN was applied to the formulation of $BaTiO_3$ – based dielectrics and for analysis of the electrical properties of PZT (**Guo *et al.*, 2002; Cai *et al.*, 2005**).

Artificial neural networks have also been used in ceramic casting (**Martinez *et al.*, 1994**), to interpret ultrasonic NDT (Non-Destructive Testing) of adhesive joints (**Bork and Challis, 1995**), for modelling the cold rolling forces (**Larkiola *et al.*, 1996**), to predict continuous-cooling transformation curves in steel from chemical composition (**Gavard *et al.*, 1996**) and to predict time-temperature transformation diagrams for titanium alloys (**Malinov *et al.*, 2000**). Bhadeshia *et al.* recently reviewed applications of neural networks in the context of materials science from their group and others (**Bhadeshia, 1999; Bhadeshia, 2009; Bhadeshia *et al.*, 2009**).

1.4 Different Kinds of Scientific Methodologies

The application of neural networks in materials science will lead us to question methodological procedures that are traditional in the discipline and which originate from quite specific and strongly held views about scientific method. It is appropriate, therefore to survey some of the principal positions in method in order to chart our position.

The processes of evolution created neural networks in the brains of living creatures. By reaching a certain degree of complexity, these networks generate electrical phenomena in space and time called consciousness, volition and memory. Such human brains have the capability to analyse the input signals received from the world, in which they have their existence. One form of this analysis, called science, has proved to be especially effective in correlating modifying and controlling the sensory input data (**Moore, 1972**).

One view of scientific method, which is called conventionalism, or abduction in logical terminology, states that the human mind created or invented certain "beautiful" logical structures that are firstly defined as laws of nature, and then devised some special ways of selecting sensory input data in order to fit into patterns ordained by the laws, which are called experiments. In this view, the scientists are like creative artists, working with the unorganized sensations from a chaotic world such as paints or marbles. Philosophers like Poincaré (**Poincaré, 1952**), Eddington (**Eddington, 1949**), and Duhem (**Duhem, 1985**) support this view.

A second view of science, which is called deductivism, also known as Popperian science (**Popper, 1963**), is based on the creative emergence of hypotheses or conjectures which gradually become well-trenched in the form of established theories as more supporting experimental evidence is sought and found. According to Popper's definition (**Popper, 1965**), "Theories are nets cast to catch what we call 'the world': to rationalize, to explain, and to master it. We endeavor to make the mesh ever finer and finer." In deductivists' opinions, there is no valid *aposteriori* logic, since general statements can never be proved from particular instances. However, a general statement can be disproved by one

contrary particular instance. As a result, a scientific theory can never be proved, but it can be disproved. The role of an experiment is therefore to subject a scientific theory to a critical test (**Moore, 1972)**. Popper therefore emphasis refutation to get around the problem of induction.

Another view of science, inductivism, preceded Popper by 350 years and was the source of the problem Popper sought to solve. It is also known as Baconian science, in which large amounts of data are firstly collected, assembled into tables, surveyed and from which theories are devised. In his *Novum Organum* of 1620 (**Bacon *et al.*, 1905**), Sir Francis Bacon argued that this was the only proper scientific method. In fact, at that time, Bacon's emphasis on observable facts was an important antidote to medieval reliance on a formal logic of limited capabilities. Although Bacon's definition sounds close to the layman's idea of what scientists do, many competent philosophers have also continued to support the essentials of inductivism, such as Russell (**Russell, 1948**) and Reichenbach (**Reichenbach, 1963**).

A central debate in the history and philosophy of science focuses on the contrasting explanations of scientific method from Popperian and Baconian science, and Gillies (**1996**) has concisely articulated the contribution and impact of artificial intelligence to philosophy of science: *"...just as earlier the use of instruments to assist observation altered the way in which science was done, so the current development of computers and artificial intelligence is also destined to change science, and in such a way that Baconian induction becomes a standard part of scientific procedure.*"

1.5 Prediction, Causation and Inference

1.5.1 Cause-Effect, Contingency and Apophenia

The central aim of many studies in the physical, behavioural, social, and biological sciences is the elucidation of cause-effect relationships among variables or events. However, the appropriate methodology for extracting such relationships from data, or even from theories, has been fiercely debated. There are two fundamental questions of causality: I) What empirical evidence is required for legitimate inference of cause-effect relationships? II) Given that the causal information about phenomenon is willingly accepted, what inferences can be drawn from such information, and how? But the fact is that these two questions have been without satisfactory answers in part because people have not had a clear semantics for causal claims and in part because people have not had effective mathematical tools for casting causal questions or deriving causal answers (**Pearl, 2000**).

David Hume, in taking an empiricist approach – that all knowledge can be derived from sense experience rather than mind – made an important distinction between statements that show the relationship between ideas (analytic) and those that describe matters of fact (synthetic). He held the idea that people can accept the idea of causality because it is a learnable habit of the imagination. The mind records constant conjunctions based on past observations (**Hume, 1896**). This led to the view that, when people say 'A causes B', it only means that A and B are constantly conjoined in observation, rather than that there is some necessary connection between them. He said that people have no other notion of cause and effect, but that of certain objects, which have been always conjoined, and they cannot penetrate further into the reason of the conjunction (**Russell, 1996**). Hume's ideas of causality therefore have particular relation to the behaviour of artificial neural networks whose main purpose is to find conjugations between observations in the form of parameters in the form of correlations but to remain silent on owning the mechanistic nature of the connection.

Contingency, based on the wider conception of association, was used to substitute the idea of cause and effect. In the third edition of his book "*The Grammar of Science*", Pearson (**1911**) treated the law of causation as a

conceptual figment extracted from phenomena, and not of their very essence. The correlation between two occurrences is actually located in a category that embraces different grades of association between two limits of absolute independence (i.e. variation of the cause produces no effect on the phenomenon) and absolute dependence (i.e. variation of the cause absolutely and alone varies the phenomenon). That is, when a cause varies, a phenomenon changes, but to a different extent; the less the variation in that change, the more nearly the cause defines the phenomena and the more closely people assert the association or the correlation to be. In this book, a contingency table was firstly used to analysis the degree of association between variables by calculating a number of correlation coefficients. Pearson believed the nature of the contingency table reflects the essence of the association between cause and effect and "…the ultimate scientific statement of description of the relation between two things can always be thrown back upon such a contingency table…". Pearson thus denies the need for an independent concept of causal relation beyond correlation (**Pearl, 2000**).

Apophenia, which has been implicated in vulnerability to schizophrenia, is defined as the tendency to perceive meaning in unrelated events. It is treated as a "pervasive tendency of human beings to see order in random configurations" (**Brugger, 2001**). However, whether it is a kind of over-mentalizing activity that involves the dysfunction in the assessment of causality, or is a consequence of a creative 'hyper-associative style' of intact causal reasoning still remains speculative (**Fyfe *et al.*, 2008**).

Apophenia can be treated as a behaviour that regards the coincidences of two events as having cause-effect association. A coincidence is defined as "…a surprising concurrence of events, perceived as meaningfully related, with no apparent causal connection", and it is the observer's psychology that makes it perceived, meaningful and apparent (**Diaconis and Mosteller, 1989**). Actually, the coincidence can be studied and analysed by using statistical techniques, and the possibility of coincidence occurring in random events can be precisely predicted with the laws of probability (**Diaconis and Mosteller, 1989; Falk and Konold, 1997; Martin, 1998; Griffiths and Tenenbaum, 2001**). In 1928, Ramsey had proved that every large structure, such as large set of numbers,

points or objects, contains a highly regular pattern, and complete disorder is an impossibility (**Graham and Spencer, 1990**). Also as mentioned by Martin (**1998**), the very nature of randomness assures that the combination of random data will yield previous unknown patterns; however, people only can use it as a hypothesis for investigating more data, but should never make a general conclusion from it.

Also, apophenia can be treated as a powerful tool for creativity, in order to make sense of the world. For creativity, the highest level is the production of a new idea or theory which is completely distinct from and not conforming to or deducible from any existing paradigm, and which is able to explain a wider range of phenomena than any existing discovery. Historically, no discovery with great importance was made by logical deduction, or by strengthening the observational basis. As a result, random thinking is the most important element of creativity (**Rao, 1997**). Also as Max Born once said "Science is not formal logic – it needs the free play of the mind in as great a degree as any other creative art".

1.5.2 Causation, Common Response and Confounding

When a strong association between variables is present, the conclusion that this association is due to a causal link between the variables is often elusive. Figure 1.5.1 shows different underlying links between variables that can explain observed association. The dashed line represents an observed association between the variables x and y. Some association can be explained by a direct cause-and-effect link between the variables. In Figure 1.5.1 (a), an arrow running from x to y shows x "causes" y.

When thinking about an association between two variables, lurking variables need to be considered. Figure 1.5.1 (b) illustrates common response, in which the observed association between the variables x and y should be explained by a lurking variable z; and both x and y change in response to changes in z. The common response creates an association even though there may be no direct causal link between x and y.

Figure 1.5.1 (c) shows confounding, in which both the explanatory variable x and the lurking variable z may influence the response variable y. Since the effect of x is confounded with the effect of z, the influence of x from the influence of z cannot be distinguished; also, it cannot be said how strong the direct effect of x on y is, it is even hard to tell if x influences y at all. This is the case in which two variables (whether explanatory variables or lurking variables) are confounded and their effects on a response variable are mixed together. Especially, when many variables interact with each other, confounding of several variables can prevent conclusions being drawn about causation.

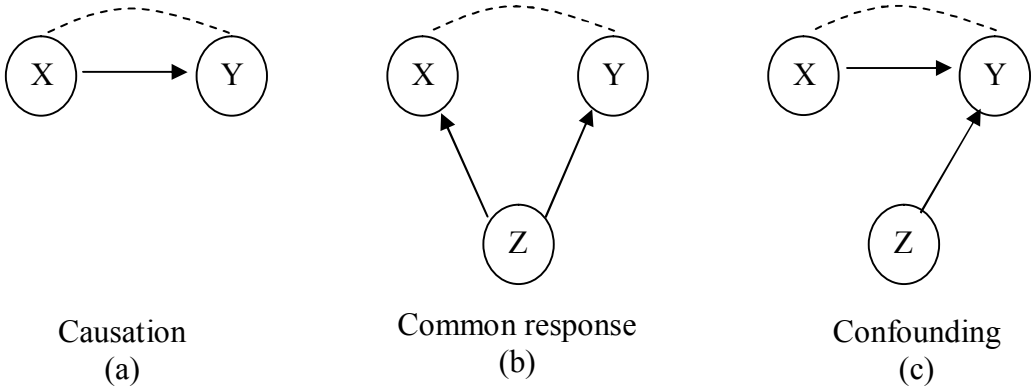

Figure 1.5.1 Some explanations for an observed association. The broken lines show an association. The arrows show a cause-and-effect link. The variables x and y are under observation, and z is a lurking variable (Redrawn from **Moore and McCabe, 1999**).

In reality, many observed associations are at least partly explained by lurking variables. Both common response and confounding involve the influence of a lurking variable (or variables) on the response variable (or variables). As a result, it has to be admitted that even a very strong association between two variables is not, by itself, good evidence that there is a cause-and-effect link between the variables; common response and confounding, along with the number of potential lurking variables, make observed associations misleading. In fact, the best method, which is the only fully compelling method, of establishing causation is to conduct a carefully designed experiment in which the effects of possible or identifiable lurking variables are controlled. (**Moore and McCabe, 1999**).

1.5.3 Correlation, Cause and Effect

A functional relationship in mathematics indicates an exact and predictable relationship, with no "ifs or buts" about it; but in practice, it is useful so long as the "ifs and buts" are only tiny voices. If a set of points (x, y) are plotted and a trend can be found, then it can be said that the variable quantities x and y are correlated. By this, it means that although there is not a strictly functional relation between them, it is possible to make some sort of prediction of the value of y, given a knowledge of the value of x. Correlation is a powerful tool for measuring the association between two variables and for expressing the dependence of one variable on the other, it measures only linear association (**Moore and McCabe, 1999**). The degree of correlation can be measured by a parameter called *product moment correlation coefficient*, *R*, which is defined as

$$R = \frac{1}{N}\sum\left(\frac{x-\bar{x}}{\sigma_x}\right)\left(\frac{y-\bar{y}}{\sigma_y}\right) \qquad \text{Equation 1.5.1}$$

where $\bar{x}$ and $\bar{y}$ are respectively the mean of all the x values and the mean of all the y values, and σ_x and σ_y are respectively the standard deviations of all the x values and all the y values.

It is only when the correlation coefficient is very high that estimation can be at all precise. Sometimes when an investigation is carried out in the presence of many disturbing factors, it is found that there is no simple relation between the factors on which the experiment was based. When plotting graphs of one variable against another and finding that, instead of the clear functional relationships sought by the investigator, and instead of straight lines and elegant-looking curves, 'plum puddings' are obtained, that is to say the points in a graph are scattered very much at random, it means that the disturbing factors have been more important than had been hoped (**Moroney, 1967**).

However, there is still the question of the significance of the correlation coefficient, even if it is high. It must be asked whether a high value of the correlation coefficient could easily have arisen by chance. Just as Whitehead (**1911**) said: "*(But in truth with more complicated instances) there is no more common error than to assume that, because prolonged and accurate*

mathematical calculations have been made, the application of the result to some fact of nature is absolutely certain". Since the method of correlation analysis is primarily used in cases where it is not possible to control the experimental conditions, but such data as can be collected as they occur are analysed (**Moroney, 1967**).

In the empiricist tradition, probabilistic relationships constitute the foundations of human knowledge, whereas causality simply provides useful ways of abbreviating and organizing intricate patterns of probabilistic relationships. Causal relationships can be taken to be the fundamental building blocks both of physical reality and of human understanding of that reality, and probabilistic relationships can be regarded as but the surface phenomena of the causal machinery that underlies and propels our understanding of the world (**Pearl, 2000**).

1.5.4 Causal and Analogical Connections

As people have tried to get to know nature's forces and laws, they often applied connections between different agents. These connections can be divided into two types: 1) causal, that is the generation of one force by the other, which has been mentioned above, and 2) analogical. While the causal connection links the forces more tightly, analogical connection is helpful in understanding these forces and in formulating theories. In history, both kinds of connections between electricity and heat were exploited by those studying these phenomena. Ideas about these connections were shaped by the changing concepts of the forces and by experimental evidence for their interaction.

Ohm based his famous 1827 theory of the electric conduction of metals on Fourier's 1822 theory of heat flow. His success in deriving analogous equations to those of Fourier for electric current indicated to him an "intimate connection" between the two phenomena. Others then shared Ohm's view. This view stimulated Wiedemann and Franz to their discovery of an approximate constant relation between the conductivity of heat and electricity in 1853. In turn, their empirical law supported an assumption of the intimate connection between the two phenomena, whose exact mechanisms were a subject of speculation until

well after the discovery of the electron. Using a combination of empirical and theoretical arguments, Lorenz claimed in 1872 that the Wiedemann-Franz constant depends linearly on the temperature, a claim that he verified experimentally by 1881. The electron theory of Drude explained Lorenz's relation on the assumption that both heat and electric currents in matter result from the motion of its electrons (**Shaul, 2005)**.

From this brief historically view, analogical connection is another kind of association, which should be distinguished from causative associations.

1.6 Developments and Applications of Hume-Rothery's Rules

Hume-Rothery's Rules, in the Baconian tradition, occupy a central space at the heart of metallurgy. In the 1920's, after surveying the available solubility data, Hume-Rothery distinguished the factors that influence compound formation and control alloying behaviour. There exists a connection between solubility, atomic size, crystal structure and a particular concentration of valence electrons in an alloy (**Hume-Rothery, 1926; Massalski, 2000**). Later, Hume-Rothery added other ideas, and developed concepts which are now known collectively as Hume-Rothery's Rules (**Hume-Rothery *et al.*, 1934; Reynolds and Hume-Rothery, 1937; Hume-Rothery, 1967**). There are already detailed reviews of Hume-Rothery's Rules, such as the work done by Massalski and King (**1963**), Massalski and Mizutani (**1978**), Massalski (**1996, 2000**) and as described in biographical sketches about Hume-Rothery (**Pettifor, 2000a**). Following the hugely significant work by Hume-Rothery and his colleagues on the prediction of solid solubility in alloys, many researchers contributed in different ways to the prediction of solid solubility in terms of a soluble/insoluble criterion. The details are discussed in part 1.6.1 and 1.6.2.

As cautioned by Pettifor (**2000a**), because different rules were expressed or stressed by Hume-Rothery at different times, it is sometimes difficult to define what constitutes 'Hume-Rothery Rules' and this confusion is extant. There is general agreement that, in order of importance, the atomic size factor is first, followed by the electronegativity effect. The importance of the electron concentration (e/a ratio) in determining solid solubility boundaries is recognised in some cases but other factors are rarely discussed in sufficient detail. Surveying metallurgical and physical science publications in general, different sources express Hume-Rothery's ideas using terms such as: "effects", "principles", "factors" or "parameters" (**Massalski, 2000**).

Researches on Hume-Rothery's Rules blossomed in the 1930s-1980s but the prediction of solubility was gradually superseded by calculation of phase diagrams (CALPHAD), and the details are discussed in part 1.6.3. However, the simplicity and generality of Hume-Rothery's Rules still make them one of the most important cornerstones in materials science. As mentioned by Watson and

Weinert (**2000**), most of these rules are still useful today as in Hume-Rothery's time.

1.6.1 Early Formation and Revision of Hume-Rothery's Rules

In 1926, after examining phase diagrams of the noble and related metals (i.e. Cu, Ag and Au), especially those alloyed with the B-subgroup elements (including Li, Be, B, C, N, O, F, Na, Mg, Al, Si, P, S, Cl, Zn, Ga, Ge, As, Se, Br, Cd, In, Sn, Sb, Te, I, Hg, Tl, Pb, Bi), Hume-Rothery published a paper on the topic of compound formation in several alloy systems (**Hume-Rothery, 1926**). In it, Hume-Rothery predicted the β phase of Cu_3Al would have the bcc structure because it satisfied an electron per atom ratio of 3/2, which was confirmed one month later by Westgren and Phragmén (**1925**).

In the 1930s, Hume-Rothery shifted his attention to characterisation of atomic size by nearest neighbour distance instead of volume (**Hume-Rothery, 1930**). At that time, two of the Hume-Rothery rules controlling solid solubility were discovered: 1) the first Hume-Rothery rule, the atomic size factor, said that if the atomic diameters of the solvent and solute differ by more than about 14-15% then the primary solid solubility will be very restricted; 2) the second rule emphasised the importance of the electron concentration (or electron per atom ratio) in determining the phase boundary. Both of these rules are presented in his classical paper in 1934 (**Hume-Rothery *et al.*, 1934**).

In 1937, after studying the silver-rich antimony-silver alloy system with Reynolds (**Reynolds and Hume-Rothery, 1937**), Hume-Rothery became aware of a third factor restricting solid solubility, that is, electrochemical factor; maximum solid solubility reduced as the electronegativity difference between solute and solvent increased because of the competition to form intermetallic compounds.

The relative valence rule was mentioned in the 1934 paper, and the importance of this rule was stressed by Hume-Rothery in early editions of his famous book *The Structure of Metals and Alloys* (**Hume-Rothery, 1936**). However, in his later versions of this book, it is stated 'more detailed examination has not confirmed

this and, in its general form, the supposed principle must now be discarded' (**Hume-Rothery and Raynor, 1962; Hume-Rothery *et al.*, 1969**).

1.6.2 Further Developments and Applications of Hume-Rothery's Rules

The development of Hume-Rothery's Rules can be classified into two categories: one is the development within each rule, and the other is the development of anamorphoses or alternatives of these rules as a whole in order to get more powerful and precise predictions.

1.6.2.1 Development and Application of Each Rule

Atomic Size Factor

The atomic size factor rule is usually presented in the following way (**Hume-Rothery *et al.*, 1934**): "if the atomic diameters of the solute and solvent differ by more than 14%, the solubility is likely to be restricted because the lattice distortion is too great for substitutional solubility." When the size factor is unfavourable, the primary solid solubility will be restricted; when the size factor is favourable, other factors limit the extent of solid solubility and it is of secondary importance. The size factor rule has been explained by using elastic theory. It has be shown that (**Friedel, 1954; Eshelby, 1956; Mott, 1962; Cottrell, 1975**), the ensuing total strain energy E in both solvent matrix and solute can be estimated as

$$E = 8\pi\mu\, r_0^3 \varepsilon^2 \qquad \text{Equation 1.6.1}$$

where μ is the shear modulus and r_0 and $(1+\varepsilon)r_0$ are the unstrained radii of the solvent and solute atoms. Taking ε as 0.14 (as the size factor rule declares) or 0.15, and $\mu\, r_0^3$=0.7 eV, this gives $E \approx 4k_BT$ at 1000 K. Darken and Gurry (**1953**) proved that at temperature T, the primary solid solubility would be restricted to below about 1 at.% when the energy of solution exceeds $4k_BT$ per atom, where k_B is Boltzmann's constant. Although elastic theory cannot be applied strictly at the atomic level, this gives a simple explanation of Hume-Rothery's size factor rule. Also, Mott (**1962**) provided a quantum mechanical basis for this elastic theory based on the Wigner-Seitz wave function $\psi_0(r)$, for an electron in the lowest state in a Wigner-Seitz cell.

The validity of the size factor has been debated since the rule was proposed. Hume-Rothery *et al.* themselves (**1934**) pointed out that the exact "atomic diameter" of an element is always difficult to define. They defined the atomic diameter as given by the nearest-neighbour distance in a crystal of the pure metal. However, this diameter cannot necessarily be transferred to the alloy because 1) the 'radius' of an atom is probably affected by coordination number. Except for the heavy elements, elements of the B sub-groups tend to crystallize with coordination number 8-N, where N is the group to which the element belongs. This is due to the partly covalent nature of the forces in these crystals and, except in Group IV B, results in the atoms having two sets of neighbours at different distances in the crystal. 2) In some structures there are great variations in the closest distance between pairs of atoms at their closest distance of approach, depending on the position and direction in the lattice. 3) On forming a solid solution, the 'sizes' of individual atoms may change according to the nature and degree of local displacements. In the case of anisotropic or complex structures or where the coordination numbers are low, the closest distance of approach does not adequately express the size of the atom when in solid solution (**Massalski, 1996**). Furthermore, atomic spacing increases or decreases as the composition changes and so differences appear between the lattice spacing in alloys and the estimated atomic sizes.

There are some attempts to derive the atomic size, such as extrapolating the size variance trend of an element in the alloy towards the pure element to give a hypothetical size (**Axon and Hume-Rothery, 1948**). Massalski and King (**1963**) pointed out that in finding the atomic size factor, it is usually the volume per atom that matters, not the distance between nearest neighbours, so they used the change in volume per atom to obtain hypothetical dimensions.

The atomic dimensions can be calculated by using pseudopotential theory, such as the work done by Hayes *et al.* (**1968**) on Li-Mg, Inglesfield (**1969a; 1969b; 1969c**) on Hg, Cd and Mg alloys, Hayes and Young (**1970**) on alkali alloys, Stroud and Ashcroft (**1971**) for Cu-Al, Li-Mg and Cu-Zn, Meyer *et al.* (**Meyer and Young, 1969; Meyer *et al.*, 1971a; Meyer *et al.*, 1971b**) on analyzing the diffusion thermopowers of dilute alkali metal alloys, on calculating the lattice

spacings and compressibilities of non-transition element solids and for analyzing residual resistivities in silver and gold and Singh and Young (**1972**) on enthalpies of solution at infinite dilution. They can also be obtained from the free-electron model developed by Brooks (**1963**) and have been used by Magnaterra and Mezzetti (**1971; 1974**).

The actual individual atomic sizes can also be estimated from static distortions in a solid solution by modulation in diffuse X-ray scattering (**Warren *et al.*, 1951; Roberts, 1954**) or from weakening of the interference maxima analogous to thermal effects (**Huang, 1947; Herbstein *et al.*, 1956; Borie, 1957; Borie, 1959**).

From the analyses cited above, and as Cottrell (**1998**) suggested, the concept of a characteristic size, which suggests hard spheres butted together is doubtful and allocating a single atomic diameter for each element, independent of its environment, and valences of solvent and solute is too simplistic an approach (**Hume-Rothery *et al.*, 1969**). At present, the importance of the size factor, of course, extends far beyond primary solubility. Many intermetallic compounds owe their existence to size-factor effects.

Relative Valence Factor

An early discovery by Hume-Rothery was that a metal of lower valence is more likely to dissolve one of higher valence than vice versa. However, more extensive investigation has not confirmed the generality of this rule. An example is that monovalent silver can dissolve about 20% aluminium but trivalent aluminium dissolves about 24% silver. However, for high valence, covalently bonded components, the relative valence factor applies well. For example, copper dissolves about 11% of silicon but silicon dissolves negligible copper (**Cottrell, 1998**). This rule seems to be valid only when monovalent metals copper, silver or gold are alloyed with the B-subgroup elements of the Periodic Table which have higher valences. This is variously attributed to the partial electron filling of the Brillouin zones in noble metals, the interaction of Fermi surfaces and Brillouin zones in B-subgroup elements (**Massalski, 1996**) and long-range charge oscillations around the impurity atoms (**Hume-Rothery, 1961**). Gschneidner (**1980**) implies that the relative valence effect is limited in

applicability; when two high valence elements are alloyed it is not always possible to predict which will form the more extensive solid solution with the other.

Besides, the valencies of transition metals are variable and complex, as analysed by Hume-Rothery *et al.* (**1951**) and Cockayne and Raynor (**1961**). Cottrell's book (**1998**) points out that due to the valency complication caused by partly filled *d* orbitals, the transition metal alloys generally do not follow the rule. Gschneidner (**1980**) revised the relative valence rule to suggest that the solubility will be low if a metal in which *d* orbitals strongly influence the valence behaviour is alloyed with a '*sp* metal'. The solubility is likely to be higher in the *d* metal than the reverse.

Electronegativity Factor

The scale for electronegativity as given by Mulliken is based on the equation:

$$\phi^* = \frac{1}{2}(I + A) \qquad \text{Equation 1.6.2}$$

where I is the ionization energy, A is electron affinity, and ϕ^* is Mulliken electronegativity. Dividing by 2.8, gives approximately Pauling's empirical scale. Watson and Bennett (**1978**) point out that in the case of transition metals, the partly filled *d* states at energies near the Fermi energy influence electronegativity. They produced an electronegativity scale for transition metals, which matches Pauling's scale, and could be scaled by 2.8 to bring it to Mulliken's scale.

As discussed by Hume-Rothery (**1961**), stable intermetallic compounds are prone to form as the more electronegative is the solute and the more electropositive is the solvent metal, or *vice versa*. Due to the lower free energy that can be obtained when the system adopts a mixture of solid solution and compound, solute atoms partition to form the stable compound rather than to enter solid solutions. Further, as stated by Pearson (**1972**), in some binary alloy systems, if one component is very electropositive relative to the other, there would be a strong tendency for them to form compounds of considerable stability in which valence rules are satisfied. This is the strongest effect in determining the constitution of alloys, which dominates all other effects.

Recently, Li and Xue (**2006**), on the basis of an effective ionic potential that is defined in terms of ionisation energy and ionic radius, calculated the electronegativities of 82 elements in different valence states and with the most common coordination numbers, and pointed out that 'although electronegativity is often treated as an invariant property of an atom, as in Pauling's scale, it actually depends on the chemical environment of the atom, e.g. valence state, coordination number and spin state'.

1.6.2.2 Mapping and Derivatives of Hume-Rothery's Rules

While extensive efforts have been made to work out the theory behind the H-R rules, it is very useful if the solubility of the materials can be mapped diagrammatically on a Cartesian system. Thus researchers can simply calculate the coordinate of the element to predict the solubility using such a diagram. This direction started from Darken and Gurry (**1953**), followed by Chelikowsky (**1979**), Gschneidner (**1980**), Alonso *et al.* (**Alonso and Simozar, 1980; Alonso *et al.*, 1982**), and Zhang and Liao (**1999a; 1999b**) among others.

Darken-Gurry Method

In 1953, Darken and Gurry (**1953**) proposed a diagrammatic method to describe the solid solubility of fifty alloy systems (DG method). They used the size factor as abscissa and electrochemical factor (electronegativity) as ordinate to plot solubilities of each alloy system and then draw an ellipse to separate the soluble elements from the insoluble elements, which is shown in Figure 1.6.1. The solubility is characterized qualitatively as "extensive" or "limited", inside the ellipse or outside the ellipse, respectively.

Waber *et al.* (**1963**) examined the universality of the Hume-Rothery size rule and the DG method for predicting solid solubilities. After analyzing 1455 binary alloy systems, they confirmed Hume-Rothery's size factor and showed that the electronegativity is an important consideration in the formation of solid solutions.

In 1980, Gschneidner (**1980**) again applied the DG method to create a soluble/insoluble classification by introducing the effect of crystal structure (electronic-crystal structure Darken-Gurry method, ECSDG). Applying the

ECSDG rules to ten solvents (Mg, Al, Fe, Ge, Pd, Ag, Cd, La, W and Pb), an improvement in the prediction of extensive solid solubility–compared with DG method was found.

Recently, Gschneidner and Verkade (**2004**) presented the complete details of their semi-empirical approach (called electronic and crystal structure, size model, ECS^2), and pointed out that their method should also be quite good at predicting the extent of another element in a binary compound. In compounds, i) the compatibility of the crystal structure of the solute with either or both of the components of the intermetallic phase is regarded as a critical factor; ii) the valence of the solute compared with the components is also decisive iii) if the above two criteria are favourable, then atomic size factor would be the final decisive issue and because of the less elastic nature of compounds compared with elemental metals, a ±10% limitation on atomic size should be applied.

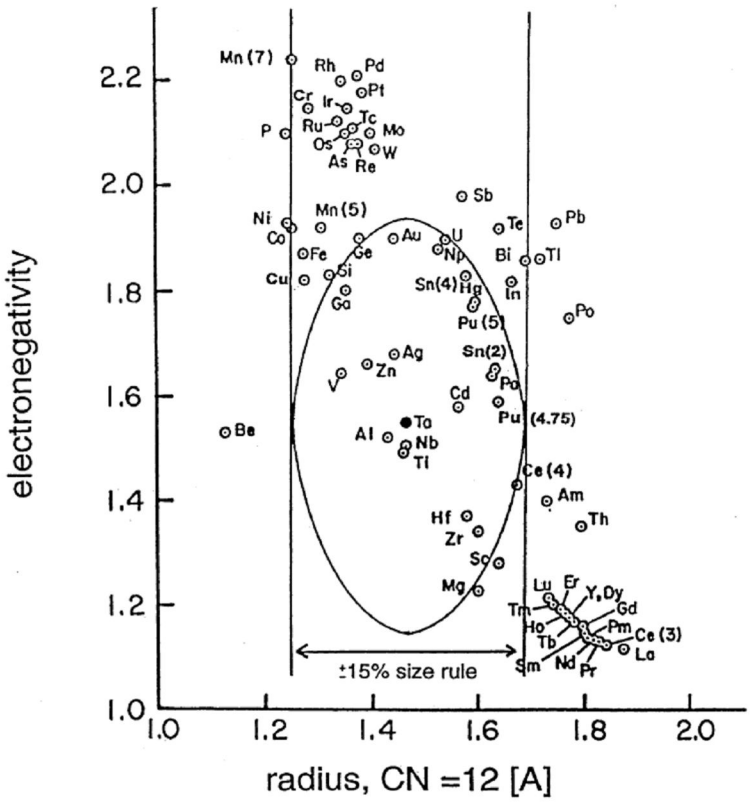

Figure 1.6.1 The electronegativity vs. the metallic radius for a coordination number of 12 (Darken-Gurry) map for Ta as the solvent. (Taken from **Gschneidner and Verkade, 2004**).

Chelikowsky's Method

In the 1970s, two events occurred to remove the barriers for understanding solid solubility in intermetallic alloys (**Chelikowsky, 1979**). 1) Miedema and collaborators predicted and classified enthalpies of formation for regular intermetallic alloys which is predominantly determined by the electronegativity difference ($\Delta\phi^*$) and the difference in electron density at the boundary of the Wigner-Seitz cell (Δn_{WS}) of pure metals (**Miedema, 1973; Miedema *et al.*, 1973; Miedema *et al.*, 1975; Miedema, 1976a; Miedema, 1976b**). 2) Kaufmann and co-workers developed ion-implantation techniques and conducted ion-implantation to provide a wide range of new and unique metastable alloy systems, unobtainable by conventional metallurgical procedures (**Kaufmann, 1977; Kaufmann and Vianden, 1977; Kaufmann *et al.*, 1977**) which led to subsequent efforts to study solid solubility in alloys (**Lopez and Alonso, 1982a; Alonso and Lopez, 1982; Zhang, 1987; Zhang and Tan, 1988**).

In 1979, Chelikowsky introduced a graphical procedure similar to the Darken-Gurry method to analyse solid solubility in the case of divalent hosts. In his work, a different pair of coordinates were introduced: the electron density at the boundary of bulk atomic cells, n_{WS}, and the electronegativity ϕ^*. As mentioned before, these two coordinates are the fundamental parameters in a successful semi-empirical theory of enthalpies of alloy formation developed by Miedema and co-workers (**Miedema, 1973; Miedema *et al.*, 1973; Miedema *et al.*, 1975; Miedema, 1976a; Miedema, 1976b; Chelikowsky, 1979**). In his new kind of plot, Chelikowsky was able to give more reliable predictions. One example of Chelikowsky plots and a comparison with Darken-Gurry plots are shown in Figure 1.6.2.

From 1.6.2(b) and other results in his paper, most of the metals which are soluble in a given host are bounded by the ellipse and this is so even if the precise location varies from host to host. This higher accuracy of prediction can be interpreted by the relation between the Miedema coordinates and more elementary descriptions of alloy formation, as developed by others (**De Chatel and Robinson, 1976; Chelikowsky and Phillips, 1978; Alonso and Girifalco,**

1979; Alonso *et al.*, 1979; Alonso and Girifalco, 1978; Hodges, 1977; Hodges, 1978; Pettifor, 1979; Varma, 1979; Williams *et al.*, 1980; Chelikowsky, 1982; Gonzalez and Alonso, 1983; Lopez and Alonso, 1983; Lopez and Alonso, 1985; Gokcen *et al.*, 1993). Recently, the Miedema parameters were used to predict the formation of quasicrystals (**Wang *et al.*, 2003; Gui *et al.*, 2006**).

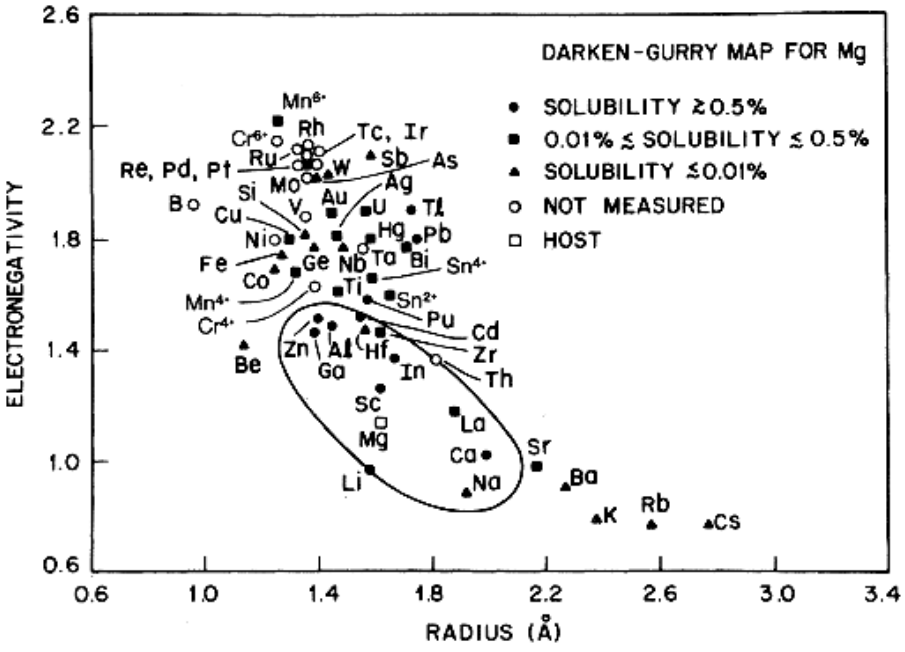

(a)

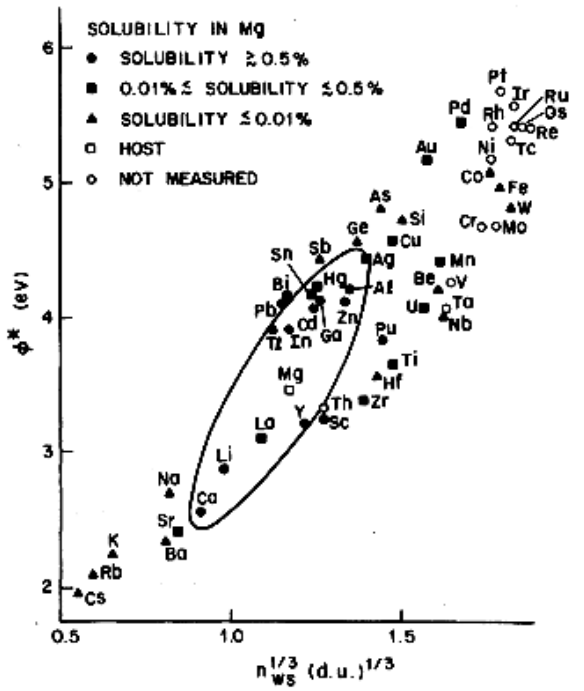

(b)

Figure 1.6.2 (a) Darken-Gurry map for Mg as host metal. (b) Chelikowsky method for Mg as host metal (Taken from **Chelikowsky, 1979**).

Although higher accuracy has been established, some exceptions remain. These exceptions suggest that Chelikowsky's method is still susceptible to some improvement (**Alonso and Simozar, 1980**).

Alonso's Method

In the 1980s, from analysis of both Darken-Gurry and Chelikowsky methods, Alonso and Simozar (**1980**) proposed a scheme containing all three coordinates (atomic size, electronegativity, electron cell-boundary density). The suggestion was also proposed by Miedema and De Chatel (**1980**). By incorporating a size factor in a new graphical method, they improved on the original Miedema coordinate scheme proposed by Chelikowsky. In their analysis, each chemical element is characterized by three parameters: the atomic volume ΔV , the electronegativity ϕ^* , and the electron density at the boundary of bulk atomic cells n_b . $\Delta\phi^*$ and Δn_{ws} (the difference of electronegativity and electron density at the boundary of bulk atomic cells) combined into a new parameter, ΔH_C , the enthalpy of formation of an equi-atomic compound (**Miedema *et al.*, 1973; Miedema, 1976b; Miedema *et al.*, 1977**). Then, the two parameters ΔH_C and ΔV (expressed as Wigner-Seitz radius, R_W) are used to construct a two-dimensional map. In this map, the chemical elements insoluble in a given host are neatly separated from the soluble ones by a straight line. The examples and the comparisons with Chelikowsky's plot are shown in Figure 1.6.3 (a) and (b). Later, Alonso *et al.* applied this method to the prediction of solid solubility in noble metals, transition metals and *sp* metal based alloys (**Alonso *et al.*, 1982; Lopez and Alonso, 1982**). Jones has applied this method to the solid solubility of two light metals, magnesium and aluminium (**Jones, 1983**).

After Miedema, the enthalpies of formation of different binary alloys have also been predicted successfully from both first-principles and semi-empirical methods (**Maarleveld *et al.*, 1986; Wei *et al.*, 1987; Terakura *et al.*, 1987; Takizawa *et al.*, 1989; Johnson, 1989; Ackland and Vitek, 1990; Johnson, 1990; Lu *et al.*, 1991; Bozzolo and Ferrante, 1992; Bozzolo *et al.*, 1992; Sluiter and Kawazoe, 2002; Ouyang *et al.*, 2003**). During the last twenty years and based on calculated enthalpies of formation of alloys and semi-empirical

theories with parameters such as electronegativity difference, atomic diameter and number of covalent bonds, a large number of predicted maximum solid solubilities of alloys, design of alloy systems or formation of compounds have appeared (**Wei *et al.*, 1990; Mohri *et al.*, 1991; Ito *et al.*, 1993; Singh *et al.*, 1993; Turchi *et al.*, 1994; Lu *et al.*, 1995; Pasturel *et al.*, 1995; Colinet *et al.*, 1997; Bacalis *et al.*, 1997; Ozolins *et al.*, 1998; Bozzolo *et al.*, 1999; Teles *et al.*, 2000; Fang *et al.*, 2002a; Zhou *et al.*, 2003a; Zhou *et al.*, 2003b; Wang *et al.*, 2004; Deibuk *et al.*, 2005; Zhang *et al.*, 2005a; Abe *et al.*, 2006; Hatano *et al.*, 2007; Liu and Zunger, 2008**). This indicates these methods still have vitality in the prediction of alloy formation even though nearly thirty years has passed.

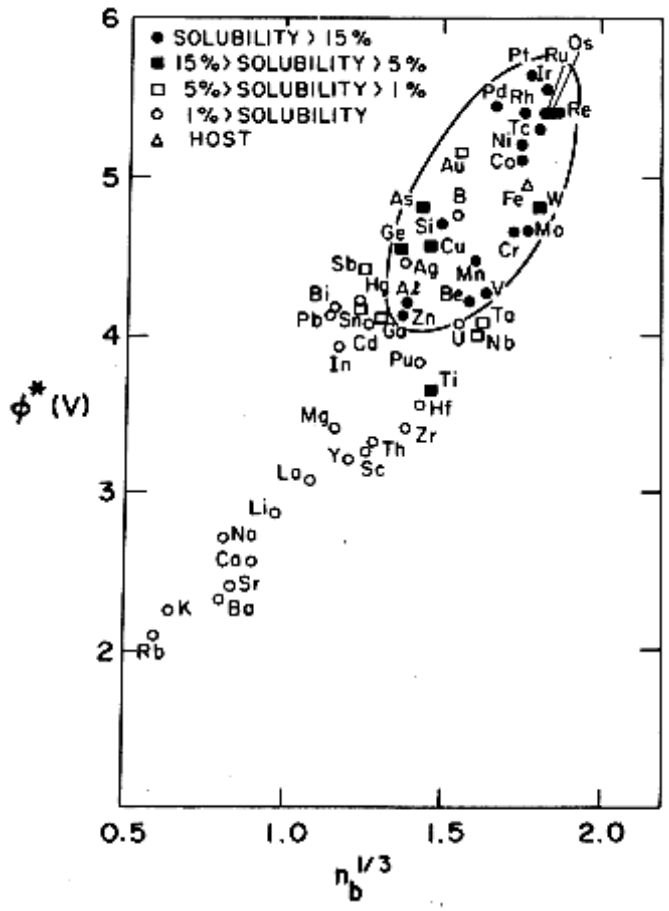

(a)

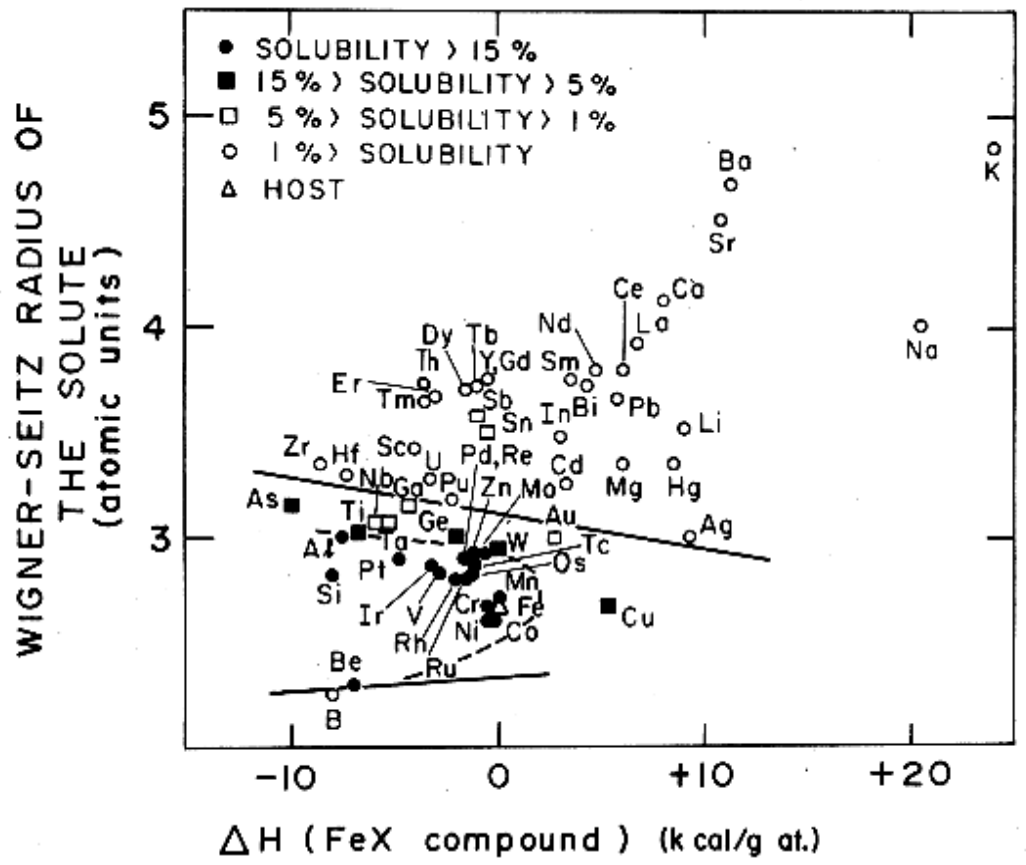

(b)

Figure 1.6.3 (a) Chelikowsky's plot for the analysis of solid solubility in Fe; (b) Alonso plot for analysis of solid solubility in Fe, the two continuous lines separate the insoluble elements from the rest (Taken from **Alonso and Simozar, 1980**).

Zhang BW Method

Zhang and his co-workers used graphical methods with various parameters/coordinates to predict the formation of amorphous alloys and solid solutions.

In 1983 (**Zhang, 1983**), they applied Miedema's coordinates to the prediction of binary amorphous alloy formation and found that this method worked quite well. The ranges of formable and non-formable binary amorphous alloys can be separated by a straight line. Of the total 157 alloys studied, the overall accuracy

was 77.7%. These results compared well with the work done by Shi *et al.* (**1979**) using bond-parametric diagrams, which had a prediction accuracy of 80%.

Taking the parameters used in Miedema's coordinates without the size factor, Zhang (**1985a**) combined the two chemical coordinates ϕ^* and $n_{ws}^{1/3}$ into one:

$$y = \left|10\left|\Delta\phi^*\right| - 39\left|\Delta\left(1/n_{ws}^{1/3}\right)\right| - 1\right| \qquad \text{Equation 1.6.3}$$

and using the radius difference of elements

$$x = \left|\frac{R_1 - R_2}{R_1}\%\right| \qquad \text{Equation 1.6.4}$$

as the other coordinate to constructed a two-dimensional map. From this, the definition of conditions for formation of binary amorphous alloys was improved. The separation of the formable and non-formable regions was given by $y = 0.05x^{-1.75}$. Of the total 157 alloys studied in that work, the overall accuracy was 83.4%. It is found that the prediction accuracy for the formation of amorphous alloys is improved when the size factor is added to the original Miedema coordinates criterion.

Zhang and co-workers proposed another graphical method, which combined bond parameters Z/r_K and Z/r_{COV} as an electron factor (where Z is atomic valence, r_K is atomic kernel radius, equal approximately to the positive ionic radius not including the valence electrons and r_{COV} is covalent radius). Then, together with a size factor to provide two coordinates for the study of solid solubility, they described the formation of amorphous alloys (**Zhang, 1981**). The two coordinates are expressed by (1) bond-parametric function $\frac{Z}{r_K}\left[x_P - \left(\frac{1}{3}\frac{Z}{r_{\mathrm{cov}}} + \frac{2}{3}\right)\right]x_P$, where x_P is the Pauling electronegativity; (2) half of the empirical interatomic distance R respectively. When the coordinate point of a host element is represented in the chart, the closer is the point of a solute element to it, the smaller the differences of the electron factors and of the size factors between the solute element and the host element. Zhang (**1987b**) applied this method to 1080 binary and got a prediction accuracy of 93%.

Zhang also used a modified electron factor

$$y = \left| \left(\frac{Z}{r_K} \right)_B \left[X_{PA} - \left(\frac{1}{3} \frac{Z}{r_{COV}} + \frac{2}{3} \right)_A \right] \left(X_{PA} - X_{PB} \right) \right| \quad \text{Equation 1.6.5}$$

as ordinate and $x = \left| \frac{R_1 - R_2}{R_1} \% \right|$ as abscissa to search for solid solubilities at room temperature in 2460 binary alloys. In this work the transition metals of the fourth, fifth and sixth long periods and 18 non-transition metals are studied. For each host element, a parabolic curve $y = a - bx^2$ can be drawn to separate the soluble elements from the insoluble ones with a criterion of 0.5 at.% solubility at room temperature. The overall reliability of this equation approached 90% for 2460 alloys. Also, it has been found that the values of a for each host metal are proportional to its cohesive energies E, and b values are proportional to $E\mu R_0^3$, where μ is the shear modulus of solvent element, and R_0 is the atomic radius of the solvent (**Zhang, 1985b**).

In 1996, Zhang and Liao (**1996**) applied this method to study the solid solubilities for the binary alloy systems based on 13 rare earth metals, and found the soluble elements can be separated from the insoluble ones by a parabola $y_1 = a - bx_1^2$, where $\boldsymbol{x_1}$ is defined in equation 1.6.4 and, $\boldsymbol{y_1}$ is defined in equation 1.6.5 or an elliptical curve

$$\left(x_2 - m \right)^2 / c^2 + \left(y_2 - n \right)^2 / d^2 = 1 \quad \text{Equation 1.6.6}$$

where $x_2 = R$ and

$$y_2 = \frac{Z}{r_K} \left[x_P - \left(\frac{1}{3} \frac{Z}{r_{\text{cov}}} + \frac{2}{3} \right) \right] x_P \quad \text{Equation 1.6.7}$$

For the solid solubilities in 897 binary alloys, the prediction accuracy was 89.2% for the parabolic separation, and 92.8% for the elliptical separation. Also, in the elliptical equation, constants m and n were dependent on the coordinates x_2 and y_2, c was proportional to $\left(\mu R^3 \right)^{-1/2}$ and d was proportional E.

In 1999, Zhang and Liao (**1999a; 1999b**) summarized different methods used by themselves and others and made a comparison in terms of prediction accuracy. Those results are shown in Table 1.6.1.

The ECS^2 method, as well as Hume-Rothery's rule and the Darken-Gurry method, are for predicting solid solubility without considering Gibbs energy. These methods are easy to use – needing only the physical parameters (radii, electronegativity, structure) of two elements **(Gschneidner and Verkade, 2004)**. The extent of primary solid solubility can be derived by using first principle calculations. Following work done by others (**Olesinski and Abbaschian, 1986; Zunger *et al.*, 1990; Ansara I. *et al.*, 1998; Fries and Jantzen, 1998; Yan and Chang, 2000; Wolverton *et al.*, 2002; Colinet, 2003**), Shin *et al.* (**2008**) described the Cu-Si system thermodynamically as an example of higher order systems (i.e. solute elements in compounds) with first-principles calculations of the ε-$Cu_{15}Si_4$ phase and solid solution phases. By considering the enthalpy of mixing and Gibbs energies of individual phases in the Cu-Si binary system, it was found that the existence of intermetallic compounds would strongly affect solubility limits. Predictions of solid solubility of other alloy systems using first principles can be found elsewhere (**Fuks *et al.*, 1975; Udovskii and Ivanov, 1977; Martin and Carstensen, 1981; Yamamoto *et al.*, 1993; Luo *et al.*, 1994; Hallemans *et al.*, 1994; Duschanek *et al.*, 1995; Sluiter *et al.*, 1996; Flandorfer *et al.*, 1997; Ding *et al.*, 1999; Grobner *et al.*, 1999; Ghosh *et al.*, 2002; Fang *et al.*, 2002b; Song *et al.*, 2003; Stuparevic, 2004; Van de Walle *et al.*, 2004; Tokunaga *et al.*, 2006; Sluiter *et al.*, 2006; Hallstedt and Kim, 2007; Ghosh and Asta, 2007; Cao *et al.*, 2008; Teyssier *et al.*, 2008**).

Table 1.6.1 Comparison of the prediction of solid solubilities by different methods (redrawn from **Zhang and Liao, 1999b**)

	No. of alloy systems and the prediction accuracy	
	Total No.	Prediction accuracy %
Hume-Rothery's rule (size factor only)	1423	67.6
D-G Method	1455	76.6
Chelikowsky Method	192	82
Alonso Method	342	90
Zhang BW Method (parabola separation)	3864	87.2
Zhang BW Method (ellipse separation)	3864	90.3

1.6.3 Calculation of Phase Diagrams (CALPHAD)

Phase diagrams offer the most basic and important information on materials systems, such as alloy systems. Traditionally, phase diagrams were determined through doing experiments. For determination of the phase boundaries, the specimens were heated over a sufficiently long time at an intended temperature to achieve equilibrium. However, the problem is that the diffusivity of atoms is generally not high enough at temperatures below half of the absolute T_m. Therefore, it is not actually possible to conduct experiments on the phase equilibrium below that temperature. On the other hand, special devices for temperature control and atmosphere adjustment are required in experiments conducted at extremely high temperatures. For these reasons, an explanation of the entire phase diagram only from experimental work is rather difficult (**Ohtani and Ishida, 1998**).

CALPHAD is an acronym for the CALculation of PHAse Diagrams, which aims to couple the phase diagrams and thermochemical properties attempting explicitly to characterise all of the possible phases in a system (**Kaufman, 1998**). In detail, it is based on the well known thermodynamic law that a system with a given composition, temperature and pressure attains the state of lowest Gibbs energy under these given conditions; and if the Gibbs energy is known for the individual phases, it is possible to calculate the equilibrium state by an energy minimization procedure (**Agren, 1996**). The procedures of doing CALPHAD can be illustrated as Figure 1.6.4.

The calculation of phase diagrams was started a century ago by Van Laar (**1908a, b**) in which he calculated a great number of prototype binary phase diagrams using ideal and regular solution models and then demonstrated the relationship of the characteristic features of a binary phase diagram in terms of the relative thermodynamic stabilities of the phases involved (**Chang *et al.*, 2004**). This situation remained unchanged for nearly half a century (**Saunders and Miodownik, 1998**) before an alternative more physical approach based on band-structure calculations (which stressed the electronic origin of solubility limits only) was employed (**Hume-Rothery *et al.*, 1940**). In the 1950s, Meijering extended Van Laar's methodology to higher order systems and calculated phase

diagrams for ternaries using a regular solution model (**Meijering, 1950; 1951; Meijering and Hardy, 1956; Meijering, 1957; Meijering, 1960**). Subsequently, people started to calculate phase diagrams for real alloy systems, mostly for binaries, using calculating machines, and then computers with software made by themselves (**Hillert, 1968; Pelton and Schmalzried, 1973; Sharma and Chang, 1979; Hillert, 1981; Lukas *et al.*, 1982; Schmid, 1983; Chuang *et al.*, 1985; Chuang *et al.*, 1986; Gabriel *et al.*, 1987; Chuang and Chang, 1987; Chen *et al.*, 1989; Kattner *et al.*, 1992; Murray *et al.*, 1992; Chen and Chang, 1993**).

Nowadays, the calculation of phase diagrams (CALPHAD) has been recognized widely as a powerful tool that enables calculation of both stable and metastable phase equilibria. Kaufman used a simple solution model to describe alloy phases and systematically calculated phase diagrams for a large number of real alloy systems, including binaries and some ternaries (**Kaufman and Cohen, 1958; Kaufman, 1959; Kaufman *et al.*, 1963; Kaufman, 1969; Kaufman and Nesor, 1976; Kaufman, 1978; Kaufman and Nesor, 1978a, b, c, d; Kaufman, 1979a, b; Kaufman and Tanner, 1979; Smith *et al.*, 1980; Kaufman *et al.*, 1981; Kaufman and Tanner, 1984; Kaufman *et al.*, 1984; Bouwstra *et al.*, 1986; Kaufman, 1991**). Many of his early published results are summarised in the monograph *Computer Calculation of Phase Diagrams* (**Kaufman and Bernstein, 1970**). Recently, more alloy systems have been evaluated (**Lim *et al.*, 1995; Yang *et al.*, 1995a; Zakulski and Moser, 1995; Yang *et al.*, 1995b; Du and Clavaguera, 1996; Gomez-A, 1998; Cui and Jin, 1999; Du *et al.*, 1999; Du and Yang, 2000; Ohnuma *et al.*, 2000; Du *et al.*, 2000; Liu *et al.*, 2001; Fries *et al.*, 2001; Luo *et al.*, 2001; Uhland *et al.*, 2001; Kaufman *et al.*, 2001; Arroyave *et al.*, 2002**; **Xiong *et al.*, 2004; He *et al.*, 2006; Guo *et al.*, 2008; Borzone *et al.*, 2009**).

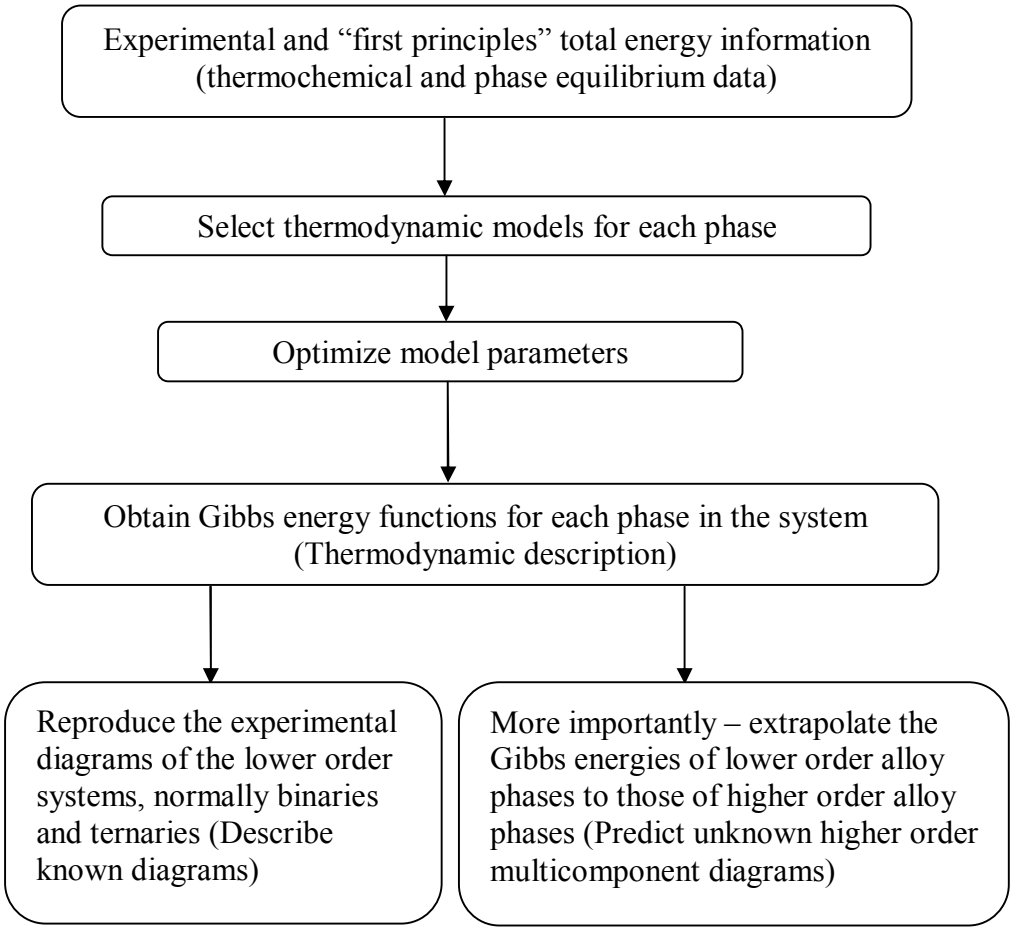

Figure 1.6.4 The CALPHAD or phenomenological approach used to obtain a thermodynamic description of a multicomponent system (Redrawn from **Chang *et al.*, 2004**).

1.7 Errors in Handbooks and Databases

1.7.1 Error as a Fundamental Dimension of Data

Physical and chemical handbooks, some having long pedigrees and an increasing number of databases are trusted for veracity of the data they contain. For a database to have scientific value, it must meet criteria of completeness and accuracy. However, as mentioned by Chrisman (**1991**), "error is inescapable, and it should be recognized as a fundamental dimension of data". The data entry mistakes, faulty sensor readings or even more malicious activities provide a large number of erroneous data sets, and then propagate these errors in each successive generation of data (**Hernández and Stolfo, 1998**). As mentioned by Redman (**1997**), error rates between 1% and 75% have been reported, and it is suggested that unless extraordinary efforts are taken, dataset field error rates of 1-5% are typically expected. Later it is reported that the error rates in the data acquisition are generally about 5% or more (**Orr, 1998; Redman, 1998**). Another study shows that as much as 40% of all collected data is dirty in one aspect or another (**Fayyad *et al.*, 2003**).

The collections in handbooks are assembled from other sources or manually transcribed from earlier handbooks and the amount is always large. Errors (most are typographical) are anticipated (**Allen, 1998**) and these errors are passed on, rather like genetic mutations, into subsequent editions and newly written handbooks and databases.

1.7.2 Existing Outlier Detection Methodologies

Outliers are defined as objects that do not comply with the general behaviour or model of the data, and have different characteristic from or are inconsistent with the remaining set of data (**Agyemang *et al.*, 2006; Han and Kamber, 2006**).

In one aspect, outliers are treated as error or noise that must be removed. There are various outlier-detection procedures to detect, and where appropriate, to remove anomalous observations, such as contaminated data and errors (**Hodge and Austin, 2004**). They have been applied to text data (**Pollock and Zamora, 1984; Pfeiffer *et al.*, 1996; Dalcin, 2005; Fan *et al.*, 2008**) and numerical data (**Walczak and Massart, 1998; Chalk *et al.*, 2001**). All of them need known

functional correlations or dependencies. Presently, with the greatly enhanced computing power available, several robust regression methods have been used to detect and reject outliers (**Liang and Kvalheim, 1996; Rousseeuw and Leroy, 2003; Colliez *et al.*, 2006; Ortiz *et al.*, 2006**). Notably, in the materials science field, statistical methods have been developed to estimate the veracity of material properties (**Ashby, 1998; Bassett *et al.*, 1998**). They seek out deviations from predefined data ranges, correlations or fit the data to a function through regression, and their performance is compared with the method used in this work (part 4.3.4). In the other aspect, outlier detection also can be used to find rare and interesting patterns for decision making, such as work done by Provost and Aronis (**1996**), Chan *et al.* (**1999**), Liu *et al.* (**2001**), Shekhar *et al.* (**2001**), Yamanish and Takeuchi (**2002**), He *et al.* (**2002**), Zhao *et al.* (**2003**), Petrovskiy (**2003**), Kou *et al.* (**2004**), Jung and Jo (**2004**).

Milleer (**1993**), Bishop (**1994**), Markou and Singh (**2003a, b**), Hodge and Austin (**2004**), Ben-Gal (**2005**), Maletic and Marcus (**2005**), Agyemang *et al.* (**2006**) and Hand and kamber (**2006**) have surveyed different methods (e.g. statistical, neural network, machine learning), used for outlier detection in different fields.

1.7.3 Policing and Correction of Errors by Exploring Correlations between Properties

In this work, the procedure that has been devised is general for collections of data in which hidden relationships can be found. It started out to see if ANNs can discover unanticipated relationships between combinations of properties of materials which might help identify potential compositional spaces for materials discovery (part 1.9 and 6.0) and in doing so, discovered that the ANN is very good at highlighting unusual data points in handbooks, tables and databases that deserve to have their veracity inspected. It is also quite good at pointing an accusing finger at the culpable values in a line-up of suspect data from different sources. The outcome is a method of sifting large amounts of data to screen out suspect values and the method could potentially be built into databases to form an immune system providing the community with self-policing databases. The method is based on the hypothesis that the data contains as-yet unknown relationships which can be discovered by the ANN; established relationships are

not essential. This work shows how correct data can be identified. Estimates can easily be found for suspect data but this is quite unethical: as mentioned before, outliers can act as a prompt for new discoveries. As mentioned by Han and Kamber (**2006**), "In general, users must check that each outlier…is indeed a 'real' outlier."

It is well known that both the boiling point and enthalpy of vaporization are very important thermodynamic properties, which are required in processes involving liquid and vapour phase transitions such as distillation, vaporization and drying (**Cachadiña and Mulero, 2007**); as the result, the quality and veracity of these data in handbooks play important roles for scientific community and industry.

In this work, a procedure was established, based on artificial neural networks (ANNs), which finds remarkable levels of error in the records of properties of the elements. Table 1.7.1 and 1.7.2 show examples of incorrect boiling point and enthalpy of vaporization values discovered by ANN in elemental data; errors that have persisted undetected into the 21st century. The representation of abbreviations in tables are as follow: CDH: *Chemistry Data Handbook* (**Stark and Wallace, 1982**); LAG: *Lange's Handbook of Chemistry* (**Speight, 2005**); ELE: *The Elements* (**Emsley, 1998**); TPC: *Tables of Physical and Chemical Constants* (**Kaye and Laby, 1995**); CRC: *CRC Handbook of Chemistry and Physics* (**David, 2000**).

In Table 1.7.2, some sources of error are self-evident when inconsistent data are thus assembled: the difference in enthalpy of vaporization of Ho is about 4 times, suggesting a missing conversion from calories to Joules; enthalpy of vaporization of Ag and Al from TPC are 10 times smaller than the data from other sources, implying a decimal point was incorrect. Sulphur and phosphorous are polyatomic molecules, so the enthalpies of vaporization differ by a factor of 4.

Table 1.7.1 Examples of inconsistent boiling point in handbooks and correct values are underlined /K.

Materials	**CDH**	**LAG**	**ELE**	**TPC**	**CRC**	**(Max-Min)/Min**
Rh	4773	4773	4000	3973	3968	20.3%
Zr	3853	3853	4650	4673	4682	21.5%
C (graphite)	5103	5103	5100	-	4098	24.5%
Ir	5573	5573	4403	4703	4701	26.6%
Pd	4253	4253	3413	3233	3236	31.5%
Si	2633	2633	2628	3533	3538	34.6%
Nb	3573	3573	5015	4973	5017	40.4%

Table 1.7.2 Examples of inconsistent enthalpy of vaporization in handbooks, and correct values are underlined /kJ mol^{-1}.

Materials	CDH	LAG	ELE	TPC	CRC	(Max-Min)/Min
Te	49.8	114	50.6	50.6	114	129%
Ir	636	231.8	564	564	-	174%
Sb	195	193	67.9	67.9	-	187%
Ho	-	71	251	251	-	253%
P (White)	12.4	12.4	51.9	-	12.4	319%
S (monoclinic)	10	45	9.62	-	45	368%
Se	14	95.5	26.3	26.3	95.5	582%
Al	284	294	294	29.1	294	910%
Ag	254	258	255	25.5	-	912%

1.8 The Prediction of Structural Stability and Formation of ABO_3-type Perovskite compounds

1.8.1 Crystal Structure Determination

Crystal-structure and materials properties are intimately linked together, so obtaining information on crystal structures continues to be an area of ongoing research. Presently, crystallographic information is a prerequisite for any extensive materials modeling and so knowledge of crystal structures is a practical and pressing quest (**Morgan and Ceder, 2005**)

There are three main approaches for determination of crystal structures. (1) Experimental determination: such work began in 1911 by von Laue and his colleagues (**Friedrich *et al.*, 1912**); and Bragg (**1913**). The experimental approach is expensive despite the emergence of high throughput automation (**Kennedy *et al.*, 1965**; **Xiang *et al.*, 1995**), as mentioned before. (2) The evolution of high-speed computers and the derivation of one-electron potentials, which greatly simplify many-body interactions, make it possible to predict structures using quantum mechanics principles, as demonstrated by Wolverton *et al.* (**2002**), Asta *et al.* (**2001**), Blum and Zunger (**2004**) and Curtarolo *et al.* (**2005**). These modelling efforts have made computational materials design a real possibility but difficulties still exist: i) As Chelikowsky (**2004**) wrote: "Although the interactions in … compounds are well understood, it is not an easy task to evaluate the total energy of solids … As the energy of an isolated atom is in the order of about 10^6 eV, but the cohesive energy only in the order of about 1-10 eV/atom, one must have a method that is accurate to one part on 10^6, or better." ii) The number of particles involved complicates the situation of evaluating the cohesive energy and makes such computations less accurate than experiment (**Villars, 2000**). (3) With the help of databases of known structures or models which have physical meaning, certain regularities, such as laws, rules, principles, factors, tendencies or patterns, might be found to help predict unknown structures. This approach, known as structure mapping, is one of the more successful non-experimental methods for crystal structure prediction and has been reviewed by Burdett and Rodgers (**1994**), Villars (**2000**) and Pettifor (**2000b**). Examples of structure mapping include Mooser-Pearson Maps (**1959**), Zunger Maps (**1980**), and Villars Maps (**1983, 1984a, b**), but the best known are

Pettifor Maps (**1984, 1986**). This method orders the very large database into domains of different structure types and can be used as an initial guide in the search for new compounds with a required structure type.

1.8.2 Data Mining Methods in Crystal Structure Prediction

The data mining (DM) method has become a powerful tool in different branches of materials science offering the possibility of making descriptive and even quantitative predictions in many areas where traditional approaches have had limited success. Generally, predictions are made through constitutive relations, that is, derived mathematically from basic laws of physics; however, in many cases, the problems are so complex that constitutive relations either cannot be derived or are too approximate or intractable for practical quantitative use. The data mining method is based on the assumption that the useful constitutive relations exist, and can be derived primarily from data rather than from basic laws of physics (**Morgan and Cerbrand, 2005**).

Because there is no generally reliable and tractable method to predict structure, and taking into account that a lot of structural data exist in crystallographic databases such as ICSD (**Bergerhoff *et al.*, 1983**), Linus Pauling files (**Villars *et al.*, 1998**), CRYSTMET (**White *et al.*, 2002**), and others as mentioned in the review paper by Allen (**1998**), crystal structure prediction is an area well suited for data mining. Examples include works by Woodley *et al.* (**1999**), Curtarolo *et al.* (**2003**), Fischer *et al.* (**2006**), Kazius *et al.* (**2006**) and, in particular, Morgan *et al.* (**2003**), who developed a clustering algorithm to automate the construction and testing of Pettifor maps based on data from a materials crystal structure database.

1.8.3 Structural Stability and Formation of ABO_3-type Perovskite Compounds

The physical and chemical properties of perovskite and perovskite-related materials are diverse and can be applied in a variety of fields, so it is useful to discover the regularities that govern the formation of perovskite-type compounds in order to guide the exploration of new materials in the huge compositional spaces available (**Zhang *et al.*, 2007**).

The study of ABO_3 compounds has a long history. Megaw (**1946**) accurately determined the structure of a number of doubled perovskites by examining high-angle lines on X-ray powder photographs. Salinas-Sanchez *et al.* (**1992**) introduced a parameter called the global instability index (**GII**), which can be used to determine the overall structural stability of perovskites. Giaquinta and Loye (**1994**) later predicted the perovskite structure for a number of compounds based on the combination of ionic radii and bond ionicities, predicting the structure of $InMO_3$ (M = Mn, Fe) with this method. Reaney and Ubic (**1999**) reviewed the relationship between the tolerance factor (***t***) and the temperature coefficient of permittivity (τ_ε) (and therefore resonant frequency, τ_f) in perovskites and also discussed the effect on τ_ε of changing ***t*** in the perovskite-related solid solution series $Ba_{6-3x}Nd_{8+2x}Ti_{18}O_{54}$. Lufaso and Woodward (**2001**) used a bond-valence model to calculate ideal $A - X$ and $B - X$ bond distances in order to calculate the bond-valence based tolerance factor (t_{BV}) which they proposed as a new criterion of the structural stability of ABO_3-type perovskite compounds. Ye *et al.* (**2002**) applied a pattern recognition method and found some regularities in the formation and the lattice distortion of perovskites. Li *et al.* (**2004**) used $r_A - r_B$ structure maps to study the perovskite formability of 197 ABO_3 compounds and then, with the knowledge of the importance of the octahedral factor (r_B/r_O) and tolerance factor ($\frac{r_A + r_O}{\sqrt{2}(r_B + r_O)}$), another structure map was constructed to predict the perovskite formability. Jiang *et al.* (**2006**) investigated the regularities governing lattice constant of ABX_3-type compounds by a statistical regression method and found a good correlation among lattice constant, the estimated bond length between ion B and ion X ($r_B + r_X$) and the ionic-radii tolerance factor t_{IR}; however, they used ionic radii of all ions A, B and X appropriate for sixfold coordination, which are inappropriate for A and X. Ubic (**2007**) later used a different approach based solely on ionic size and derived a simpler and more accurate empirical relationship between ionic size and lattice constant. In 2007, Zhang *et al.*, based on the bond-valence model (BVM) and structure-map technology, investigated the structural stability and formability of ABO_3-type perovskite compounds, established new criteria for the structural stability of such compounds, and created new structure maps that can be used for exploring novel perovskite-related compounds. In that work, the

calculated global instability indices **GII**s are compared with bond-valence based tolerance factors t_{BV}s for 232 ABO_3-type perovskite compounds, and the results are shown in Figure 1.8.1. From this result, they found the **GII** values are close to 0 when t_{BV} values approach 1, and all **GII** values are less than 1.2 v.u. for ABO_3-type perovskite compounds. Also, it was found that the structural stability of ABO_3-type perovskite compounds follows the order $A^{1+}B^{5+}O_3$-type > $A^{2+}B^{4+}O_3$-type > $A^{3+}B^{3+}O_3$-type, which agrees with the experimental measurements. In 2008, Feng *et al.* (**2008**) used a method similar to that of Li *et al.* (**2004**) to predict the formability of ABO_3 cubic perovskite using the octahedral factor and tolerance factor. Recently, Verma *et al.* (**2008**) developed an equation to predict lattice constant values for cubic perovskites by using the product of ionic charges and average radii of ions A, B and X, but the results are much less accurate than those of either Lufaso and Woodward (**2001**) or Ubic (**2007**).

This work is based on the structural stability and formability data of ABO_3-type perovskites used by Zhang *et al.* (**2007**) and makes use of the neural network data-mining method i) to test whether it is possible to use a backpropagation neural network to make the prediction of **GII** from t_{BV} within each ABO_3-type perovskite subclass (*i.e.*, in $A^{1+}B^{5+}O_3$ type, $A^{2+}B^{4+}O_3$ type, and $A^{3+}B^{3+}O_3$ type), and within the whole ABO_3-type perovskite; ii) to test whether using a probabilistic neural network could improve the prediction accuracy for perovskite formability based on the ideal A-O and B-O bond distances ($d_{A\text{-}O}$ and $d_{B\text{-}O}$) compared to the work done by Zhang *et al.* (**2007**).

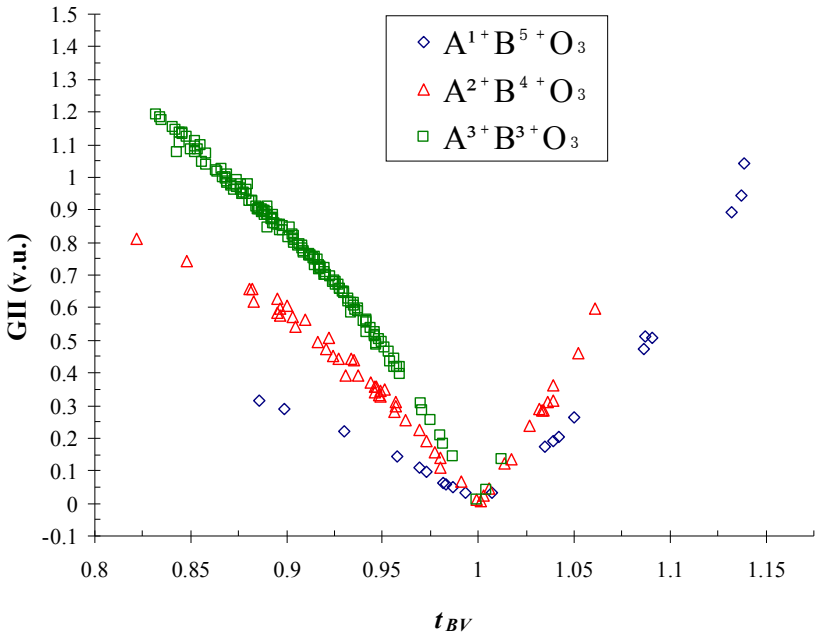

Figure 1.8.1 Global instability indices (**GII**) *versus* bond-valence based tolerance factors (t_{BV}) for ABO_3-type perovskite compounds. (Redrawn from **Zhang *et al.*, 2007**).

1.9 Exploring Multiple Correlations of Properties using Artificial Neural Networks

Materials Science and Engineering, "is concerned with the generation and application of knowledge relating the composition, structure, and processing of materials to their properties and uses" as defined in The Summary Report of the Committee on the Survey of Materials Science and Engineering (COSMAT) of the United States National Academy of Sciences (**1974**), or "the study of substances from which something else is made or can be made; the synthesis, properties, and applications of these substances." in European White Book on Fundamental Research in Materials Science (**2001**). As mentioned in part 1.2.2, it is an axiom that the properties of a material are causally related to the structure at a hierarchy of scales, that is, the properties of a material depend on the chemical nature of its atoms, its structure at the atomic or molecular level, its microstructure and macrostructure. The traditional methodological framework for materials science is the identification of the *composition-processing-structure-property* causal pathways that link hierarchical structure to properties, and many successes in materials science have emerged from its careful implementation.

People are introduced to the materials sciences through a methodology predicated on discovery of the relationships between composition and structure on the one hand and properties on the other. Once these relationships are in place, it will be possible to both understand why existing materials behave as they do and predict how materials can be chosen and modified to behave as we want. Nevertheless, the quantitative inference of properties from structures is very complex; many levels of structure must be considered; low levels of impurity or imperfection sometimes have an overwhelming influence on properties. Partly because of the slow progress in the predictive capacity of materials science as conceived in terms of structure-property relationships, alternative methodologies have emerged, such as high throughput experimental methods and computational methods, as discussed in part 1.2.1 and 1.2.3.

1.9.1 Are different material properties related?

As observed by Ashby (**1998**), all the properties of materials can be derived ultimately from structure and bonding or can be considered to have their ultimate origin in Schrödinger's equation. This means that the properties of a material are, to varying degrees, interrelated. This can be schematically shown in Figure 1.9.1. A few such correlations are well known because they arise from the same structural level. The relationship between permittivity and refractive index at the level of electronic polarisation is a good example. A journey into materials science that explores correlations of properties is rather unconventional but the considerable success of Ashby's property mapping (**Ashby, 1989, 1999; CES EduPack 2008**) suggests that it could provide a way of identifying compositional zones that are worthy of more detailed exploration and therefore narrow the hugely complex space that confronts the discovery of new materials. This part of work participates in this journey.

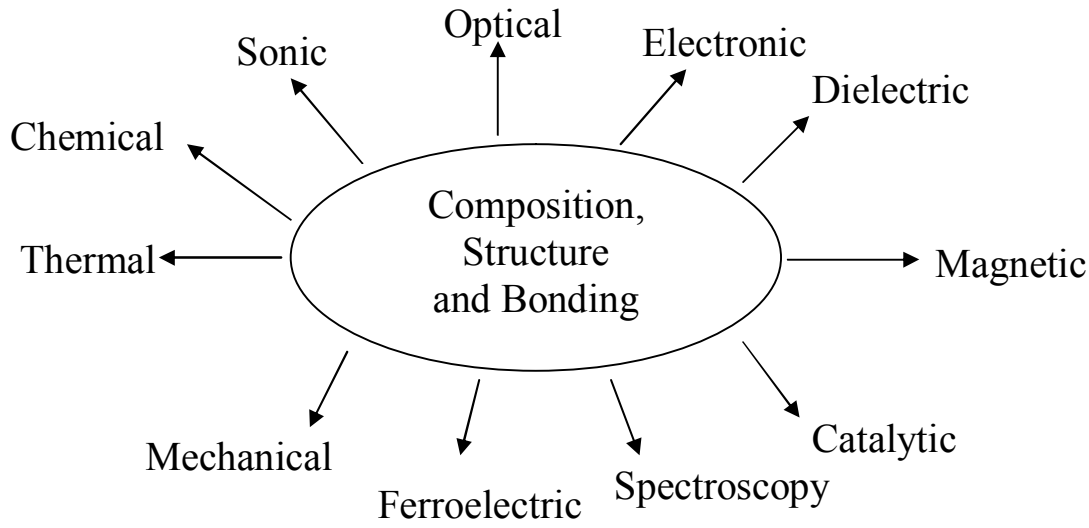

Figure 1.9.1 Schematic arrangement of causation in materials science.

As shown in Figure 1.5.1 and the discussions made in part 1.5.2, there are three types of connection between variables that can explain a correlation between x and y (**Moore and Notz, 2006**): direct causation, common response, or confounding. An observed relationship can be used for prediction without worrying about causation as long as the patterns found in past data continue to

hold true. The purpose of exploring a correlation is to make predictions, which are usually based on correlation of known information, with interpolation or extrapolation as required.

1.9.2 Examples of Known Correlations between Properties

The idea of exploring property-property relationships rather than structure-property relationships seems less unconventional when it is noticed that examples of binary correlations among materials properties abound. In most cases there is a sound mechanistic connection and the scientific practitioner uses a well-trenched *circumferential* path in Figure 1.9.1 while being barely conscious of the two radii that relate them. Examples include:

(i) The specific heat and atomic/molecular mass: specific heat is a measure of the heat energy required to increase the temperature of a unit mass of a substance by a unit temperature. The heat energy arises, partly due to the number of atoms or molecules that are vibrating and if a substance has a lower molar mass, then each unit mass has more atoms or molecules available to store heat energy.

(ii) Specific heat and density in solids: they are related because atoms differ greatly in mass but little in size, and so the density of a solid is mainly determined by its atomic weight and to a lesser degree by atom size and the way in which they are packed (**Ashby *et al.*, 2007**). Because of this correlation between density and atomic weight and the correlation between atomic weight and specific heat capacity, there is a strong, inverse correlation between solid density and specific heat.

(iii) Melting and boiling temperatures: they can be correlated with the depth of the energy well (**Van Vlack, 1989**) as shown in Figure 1.9.2. Atoms have minimum energy (at the bottom of the well) at a temperature of absolute zero. Increased temperatures raise the energy until atoms are able to separate from one another.

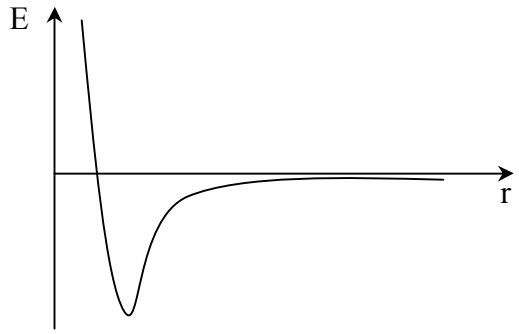

Figure 1.9.2 The interatomic distance – potential energy curve.

(iv) Electrical and thermal conductivity in metals provides another example. In 1827, Ohm, based on Fourier's 1822 theory of heat flow (**Fourier, 1822**), derived theory of the electric conduction of metals (**Ohm, 1827**). His success in deriving analogous equations to those of Fourier for electric current indicated to him an "intimate connection" between the two phenomena. This view stimulated Franz and Wiedemann to their discovery of an approximate constant relation between the conductivity of heat and electricity in 1853 (**Franz and Wiedemann, 1853**). Using a combination of empirical and theoretical arguments, Lorenz claimed in 1872 that the Wiedemann-Franz constant depends linearly on the temperature (**Lorenz, 1872**), which was verified experimentally in 1881 (**Lorenz, 1881a, 1881b**). The electronic theory of Drude explained Lorenz's relation on the assumption that both heat and electric currents in matter results from the motion of its electrons (**Drude, 1900a, 1900b**). According to Drude's theory, the value of the temperature-dependent Wiedemann-Franz constant (i.e. the Lorenz number) is (**Wilson, 1953; Kittel, 2005**):

$$L \equiv \frac{\kappa}{\sigma T} = \frac{\pi^2}{3}\left(\frac{k}{\varepsilon}\right)^2 \qquad \text{Equation 1.9.1}$$

where L is Lorenz number, κ is thermal conductivity, σ is electrical conductivity, T is temperature, k is Boltzmann's constant, and ε is the charge of an electron. Rosenberg (**1988**) has mentioned that this relationship holds remarkably well; the only exception is in very pure specimens at intermediate temperatures, where small angle phonon scattering is important, and it is not very satisfactory.

However, it should be mentioned that although modern electron theory succeeds in explaining the Wiedemann-Franz constant and the Lorenz number, closer studies of the conduction of heat and electricity through metals showed that this simple theory, which only considered the electrons to move freely through metals, was unable to explain the manifold and complicated phenomena in a satisfactory way, such as in the alkali metals where the ratio of κ / σ is extremely low (**Hornbeck, 1913**). In general, the Lorenz number *L*, while roughly constant, is not exactly the same for all materials; Kittel (**2005**) gives some values of *L* ranging from $L = 2.23 \times 10^{-8}$ W Ω K^{-2} for Cu at 0 ºC to $L = 3.2 \times 10^{-8}$ W Ω K^{-2} for W at 100 ºC.

(v) Thermal expansion coefficients of materials with comparable atomic packing vary inversely with their melting temperatures (**Van Vlack, 1989**). This indirect relationship exists because the higher-melting-point materials have deeper and therefore more symmetrical energy wells. Thus, the mean interatomic distances of more strongly bonded materials increase less with a given change in thermal energy.

(vi) Hardness and melting point are related because hardness is related to the stress required to separate atoms during dislocation motion (**Van Vlack, 1989**). Since larger interatomic forces of attraction imply deeper energy wells, materials with high melting points are the harder materials, such as diamond, Al_2O_3 and TiC. The correlation holds for materials with weaker bonds. However, there are exceptions to these generalizations when more than one type of bond is present, such as graphite and polyethylene.

(vii) The melting point and bulk modulus are related since both the melting temperature, T_m, and the elastic modulus, E, relate to the bonding energy (**Van Vlack, 1989**).

Other binary correlations exist between dielectric constant and refractive index, toughness and hardness, an inverse correlation between dielectric loss and dielectric strength and in porous materials, the mechanical strength and the dielectric strength (**Kishimoto *et al.*, 1991**). In functional ceramics, a dielectric

which has high loss at low temperature may show ionic conduction at a higher temperature, in oxides, a change of colour may be associated with electrical conduction.

Ashby notes (**Ashby, 1998**) that some correlations have a simple theoretical basis while others can be found by empirical methods by an appropriate search routine. Generally, the correlations derived in a direct way from the nature of the atomic bonding and structure are strong, such as modulus and melting point, or specific heat and density; while those derived from properties which depend on defects in the structure are less strong, such as strength and toughness and are weakest when interaction with the environment is involved, such as corrosion and wear.

1.9.3 Methods for Exploring Property Correlations

Exploration of property correlations can be classified into three types: I) purely empirical, II) partly empirical but based on some theoretical concept, III) and purely theoretical (**Reid and Sherwood, 1958**). In this work, we use artificial neural networks to explore property correlations not only for binary, but also for ternary and more complex systems.

Examples of applying neural networks to explore property correlations include Egolf and Jurs (**1993**) who used both regression and neural network techniques to predict boiling points of organic heterocyclic compounds using the molecular weight, dipole moment, 1^{st} order molecule connectivity and other structure descriptors. Michon and Hanquet (**1997**) used methods of quantitative structure property relationships (QSPR) and neural networks to find non-linear relations between chemical and rheological properties. Homer *et al.* (**1999**) developed ANN with equilibrium physical properties and structural indicators for prediction of viscosity, density, heat of vaporization, boiling point and Pitzer's acentric factor for pure organic liquid hydrocarbons at $T_{reduced}$ over 0.45-0.7 range. Boozarjomehry *et al.* (**2005**) developed a set of ANNs to predict basic properties (including critical temperature, acentric factor and molecular weight) of pure compounds and petroleum fractions based on their normal boiling point and liquid density at 293 K. Strechan *et al.* (**2006**) obtained correlations between the enthalpy of vaporization, the surface tension, the molar volume and the molar

mass of a substance using ANNs. Mohammadi and Richon (**2007**) used ANN to predict the enthalpy of vaporization of hydrocarbons, especially heavy hydrocarbons and petroleum fractions, from the specific gravity and normal boiling temperatures. Karabulut and Koyuncu (**2007**) developed neural network models to establish correlation of thermal conductivity with temperature and density for propane. Recently, Giordani *et al.* (**2009**) used ANN for multiple correlation of the mechanical properties of modified natural rubber.

The difference between these approaches and method used in this work is that all of them needed prior knowledge to select the properties that are perceived to be significant for the prediction. In this work, it is hoped to prepare the ground for a wider scope which makes use of the remarkable information processing characteristics of the computer to find the correlation between specific properties drawn from a large number of different properties. The physical principles behind multiple correlations found by ANNs might be deduced *post facto* but the primary aim of this work is to accelerate the pace for discovering new materials by narrowing down the compositional spaces for subsequent search either by high throughput methods or molecular modelling.

2.0 Methods for Construction of Neural Networks (BPANN and PNN)

For each case, there are two main works included: one is the data collection, and the other is the neural network construction. The collected data are trained on the constructed neural network and then this neural network is used to predict the result based on the known parameters. In this part, the constructions of neural network are described. The collection of data and the determination of inputs and outputs are described separately in chapters for each case. In the work, two different neural networks are used: one is the backpropagation neural network (BPANN), and the other is probabilistic neural network (PNN). (**Appendix 1**)

2.1 Selection of Architecture of Neural Networks (BPANN)

2.1.1 Selection of the Number of Hidden Layers

It has been said that in most function approximation problems, one hidden layer is sufficient to approximate continuous functions (**Hecht-Nielsen, 1990; Basheer, 2000**); two hidden layers must generally be necessary for learning functions with discontinuous (**Masters, 1994**). Any functional relationship between inputs and outputs, as mentioned in the neural networks user's guide (**Mathworks**), can be represented by the two-hidden layers sigmoid/linear network, if the sigmoid layer has enough neurons. As the result, a two-hidden layer network, with tan-sigmoid transfer function in the first hidden layer and a linear transfer function in the second hidden layer, is adopted.

2.1.2 Selection of the Number of Neurons in Hidden Layers

The size, i.e. the number of neurons, in the second hidden layer is constrained by the number of outputs required by the problem. The outputs of the network in all these works are always one, so there is one neuron in the second hidden layer.

The choice of number of neurons in the first hidden layer is up to the designer. The optimum number of neurons in the first hidden layers may be a function of (1) input/output vector size, (2) size of training and testing sub-sets and, more importantly, (3) the problem of non-linearity (**Basheer and Hajmeer, 2000**). The optimum number can be found by trial and error by placing a different number of neurons in the first hidden layer for the same dataset.

2.2 Selection of the Methods for Improving Generalization (BPANN)

One of the problems that occur during neural network training is called overfitting. This happens when the error on the training set is driven to a very small value, but the error is large when new data is presented to the network. This is the case at which the network has memorized the training examples, but it has not learned to generalize to new situations.

One method for improving network generalization is to use a network that is just large enough to provide an adequate fit. The larger a network used, the more complex the functions the network can create. If a small enough network is used, then the network will not have enough power to overfit the date. However, it is hard to know beforehand how large a network should be for a specific application.

There are two other methods for improving generalization that have been implemented in the Neural Network Toolbox: one is *Bayesian Regularization* and the other is *Early Stopping* (**Mathworks**).

- *Bayesian Regularization*: regularization involves automatically setting the optimal performance function, which is normally chosen to be the sum of squares of the network errors on the training set, to achieve the best generalization. The improvement of generalization is reached by modifying the performance function through adding a term that consists of the mean of the sum of squares of the network weights and biases. In Bayesian regularization framework, the weights and biases of the network are supposed as random variables with specified distributions. Then, the regularization parameters are estimated using statistical techniques, which are related to the unknown variances associated with these distributions (**Mackay, 1992a; 1992b**).
- *Early Stopping*: in this technique the available data is divided into three subsets. The first subset is the training set, which is used for computing the gradient and updating the network weights and biases. The second subset is the validation set. The error on the validation set is monitored during the training process. The validation error will normally decrease during the initial phase of training, as does the training set error. However, when the

network begins to overfit the data, the error on the validation set will typically begin to rise. When the validation error increases for a specified number of iterations, the training is stopped, and the weights and biases at the minimum of the validation error are returned.

Bayesian Regularization tends to provide better generalization performance than *Early Stopping* in training function approximation networks, specially when the size of the data set is small (**Mathworks**). As a result, *Bayesian Regularization*, in combination with Levenberg-Marquardt training, is used for improving generalization.

2.3 Partitioning of the Database (BPANN)

The generalizing ability of the network depends on the training database size (**Basheer and Hajmeer, 2000**). Although ANN can be obtained from a training database of any size, like other empirical models, generalization of these models outside the model domain is adversely affected. Since ANN are required to generalize for the unseen data, data used for training should be large enough to cover the possible known variation in the problem domain.

The development of an ANN based on Bayesian Regularization requires partitioning of the parent database into two sub-sets: training and testing. Currently, there are no definitive rules for determining the required sizes of the data sub-sets. Rules of thumb derived from experience and analogy between ANN and statistical regression exist (**Basheer and Hajmeer, 2000**). Following the method suggested by MATLAB (**Mathworks**), the sets are picked as equally spaced points throughout the original data. Ratio 4:1 is selected, i.e., partitioning the whole data set into five groups, four groups being used for training, while one group is used for testing. The size of the training set and testing set are thus determined, but the choice of testing set still plays a crucial role, because the training set should include all the data belonging to the problem domain. In the problems of materials science, it is always that the data size is small and the problem domains are not clear, so referring to Malinov and Sha's work (**2003**), a loop program was used to redistribute the database in order to make the training set cover the problem domain. The distribution was selected on the basis of

regression coefficient R (R = 1 corresponds to prefect correlation) for both training set and testing set. It is desirable that the R values for both training and testing are as close to 1 as possible, and the difference between them are as close to zero as possible. However, where M, the slope of the linear regression line, is smaller than 0.9, the regression coefficient provides an unreliable criterion, and so the selection was at the beginning based on $\varphi = |M - 1| + (1 - R) + \left|\frac{B}{B_{\max}}\right|$ where B is the intercept on 'A' axis and B_{max} is the maximum property value. The ideal value of this parameter is zero. In section 3.0 (i.e. Revisiting Hume-Rothery's Rules with Artificial Neural Networks), the distribution is selected on the basis of φ for the testing set.

Later, considering the slope M could determine the value of intercept B, and also in order to find the closest and highest performance for both training and testing sets, the criterion has been improved to $\omega = \left|\varphi^2_{\text{training}} - \varphi^2_{\text{testing}}\right|$, where $\varphi = |M - 1| + (1 - R)$, and the smallest value of ω is chosen. This criterion applied in other three applied examples.

2.4 Data Normalization (BPANN)

It has been suggested by Basheer and Hajmeer (**2000**) that, the data should be normalized (scaled) within a uniform range (e.g., [0 1] or [-1 1]) in order to i) prevent larger numbers from overriding smaller ones, ii) prevent premature saturation of the neurons of hidden layers, which would impede the learning process.

There are two functions for scaling the inputs and targets of networks that have been implemented in the Neural Network Toolbox:

- **PREMNMX**: which is used to scale inputs and targets so that they fall in the range [-1, 1];
- **PRESTD**: which normalizes the inputs and targets so that they will have zero mean and unity standard deviation.

As the transfer functions employed in these works are tan-sigmoid transfer function and linear function, **PREMNMX** is adopted.

In all of these four applied examples, the size of dataset is not very large. Nevertheless, there are many situations where materials scientists would like to benefit from ANNs in situations where the data set has inherent limitations. It has been proved that ANN methods provide an efficient tool for experimental data analysis even when the database size is small (**Guessasma *et al.*, 2003**).

2.5 Construction of Probabilistic Neural Network (PNN)

2.5.1 Partitioning of the Database for PNN

Probabilistic neural network (PNN) is a type of radial basis network suitable for classification problems (**Specht, 1990; Vicino, 1998**). As for BPANN, the generalizing ability of PNN depends on the training database size. It is necessary to generalize for the unseen data, so the data set used for training should be large enough to cover the possible known variation in the problem domain. The parent database here is partitioned into two sub-sets: training and testing. Following the method used in construction of BPANN, as discussed previously, the sets are picked as equally spaced points throughout the original data. The whole data set is partitioned into five groups, four groups being used for training, and one group is used for testing. Also due to the problem domain is not clear, a loop program is used to redistribute the database in order to make the training set cover the problem domain. One way that can be used to view the results is a confusion matrix, where matrix element $\boldsymbol{m_{ij}}$ gives the number of times a sample belonging in class $\boldsymbol{C_i}$ was assigned to $\boldsymbol{C_j}$. As a result, the distribution was selected on the basis of the total number of samples incorrectly placed into the class $\sum m_{ij}$ (false positives). The ideal value of $\sum m_{ij}$ should be zero.

2.5.2 Choice of Spread for PNN

The spread of radial basis functions in PNN needs to be chosen. As mentioned in MATLAB (**Mathworks**), if the spread is near zero, the network acts as a nearest neighbour classifier; as spread becomes larger, the designed network takes into account several nearby design vectors. In this work, a looped program, referring to Malinov and Sha's work (**2003**), is used in order to find the best combination of database distribution and value of spread.

3.0 Revisiting Hume-Rothery's Rules with Artificial Neural Networks

3.1 Special Experimental Details

3.1.1 Data Collection

- *Solubility Limit Collection*: the solid solubility limits (at.%) for silver, copper and gold alloys are recorded from Massalski *et al.* (**1987**), Moffatt (**1994**) and ASM Handbook Vol. 3, Alloy Phase Diagrams (**1992**). (**Listed in Appendix 2**)
- *Physical Parameters Collection*: the physical parameters, radii (Å), valences and electrochemical factors (electronegativity) of solvent and solute atoms are taken from Stark and Wallace (**1982**) and from Aylward and Findlay (**1998**). The valences of elements, which were mentioned by Hume-Rothery in 1934, follow his representation (**Hume-Rothery, 1934**). Radii of Al, Ga, and α-Fe also followed Hume-Rothery's representations (**Hume-Rothery, 1961**). The structure parameter is taken from ASM Handbook Vol. 3, Alloy Phase Diagrams (**1992**). (**Listed in Appendix 2**)

The whole dataset is used in three different ways: i) the 60 silver and copper alloy systems, which were first mentioned by Hume-Rothery in 1934, are used for training the neural network and testing whether the Hume-Rothery's Rules work in this range of alloy systems; ii) all the 408 silver and copper alloy systems collected are used to represent the process, and then to test the effect of introduced melting point of both solvent and solute iii) all the 566 silver, copper and gold alloy systems are used to test the effect of melting point of both solvent and solute, as well as for Hume-Rothery's Rules for wider range of alloy systems.

3.1.2 Determination of Inputs and Outputs

Determination of Input Parameters

The network input parameters are the physical parameters including i) atomic size parameter, ii) valence parameter, iii) electrochemical parameter, i.e. electronegativity, and iv) structure parameter of solvent and solute atoms, which were not mentioned in 1934 by Hume-Rothery, but were introduced in 1948 (**Axon and Hume-Rothery, 1948**) concerning the detailed examination of Vegard's law (**Vegard, 1921**) in the case of metallic solid solutions.

Three different expressions of these parameters are used:

1. The raw data that Hume-Rothery used. Details are discussed below.
2. The original collected values for each parameter of solvent and solute atoms.
3. The original collected parameters are converted into functionalized values before putting them into the networks:

a) ***For Size Factor***: The difference between the atomic diameters of solvent and solute atoms divided by the diameter of the solvent atom is used.

b) ***For Valence Factor***: These are integers and the original values are used, leaving the neural network to decide the relations between valence of solvents and solutes.

c) ***For Electrochemical Factor***: The difference between that of the solvent and solute atoms is used.

d) ***For Structure Parameter***: The expressions of the structures can be put in terms of numbers 1-14 for the Bravais lattices, but this revealed little effect of structure. They can also be expressed in three sets of numbers representing primitive cell dimensions, angles and systems. This allows some similarities to be explored. The three sets are i) unit cell length ($a=b=c$; $a=b\neq c$; $a\neq b\neq c$), ii) axes angles ($\alpha=\beta=\gamma=90^o$; $\alpha=\beta=90^o$, $\gamma=120^o$; $\alpha=\beta=\gamma\neq90^o$; $\alpha=\gamma=90^o\neq\beta$; $\alpha\neq\beta\neq\gamma\neq90^o$) and iii) crystal system (simple; base-centred; face-centred; body-centred).

Later, we were curious if more rules are needed to extend Hume-Rothery's principle into quantitative solubility prediction of a wider range of alloy systems using ANN. As the result, one new parameter was introduced:

e) ***Melting point (T_m)***: It is well known that the solubility of many solids depends on temperature. As a result, it is reasonable to consider improving the performance of prediction by introducing temperature as a parameter. The melting temperature (T_m, in the unit of ^oC), above which two metals are miscible in any proportions, was proposed as an additional parameter.

Determination of Output Parameters

In Hume-Rothery's Rules, a soluble/insoluble criterion is described (The quantitative maximum solid solubilities of Zn, Ga, and Ge in copper, Cd, In and Sn in silver can be predicted from electron concentration of 1.4, but this is not a general case). However, it would be more advantageous to attempt to predict the original value of solubility. The output parameters, which are the solubility limits of each alloy system, are therefore expressed in two ways:

1) Following the specified criterion: if the solubility of solute metal in solvent metal exceeds 5 at.% (**Hume-Rothery, 1969; Zhang and Liao, 1999a**), then it is said that this solute metal is soluble in the solvent metal.

2) Original maximum solubility limits of each alloy system are used.

3) T_{max}, under which the maximum solubility is reached, is always associated with the maximum solubility values. As a result, it is interesting to see whether T_{max} can be predicted as well, without knowing the maximum solubility values. So, T_{max} (in the unit of ºC) is also used as an output parameter.

3.2 Results

Here, the results are shown as follows: i) The first 60 alloy systems mentioned by Hume-Rothery in 1934, are used as a start; ii) The whole 408 alloy systems are then used to test whether Hume-Rothery's Rules work for copper and silver alloy systems in general; iii) Relative importance of the rules; iv) Introduction of the melting points for both solvent and solute to test their effect on the solid solubility prediction; v) Testing both the melting point effect and Hume-Rothery's Rules for a wider range of alloy systems (copper, silver and gold).

3.2.1 Testing Hume-Rothery's Rules within 60 Alloy Systems

Of the four parameters, the size factor, the electrochemical factor and the relative valency factor were those used by Hume-Rothery in 1934, so these are used in initial tests for predicting solubility.

Following the Method that Hume-Rothery's Definition Suggests

During this trial, the following criteria are used:

1. If the atomic diameters differ by more than 14%, then it means that size factor is "unfavourable", and the input number for this parameter is zero, or it is one.

2. If the valency of solvent atom is lower than that of solute atom, then the input number for this parameter is one, or else the number is zero.

3. If the difference of the electronegativity of solvent and solute atom is more than 0.4, mentioned by Darken and Gurry (**1953**) and Zhang and Liao (**1999a**), then the input number for this parameter is zero, or else it is one.

4. If the solubility of solute metal in solvent metal exceed 5 at.%, then the output number is one, or else it is zero.

In this case, the problem to be solved is a classification problem, so a probabilistic neural network was designed for use. The modified criterion of 15% for the diameter difference mentioned by Darken and Gurry (**1953**) is used in the next trial, also with soluble/insoluble as output and both results are listed in Table 3.2.1 in terms of the percentage of all the sixty predictions that are wrong.

Comparing these results, a slight difference is found: the percentage error of predicted results based on experimental results for the whole dataset using the 15% criterion is slightly lower than that for 14%. This result shows the consistency with the modified criterion of size factor, although Hume-Rothery stated in his later work (**1966**) "the 14% difference does give a better correlation with solubility data than the commonly accepted 15%".

Using the same approach and including the 15% criterion, the structure parameter is introduced next in terms of whether the structure of solvents and solutes are the same or not (i.e. 1 same, 0 not same). The results are listed in the last row of Table 3.2.1. Comparing these results with the previous one, there is no improvement in correlation. This indicates that the structure parameter does not play a very important role in solubility when the 5 at.% solubility limit is selected as the threshold. Zhang and Liao (**1999a**) commented that taking the 5 at.% threshold at any temperature is not precise enough and solubility limits are not accurately predicted when the rules are deployed in this way.

Table 3.2.1 Testing Hume-Rothery's Rules with 60 alloy systems using his criterion (14% variation), the later suggestion of 15% and the 15% criterion with structural identity (same or not).

Choice	Error of Prediction (%)	
	Testing	Whole Data
14%	8.3	15
15%	8.3	13
Structure Parameter	8.3	13

Using the Exact Collected Values

In the next trial, the original values of input parameters and of output original solubility values are used and structure parameter is incorporated by using an integer for each of the 14 Bravais lattices. From this trial to the end of this part, all the problems modelled are mapping problems, so backpropagation artificial neural networks (BPANNs) are adopted throughput. The separate results are shown in Figure 3.2.1 in which the training set (a) is distinguished from the testing set (b). For the training set, the regression coefficient R is 0.996 and slope

M is 0.984. However, the prediction for the testing data from the trained network in this case is very poor (M is 0.193 and R is 0.383) and this clearly indicates that although the network trains satisfactorily on the actual values of input data it is unable to use these for prediction.

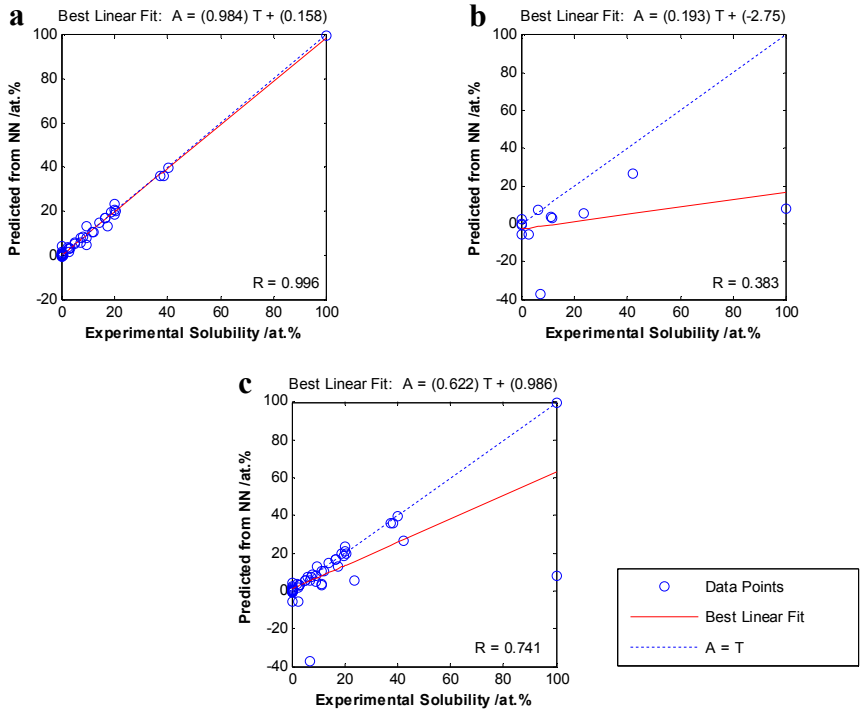

Figure 3.2.1 Prediction of solubility using original values of input parameters for the 60 alloy system dataset: atomic size, valency and electronegativity and structure. a) Training set, b) Testing set, c) Whole set.

Using Functional Parameters

In the next trial, input variables are based on functionalized values, structure parameter is omitted and the results are shown in Figure 3.2.2. The values of M, B and R for the training set are 0.977, 0.23 and 0.993 respectively and for the testing set they are 0.962, -1.19 and 0.992 respectively. This demonstrates reasonable correlation (the ideal values are M=1, B=0 and R=1).

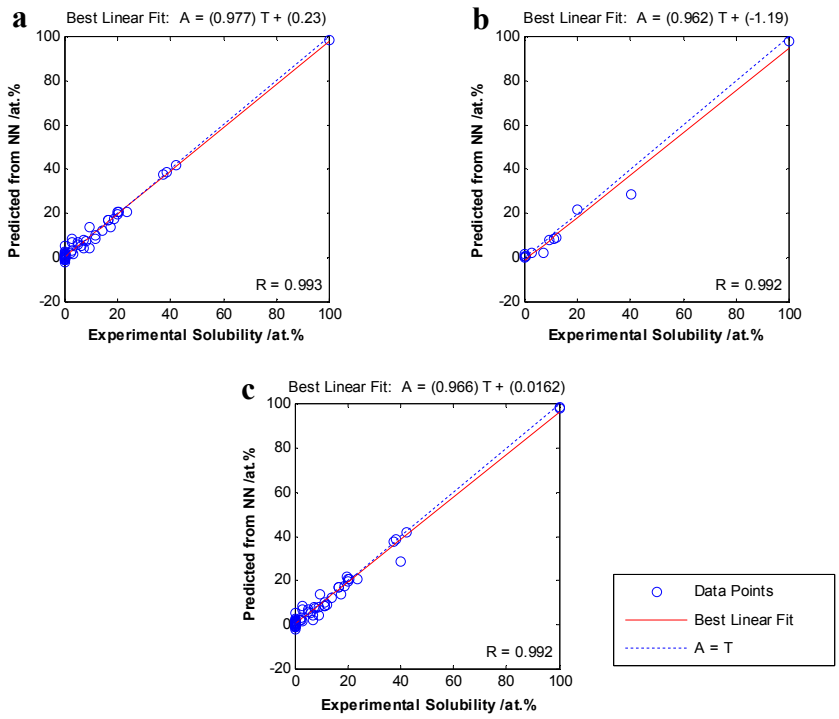

Figure 3.2.2 Prediction of solubility using 3 functionalized parameters for the 60 alloy system dataset: atomic size, valency and electronegativity. a) Training set, b) Testing set, c) Whole set.

The functionalized structural parameter described above is then incorporated in place of the Bravais lattice number are the results are shown in Figure 3.2.3. Comparing this with Figure 3.2.2, the difference is not great, nor can it be said that one is superior to the other. This could imply that the structure parameter does not play a very important role, and indeed Hume-Rothery did not include it in 1934.

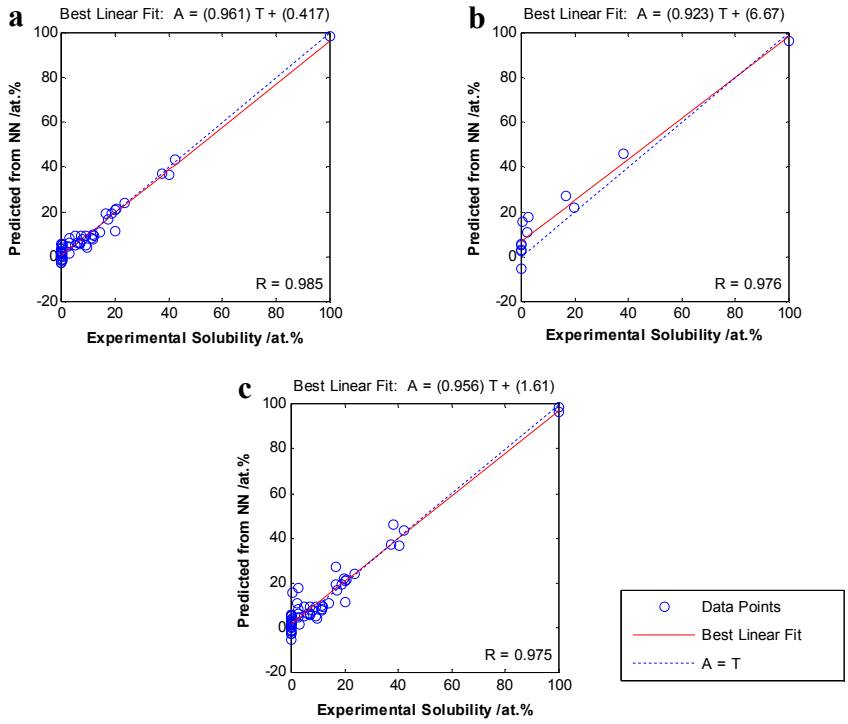

Figure 3.2.3 Prediction of solubility using 4 functionalized parameters for the 60 alloy systems: atomic size, valence, electronegativity and structure. (a) Training set, (b) Testing set, (c) Whole set.

There are several ways to evaluate the performance of neural network predictions. The first and simplest is based on the value of the linear regression coefficient R for the plot of predicted vs. experimental output. A problem occurs when R is low (<0.9) and the slope, M, is close to unity or *vice versa*. Under these circumstances slope, M, and R can be combined to give one parameter $\varphi=|M-1|+(1-R)+\left|\frac{B}{B_{\max}}\right|$ as defined in section 2.3 which should be as close as possible to zero. This has the advantage of providing a single value that can be used as a criterion for parameter selection in a looped optimization program. However, in this composite parameter, the contribution of each of M and R is treated as equal whereas a weighting might be preferable. An alternative method is to consider the mean error of the predicted value from experimental value. There are three ways in which this error can be calculated: (i) the mean true error having the same unit as target values, (ii) the mean modulus of error again having the same unit as target and (iii) the percentage error (as modulus) based

on the experimental value. The problem of (i) is that a zero mean error can be obtained from large deviations from the line and the problem with (iii) is that when many experimental values are zero or close to zero, the percentage is infinite or very high respectively, such as in this case. Thus, here (ii) provides the best criterion and furthermore the standard deviation of this modulus of error gives a measure of spread and hence, if large, indicates that the error is not systematic. So in assessing the correlation two parameters are used: the correlation coefficient R and the average absolute deviation between theory and prediction (mean modulus of error). The two are plotted in Figure 3.2.4 for all data sets and show a good correlation at high R: at R=1, the mean modulus of error is zero.

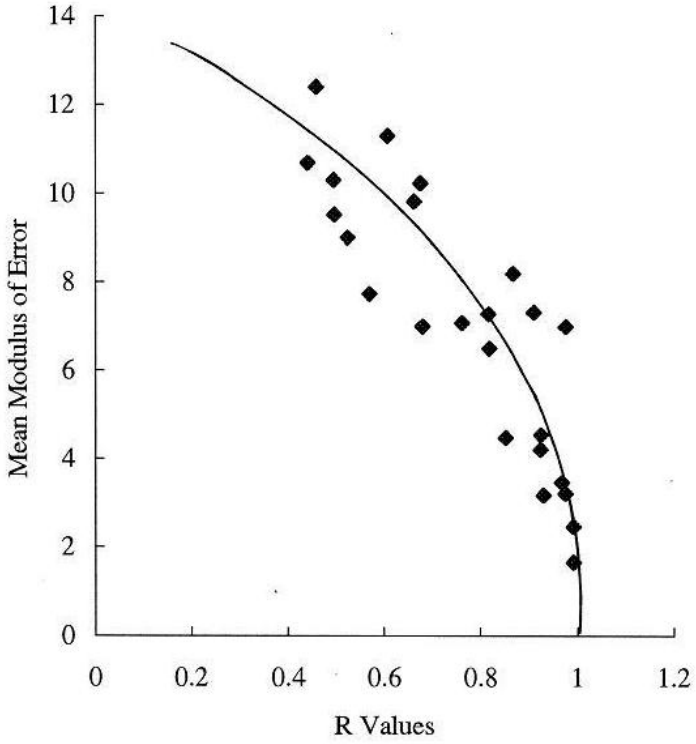

Figure 3.2.4 The correlation between R-values and mean modulus of error.

These criteria are compared in the first two data rows of Table 3.2.2 for the testing set and whole set of the 60 alloy system from plots of predicted solubility against experimental solubility. The first thing to notice about this table is that the four ways of assessing the accuracy of prediction (testing set) concur. As the linear regression coefficient decreases, the parameter φ increases much more

dramatically and can be regarded as a more sensitive indicator for this reason. Also a simple calculation of the mean deviation of the predicted values from the best fit line (mean modulus of error) gives an estimate of the accuracy of prediction. This follows the trend of increasing φ and reduced R. The standard deviation for this error is an indicator that the error is random rather than systematic and if so, the standard deviation is expected to increase with the mean as it, in fact, does. The ratio of standard deviation of error to mean error is, in all but one case, greater than unity. This trends in the assessment criteria are consistent for both the testing set and the whole set.

The best predictive results for the network are obtained by using the functionalized values of atomic size, valence and electronegativity to predict original values of solubility for the 60-alloy dataset used by Hume-Rothery himself and the data are plotted in Figure 3.2.2. Inclusion of the structural factor using the parameter described above weakens the predictive power of the network (Figure 3.2.3). The reason for this slightly counter-intuitive finding is that crystallographic compatibility is likely to become more important at higher solubility levels, being essential for continuous solubility. However, the majority of data are at the low solubility end where substitutional atoms are at low co-ordination number. Another reason is that the number used to represent structure actually conceals crystallographic similarities as discussed in more detail below and there is not enough training data for the network to establish these similarities by itself. The structure parameter is used to assess the criterion for solubility that "the same crystal structure for the two elements favours a wide solubility range" (**Wyatt and Dew-Hughes, 1974**). This makes it a kind of classification problem, not completely the same as a mapping problem and it could be argued that including it in this type of network is inappropriate.

3.2.2 Testing Hume-Rothery's Rules within 408 Alloy Systems

From the results for the 60 alloy systems, it is clear that using the 3 functionalized values of parameters provides better results, so the same approach is adopted for testing the 408 alloy systems. This represents a nearly exhaustive set of known silver and copper alloys. The results, shown in the last row of Table 3.2.2 and plotted in Figure 3.2.5, use the same format of inputs as those used for

the 60 alloys set. When this method (omitting structural parameter) is applied to the larger 408 alloys dataset, the regression coefficient is low (less than 0.9) and the comparison between different regression coefficient values has less meaning. Calculation of the mean modulus of error gives a less ambiguous estimate of the accuracy of prediction. The mean error of the prediction (testing set) increases by a factor of three and the linear regression coefficient drops well below 0.9. The mean error for the testing set and the whole set becomes closer showing that this set does not train well whereas for the 60 alloy set, the whole set errors are much lower than the testing set errors. It is an inevitable conclusion that the wider application of the rules introduces difficulties some of which are discussed below.

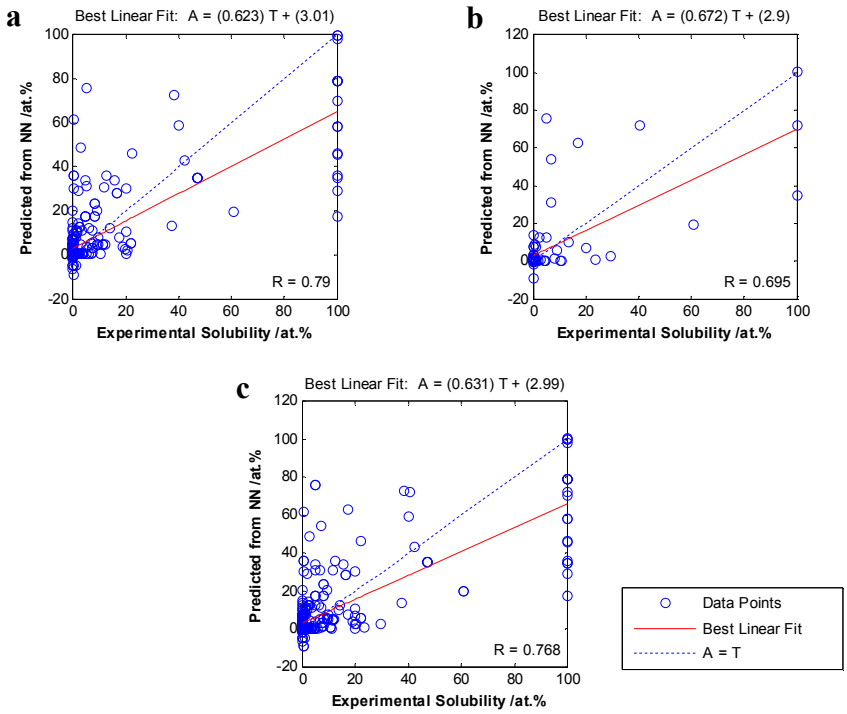

Figure 3.2.5 Prediction of solubility using 3 functionalized parameters for the 408 alloy systems: atomic size, valency and electronegativity. (a) Training set, (b) Testing set, (c) Whole set.

Table 3.2.2 Comparison of criteria for predicting solubility using different combinations of parameter groups.

Conditions*	Test Set				Whole Set			
	R	φ	Mean modulus of error /atom %	S.D. of modulus of error /atom %	R	φ	Mean modulus of error /atom %	S.D. of modulus of error /atom %
Size, Valence, Electronegativity (60 alloys)	0.992	0.0579	2.46	3.21	0.992	0.0422	1.65	1.94
Size, Valence, Electronegativity, Structure (60 alloys)	0.976	0.168	6.98	4.58	0.975	0.0851	3.21	3.21
Size, Valence, Electronegativity (408 alloys)	0.695	0.662	7.01	14.1	0.768	0.631	6.30	12.7

* Using functionalized parameters

3.2.3 Relative Importance of the Rules

It is interesting to enquire which of the four parameters, i.e. atomic size, valence, structure and electronegativity, is the most influential parameter assuming that they are independent of each other. The importance of structural parameter has been tested and found not to play a very important overall role, although of course it does influence the possibility of continuous solubility.

The relative importance of size factor, valence and electronegativity is shown from Figure 3.2.6 to Figure 3.2.8, and compared in Table 3.2.3. Using the same procedure (functionalized parameters including structure), the network is run with one parameter omitted at a time on the set of 60 systems.

In general, mean error (data columns 3 and 7) varies inversely with regression coefficient (data columns 1 and 5) and the standard deviation of error is between 1.1 and 1.8 times higher than the mean error. Using the mean error of the testing set as main criterion for accuracy of prediction, the parameters atomic size, valence and electronegativity provide the strongest prediction of solubility and of these, atomic size has the strongest effect because when omitted the error is highest (data row 2). Electronegativity appears to have a stronger influence than valence (data row 3 and 4). In fact, these parameters are not wholly independent of each other. This is a confounding case, as shown in Figure 1.5.1(c), in which the effect of each parameter is confounded with others. As mentioned by Hume-Rothery, they are related and their interplay makes the determination of solubility very difficult (**Hume-Rothery *et al.*, 1934**). As a result, the determination of relative importance of each parameter is not easy; it can only be said descriptively that the atomic size and electronegativity play more important roles than the valence and structural parameters.

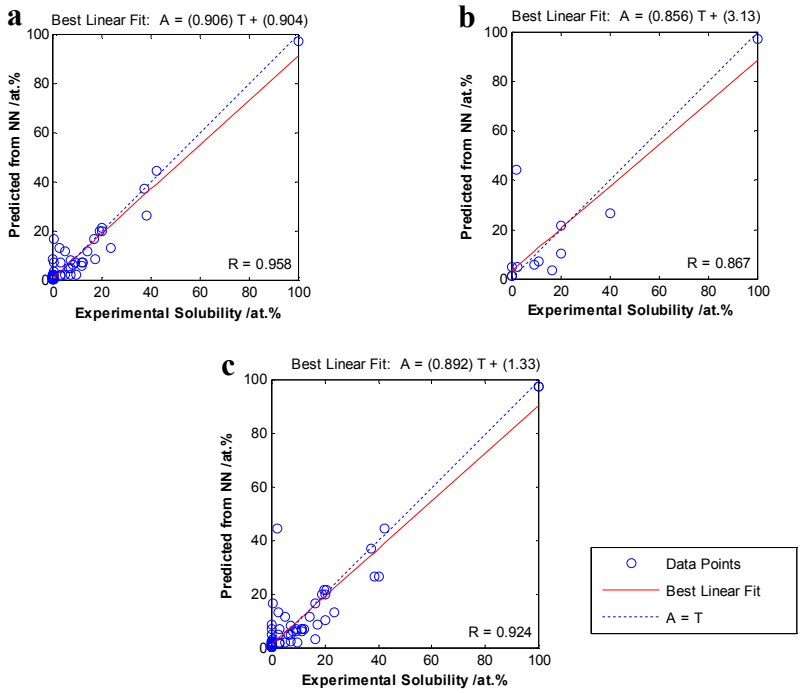

Figure 3.2.6 Prediction of solubility using 3 functionalized parameters for the 60 alloy systems: valency, electronegativity and structure. (a) Training set, (b) Testing set, (c) Whole set.

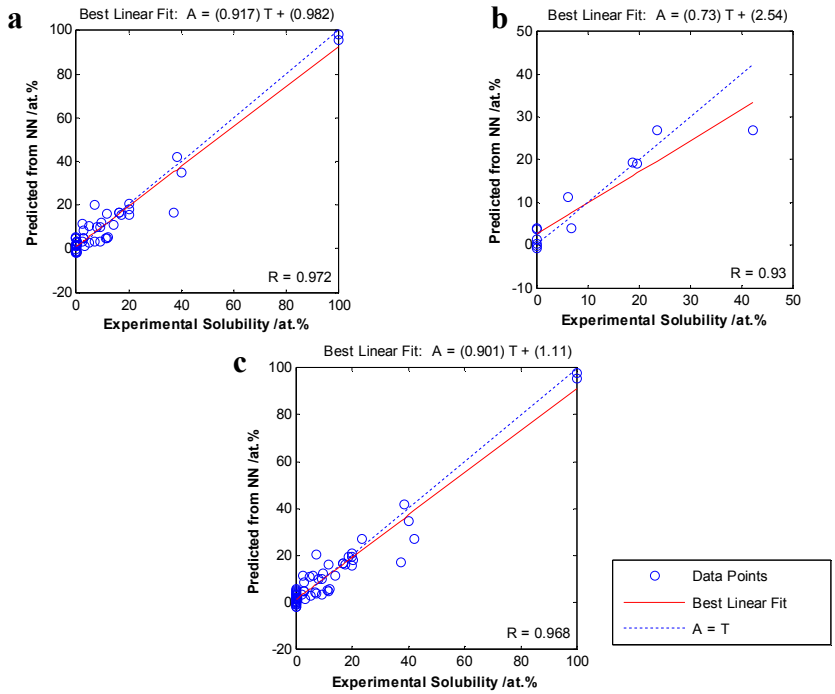

Figure 3.2.7 Prediction of solubility using 3 functionalized parameters for the 60 alloy systems: size, electronegativity and structure. (a) Training set, (b) Testing set, (c) Whole set.

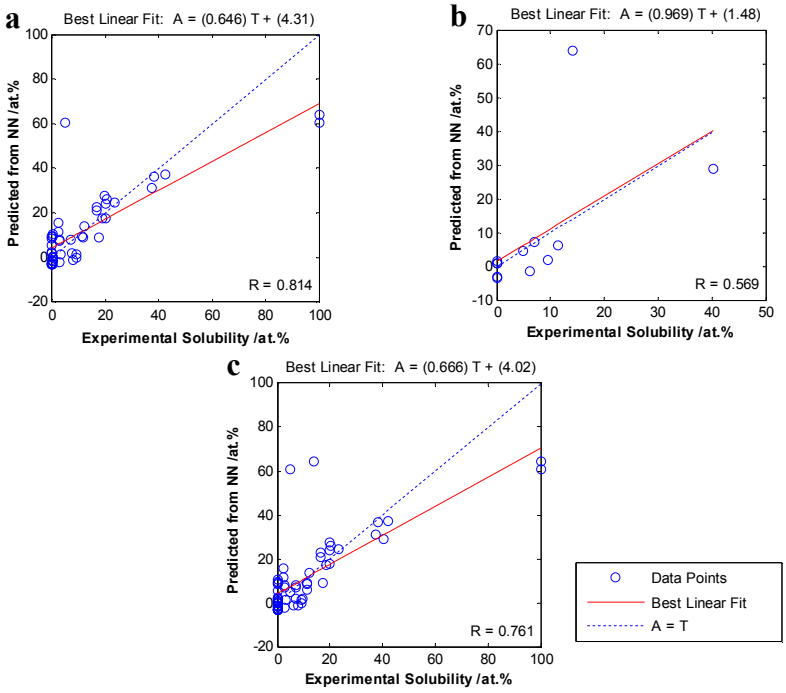

Figure 3.2.8 Prediction of solubility using 3 functionalized parameters for the 60 alloy systems: size, valence and structure. (a) Training set, (b) Testing set, (c) Whole set.

Table 3.2.3 Comparison of criteria for predicting solubility using different combinations of three parameters.

Conditions*	Test Set				Whole Set			
	R	φ	Mean modulus of error /atom %	S.D. of modulus of error /atom %	R	φ	Mean modulus of error /atom %	S.D. of modulus of error /atom %
Size, Valence, Electronegativity (60 alloys)	0.992	0.0579	2.46	3.21	0.992	0.0422	1.65	1.94
Valence, Electronegativity, Structure (60 alloys)	0.867	0.308	8.19	11.7	0.924	0.197	4.20	6.34
Size, Structure, Electronegativity (60 alloys)	0.93	0.365	3.17	4.19	0.968	0.142	3.46	3.66
Size, Valence, Structure (60 alloys)	0.569	0.477	7.73	13.8	0.761	0.613	7.07	11.0

* Using functionalized parameters

In the next stage, pairs of parameters are selected to predict solubility: (1) atomic size and valence factors, (2) atomic size and electronegativity factors, (3) atomic size and structural factors, (4) valence and electronegativity factors, (5) valence and structural factors and (6) structure and electronegativity factors. The results are shown from Figure 3.2.9 to Figure 3.2.14, and the comparisons are shown in Table 3.2.4. The first thing to notice is that most of the mean errors are increased compared to the three input tests reported in Table 3.2.3. The correlation coefficient for the testing set is generally higher than that for the whole set because the partitioning procedure described above selects minimum φ for the testing set as criteria rather than for the training set, as mentioned in section 2.3. An ideal procedure would be to find the correlation for both sets for each partition and select the distribution that gives the closest and highest R-values as described by Malinov and Sha (**2003**). When the correlation is poor however, as for the effects of valence and structure, the value of R has little meaning. Table 3.2.4 confirms the deductions from the three-parameter tests that atomic size has the strongest effect on solubility and the structural parameter the least effect. However some ambiguity attends the relative role of electronegativity and valence which are reversed in this assessment of ranking. As mentioned in section 1.6.2.1, Pearson states (**1972**) that "when one component in a binary alloy is very electronegative relative to the other, there is a strong tendency for them to form compounds of considerable stability in which valence rules are satisfied. Such alloys are said to exhibit a strong electrochemical factor and this is the strongest effect in determining the constitution of alloys, and one which dominates all other effects such as energy band or geometrical factors".

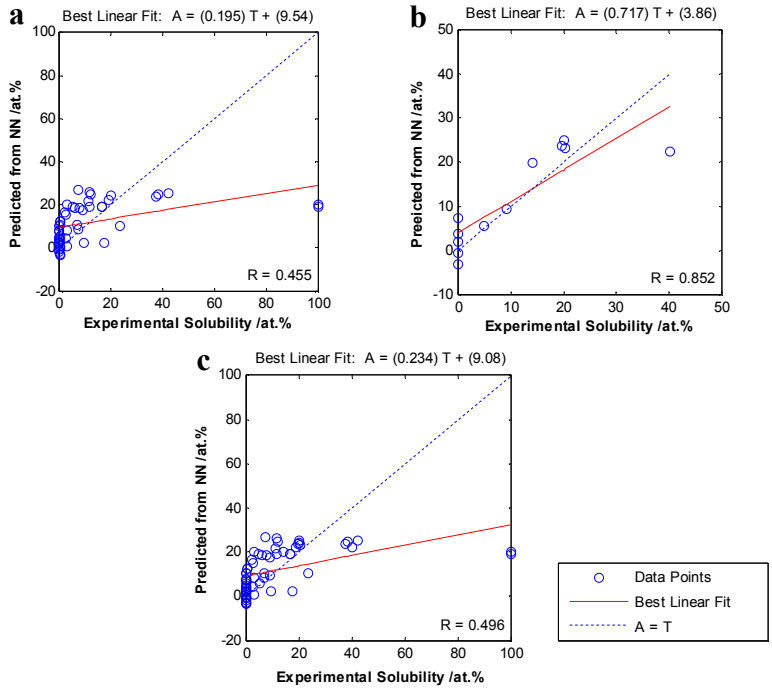

Figure 3.2.9 Prediction of solubility using 2 functionalized parameters for the 60 alloy systems: size, valence. (a) Training set, (b) Testing set, (c) Whole set.

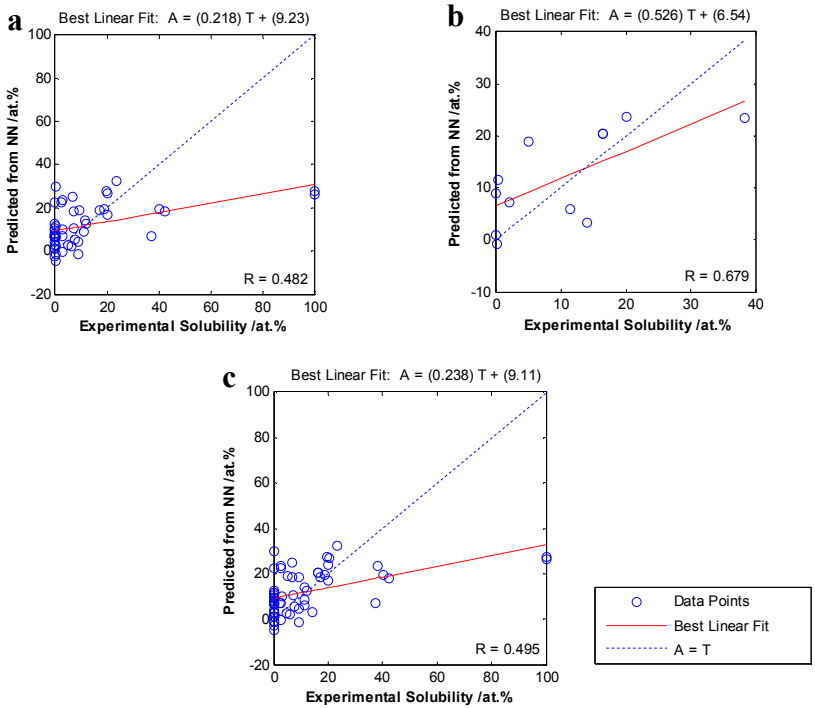

Figure 3.2.10 Prediction of solubility using 2 functionalized parameters for the 60 alloy systems: size, electronegativity. (a) Training set, (b) Testing set, (c) Whole set.

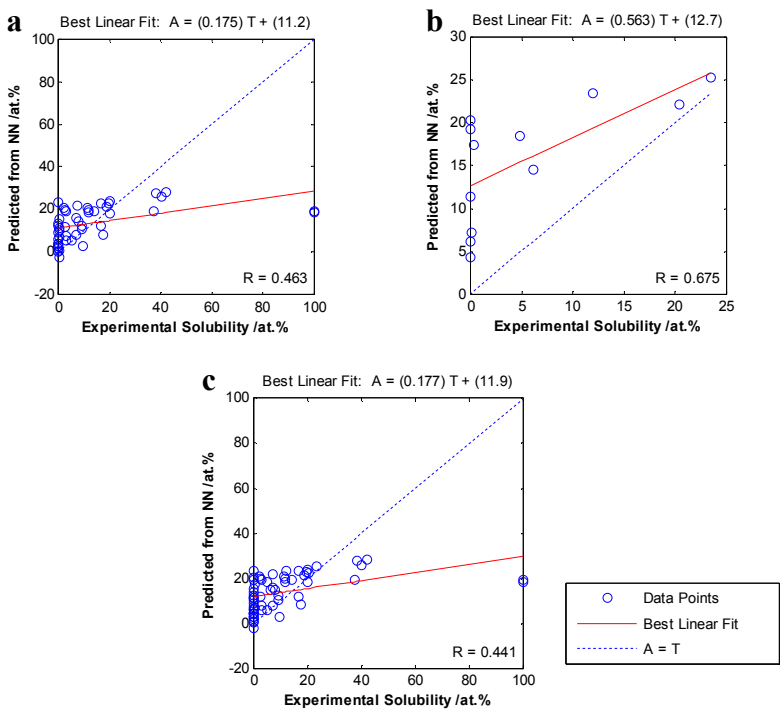

Figure 3.2.11 Prediction of solubility using 2 functionalized parameters for the 60 alloy systems: size, structure. (a) Training set, (b) Testing set, (c) Whole set.

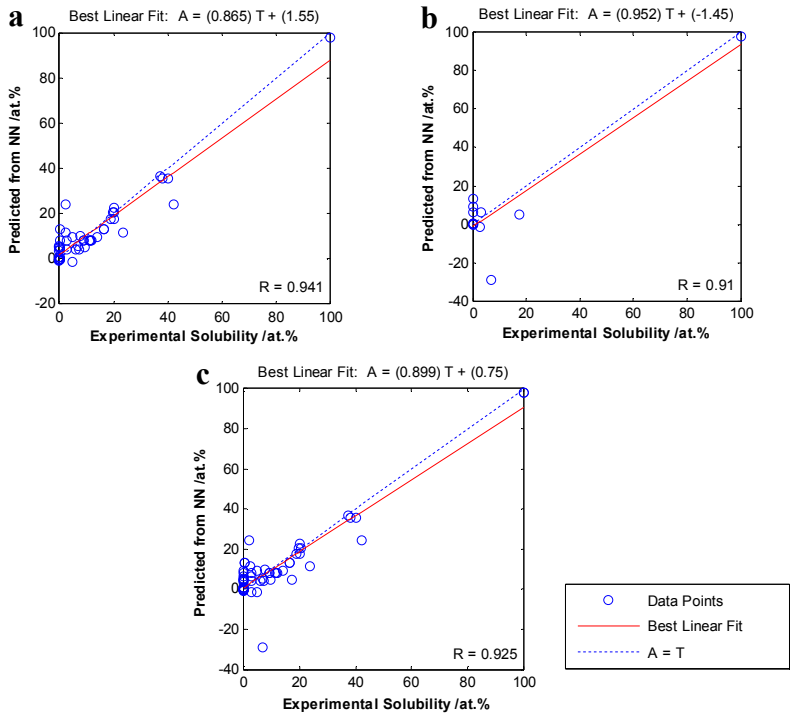

Figure 3.2.12 Prediction of solubility using 2 functionalized parameters for the 60 alloy systems: valence, electronegativity. (a) Training set, (b) Testing set, (c) Whole set.

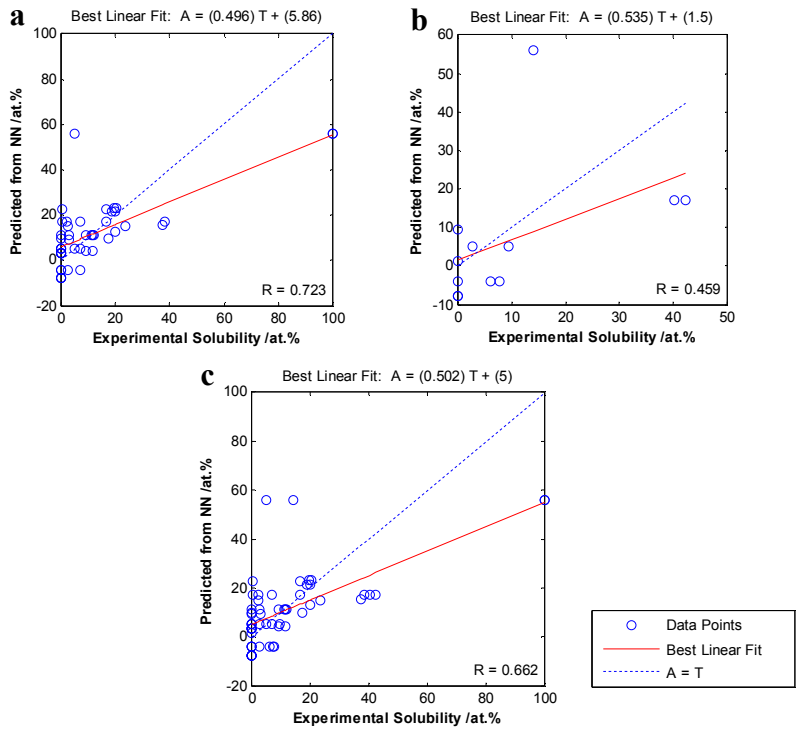

Figure 3.2.13 Prediction of solubility using 2 functionalized parameters for the 60 alloy systems: valence, structure. (a) Training set, (b) Testing set, (c) Whole set.

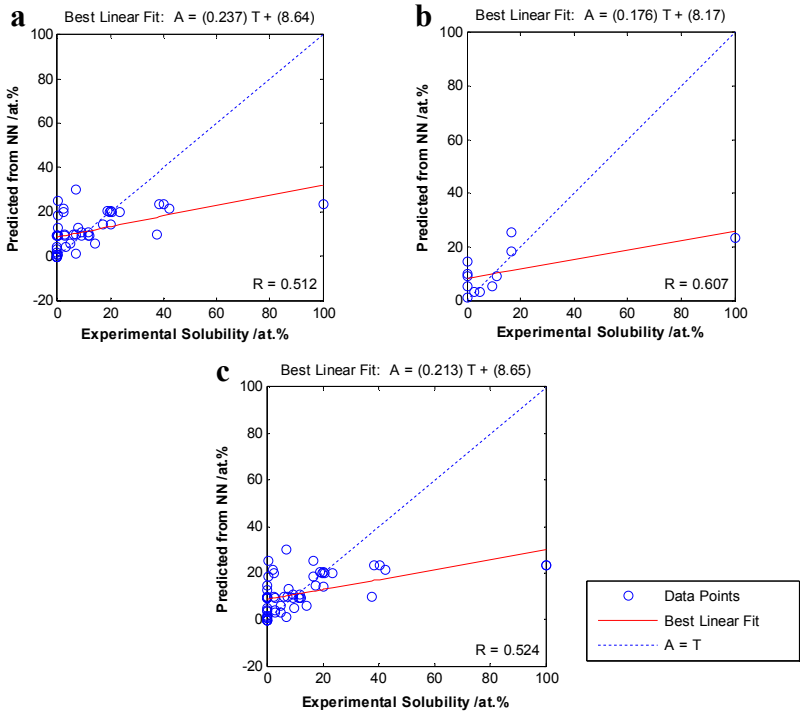

Figure 3.2.14 Prediction of solubility using 2 functionalized parameters for the 60 alloy systems: structure, electronegativity. (a) Training set, (b) Testing set, (c) Whole set.

Table 3.2.4 Comparison of criteria for predicting solubility using different combinations of two parameters.

Conditions*	Test Set				Whole Set			
	R	φ	Mean modulus of error /atom %	S.D. of modulus of error /atom %	R	φ	Mean modulus of error /atom %	S.D. of modulus of error /atom %
Size, Valence (60 alloys)	0.852	0.470	4.47	2.50	0.496	1.36	9.52	14.3
Size, Electronegativity (60 alloys)	0.679	0.860	6.99	4.83	0.495	1.36	10.3	13.8
Size, Structure (60 alloys)	0.675	0.889	10.2	6.42	0.441	1.50	10.7	14.4
Valence, Electronegativity (60 alloys)	0.91	0.153	7.31	10.1	0.925	0.184	4.54	6.06
Valence, Structure (60 alloys)	0.459	1.02	12.4	11.9	0.662	0.886	9.82	11.3
Structure, Electronegativity (60 alloys)	0.607	1.30	11.3	21.1	0.524	1.35	9.00	14.5

* Using functionalized parameters

3.2.4 The Effect of Temperature Parameters

Based on the 408 alloy systems used before, T_m is introduced, and the results are shown in Figure 3.2.15, in which the circles represent the training data set and stars represent the testing data set. Comparison of this result with Figure 3.2.5 (c) shows there is little improvement. On further consideration of the problem, it can be seen that for the systems with complete solubility (i.e., 100 at.%) or complete insolubility (0 at.%) the solubility stays as 100 at. % or 0 at. % within the whole temperature range of the solid phase. That is, the solid solubility in the solid phase temperature range is independent of temperature. For this reason, the introduction of temperature does change the performance of the prediction for 100 at.% and 0 at.%, and so the regression coefficient cannot be improved. As a result, for the following tests, which aim to test the effect of introducing temperature parameters, the systems that have 100 at.% or 0 at.% solubility were eliminated.

In the following tests, the whole data set was used in two different ways: (1) 155 silver and copper alloy systems, which were generated from the 408 alloy systems used in previous work but excluding the systems with 100 at.% or 0 at.% solubility; (2) to introduce 76 gold alloy systems in. A total of 231 alloy systems including silver, copper and gold were used.

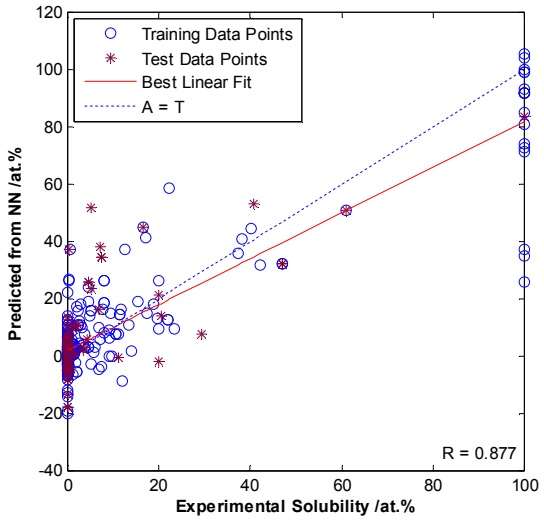

Figure 3.2.15 Prediction of solubility of 408 silver and copper alloy systems using 3 functional parameters: atomic size, valence and electronegativity and melting point of solvents and solutes.

Testing Extended Hume-Rothery's Rules with the 155 Alloy Systems

At first, the functionalized values of atomic size, valence and electronegativity were used to make the prediction of original solubility limits within the 155 alloy systems (without using melting point, in order to compare the melting effect later). The result is shown in Figure 3.2.16 (a).

Next, the melting point T_m of both solvents and solutes were included to make another prediction. The result is shown in Figure 3.2.16 (b). From comparison of Figure 3.2.16 (b) with Figure 3.2.16 (a), the performance has been greatly improved (the regression coefficient increases from 0.79 to 0.963). This improvement indicates the melting point T_m plays a significant role in the prediction. The reasons will be discussed later and the statistical analysis are listed in 1st and 2nd rows of Table 3.2.5.

Testing the Extended Hume-Rothery's Rules with 231 Noble Metal (Au, Ag, Cu) Alloy Systems

Figure 3.2.17 (a) and (b) show the prediction of solubility for 231 noble metal alloy systems. The statistical analysis results are shown in 3rd and 4th rows in Table 3.2.5. The same trend of improvements can be found, confirming the effects of melting point of solutes and solvents. From these results, it can be seen that melting point has a great effect on the solubility prediction. It is interesting to unveil the mechanism of this effect, and the details are shown in discussion part.

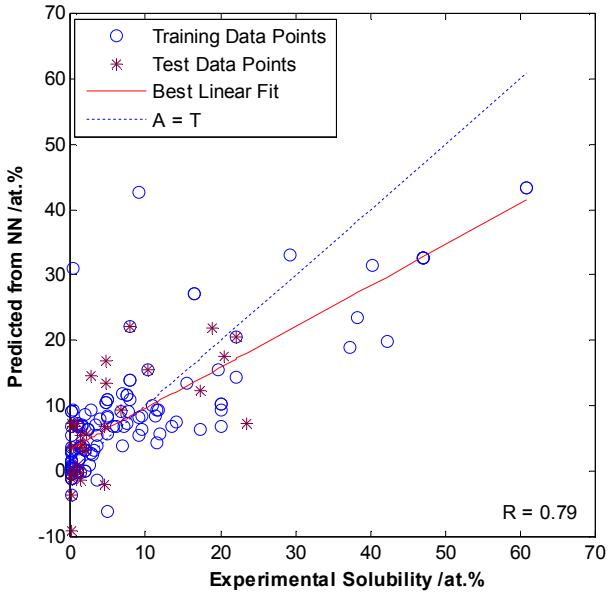

(a)

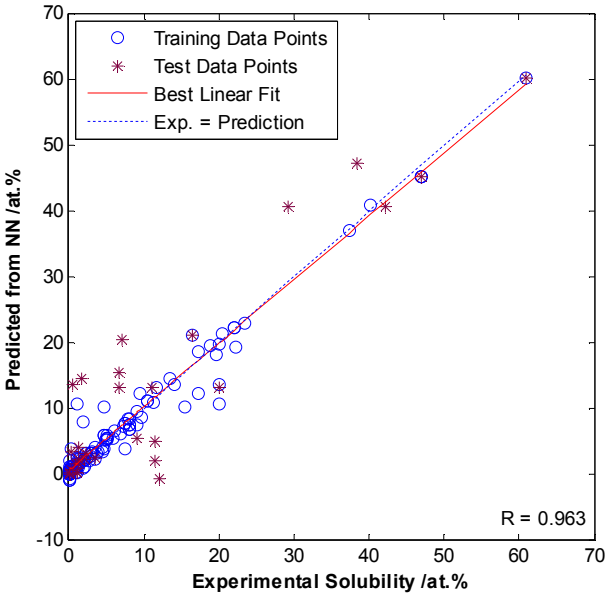

(b)

Figure 3.2.16 Prediction of solubility for 155 silver and copper alloy systems using: (a) 3 functional parameters: atomic size, valence and electronegativity; (b) melting points of solvents and solutes plus parameters used in (a).

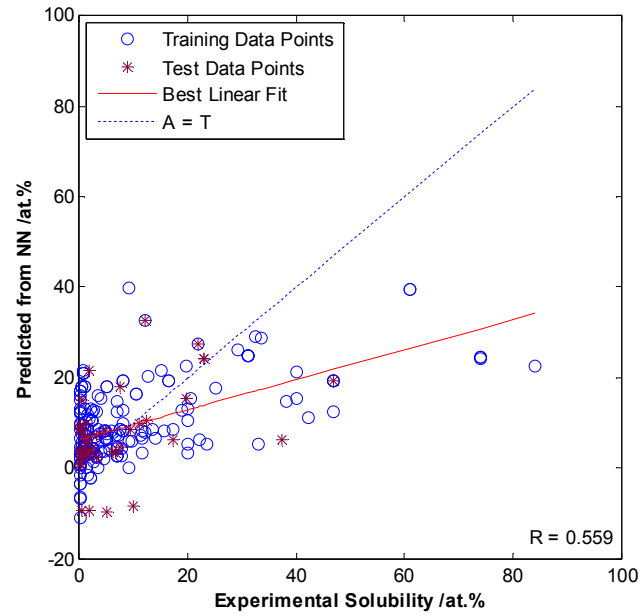

(a)

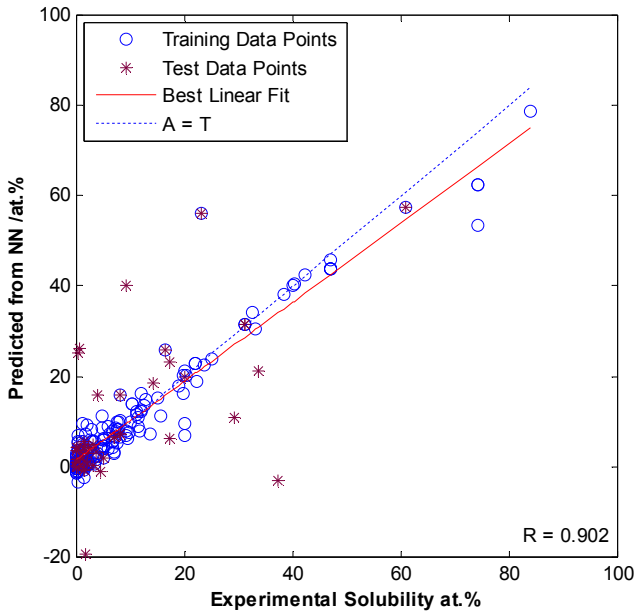

(b)

Figure 3.2.17 Prediction of solubility for 231 noble metal alloy systems using: a) 3 functionalized parameters: atomic size, valence and electronegativity; b) melting points of solvents and solutes plus parameters used in a).

Table 3.2.5 Statistical analysis of the results shown for Figure 3.2.16 and Figure 3.2.17.

Results		Test set			Whole set		
		R	Mean of error modulus /at. %	SD of error modulus /at. %	R	Mean of error modulus /at. %	SD of error modulus /at. %
Figure 3.2.16	(a)	0.653	5.00	4.19	0.790	5.07	5.47
	(b)	0.926	4.45	4.66	0.963	1.71	2.88
Figure 3.2.17	(a)	0.480	6.58	7.16	0.559	8.14	9.20
	(b)	0.643	6.86	9.89	0.902	3.18	5.67

3.2.5 Prediction of T_{max}

Testing for the 155 alloy systems

As before, at the beginning, the functionalized values of atomic size, valence and electronegativity were used to make the prediction of T_{max}. The result is shown in Figure 3.2.18 (a).

Next, the melting points T_m of both solvents and solutes were added to make the prediction. The result is shown in Figure 3.2.18 (b). From comparison of these two figures, the performance has been dramatically improved (the regression coefficient increases from 0.214 to 0.881). This improvement confirms the significant contribution of melting point to the maximum solubility.

Further, it is interesting to see the sole effects of melting points to T_{max}, since all of them are temperature parameters. The result is shown in Figure 3.2.18 (c). From this result, it can be found that the melting points alone play very important role in the prediction of T_{max}. The statistical analyses for all these three cases are listed in Table 3.2.6, from 1st to 3rd rows. In these cases, the experimental values are far greater than zero, the percentage error therefore can be adopted for evaluating the performance of neural network predictions.

Testing for the 231 alloy systems

The same procedure applied to the 231 noble metal systems. The results are shown in Figure 3.2.19, and the statistical analysis results are shown in Table 3.2.7 from 4th to 6th rows.

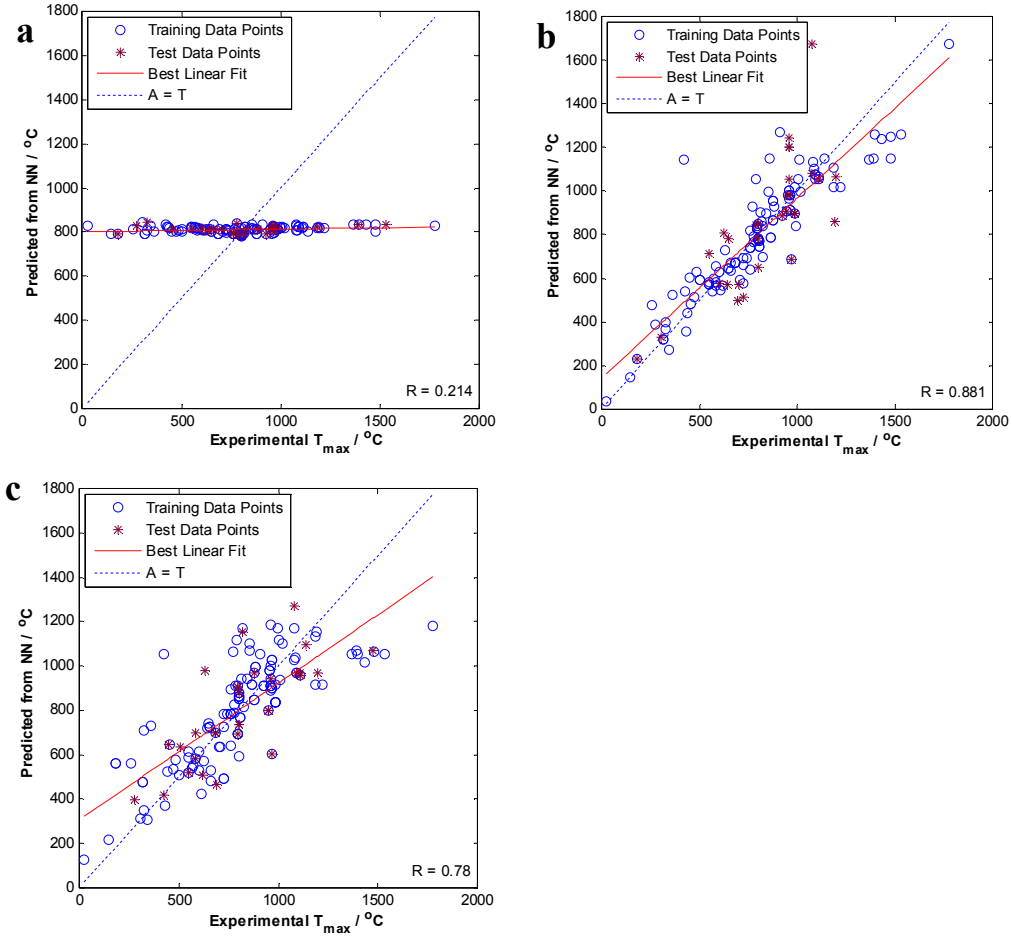

Figure 3.2.18 Prediction of T_{max} for 155 silver and copper alloy systems using a) 3 functionalized parameters: atomic size, valence and electronegativity; b) melting points of solvents and solutes plus parameters used in a); c) melting points of solvents and solutes only.

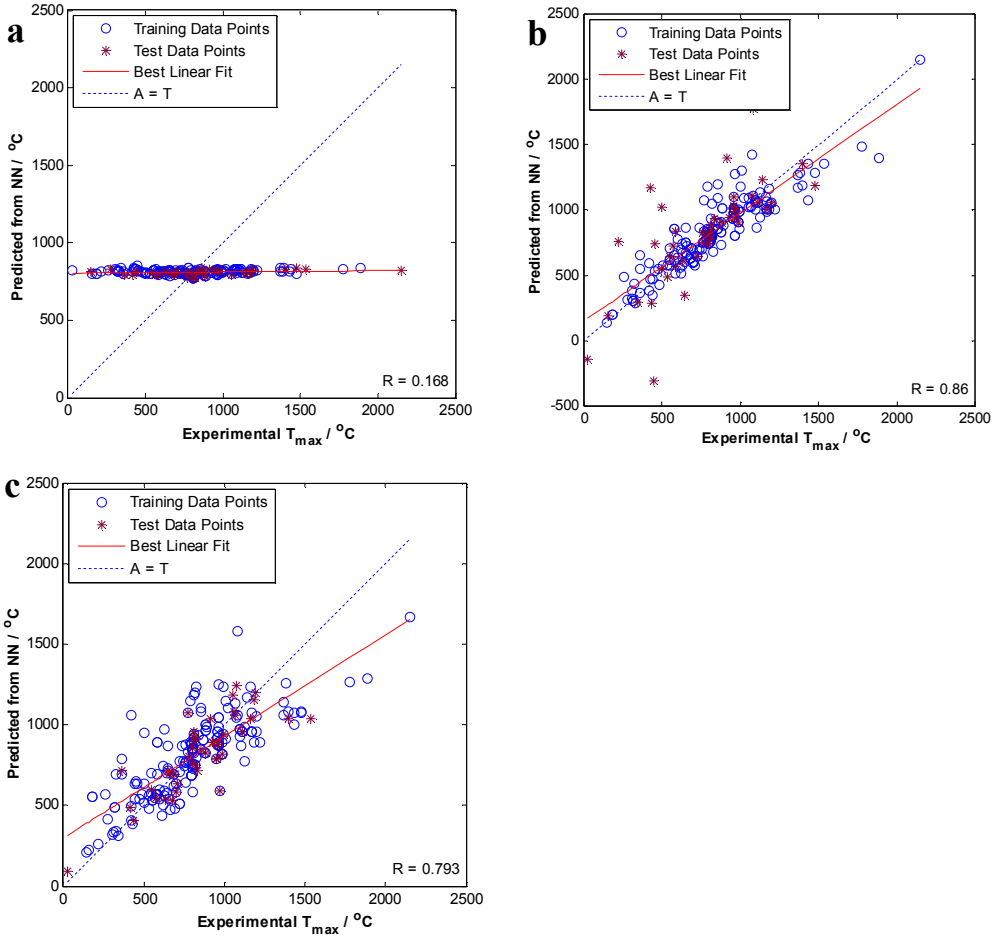

Figure 3.2.19 Prediction of T_{max} for 231 silver and copper alloy systems using a) 3 functionalized parameters: atomic size, valence and electronegativity; b) melting points of solvents and solutes plus parameters used in a); c) melting points of solvents and solutes only.

Table 3.2.6 Statistical analysis of the results shown for Figure 3.2.18 and Figure 3.2.19.

Results		Test set					Whole set				
		R	Mean of error modulus /ºC	SD of error modulus /ºC	Mean of percentage error modulus /%	SD of percentage error modulus /%	R	Mean of error modulus /ºC	SD of error modulus /ºC	Mean of percentage error modulus /%	SD of percentage error modulus /%
Figure 3.2.18	(a)	0.205	205	193	40.1	70.6	0.214	209	190	57.5	263
	(b)	0.775	133	125	16.2	12.7	0.881	88.2	104	12.3	17.7
	(c)	0.752	137	108	17.6	14.3	0.78	130	122	22.2	42.9
Figure 3.2.19	(a)	0.336	213	260	35.5	73.6	0.168	219	205	51.1	216
	(b)	0.744	156	203	42.8	108	0.86	98.5	123	17.4	50.7
	(c)	0.82	110	108	18.8	38.8	0.793	134	126	20.5	31.4

3.3 Discussion

It is important to recognize that there are four different factors that limit the predictive capability of the networks: (i) imperfections in the network configuration which we have attempted to minimize through design, (ii) paucity of learning data which has been mentioned in section 2.0, (iii) the generality of Hume-Rothery's Rules which were conceived as guidelines and (iv) the fact, recognized by Hume-Rothery and co-authors, that the available data are subject to inexactitudes.

3.3.1 The Reliability of Input Parameters

Hume-Rothery *et al.* (**1934**) themselves made it clear that the exact "atomic diameter" of an element is always difficult to define. Their definition of atomic diameter, as given by the nearest-neighbour distance in a crystal of the pure metal, was used here but the "radius" of an atom is probably affected by coordination number. Except for the heavy elements, elements of the B sub-groups tend to crystallize with coordination number 8-N, where N is the group to which the element belongs. This is due to the partly covalent nature of the forces in these crystals, and except in Group IV B (diamond structure) results in the atoms having two sets of neighbours at different distances in the crystal. Cottrell (**1998**) suggests that the concept of a characteristic size, which suggests hard spheres butted together, is doubtful. Allocating a single atomic diameter for each element, independent of its environment, and valences of solvent and solute is too simplistic an approach (**Hume-Rothery *et al.*, 1969**). Furthermore, within the 408 alloy systems, the metallic radius of some elements could not be found and covalent radius used instead. These factors contribute to the errors for the prediction of solid solubility limit and are to be distinguished from intrinsic weakness of the ANN.

An early discovery by Hume-Rothery was that a metal of lower valence is more likely to dissolve one of higher valence than *vice versa*. However, more detailed examination has not confirmed this. As mentioned before, silver dissolves about 20% aluminium but aluminium dissolves about 24% silver. For high valence, covalently bonded components, the relative valence factor applies. For example, copper dissolves about 11% of silicon, which behaves as a 4-valent metal in

forming Cu-Si electron phase alloys, but the solubility of copper in covalently bonded silicon is negligible (**Cottrell, 1998**). As a result, although Hume-Rothery (**Hume-Rothery *et al.*, 1969**) accepted that it is still a general principle that the solubility in the element of lower valency is of greater extent when dealing with alloys of univalent metals copper, silver and gold with metals with higher valency, in its general form, this principle must be treated with caution.

Also, the valencies of transition metals are variable and complex and have been analyzed by Hume-Rothery *et al.* (**1951**) and Cockayne and Raynor (**1961**). As suggested by Cottrell (**1998**), due to the valency complication caused by partly-filled *d* shells, the transition metal alloys generally do not follow the rule. Gschneider (**1980**) modified the relative valence rule so that the solubility is low when a metal in which *d* orbitals strongly influence the valence behaviour, is alloyed with a simple '*sp* metal', but that the solubility is likely to be better in the *d* metal than the reverse.

The electronegativity rule needs a scale, such as that given by Mulliken, based on the equation $\chi = \frac{1}{2}(\mathrm{I} + \mathrm{A})$, where I is the *ionization energy*, A is *electron affinity* and χ is *Mulliken electronegativity*. When divided by 2.8, this scale matches the empirical scale of Pauling reasonably well. In the case of transition metals, as emphasized by Watson and Bennett (**1978**), the partly-filled *d* states of transition metals at energies near the *Fermi energy* influence electronegativity. Watson and Bennett presented an electronegativity scale for transition metals that matched Pauling's scale, and could be scaled by 2.8 to bring it to Mulliken's scale of χ values. Most importantly, Li and Xue (**2006**) recently have mentioned that "although electronegativity is often treated as an invariant property of an atom, as in Pauling's scale, it actually depends on the chemical environment of the atom, e.g. valence state and coordination number", which was also mentioned in Hume-Rothery *et al.* (**1969**). The electronegativity values adopted in this part of work are based on Pauling's work, so the above effects are not entirely taken into account.

The method adopted for expressing structure parameter has some limitations. Firstly, the expressions used to distinguish different crystal structures can conceal similarities. For unit cell length, a=b=c and a=b≠c are distinguished but can have considerable similarity. Secondly, from this expression, the face centered cubic (FCC) and the hexagonal close packed (HCP) systems are expressed as quite distinct sets but there are some similarities between these two structures. They are both close packed systems and stacking faults can blur the difference. Indeed the Cu and Zn systems demonstrate high solubility even though one component, Zn, is HCP and the Cu is FCC. The Ag and α-Li system is a similar case. Thirdly, there are several complex structural systems that cannot be distinguished from other systems by using this expression, such as α-Mn, whose structure is cI58, and β-Mn, whose structure is cP20. These all affect the ability of the structure parameter to contribute to predicting the solubility.

3.3.2 The Effect of Melting Point

The melting point effect actually has been interpreted from some aspects by Hume-Rothery *et al.* (**Buckley and Hume-Rothery, 1963; Hume-Rothery, 1965**). The solid solubility of an alloy system can be treated as the capability to stabilize in the solid phase at that solubility value of added elements, under a certain temperature and this is the competition between the liquid and solid phase for these conditions (certain solubility values and temperature) under free energy minimisation routine. Hume-Rothery *et al.* assessed the stabilizing power of liquid and solid phase in terms of the free energy difference (ΔG), which is the free energy of transfer one mole of solute from the solid to the liquid phase, and includes the melting point effect and other effects (such as atomic diameters, electronic effects, etc.). This can be written as

$$\Delta G = f(mp) + \Delta F \qquad \text{Equation 3.3.1}$$

where the $f(mp)$ is the melting point effect, and ΔF is the effect due to atomic diameters, electronic effects and so on.

From Equation 3.3.1, it can be seen that the stability of one phase can be interpreted in terms of size effects, electronic effects, melting points etc. The effects that contribute to ΔF actually are the parameters in Hume-Rothery's

Rules, as mentioned in a previous paper (**Zhang *et al.*, 2008**); and the melting point effect is the extra effect. For detail, the melting point effect $f(mp)$can be expressed as $-\Delta S_F \times \Delta T$, where ΔS_F is the entropy of freezing of solute element, and ΔT is the difference between T and the melting point of the pure solute.

The above equation explains the effect of melting points of solutes and the temperature at which the stable phase is obtained. This is why the performance of solubility prediction can be improved by introducing the melting point of solutes and the temperature at which the maximum solubility is attained.

3.3.3 The Generality of Hume-Rothery's Rules

Hume-Rothery and co-workers state: "In general, the solubility limit is mainly determined by these factors, and it is their interplay that makes the results so complex" (**Hume-Rothery *et al.*, 1934**). For the 60 alloy systems mentioned by Hume-Rothery in 1934, and using some of the parameter values that can be found in Hume-Rothery's paper or his book and others that follow his representations, the results for prediction of solid solubility limit are satisfactory.

However, from theory as analyzed by others in later work (**Zhang and Liao, 1999a, b; Cottrell, 1998; Miedema, 1973**), and also from the attempts to predict solid solubility limit of the 408 alloy systems, it can be said that Hume-Rothery's Rules work properly in a certain range of alloy systems, but cannot be treated as general principles. Also it needs to be said that despite using Hume-Rothery's Rules, one cannot predict the solid solubility limits accurately. However, these rules are still useful guidelines for judging the solubility of alloy systems.

Further, the introduction of the melting temperatures of both solvents and solutes has a significant effect for the prediction of solid solubility values and its related parameter T_{max}.

4.0 The Policing and Correction of Handbooks and Databases by Artificial Neural Networks

4.1 Data Collection

In this work, the properties of the elements were used as a test dataset for scrutiny by the ANN since these data were expected to be very reliable. Only elements with short half lives were excluded. The majority were taken from Chemistry Data Handbook (CDH) (**Stark and Wallace, 1982**). When suspects were identified, more handbooks were called upon including The Lange's Handbook of Chemistry (LHC) (**Speight, 2005**), The Elements (ELE) (**Emsley, 1998**), Tables of Physical and Chemical Constants (TPC) (**Kaye and Laby, 1995**) and CRC Handbook of Chemistry and Physics (CRC) (**David, 2000**).

4.2 General Steps for Policing/Correction of Errors and Results

This process involves four different stages.

Stage 1: A dataset is examined for internal relationships and inconsistent data-points are identified. In one example, the ANN was used to explore the indirect relationship between boiling point and enthalpy of vaporization using data from CDH (Table 4.1.1 and Figure 4.1.1). The best linear fit equations have regression coefficients R=0.973 and 0.972. On this basis, the correlation hypothesis was raised that the correlation applies to all elements. However, some data points fall well away from the line: e.g. Ho, Se, S, Te, I, As (α), Nb, P, Cd and Pd for which there are two possible causes. The first is that the correlation hypothesis is violated for these special cases; and the second is incorrect handbook data. So at this stage, data from other sources (ELE, TPC and CRC), if available, are brought in (Table 4.1.2 and 4.1.3).

Table 4.1.1 The dataset used to train the ANN shown in Figure 4.1.1. Majority were taken from Chemistry Data Handbook (CDH, 1982) without judgement. A few data unavailable in CDH were taken from LAG and ELE. (BP: Boiling Point; ΔH_V: Enthalpy of Vaporization).

Elements	BP /K	ΔHv /kJ mol^{-1}	Elements	BP /K	ΔHv /kJ mol^{-1}	Elements	BP /K	ΔHv /kJ mol^{-1}
Ag	2483	254	**H**	21.15	0.90	**Pt**	4803	510
Al	2743	284	**He**	4.150	0.08	**Rb**	961.2	69.0
Ar	87.20	6.53	**Hf**	5673	648	**Re**	5903	636
As (grey)	886.2	32.4	**Ho**	2873	71.0	**Rh**	4773	531

Au	3243	342	**I (I_2)**	457.2	22.0	**Ru**	5173	619
B	4203	540	**In**	2273	225	**S (mono.)**	718.2	10.0
Ba	1913	149	**Ir**	5573	636	**Sb**	1653	195
Be	2750	309	**K**	1047	79.1	**Sc**	3003	310
Bi	1833	179	**Kr**	121.2	9.04	**Se**	958.2	14.0
Br	331.7	30.0	**La**	3743	400	**Si**	2633	300
C (graphite)	5103	715	**Li**	1603	136	**Sm**	2173	165
Ca	1760	153	**Lu**	3603	414	**Sn**	2543	290
Cd	1038	100	**Mg**	1383	132	**Sr**	1653	141
Ce	3743	398	**Mn**	2373	225	**Ta**	5693	753
Cl	238.5	20.4	**Mo**	5833	536	**Tb**	3073	293
Co	3173	390	**N**	77.15	5.58	**Te**	1263	49.8
Cr	2755	347	**Na**	1163	101	**Ti**	3533	427
Cs	963.2	66.1	**Nb**	3573	694	**Tl**	1733	162
Cu	2868	305	**Nd**	3303	289	**Tm**	2003	247
Dy	2873	280	**Ne**	27.15	1.80	**V**	3273	444
Er	3173	280	**Ni**	3003	379	**W**	6203	774
Eu	1713	176	**O**	90.15	6.82	**Xe**	165.2	12.6
F	85.15	6.32	**Os**	5273	678	**Y**	3203	390
Fe	3273	354	**P (white)**	553.2	12.4	**Yb**	1703	159
Ga	2673	256	**Pb**	2017	177	**Zn**	1180	115
Gd	3273	301	**Pd**	4253	380	**Zr**	3853	502
Ge	3103	330	**Pr**	3403	331			

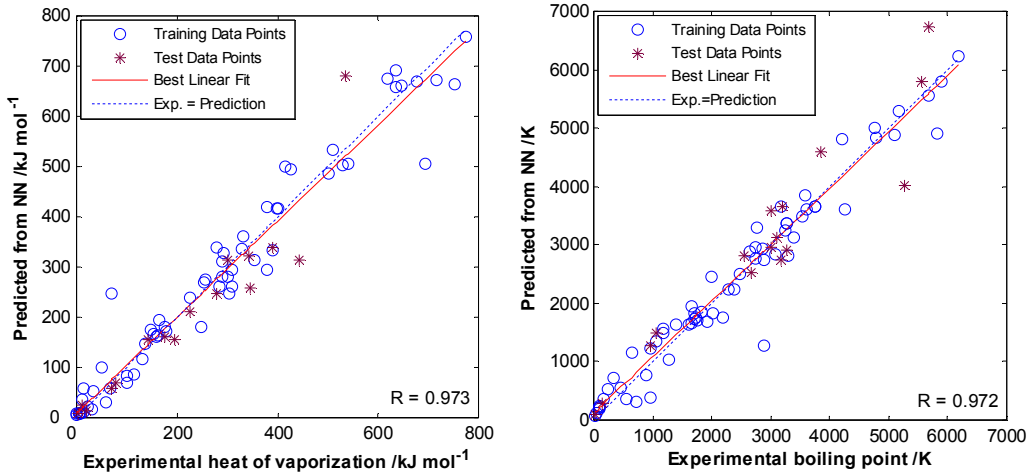

(a) (b)

Figure 4.1.1 Prediction of a) enthalpy of vaporization from boiling point; b) boiling point from enthalpy of vaporization; using data from CDH , LHC and ELE.

Table 4.1.2 List of boiling points from five handbooks (*acronyms as in text*). Dataset does not have exclusions based on judgement. The elements are sorted in ascending (Max.-Min.)/Min.

Elements	CDH	LAG[&]	ELE	TPC	CRC	(Max-Min)/Min
Se[I]	958.2	958.2	958.1	958.2	958.2	0.01%
O	90.15	90.15	90.19	90.19	90.2	0.06%
S (monoclinic)[I]	718.2	718.2	717.8	717.8	717.8	0.06%
Hg	630.2	630.2	629.7	629.8	629.9	0.08%
I (I_2)[I]	457.2	457.2	457.5	457.2	457.6	0.09%
Ge	3103	3103	3103	3103	3106	0.10%
Br	331.7	332	331.9	332.1	332	0.12%
Te[I]	1263	1263	1263	1263	1261	0.16%
F	85.15	85.15	85.01	85.05	85.03	0.16%
Ca	1760	1760	1757	1757	1757	0.17%
Ar	87.15	87.15	87.29	87.29	87.3	0.17%
Rb	961.2	961.2	961	963.2	961.2	0.23%
Sr	1653	1653	1657	1653	1655	0.24%
Zn	1180	1180	1180	1183	1180	0.25%
Cl	238.5	238.5	239.2	239.2	239.1	0.29%
Ne	27.15	27.15	27.1	27.07	27.07	0.30%
N	77.15	77.15	77.4	77.35	77.36	0.32%
La	3743	3743	3730	3733	3737	0.35%
Cd	1038	1038	1038	1043	1040	0.48%
Pb	2017	2017	2013	2023	2022	0.50%
Os[I]	5273	5273	5300	5273	5285	0.51%
Re[I]	5903	5903	5900	5873	5869	0.58%
P (White)[I]	553.2	553.2	553	550.2	553.7	0.64%
Xe	165.2	165.2	166.1	165.1	165	0.67%
Ti	3533	3533	3560	3563	3560	0.85%
Na[I]	1163	1163	1156	1153	1156	0.87%
Tl	1733	1733	1730	1743	1746	0.92%
Li	1603	1603	1620	1613	1615	1.06%
Kr[I]	121.2	121.2	120.9	120	119.9	1.08%
Cu	2868	2868	2840	2833	2835	1.24%
Er	3173	3173	3136	3133	3141	1.28%
Nd	3303	3303	3341	3343	3347	1.33%
Ce[I]	3743	3743	3699	3693	3716	1.35%
Dy	2873	2873	2835	2833	2840	1.41%
K	1047	1047	1047	1033	1032	1.45%
As (grey)**	886.2	886.2	889	883.2	876.2	1.46%
Mg	1383	1383	1363	1363	1363	1.47%
Co	3173	3173	3143	3203	3200	1.91%

Al^{I}	2743	2743	2740	2793	2792	1.93%
Lu	3603	3603	3668	3663	3675	2.00%
Cs	963.2	963.2	951.6	943.2	944.2	2.12%
Ag^{I}	2483	2483	2485	2433	2435	2.14%
Ta	5693	5693	5698	5833	5731	2.46%
Bi^{I}	1833	1833	1883	1833	1837	2.73%
Ho^{I}	2873	2873	2968	2973	2973	3.48%
In	2273	2273	2353	2343	2345	3.52%
Sc	3003	3003	3104	3103	3109	3.53%
H	21.15	21.15	20.28	20.28	20.28	4.29%
Au	3243	3243	3080	3123	3129	5.29%
He	4.15	4.15	4.216	4.37	4.22	5.30%
Sm^{I}	2173	2173	2064	2063	2067	5.33%
Mn	2373	2373	2235	2333	2334	6.17%
W	6203	6203	5930	5823	5828	6.53%
Cr	2755	2755	2945	2943	2944	6.90%
Ga	2673	2673	2676	2473	2477	8.21%
Fe	3273	3273	3023	3133	3134	8.27%
Gd	3273	3273	3539	3533	3546	8.34%
Ni$^{\&}$	3003	3003	3005	3263	3186	8.66%
B^{I}	4203	4203	3931	4273	4273	8.70%
Eu	1713	1713	1870	1873	1802	9.34%
Tm^{II}	2003	2003	2220	2223	2223	11.0 %
Pr^{II}	3403	3403	3785	3783	3793	11.5%
V^{II}	3273	3273	3650	3673	3680	12.4%
Y^{II}	3203	3203	3611	3613	3618	13.0%
Sn^{II}	2543	2543	2543	2893	2875	13.8%
Ba^{II}	1913	1913	1910	2173	2170	13.8%
Tb^{III}	3073	3073	3396	3493	3503	14.0 %
Sb^{III}	1653	1653	1908	1860	1860	15.4%
Yb^{II}	1703	1703	1466	1473	1469	16.2%
Hf^{III}	5673	5673	5470	4873	4876	16.4%
Pt$^{\#\,\&}$	4803	4803	4100	4093	4098	17.4%
Be^{II}	2750	2750	3243*	2743	2744	18.2%
Mo^{III}	5833	5833	4885	4913	4912	19.4%
Rh^{II}	4773	4773	4000	3973	3968	20.3%
Zr^{III}	3853	3853	4650	4673	4682	21.5%
Ru$^{\#}$	5173	5173	4173	4423	4423	24.0 %
C (Graphite)^{II}	5103	5103	5100**	-	4098**	24.5%
Ir^{III}	5573	5573	4403	4703	4701	26.6%
Pd^{II}	4253	4253	3413	3233	3236	31.6%
Si^{III}	2633	2633	2628	3533	3538	34.6%
Nb^{II}	3573	3573	5015	4973	5017	40.4%

* Under pressure

** Sublimation

& the boiling point is different in different tables of LAG. For example, Nickel (Ni) is 2884°C in Page 1.43 (Table 1.3) and 2730°C in page 1.125 (Table 1.19). We selected most of the boiling points from the later table.

The variation of boiling points of Pt and Ru are greater than 10% but here due to shortage of data in range of 3603.15 to 5693.15 K in Category IV, they were classified into Category IV by identifying the closest value from the literature to reduce the uncertainty in that range (**Arblaster, 2005; 2007**).

I. Category I: The data of boiling point for these elements are consistent in different handbooks but that of enthalpy of vaporization are not.

II. Category II: The data of enthalpy of vaporization for these elements are consistent in different handbooks but that of boiling point are not.

III. Category III: The data of neither boiling point nor enthalpy of vaporization for these elements are consistent in different handbooks

Table 4.1.3 List of enthalpies of vaporization from five handbooks (*acronyms as in text*). Dataset does not have exclusions based on judgement. The elements are sorted in ascending (Max.-Min.)/Min.

Elements	CDH	LAG	ELE	TPC	CRC	(Max-Min)/Min
Tm^{II}	-	247	247	-	-	0.00%
Yb^{II}	-	159	159	-	-	0.00%
O	6.82	6.82	6.82	6.82	6.82	0.00%
Eu	-	176	176	176	-	0.00%
Cl	20.4	20.4	20.4	20.4	20.4	0.00%
Cd	100	99.9	99.9	99.9	99.9	0.10%
N	5.58	5.57	5.58	5.59	5.57	0.36%
La	400	402	400	400	-	0.50%
C (Graphite)^{II}	715	-	711	-	-	0.56%
Pr^{II}	-	331	333	333	-	0.60%
Ga	256	254	256	256	254	0.79%
Xe	12.6	12.6	12.7	12.6	12.6	0.79%
Ti	427	425	429	425	-	0.94%
Nb^{II}	694	690	697	690	-	1.01%
Ge	330	334	334	334	334	1.21%
Br	30	30	30	29.6	30	1.35%
Ar	6.53	6.43	6.53	6.52	6.43	1.56%
As (grey)	32.4	-	31.9	-	-	1.57%
Cu	305	300	305	301	-	1.67%
Pb	177	180	179	178	180	1.69%
Hg	58.2	59.1	59.2	59.1	59.1	1.72%
Nd	-	289	284	284	-	1.76%
Tl	162	165	162	162	-	1.85%
Ni	379	378	372	378	-	1.88%
Sn^{II}	290	296	290	290	-	2.07%
H	0.9	-	0.92	0.9	0.9	2.22%
Mn	225	221	220	220	-	2.27%
Cr	347	340	349	340	-	2.65%
Ta	753	733	753	737	-	2.73%
K	79.1	76.9	77.5	76.9	-	2.86%
Sr	141	137	139	137	-	2.92%
In	225	232	226	226	-	3.11%
Mg	132	128	129	128	-	3.13%
Ca	153	155	150	155	-	3.33%
V^{II}	444	459	459	447	-	3.38%
Lu	-	414	428	-	-	3.38%
Gd	-	301.3	311.7	311.7	-	3.45%
Be^{II}	309	297	309	298	-	4.04%

Fe	354	340	351	350	-	4.12%
W	774	807	799	806	-	4.26%
Co	390	377	382	373	-	4.56%
Er	-	280	293	293	-	4.64%
Dy	-	280	293	-	-	4.64%
F	6.32	6.62	6.55	6.54	6.62	4.75%
He	0.084	0.083	0.082	0.08	0.08	5.00%
Ne	1.8	1.71	1.74	1.77	1.71	5.26%
Au	342	324	324	324	324	5.56%
Cs	66.1	63.9	65.9	67.8	-	6.10%
Rh^{II}	531	494	495	495	-	7.49%
Y^{II}	390	365	393	393	-	7.67%
Zn	115	124	115	115	-	7.83%
Ba^{II}	149	140	151	140	140	7.86%
Pd^{II}	380	362	393	393	-	8.56%
Li	136	147	135	147	-	8.89%
Pt	510	469	511	511	-	8.96%
Ru	619	592	568	568	-	8.98%
Sc	310	333	305	305	-	9.18%
Rb	69	75.8	69.2	69.2	-	9.86%
Kr^{I}	10	9.08	9.05	9.03	9.08	10.7%
Re^{I}	636	704	707	707	-	11.2%
B^{I}	540	480	539	508	480	12.5%
Na^{I}	101	97.4	89	97.4	-	13.5%
Mo^{III}	536	617	594	590	-	15.1%
Hf^{III}	648	571	661	661	-	15.8%
Sm^{I}	-	165	192	192	-	16.4%
Os^{I}	678	738	628	628	-	17.5%
Zr^{III}	502	573	582	591	-	17.7%
Bi^{I}	179	151	179	187	151	23.8%
Ce^{I}	-	398	314	314	-	26.8%
Si^{III}	300	359	383	359	-	27.7%
Tb^{III}	-	293	391	-	-	33.5%
I (I_2)^{I}	22	41.6	41.7	41.9	41.6	90.5%
Te^{I}	49.8	114	50.6	50.6	114	129%
Ir^{III}	636	232	564	564	-	174%
Sb^{III}	195	193	67.9	67.9	-	187%
Ho^{I}	-	71	251	251	-	254%
P (White)^{I}	12.4	12.4	51.9	-	12.4	319%
S (monoclinic)^{I}	10	45	9.62	-	45	368%
Se^{I}	14	95.5	26.3	26.3	95.5	582%
Al^{I}	284	294	294	29.1	294	910%
Ag^{I}	254	258	255	25.5	-	912%

I. Category I: The data for boiling point for these elements are consistent in different handbooks but those for enthalpy of vaporization are not.

II. Category II: The data for enthalpy of vaporization for these elements are consistent in different handbooks but those of boiling point are not.

III. Category III: The data for neither boiling point nor enthalpy of vaporization for these elements are consistent in different handbooks

Stage 2: This involves the selection of a conformity criterion. Remarkably, there were 21 elements having inconsistent boiling point at the 10% level or above; and 23 elements having inconsistent enthalpy of vaporization at the 10% level or above in these five handbooks. These are not trivial numbers in only 82 elements inspected and this is far above Chapman's 1-5% field error rate (**Chapman, 2005**). Elements were then classified into four categories on the basis of a 10% variation between minimum and maximum values (a full list of categories is in Table 4.1.4 – 4.1.7):

I) boiling points of the elements are consistent but enthalpy of vaporization are inconsistent;

II) enthalpy of vaporization are consistent but boiling points are inconsistent;

III) both boiling point and enthalpy of vaporization are inconsistent and;

IV) both boiling point and enthalpy of vaporization are consistent.

Consistency across the five handbooks does not imply accuracy (all could have been copied from the same incorrect source) but the ANN may still detect a deviation from the correlation line.

Table 4.1.4 List of Category I elements: boiling points of the elements are consistent but enthalpy of vaporization are inconsistent.

Elements	Boiling point /K	Enthalpy of vaporization /kJ mol^{-1}					
		CDH	LAG	ELE	TPC	CRC	(Max-Min)/Min
Ag	2483	254	258	255	25.5	-	912%
Al	2743	284	294	294	29.1	294	910%
B	4203	540	480	539	508	480	12.5%
Bi	1833	179	151	179	187	151	23.8%
Ce	3743	-	398	314	314	-	26.8%
Ho	2873	-	71	251	251	-	254%
I (I_2)	457.2	22	41.6	41.7	41.9	41.6	90.5%
Kr	121.2	10	9.08	9.05	9.03	9.08	10.7%
Na	1163	101	97.4	89	97.4	-	13.5%
Os	5273	678	738	628	628	-	17.5%
P (white)	553.2	12.4	12.4	51.9	-	12.4	319%
Re	5903	636	704	707	707	-	11.2%
S	718.2	10	45	9.62	-	45	368%
Se	958.2	14	95.5	26.3	26.3	95.5	582%
Sm	2173	-	165	192	192	-	16.4%
Te	1263	49.8	114	50.6	50.6	114	129%
Average							**231%**

Table 4.1.5 List of Category II elements: enthalpies of vaporization are consistent but boiling points are inconsistent.

Elements	Enthalpy of vaporization /kJ mol^{-1}	Boiling point /K					
		CDH	LAG	ELE	TPC	CRC	(Max-Min)/Min
Ba	149	1913	1913	1910	2173	2170	13.8%
Be	309	2750	2750	3243	2743	2744	18.2%
C (graphite)	715	5103	5103	5100	-	4098	24.5%
Nb	694	3573	3573	5015	4973	5017	40.4%
Pd	380	4253	4253	3413	3233	3236	31.6%
Pr	331	3403	3403	3785	3783	3793	11.5%
Rh	531	4773	4773	4000	3973	3968	20.3%
Sn	290	2543	2543	2543	2893	2875	13.8%
Tm	247	2003	2003	2220	2223	2223	11.0%
V	444	3273	3273	3650	3673	3680	12.4%
Y	390	3203	3203	3611	3613	3618	13.0%
Yb	159	1703	1703	1466	1473	1469	16.2%
Average							**18.9%**

Table 4.1.6 List of Category III elements: both boiling point and enthalpy of vaporization are inconsistent.

Elements	Boiling point /K					Enthalpy of vaporization /kJ mol^{-1}				
	CDH	LAG	ELE	TPC	CRC	CDH	LAG	ELE	TPC	CRC
Tb	3073	3073	3396	3493	3503	-	293	391	-	-
Hf	5673	5673	5470	4873	4876	648	571	661	661	-
Ir	5573	5573	4403	4703	4701	636	232	564	564	-
Mo	5833	5833	4885	4913	4912	536	617	594	590	-
Sb	1653	1653	1908	1860	1860	195	193	67.9	67.9	-
Si	2633	2633	2628	3533	3538	300	359	383	359	-
Zr	3853	3853	4650	4673	4682	502	573	582	591	-

Table 4.1.7 List of Category IV elements: both boiling point and enthalpy of vaporization are consistent.

Elements	Boiling point /K	Enthalpy of vaporization /kJ mol^{-1}	Elements	Boiling point /K	Enthalpy of vaporization /kJ mol^{-1}
Ar	87.15	6.53	**K**	1047	79.1
As	886.2	32.4	**La**	3743	400
Au	3243	342	**Li**	1603	136
Br	331.7	30.0	**Lu**	3603	414
Ca	1760	153	**Mg**	1383	132
Cd	1038	100	**Mn**	2373	225
Cl	238.5	20.4	**N**	77.15	5.58
Co	3173	390	**Nd**	3303	289
Cr	2755	347	**Ne**	27.15	1.90
Cs	963.2	66.1	**Ni**	3003	379
Cu	2868	305	**O**	90.15	6.82
Dy	2873	280	**Pb**	2017	177
Er	3173	280	**Pt**	4100	510
Eu	1713	176	**Rb**	961.2	69.0
F	85.15	6.32	**Ru**	4423	619
Fe	3273	354	**Sc**	3003	310
Ga	2673	256	**Sr**	1653	141
Gd	3273	301	**Ta**	5693	753
Ge	3103	330	**Ti**	3533	427
H	21.15	0.90	**Tl**	1733	162
He	4.15	0.0840	**W**	6203	774
Hg	630.2	58.2	**Xe**	165.2	12.6
In	2273	225	**Zn**	1180	115

Stage 3: This uses the data falling into Category IV to train a second set of ANNs. ANN1 is used to predict enthalpy of vaporization; ANN2 is used to predict boiling point. The constructions for these two ANNs are given in Table 4.1.8 and 4.1.9 and it is supposed that these to have been trained on "consistent" data providing a robust correlation against which the consistency of other data can be judged. The performance of the ANNs (ANN1 and ANN2) using consistent data is improved dramatically. The general correlation performance has been increased and the values of M and R are greater being M=0.990, R=0.994 and M=0.993, R=0.995 (Figure 4.1.2), which is greater than the case in Figure 4.1.1 which are M=0.96, R=0.973 and M=0.953, R=0.972.

Table 4.1.8 The weights and biases of the network ANN1.

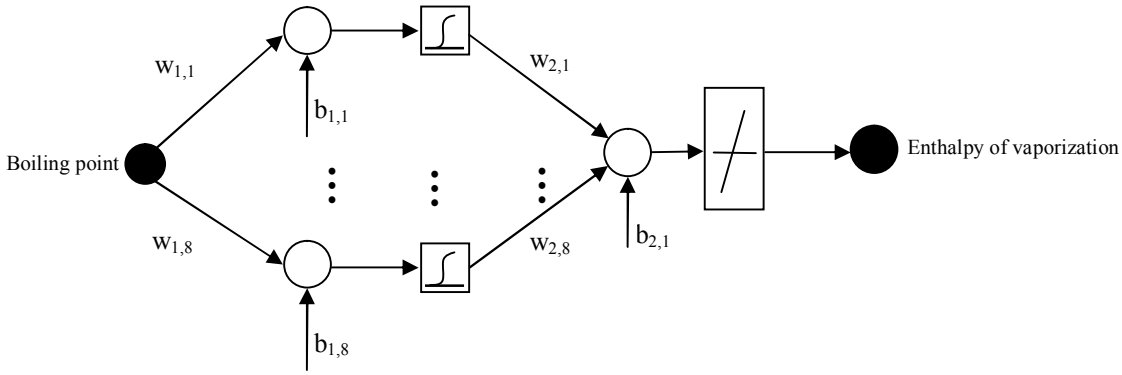

Weights		Biases		Weights		Biases	
$w_{1,1}$	*0.232*	$b_{1,1}$	*0.0228*	$w_{2,1}$	*0.2376*	$b_{2,1}$	*0.1465*
$w_{1,2}$	*0.232*	$b_{1,2}$	*0.0228*	$w_{2,2}$	*0.2376*		
$w_{1,3}$	*-0.9475*	$b_{1,3}$	*0.3703*	$w_{2,3}$	*-0.9277*		
$w_{1,4}$	*0.232*	$b_{1,4}$	*0.0228*	$w_{2,4}$	*0.2376*		
$w_{1,5}$	*-0.232*	$b_{1,5}$	*-0.0228*	$w_{2,5}$	*-0.2376*		
$w_{1,6}$	*-0.232*	$b_{1,6}$	*-0.0228*	$w_{2,6}$	*-0.2376*		
$w_{1,7}$	*-0.232*	$b_{1,7}$	*-0.0228*	$w_{2,7}$	*-0.2376*		
$w_{1,8}$	*-0.232*	$b_{1,8}$	*-0.0228*	$w_{2,8}$	*-0.2376*		

Table 4.1.9 The weights and biases of the network ANN2.

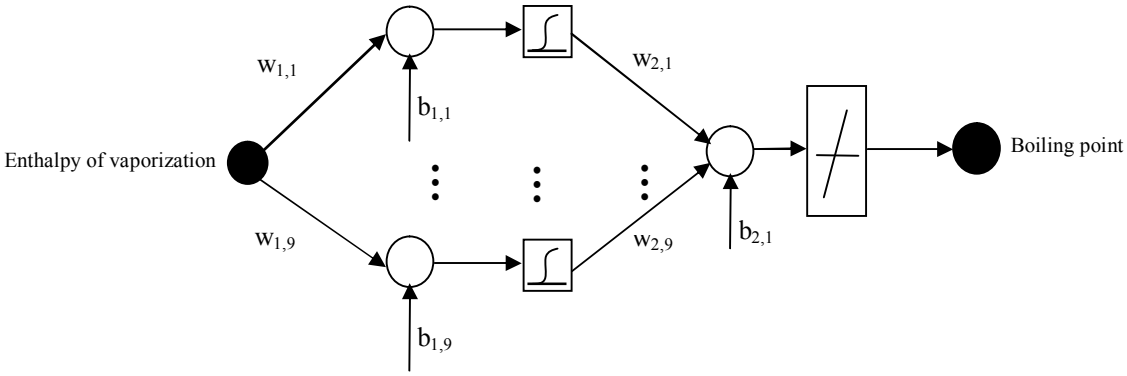

Weights		Biases		Weights		Biases	
$w_{1,1}$	*0.9919*	$b_{1,1}$	*-0.9737*	$w_{2,1}$	*1.2827*	$b_{2,1}$	*-0.0252*
$w_{1,2}$	*0.3945*	$b_{1,2}$	*-0.0551*	$w_{2,2}$	*0.5929*		
$w_{1,3}$	*-0.3945*	$b_{1,3}$	*0.0551*	$w_{2,3}$	*-0.5929*		
$w_{1,4}$	*4.6083*	$b_{1,4}$	*-0.162*	$w_{2,4}$	*1.2808*		
$w_{1,5}$	*2.1463*	$b_{1,5}$	*0.2939*	$w_{2,5}$	*-1.8117*		
$w_{1,6}$	*2.1463*	$b_{1,6}$	*0.2939*	$w_{2,6}$	*-1.8117*		
$w_{1,7}$	*4.4243*	$b_{1,7}$	*1.5236*	$w_{2,7}$	*1.2084*		
$w_{1,8}$	*0.3945*	$b_{1,8}$	*-0.0551*	$w_{2,8}$	*0.5929*		
$w_{1,9}$	*-1.2974*	$b_{1,9}$	*-1.3249*	$w_{2,9}$	*-1.4823*		

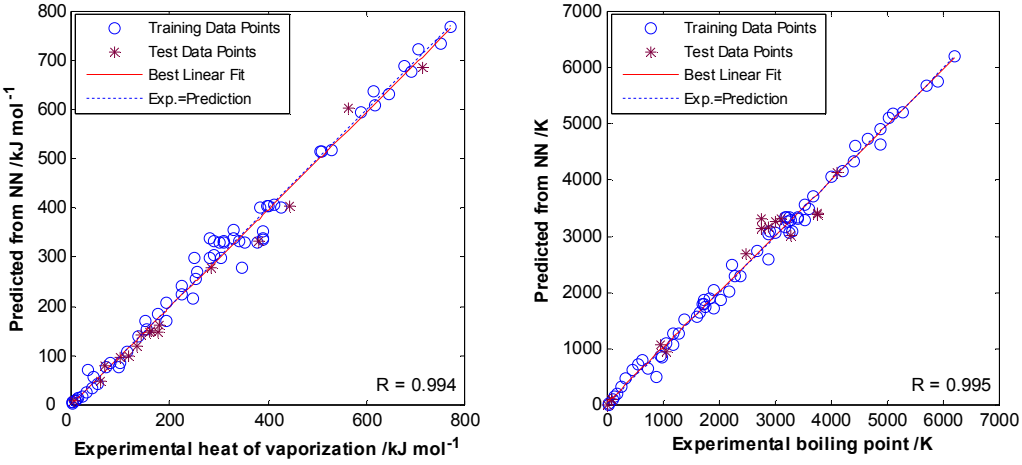

(a) (b)

Figure 4.1.2 Prediction of a) enthalpy of vaporization from boiling point; b) boiling point from enthalpy of vaporization; using "consistent" data.

Stage 4: The consistent values are used to identify inconsistent data. First, the robust ANN1 predicts the enthalpies of vaporization of elements in Category I using their consistent boiling point as inputs. The outputs are compared with the handbook data to isolate suspect enthalpy of vaporization data. After this, most of the differences between the predicted and the closest recorded values of enthalpy of vaporization are less than 10%. The average error for enthalpy of vaporization in Category I decreased from 231% (Table 4.1.4) to 8.8% (Table 4.1.10).

The second part of stage 4 is to use consistent enthalpies of vaporization as input values for ANN2 to predict boiling points of elements in Category II, which are then used to isolate the suspect boiling point data in that set. Predicted and closest recorded values of boiling points for most of the samples now differ by less than 10% (Table 4.1.11). The average error of boiling point in Category II decreased from 18.9% (Table 4.1.5) to 6.43% (Table 4.1.11). So among a set of inconsistent data, the ANN is able to find which are the most likely to be correct. Indeed, the predicted value might even be more accurate in the case of experimentally difficult measurements but the ethics of data correction preclude its use.

Table 4.1.10 List of Category I elements with predicted and selected correct values of enthalpy of vaporization and difference percentage.

Elements	Boiling point /K	Predicted enthalpy of vaporization /kJ.mol^{-1}	Selected enthalpy of vaporization /kJ.mol^{-1}	Difference percentage
Na	1163	97.6	97.4	0.21%
Al	2743	281	284	1.06%
B	4203	499	508	1.77%
Os	5273	664	678	2.06%
Kr	121.2	8.8	9.03	2.55%
Ag	2483	246	254	3.15%
Te	1263	107	114	6.14%
Bi	1833	168	179	6.15%
Re	5903	752	707	6.36%
Ce	3743	427	398	7.29%
Sm	2173	207	192	7.81%
I_2	457.2	35.1	41.6	15.6%
P (white)	553.2	43	51.9	17.2%
Se	958.2	78.4	95.5	17.9%
Ho	2873	299	251	19.1%
S	718.2	57	45	26.7%
Average				**8.81%**

Table 4.1.11 List of Category II elements with predicted and selected correct values of boiling point and difference percentage.

Elements	Enthalpy of vaporization /kJ mol^{-1}	Predicted boiling point /K	Selected boiling point /K	Difference percentage
Pd	380	3221	3233	0.37%
Nb	694	5078	5017	1.22%
Yb	159	1671	1703	1.88%
Rh	531	4137	4000	3.43%
Y	390	3317	3203	3.56%
C (graphite)	715	5326	5103	4.37%
Be	309	3100	3243	4.41%
Sn	290	3060	2893	5.77%
V	444	3939	3680	7.04%
Pr	331	3081	3403	9.46%
Ba	149	1600	1910	16.2%
Tm	247	2655	2223	19.4%
Average				**6.43%**

The data in Category III are treated as follows. It is supposed that if one of the inconsistent values in one property is correct, it might be used to predict a value close to one of the inconsistent values in the other property. For example, for Si, it has a very wide range of handbook boiling points of 2633 K, 2628 K, 3533 K and 3538 K and handbook enthalpies of vaporization of 300, 359 and 383 kJ/mol. So its possible boiling points were predicted using all three enthalpies of vaporization and ANN2 obtaining 3091K, 3096 K, and 3250 K respectively. The differences of predicted boiling points with handbook data can be calculated (12 different combinations). The minimum difference is 8 % between 3533 K (handbook) and 3250 K (predicted from enthalpy of vaporization 383 kJ/mol). So a possible pair is obtained: 3533 K and 383 kJ/mol. Then the ANN1 was used to predict possible enthalpies of vaporization using four handbook boiling points, giving another 12 combinations. The minimum difference corresponds to the pair 3533 K and 383 kJ/mol again (predicted enthalpy of vaporization 395 kJ/mol gives a 3% difference with 383 kJ/mol). This points to the correct boiling point of Si as 3533 K and enthalpy of vaporization, 383 kJ/mol.

The case of silicon may have been lucky – the same pair was obtained in both prediction directions and identification is easily. In some cases the pairs are different in different prediction directions. For iridium, the two pairs are 4701 K and 564 kJ/mol, and 4403 K and 636 kJ/mol. In the first pair, the predicted enthalpy of vaporization is 577 kJ/mol (2.4% difference from 564 kJ/mol) predicted from 4701 K. But in the reverse direction, the prediction of boiling point from 564 kJ/mol is 4158 K, which has 12% difference with 4701 K. In the second pair, the predicted boiling point 4510 K has the smallest difference with 4403 K (2.4%), but in the reverse direction, the difference is 16.6%. It is difficult to point out which pair is more favourable and it looks as though a lengthy indagation of the original sources is inevitable; a quest made problematic because many handbooks are now silent about sources. There is however one other trick that sometimes works.

In such cases, a comprehensive minimum of difference can be calculated. For the general situation, m boiling points B_{oi} (i=1,2…m), and n enthalpies of vaporization H_{oj} (j=1,2…n) from handbooks are available. The ANN will predict

n boiling point B_{pj} (***j***=1,2…***n***) from those ***n*** enthalpy of vaporization, and predict ***m*** enthalpy of vaporization H_{pi} (***i***=1,2…***m***) from ***m*** boiling point. The percentage errors of boiling point prediction, X={x_{ij}}, where $x_{ij} = \left|1 - \frac{B_{pj}}{B_{oi}}\right|$, ***i***=1,2…***m***, ***j***=1,2…***n***, and the percentage errors of enthalpy of vaporization prediction, Y={y_{ij}}, where $y_{ij} = \left|1 - \frac{H_{pi}}{H_{oj}}\right|$, ***i***=1,2…***m***, ***j***=1,2…***n***.

The comprehensive error of the pair is $e_{ij} = \sqrt{(x_{ij} + y_{ij})^2 + (x_{ij} - y_{ij})^2}$. The pair corresponding to the minimum e_{ij} is treated as the correct pair. In this way, two criteria are considered. The sum of the differences (x_{ij}+y_{ij}) should be as small as possible to assess overall performance. Secondly the margin (x_{ij}-y_{ij}) should be minimised to compromise. The parameter e_{ij} is used to select the correct pair. In a few cases, there may be several similar minima and it is likely that resort must be made to an original literature search (Results are shown in Table 4.1.12).

Further inspection of data showed that although the pairs are different in different prediction directions, this difference is often very small. For example, Tb has two pairs 391 kJ/mol and 3396 K, and 391 kJ/mol and 3493 K. Actually the difference between 3396 K and 3493 K is very small and the two pairs are really just one.

Finally, an ANN was trained with the "consistent" values inserted and the result is shown in Figure 4.1.3, the statistics are given in the third and fourth row of Table 4.1.13. The general correlation performance has been increased and the values of M and R are greater being M=0.99, R=0.994 and M=0.993, R=0.995 (for forward and backward predictions respectively) than the case in Figure 4.1.1 which are M=0.96, R=0.973 and M=0.963, R=0.972, and the statistics are shown in the first and second row of Table 4.1.13.

Table 4.1.12 List of Category III elements with predicted and selected correct values and difference percentage (only the corrected pairs are shown).

Elements	Predicted enthalpy of vaporization /kJ mol^{-1}	Selected enthalpy of vaporization /kJ mol^{-1}	Difference percentage	Predicted boiling point /K	Selected boiling point /K	Difference percentage
Hf	604	648	6.79%	4610	4876	5.46%
Ir	530	564	6.03%	4158	4403	5.56%
Mo	605	617	1.94%	4375	4885	10.4%
Sb	176	193	8.81%	1968	1908	3.14%
Si	395	383	3.13%	3250	3533	8.01%
Tb	374	391	4.35%	3328	3396	2.00%
Zr	569	591	3.72%	4236	4650	8.90%

Table 4.1.13 Statistical analysis for ANN performance in Figures 4.1.1, Figure 4.1.3 and Figure 4.1.5.

Conditions (Figures)	Test set						Whole set					
	M	R	Mean of error modulus	SD of error modulus	Mean of percentage error modulus /%	SD of percentage error modulus /%	M	R	Mean of error modulus	SD of error modulus	Mean of percentage error modulus /%	SD of percentage error modulus /%
4.1.1(a)	0.991	0.943	38.1 kJ mol^{-1}	44.1 /kJ mol^{-1}	35.4	57.2	0.96	0.973	32.4 kJ mol^{-1}	36.9 kJ mol^{-1}	114	720
4.1.1 (b)	0.982	0.954	409 K	354 /K	36.9	64.1	0.963	0.972	269 K	284 K	45.9	139
4.1.3 (a)	0.986	0.995	18.1 kJ mol^{-1}	14.8 /kJ mol^{-1}	10.1	6.38	0.99	0.994	16.7 kJ mol^{-1}	15.7 kJ mol^{-1}	48.5	308
4.1.3(b)	1	0.986	196 K	167 /K	35.9	109	0.993	0.995	119 K	108 K	14.7	50.5
4.1.5 (a)	0.974	0.94	55.0 kJ mol^{-1}	65.4 /kJ mol^{-1}	48.4	121	0.944	0.964	35.3 kJ mol^{-1}	42.7 kJ mol^{-1}	202	1342
4.1.5 (b)	0.99	0.956	294 K	368 /K	74.1	201	0.964	0.974	231 K	278 K	30.0	98.8

4.3 Discussion

4.3.1 Comparisons of ANN Curves

In this work, error detection and correction is based on the binary correlation between properties, so it is possible to interpret the results visually by drawing a 2-D diagram. The interpretation is shown in Figure 4.1.4, which is constructed as follows:

1. The boiling point is placed on the abscissa and enthalpy of vaporization on the ordinate for both ANNs.
2. The data in Category IV are plotted directly and are shown as blue dots. For these data, the boiling point values are within the range 0 K –7000 K; while the enthalpy of vaporization values are within the range 0 kJ mol^{-1} – 800 kJ mol^{-1}.
3. The ANN1 was fed with *artificial* boiling point data from 0 to 7000 (taking 1 as interval) to predict corresponding enthalpy of vaporization. Those data were used to draw a complete curve 1. This curve is shown as the green dot-dash line.
4. Similarly, the ANN2 was fed with *artificial* enthalpy of vaporization prediction from 0 to 800 (taking 0.02 as interval) to predict the corresponding boiling point. These data were used to draw curve 2. This curve is shown as a red solid line.
5. The data in Category IV have up to 10% variation between minimum and maximum values so it is reasonable to put ±10% bounds for each curve to show the uncertainty of the prediction. For curve 1, the enthalpy of vaporization was multiplied by 110% and 90%, and for curve 2, the boiling point was multiplied by 110% and 90%. The boundaries are shown as green or red dotted lines.

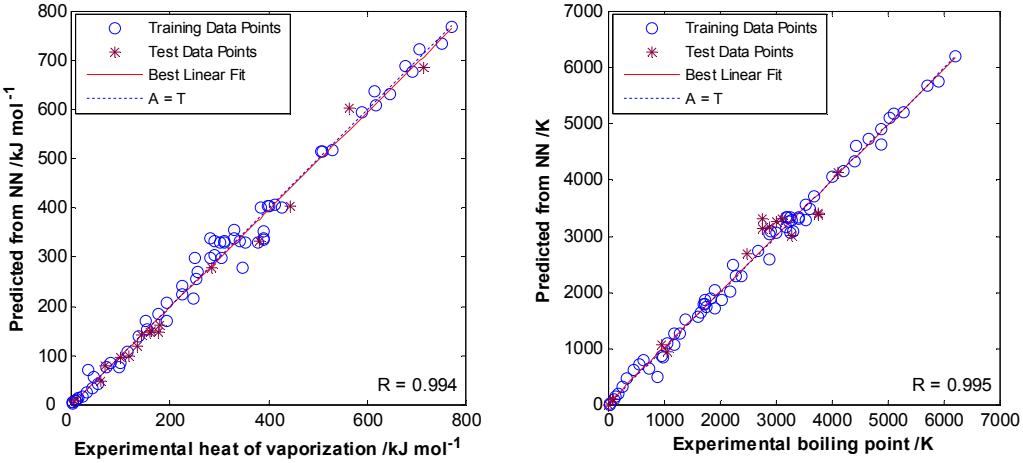

(a) (b)

Figure 4.1.3 Prediction of a) enthalpy of vaporization from boiling point; b) boiling point from enthalpy of vaporization; using "consistent" data.

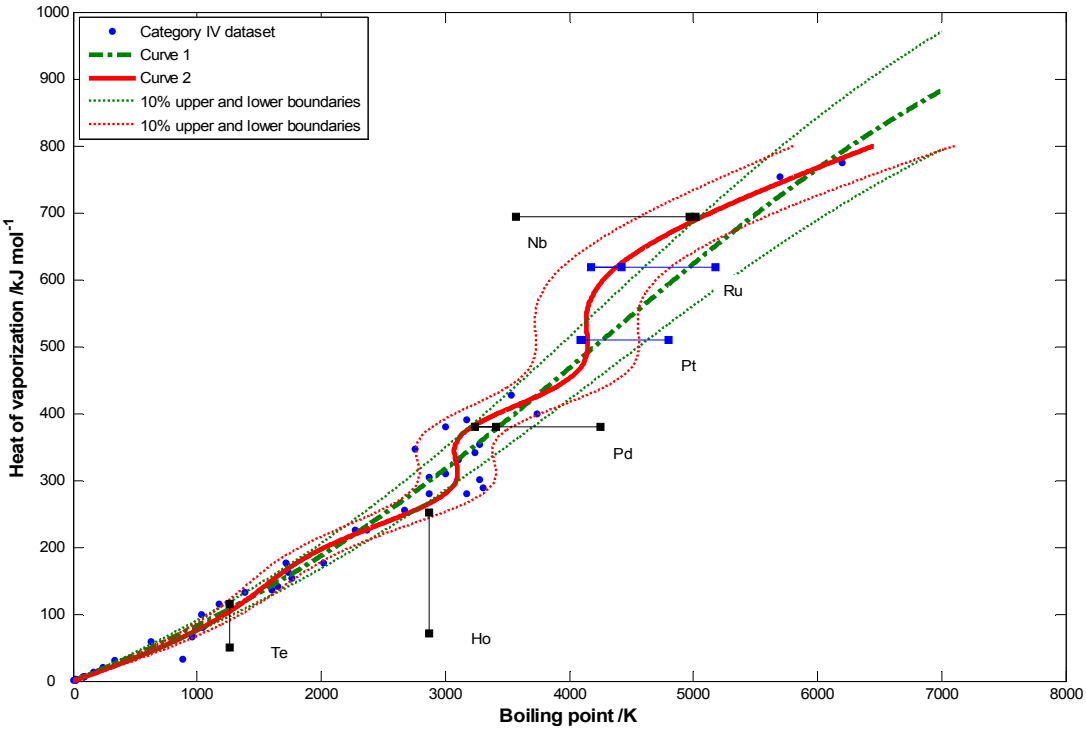

Figure 4.1.4 Neural network fitting curves with ±10% boundaries for both boiling point and enthalpy of vaporization prediction of the Category IV dataset.

In Figure 4.1.4, almost all the elements in Category IV are located within the acceptable zone, which indicates the trained neural networks capture the correlation that exists between boiling point and enthalpy of vaporization for

Category IV elements. This enhanced the confidence in using the trained network derived from stage 3 to identify inconsistent data in stage 4.

If the ideal equation between enthalpy of vaporization and boiling point was found by the ANN then curves 1 and 2 should be identical. However, curves 1 and 2 are different in shape and this means the neural networks found two different equations to represent the correlation between boiling point and enthalpy of vaporization. The reasons for that could be a) noise from the data; b) other unknown properties influence enthalpy of vaporization and/or boiling point. As a result, the neural network cannot find an exact function but a correlation. It minimizes the estimate uncertainty of one quantity, when given a value for the other. The uncertainty makes the two curves different.

Although the ANN found that curve 1 is the best prediction for enthalpy of vaporization, it is interesting to test whether curve 2 performs better on the prediction of enthalpy of vaporization; and *vice versa*. Here, the sum of the squared residuals (SSE) in both boiling point and enthalpy of vaporization for each curve were used as a criterion, which is the same criterion used in regression analysis. When curve 1 is used to predict the enthalpy of vaporization, the sum of the squares of discrepancies is 3.75×10^{4} $kJ^{2}\,mol^{-2}$, and when curve 2 is used to do the same prediction, the value is 5.75×10^{4} $kJ^{2}\,mol^{-2}$. Similar, when the curve 2 is used to predict the boiling point, the value is 1.02×10^{6} K^{2} and when curve 1 is used, the value is 1.99×10^{6} K^{2}.

From comparison of these values, it can be found that for enthalpy of vaporization, the SSE calculated from curve 1 is smaller, but not significantly so, than the value calculated from curve 2; and for boiling point, the SSE calculated from curve 2 is smaller, but not significantly so, than the value calculated from curve 1. As the result, it can be said curve 1 is better for predicting the enthalpy of vaporization, and curve 2 is better for predicting the boiling point, and the neural network found the right one for each. Also, from the comparison made above, the difference in each case is not great, which suggests both of the fitting curves are sensible.

To illustrate the relationship between the curve and the inconsistent data, the data of some elements were drawn in Figure 4.1.4. Clearly, the correct values should be the points close to the curves.

4.3.2 Measurement Methods for Boiling Points and Enthalpy of Vaporization

It is important to remember that these two properties are not directly related. They are based on the Clausius-Clapeyron equation: that is $\frac{dP_{vp}}{dT} = \frac{\Delta H_v}{T\Delta V_v} = \frac{\Delta H_v}{(RT^2 / P_{vp})\Delta Z_v}$, which in its integrated form gives, $P_{vp} = i\exp\left(\frac{\Delta H_v}{RT}\right)$. The boiling point is the temperature at which P_{vp} reaches ambient but the pre-exponential coefficient is not included in the ANN making the relationship indirect.

Boiling point is the temperature at which the vapour pressure of a liquid is equal to the external pressure; and when the external pressure equals 1 atmosphere, the boiling point is called the normal boiling point, which is the meaning in this work.

The enthalpy of vaporization of materials is not a property which can be measured directly as can boiling point. In Poling *et al.*'s book (**2000**), three categories of method to estimate the enthalpy of vaporization are summarised: 1) Based on the Clausius-Clapeyron equation $\frac{dP_{vp}}{dT} = \frac{\Delta H_v}{T\Delta V_v} = \frac{\Delta H_v}{(RT^2 / P_{vp})\Delta Z_v}$, $\frac{dP_{vp}}{dT}$ is found from a vapour-pressure temperature correlation, and then ΔH_v can be obtained after the estimation of ΔZ_v, which is the difference in compressibility factor of saturated vapour and saturated liquid; 2) Use of the principle of corresponding states to make the estimation, such as the equations developed by Pitzer *et al.* (**1955**), Fish and Lielmezs (**1975**), Nath (**1979**), Sivaraman *et al.* (**1984**), Meyra *et al.* (**2004**), Malagoni *et al.* (**2005**), Cachadiña and Mulero (**2007**); 3) In the case of estimating ΔH_v from normal boiling point, there are some additional techniques available, such as Giacalone's equation which was

first developed in 1951 and with improved accuracy by Fishtine and Klein (**Poling *et al.*, 2000**), the Riedel method (**1954**), McCurdy and Laidler (**1963**), the Chen method (**1965**), the Vetere method (**1973**), and also some others done by Fedors (**1974**), Lawson (**1980**), Guthrie and Taylor (**1983**), Hoshino *et al.* (**1983**), Ma and Zhao (**1993**), Constantinou and Gani (**1994**), Tu and Liu (**1996**).

For most of the correlations in these three categories, critical constants T_c and P_c are required either directly or indirectly. As a result, it is reasonable to say that there is a correlation, which is a confounding association, between the boiling point and enthalpy of vaporization, although the function is not known exactly. This is an example of the situation in which the ANN can be applied.

4.3.3 Original Sources of Property Values

To verify the method, original sources were consulted where possible 1) to check whether the refined values were sensible, 2) to reveal and analyse the origin of the differences between handbook data and 3) to find whether the neural network can give values closer to the original literature. Representative examples are shown below. Some errors are attributable to incorrect unit conversions, some to different reference conditions.

Table 4.1.10 indicates that predicted and closest recorded values of enthalpy of vaporization for most elements differ by less than 10% after removal of incorrect data. The exceptions are I_2 (15.5%), P (17.1%), Se (17.9%), Ho (19.0%) and S (26.7%). Data for elements I_2, P and S depend on the polyatomic nature of these molecules and this accounts for the differences as shown in Table 4.1.3 but handbooks do not always state how the value is normalised. In these cases, where the substances always exist in their molecular forms, the corresponding enthalpy of vaporization should be accounted for molecular form. From Table 4.1.10, the corrected values are reasonable choices, although the differences are still greater than 10%. The detailed investigations of Ho and Se are shown below. These results show that the ANNs can predict more reliable data.

For holmium (Ho), there are two sources of discrepancy. Original sources for $\Delta H_{v,st}$ offer 71910 cal mol^{-1} (**Hultgren *et al.*, 1973**), 69500 cal mol^{-1} (**White *et al.*, 1961**), 75040 cal mol^{-1} (**Trulson *et al.*, 1961**), 81150 cal mol^{-1} (**Hultgren *et al.*, 1973**) and 70600 cal mol^{-1} (**Wakefield *et al.*, 1967**). Clearly these results indicate the enthalpy of vaporization of holmium is around 71 kcal mol^{-1}, corresponding to 297 kJ mol^{-1}, rather than the 71 kJ mol^{-1} recorded in *Lange's Handbook of Chemistry* and the source of error is transcription of units. Indeed in the earlier 12th edition of *Lange's Handbook Chemistry* (**Dean, 1979**), the value was 60 kcal mol^{-1}, placing it in the correct range.

The selected handbook value of 251 kJ mol^{-1} still differs by more than 10% from the ANN predicted value of 299 kJ mol^{-1}. The second source of discrepancy is the reference temperature. All the above values are corrected to standard temperature. However the Category IV values used for training ANNs 1 and 2 are all referenced to normal boiling point (with the exception of four elements). Values for the enthalpy of vaporization of Ho at normal boiling point are available: 67 kJ mol^{-1} corresponding to 280 kJ mol^{-1} (**Daane, 1961**) and 64.7 $\mathrm{cal\,mol^{-1}}$ corresponding to 270 kJ mol^{-1} (**Wakefield *et al.*, 1967**). These values are close to the value predicted by the ANN and this demonstrates the remarkable discernment of the ANN in detection of errors and identification of true values.

The case of selenium is different. The handbook values are 14, 26.3 and 95.5 kJ mol^{-1} and the ANN predicts 78.4 kJ mol^{-1} from the well-established boiling point of 958 K (as a fixed point in International Temperature Scale) (**De Selincourt, 1940; Brooks, 1952**). The source for 95.5 kJ mol^{-1} can be found (**Brooks, 1952**), in which Brooks used the Bourdon gage method and Clapeyron equation $\ln P_{VP} = A - \frac{B}{T}$, and determined the enthalpy of vaporization for Se at the normal boiling point which is 22.02 ± 0.02 kcal/mol and corresponds to 95.48 ± 0.08 kJ/mol. This is supported by Hutlgren *et al.* (**1973**) who gives a value at 625 K where, of the eight chemical allotropes for gaseous Se, Se_6 predominates (**Bagnall, 1966**). The value of 13.8 kJ mol^{-1} for atomic Se corresponds to 82.8 kJ

mol^{-1} for Se_6 (**Hultgren *et al.*, 1973**). This may explain the handbook value of 14 kJ mol^{-1}, if that value be for atomic Se. The handbook value of 26.3 kJ mol^{-1} begins to look like a transcription of units error of x4.18 J cal^{-1}. The selected value of 95.5 kJ mol^{-1} still deviates by more than 10% from the ANN predicted value 78.4 kJ mol^{-1}. A possible reason for this, as discussed by Bagnall (**1966**) and Reid *et al.* (**1987**), is associated with constants in the Clapeyron equation and is described in the part 4.3.5.

4.3.4 Comparison with the Method used by Ashby

The ANN technique was also used to double-check the statistical approach (**Ashby, 1998; Bassetti *et al.*, 1998**) used for CES software (previously Cambridge Materials Selector, CMS). The CES data was used to train an ANN and it gave correlation coefficients of 0.964 and 0.974 compared with 0.994 and 0.995 when using the "consistent" data (shown in Figure 4.1.5, and statistical analysis as shown in fifth and sixth row of Table 4.1.13). For example, consider the enthalpy of vaporization for Se. The value taken from CES Software is 207 kJ mol^{-1} but other sources give 14, 26.3 and 95.5 kJ mol^{-1}. The value for enthalpy of vaporization for phosphorous (P, white) in CES software is 316 kJ mol^{-1}, while the values quoted by Dainton and Kimberley (**1950**) and other sources is 12.4 kJ mol^{-1} for ¼ P_4 or 51.9 kJ mol^{-1} for P_4. These are large discrepancies for elemental data.

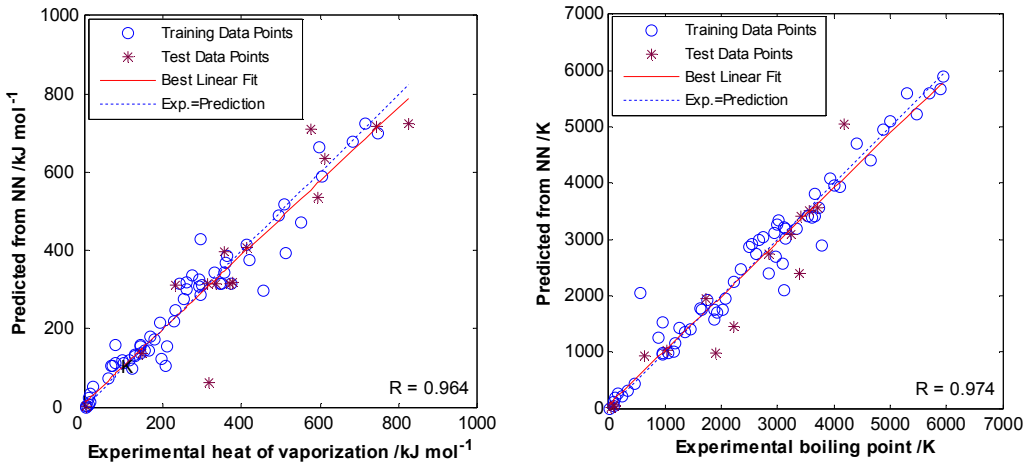

(a) (b)

Figure 4.1.5 Prediction of a) enthalpy of vaporization from boiling point; b) boiling point from enthalpy of vaporization using dataset all recorded from CES 2008.

4.3.5 Factors that Affect the Accuracy of the Prediction

In this part, several factors that affect the accuracy of prediction are discussed.

1. *The determination of the constant after Clausius-Clapeyron integration*. As mentioned in Reid *et al.* (**1987**), it is not easy to trace the origin of many experimental enthalpies of vaporization. A few were determined from calorimetric measurements, but in a large number of cases the values were obtained directly from Clausius-Clapeyron equation $\frac{d\ln P_{vp}}{d(1/T)} = -\frac{\Delta H_v}{R\Delta Z_v}$, in which the ΔZ_v were determined separately using various techniques, and $(d\ln P_{vp})/dT$ was found by numerical differentiation of experimental vapour pressure data or by differentiating some P_{vp} – T correlation analytically. The constants in one equation may be optimized for correlating vapour pressures, but it does not necessarily follow that these same constants give the best fit for computing slopes. For this reason, uncertainty is present in using any analytical vapour pressure – temperature equation to obtain accurate values of slopes $(d\ln P_{vp})/dT$.

2. *Enthalpy of vaporization varies with temperature*. ΔH_v is always treated as a weak function of temperature, and an assumption is made that this value

does not vary with temperature (**Reid *et al.*, 1987; De Podesta, 2001**) during the integration of Clausius-Clapeyron equation. However, it is not true for each element (**Hultgren *et al.*, 1973**). For some elements, the variation is narrow, such as Ga (from 260 kJ mol^{-1} at normal boiling point to 273 kJ mol^{-1} at room temperature, 5% difference), Zr (from 58.4 kJ mol^{-1} at normal boiling point to 61.3 kJ mol^{-1} at room temperature, 5.0% difference), W (from 827 kJ mol^{-1} at normal boiling point to 852.6 kJ mol^{-1} at room temperature, 3.1% difference) and others, the variation is wide, and the value of ΔH_v decreases with rising temperature, such as Ba (from 142 kJ mol^{-1} at normal boiling point to 182.7 kJ mol^{-1} at room temperature, 28.7%), Tm (from 191.5 kJ mol^{-1} at normal boiling point to 233 kJ mol^{-1} at room temperature, 21.7%). The data for enthalpies of vaporization are recorded in most of handbooks (such as CDH, LAG, ELE, TPC) in a mixed fashion without mention of the temperatures to which the values apply. This introduces uncertainties in finding the correlation and reduces the accuracy of predictions. After comparing the values in Category IV with the values recorded in *Selected Values of the Thermodynamic Properties of the Elements* (**Hultgren *et al.*, 1973**), which tabulates enthalpies of vaporization over a temperature range, it is found that all but four (Dy, Eu, Gd and Lu) are recorded at normal boiling points. Thus, Pb (Category IV) for example, has a value 175 kJ mol^{-1} at boiling point and 192 kJ mol^{-1} at room temperature (**Hultgren *et al.*, 1973**) and so it is infered that 177 kJ mol^{-1} is enthalpy of vaporization at normal boiling point. Thus neural networks (ANN1 and ANN2) have found the correlation between normal boiling points and enthalpy of vaporization under normal boiling points.

3. *The Clausius-Clapeyron equation is not the only equation for estimating enthalpies of vaporization*. Other methods such as Pitzer's acentric factor correlation, Riedel's method, Chen's method and Vetere's method are also used. More accurate estimates may be obtained when specific correlations are employed and demand a recourse to original sources (**Reid *et al.*, 1987**).

These factors mean that differences between predicted and corrected values cannot be avoided. The 1st and 3rd factors account for small differences (<10%)

since these just affect the accuracy of the enthalpies of vaporization. The large deviations (>10%) may be attributed to the 2nd factor. For Category I, the problems of the 2nd factor do not attend the records of boiling point so the prediction of enthalpy of vaporization for these elements from the consistent boiling point can be treated as reliable. However, the 2nd factor affects predictions for the elements in Category II and so enthalpies of vaporization used for these elements were rechecked with the values recorded in *Selected Values of the Thermodynamic Properties of the Elements* (**Hultgren *et al.*, 1973**) and another set of predictions based on the enthalpies of vaporization referenced to normal boiling point was made. The results are shown in Table 4.1.14.

Table 4.1.14 List of Category II elements with predicted and selected correct values of boiling point and difference percentage (with reference to normal boiling point).

Elements	Enthalpy of vaporization /kJ mol^{-1}	Predicted boiling point /K	Selected boiling point /K	Difference percentage
Yb	129	1460	1466	0.41%
Nb	682	4944	4973	0.58%
Y	363	3111	3203	2.87%
C (graphite)	709	5254	5103	2.96%
Tm	191	1943	2003	3.00%
Rh	493	4144	4000	3.60%
Pd	358	3093	3233	4.33%
Be	292	3068	3243	5.40%
Sn	296	3081	2893	6.50%
V	451	3995	3680	8.56%
Pr	297	3084	3403	9.37%
Ba	142	1551	1910	18.8%
Average				**5.53%**

From comparison of the results in Table 4.1.11 with Table 4.1.14, it can be seen that most of the boiling points are the same, except Yb and Tm. As a result, it is interesting to analyse which prediction is more sensible.

For Yb, 159 kJ mol^{-1} is corresponding to the value recorded under the room temperature according to Hultgren *et al.* on page 564 (**Hultgren *et al.*, 1973**), which gives 129 kJ mol^{-1} at normal boiling point and 152 kJ mol^{-1} at room temperature. A higher value of enthalpy of vaporization at normal boiling point corresponds to a higher value of normal boiling point, so 159 kJ mol^{-1} was used

to predict boiling point giving the higher value of boiling point for Yb. Two factors need to be considered: 1) For different elements, those having higher normal boiling points always have higher enthalpies of vaporization at the normal boiling point; 2) For a given element, the enthalpy of vaporization varies inversely with temperature. For Yb, the boiling point is higher than ambient and so the enthalpy of vaporization at boiling point is lower than the value at ambience. Previously, the enthalpy of vaporization at room temperature was used to predict boiling point, and the first factor means the boiling point was over-estimated. Now the enthalpy of vaporization at normal boiling point is employed and the boiling point prediction is correct. Using 129 kJ mol^{-1}, the corresponding boiling point is 1460 K, which is closer to 1466 K (within 0.40%), and this value is confirmed by the work of Habermann and Daane (**Habermann and Daane, 1964**). In their work, the vapour pressures of the rare-earth metals were measured by the Knudsen effusion technique using a quartz-fibre microbalance, and then a combination of Second and Third Law methods were used to calculate the normal boiling point for each rare-earth metal, and for Yb this value is 1466 (±5)K.

For Tm, 247 kJ mol^{-1} is the value corresponding to ambient temperature, according to Hultgren *et al.* on page 533 (**Hultgren *et al.*, 1973**), which gives 191 kJ mol^{-1} at normal boiling point and 232 kJ mol^{-1} at room temperature and is greater than the value recorded at normal boiling point which is about 191 kJ mol^{-1}. For similar reasons, 247 kJ mol^{-1} was used to predict boiling point producing a higher value. Using the value of 191 kJ mol^{-1}, it is found the boiling point is 1943 K, which is closer to 2003K (within 3.00%), and is consistent with the value obtained by Spedding *et al.* after purifying this element at the Ames Laboratory of the U. S. Atomic Energy Commission (**Spedding *et al.*, 1957**), which was 2000 K.

From this analysis, the prediction of boiling point in these cases is more justifiable, than before. So it emerges that although there are several factors, especially the 2^{nd}, that may mislead the neural network method, when care is taken and critical surveys are employed, it turns out to be robust and reliable.

4.3.6 The Generality and Limitations of This Method

Generality

In a general situation, there may be more than two properties correlated. All that is required is sufficient correlation, as established by the ANN, to give demarcation between a majority of well correlated data-points and an outlying minority. If more than two properties are correlated, a similar procedure can also be applied. In the following, the mathematical expressions for use when three properties are correlated and given. The situation for more properties is derived by analogy with this.

The first step is to find a database of consistent records of all three properties (Category I in Table 4.1.15). Those data will be used to train three ANNs (i.e., ANN1, the prediction of C using A and B, ANN2, the prediction of B using A and C, and ANN3, the prediction of A using B and C). The other records are classified into categories 2-8 according to the number of inconsistent properties.

Table 4.1.15 Systematic methodology for error checking in handbooks.

Categories	A	B	C	Methodology
1	1	1	1	Used to train three ANNs.
2	1	1	0	Method 1
3	1	0	1	
4	0	1	1	
5	0	0	1	Method 2
6	0	1	0	
7	1	0	0	
8	0	0	0	Method 3

1 = property records are consistent in different handbooks

0 = property records are inconsistent in different handbooks

The Methods 1, 2 and 3 listed in Table 4.1.15 can be described as follows:

Method 1: Take Category 2 as an example. Inconsistent properties C can be predicted directly from properties A and B by using ANN1.

Method 2: Take Category 5 as an example. For a general situation, we may have l records of property **A** $\{A_{(o)i}, i = 1, 2, \ldots l\}$, m records of property **B** $\{B_{(o)j}, j = 1, 2, \ldots m\}$ from handbooks.

The ANN3 will predict m property **A** $\{A_{(p)j}, j = 1, 2, \ldots m\}$ from m property **B** and the correct property **C**. The percentage errors of property A prediction are X=$\{x_{ij}\}$, where $x_{ij} = \left|1 - \frac{A_{(p)j}}{A_{(o)i}}\right|$, $i = 1, 2, \ldots l, j = 1, 2, \ldots m$.

Similarly, ANN2 will predict l property **B** $\{B_{(p)i}, i = 1, 2, \ldots l\}$ from l property **A** and the correct property **C**. The fractional errors of property B prediction are Y=$\{y_{ij}\}$, where $y_{ij} = \left|1 - \frac{B_{(p)i}}{B_{(o)j}}\right|$, $i = 1, 2, \ldots l, j = 1, 2, \ldots m$.

The comprehensive error of each pair is $e_{ij} = \sqrt{(x_{ij} + y_{ij})^2 + (x_{ij} - y_{ij})^2}$. The correct properties are the pair which presents minimum e_{ij}.

Method 3: Suppose we have l different records of property **A** $\{A_{(o)i}, i = 1, 2, \ldots l\}$, m different records of property **B** $\{B_{(o)j}, j = 1, 2, \ldots m\}$, and n different records of property **C** $\{C_{(o)k}, k = 1, 2, \ldots n\}$ from handbooks. The ANN3 will predict $m \times n$ records of property **A** $\{A_{(p)jk}, j = 1, 2, \ldots m, k = 1, 2, \ldots n\}$ from m property **B** and n property **C**. The fractional errors of property A prediction are X=$\{x_{ijk}\}$, where $x_{ijk} = \left|1 - \frac{A_{(p)jk}}{A_{(o)i}}\right|$, $i = 1, 2, \ldots l, j = 1, 2, \ldots m, k = 1, 2, \ldots n$.

Similarly, ANN2 will predict $l \times n$ records of property **B** $\{B_{(p)ik}, i = 1, 2, \ldots l, k = 1, 2, \ldots n\}$ from l property **A** and n property **C**. The fractional errors of property B prediction are Y=$\{y_{ijk}\}$, where $y_{ijk} = \left|1 - \frac{B_{(p)ik}}{B_{(o)j}}\right|$, $i = 1, 2, \ldots l, j = 1, 2, \ldots m, k = 1, 2, \ldots n$.

Again, ANN1 will predict $\boldsymbol{l} \times \boldsymbol{m}$ records of property **C** $\{\boldsymbol{C_{(p)ij}}, \boldsymbol{i} = 1, 2, \ldots \boldsymbol{l}, j = 1, 2, \ldots \boldsymbol{m}\}$ from $\boldsymbol{l}$ property **A** and $\boldsymbol{m}$ property **B**. The fractional errors of property C prediction are $Z=\{z_{ijk}\}$, where $z_{ijk} = \left|1 - \frac{C_{(p)ij}}{C_{(o)k}}\right|$, $\boldsymbol{i} = 1, 2, \ldots \boldsymbol{l}, \boldsymbol{j} = 1, 2, \ldots \boldsymbol{m}, \boldsymbol{k} = 1, 2, \ldots \boldsymbol{n}$.

The comprehensive error of each group is

$$e_{ijk} = \sqrt{\left(x_{ijk} + y_{ijk} + z_{ijk}\right)^2 + \left(x_{ijk} - y_{ijk}\right)^2 + \left(y_{ijk} - z_{ijk}\right)^2 + \left(x_{ijk} - z_{ijk}\right)^2}$$

The combination corresponding to the minimum $\boldsymbol{e_{ijk}}$ is the correct combination.

Limitation of this method and improvement

Although the method developed here is a powerful method, there are still some limitations. Error pairs may be difficult to detect if:

(1) both single source data are wrong but obey the relationship by coincidence, then they cannot be detected.

(2) both single source data are wrong but do *not* obey the relationship, they can be detected but we cannot identify which is wrong or if both are wrong (Examples are the enthalpy of vaporization of elements of Yb and Tm which have been discussed in part 4.3.5)

However, both of those two limitations could be overcome by introducing more properties into the correlation, based on an assumption that the probability that all data are wrong but still obey the relationship by coincidence is very low.

5.0 The Prediction of Structural Stability and Formability of ABO_3-type Perovskite Compounds using Artificial Neural Networks

5.1 Special Experimental Details

5.1.1 Data Collection

This part of work is based on the work done by Zhang *et al.* (**2007**), the values of global instability indices (**GII**), bond-valence based tolerance factor (t_{BV}), and A-O and B-O bond distances ($d_{A\text{-}O}$ and $d_{B\text{-}O}$) are recorded. These data are taken from their supplementary data (Reference: BS5049) and can be accessed from the *Acta Crystallographica Section B* journal site.

5.1.2 Determination of Input and Output Parameters

This part of work is composed of two different parts: 1) prediction of the global instability indices (**GII**) from bond-valence based tolerance factor (t_{BV}) using backpropagation neural network (BPANN); 2) prediction of the perovskite formability based on the ideal A-O and B-O bond distances ($d_{A\text{-}O}$ and $d_{B\text{-}O}$) bond distances using probabilistic neural network (PNN).

In part 1, the bond-valence based tolerance factor (t_{BV}) and global instability indices (**GII**) are input and output of BPANN, respectively; in part 2, the inputs are A-O ($d_{A\text{-}O}$) and B-O ($d_{B\text{-}O}$) bond distances, and the output are the formability of perovskites.

5.2 Results and Discussion

5.2.1 Prediction of GII from bond t_{BV}

From the three curves in Figure 1.8.1, it is interesting to see whether there is a correlation between **GII** and t_{BV}, that is, can one of them, say t_{BV}, be used to predict the other (**GII** in this case)? The results of using t_{BV} to predict **GII** for $A^{1+}B^{5+}O_3$ type perovskites, $A^{2+}B^{4+}O_3$ type perovskites and $A^{3+}B^{3+}O_3$ type perovskites are shown in Figures 5.2.1(a) to 5.2.1(c) in which the blue circles represent the training datasets and the purple stars represent the testing datasets. The best linear fit equations and regression coefficients, R, show that they give sensible correlations; R=0.999 for Figure 5.2.1(a), R=0.997 for Figure 5.2.1(b) and R=0.999 for Figure 5.2.1(c). These three results indicate that correlations exist between the tolerance factor (t_{BV}) and global instability index (**GII**) for each subclass of perovskites (*i.e.*, $A^{1+}B^{5+}O_3$, $A^{2+}B^{4+}O_3$, $A^{3+}B^{3+}O_3$). The reasons will be discussed later.

It is also interesting to know whether a uniform correlation between the tolerance factor (t_{BV}) and global instability index (**GII**) exists for the whole class of ABO_3 perovskites. In order to address this question, a similar procedure is used to make predictions of **GII** from t_{BV}. The result is shown in Figure 5.2.1(d). By comparing the best linear fit equation and regression coefficient, R, in this figure (R=0.949) with the results shown in Figure 5.2.1(a-c), it is found that a correlation between **GII** and t_{BV} for all ABO_3 perovskites exists, but is not as straightforward as those shown for the individual classes.

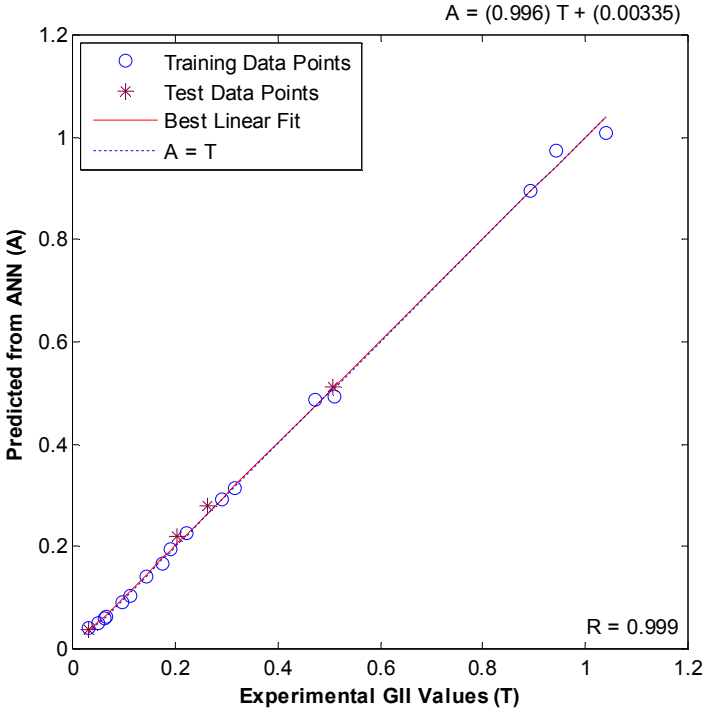

Figure 5.2.1 (a) Prediction of global instability indices (**GII**) from bond-valence based tolerance factors (t_{BV}) for $A^{1+}B^{5+}O_3$.

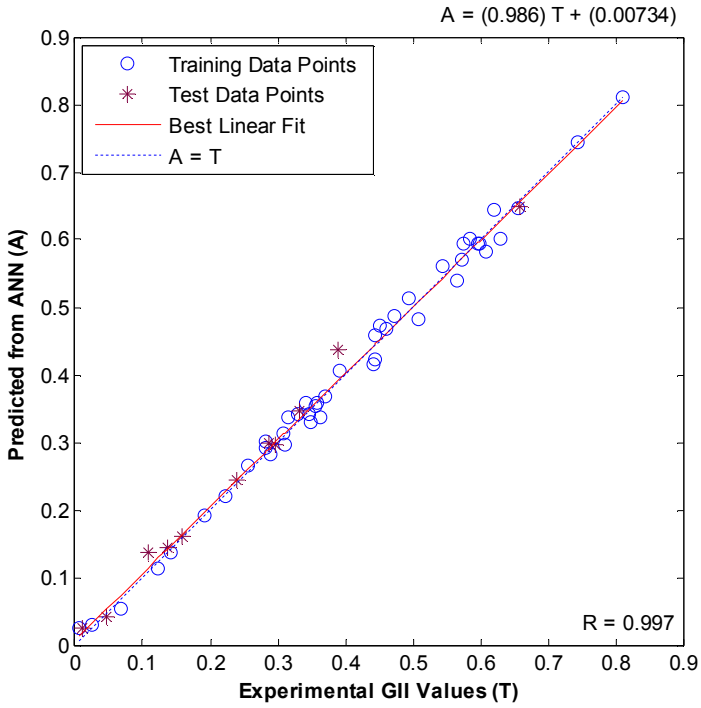

Figure 5.2.1 (b) Prediction of global instability indices (**GII**) from bond-valence based tolerance factors (t_{BV}) for $A^{2+}B^{4+}O_3$.

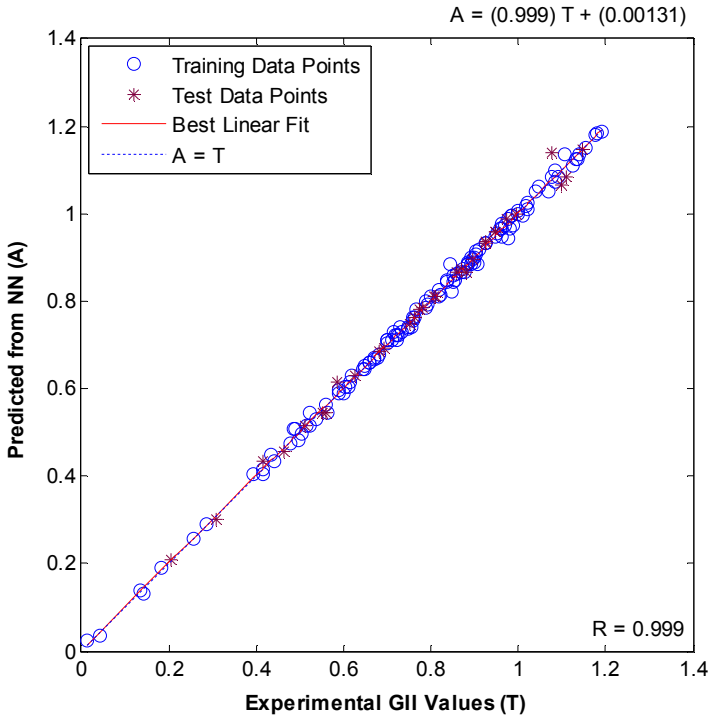

Figure 5.2.1 (c) Prediction of global instability indices (**GII**) from bond-valence based tolerance factors (t_{BV}) for $A^{3+}B^{3+}O_3$.

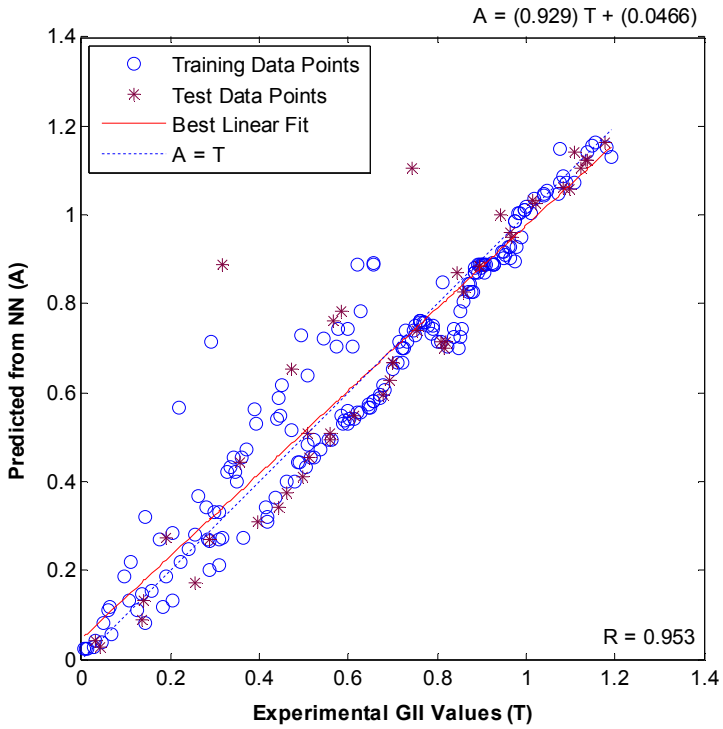

Figure 5.2.1 (d) Prediction of global instability indices (**GII**) from bond-valence based tolerance factors (t_{BV}) for all type of ABO_3 perovskite compounds.

Now the correlations between the tolerance factor and the overall structural stability are explained. The overall structural stability, referred to as the global instability index (**GII**), is determined by comparing the calculated atomic bond-valence $V_{i(\text{calc.})}$ and formal valence $V_{i(OX)}$, as used by Zhang *et al.* (**2007**),

$$GII = \left\{ \left[\sum_{i=1}^{N} \left(d_i^2 \right) \right] / N \right\}^{1/2} \qquad \text{Equation 5.2.1}$$

where N is the number of atoms in the asymmetric unit, and

$$d_i = V_{i(OX)} - V_{i(calc)}, \qquad V_{i(calc)} = \sum_j s_{ij} \qquad \text{Equation 5.2.2}$$

and

$$s_{ij} = \exp\left(\frac{R_{ij} - d_{ij}}{B} \right) \qquad \text{Equation 5.2.3}$$

where d_{ij} is the cation-anion bond distance; R_{ij} is empirically determined for each cation-anion pair based on a large number of well-determined bond distances for the cation-anion pair in question, and has been tabulated; and B is an empirically determined universal constant with a value of 0.37.

The bond-valence based tolerance factor, $\boldsymbol{t_{BV}}$, shown in Equation 5.2.4, is calculated like the tolerance factor ($\frac{r_A + r_O}{\sqrt{2}(r_B + r_O)}$), but substituting r_A+r_O and r_B+r_O with bond distances A-O (d_{AO}) and B-O (d_{BO}) calculated from the bond-valence model.

$$\boldsymbol{t}_{\mathbf{BV}} = \frac{d_{AO}}{\sqrt{2} d_{BO}} \qquad \text{Equation 5.2.4}$$

From the analysis above, it can be found that both the global instability index (**GII**) and bond-valence tolerance factor ($\boldsymbol{t_{BV}}$) are calculated fundamentally from d_{ij} and other parameters, and so there is a common response, as indicated in Figure 1.5.1 (b), between **GII** and $\boldsymbol{t_{BV}}$. This can explain the results for each ABO_3 type ($A^{1+}B^{5+}O_3$, $A^{2+}B^{4+}O_3$, $A^{3+}B^{3+}O_3$) shown in Figure 5.2.1 (a)-(c); however, for the whole range of ABO_3-type perovskites, the correlation is rather poor, which indicates that there is no unified relationship between $\boldsymbol{t_{BV}}$ and **GII** for all the types of ABO_3 perovskite. However, if each **GII** value in Figure 1.8.1 were

normalized by the valence of A-site cations, a unified correlation would emerge. The result is shown in Figure 5.2.2. Again, ANN was used to make the prediction of **GII** values from t_{BV} and the valences of A-site cations, and the result is shown in Figure 5.2.3.

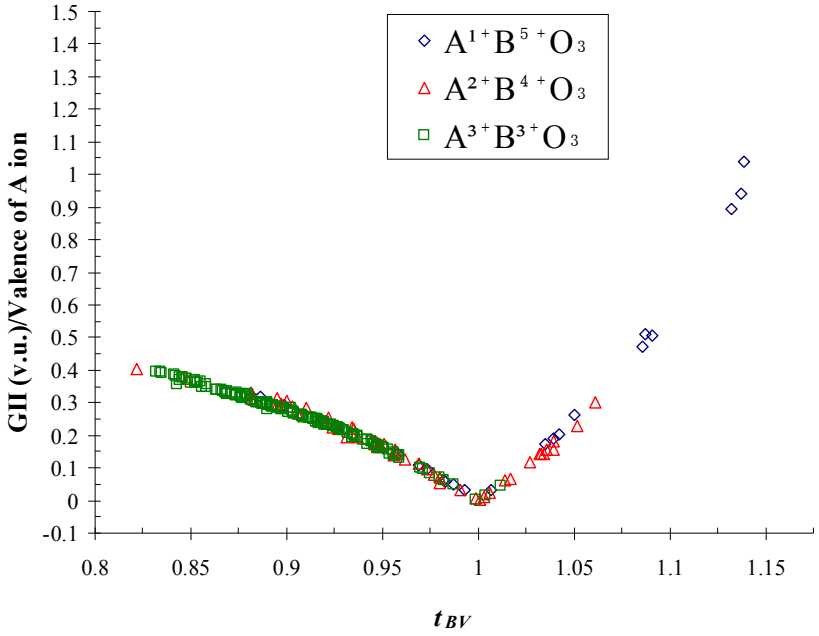

Figure 5.2.2 Global instability indices (**GII**) normalised by the valences of A-site cations *versus* bond-valence based tolerance factors (t_{BV}) for ABO_3-type perovskite compounds.

5.2.2 Prediction of Perovskite Formation

Here, a probabilistic neural network (PNN) is used to simulate the work done by Zhang *et al.* (**2007**) to predict the likelihood zone of perovskite compounds being formed, based on the same parameters they used, *i.e.*, ideal A-O and B-O bond distances derived from bond-valence model (BVM). The predictions are made for each type of perovskite ($A^{1+}B^{5+}O_3$, $A^{2+}B^{4+}O_3$ and $A^{3+}B^{3+}O_3$) and also for all ABO_3-type perovskites collectively. The results are shown in Figure 5.2.4 (a)-(d).

Figure 5.2.4 (a) shows that six $A^{1+}B^{5+}O_3$ structures are located in the wrong zone (six non-perovskites locate in perovskite zone), whereas in Zhang *et al.*'s (**2007**) work, seven such structures are located in the wrong zone. Similarly, Figure 5.2.4 (b) shows nine incorrect $A^{2+}B^{4+}O_3$ perovskite assignments, whereas Zhang

et al.'s (**2007**) have seventeen incorrect predictions; and Figure 5.2.4 (c) shows five incorrect $A^{3+}B^{3+}O_3$ perovskite assignments where Zhang *et al.* (**2007**) shows two, but all no non-perovskite assignment.

From these three comparisons, it is found that in the first two cases, the neural network performs a bit better in terms of predictive accuracy; however, in Zhang *et al.*'s work (**2007**), the boundaries for separating perovskite and non-perovskite zones are regular, which helped them to point out the conditions that determine the formability of ABO_3-type perovskite compounds. In the third case, Zhang *et al.* (**2007**) made all the predictions of non-perovskite structures correct but made two incorrect predictions of perovskites, while the neural network makes predictions of all perovskites correctly, but makes four false predictions of non-perovskites.

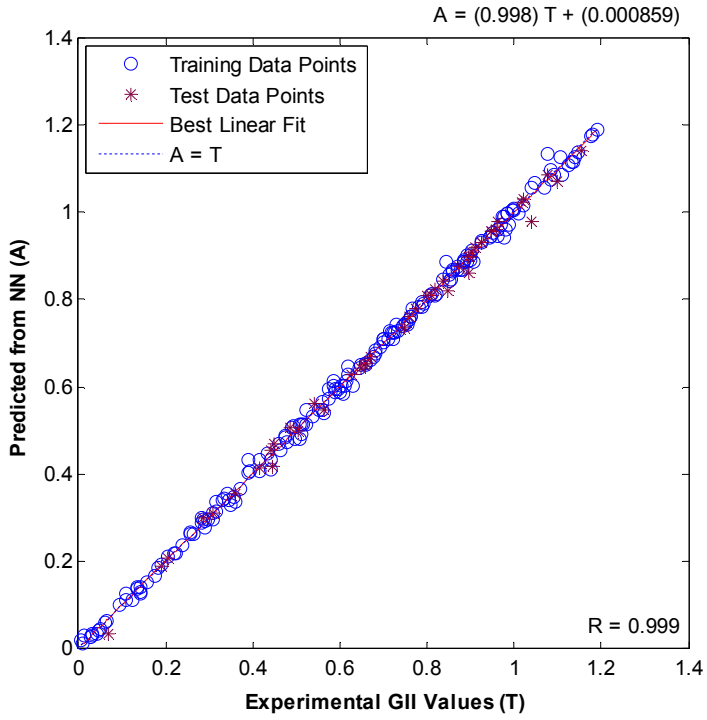

Figure 5.2.3 Prediction for perovskite formability of all ABO_3-type compounds from t_{BV} and valences of A ions by ANN.

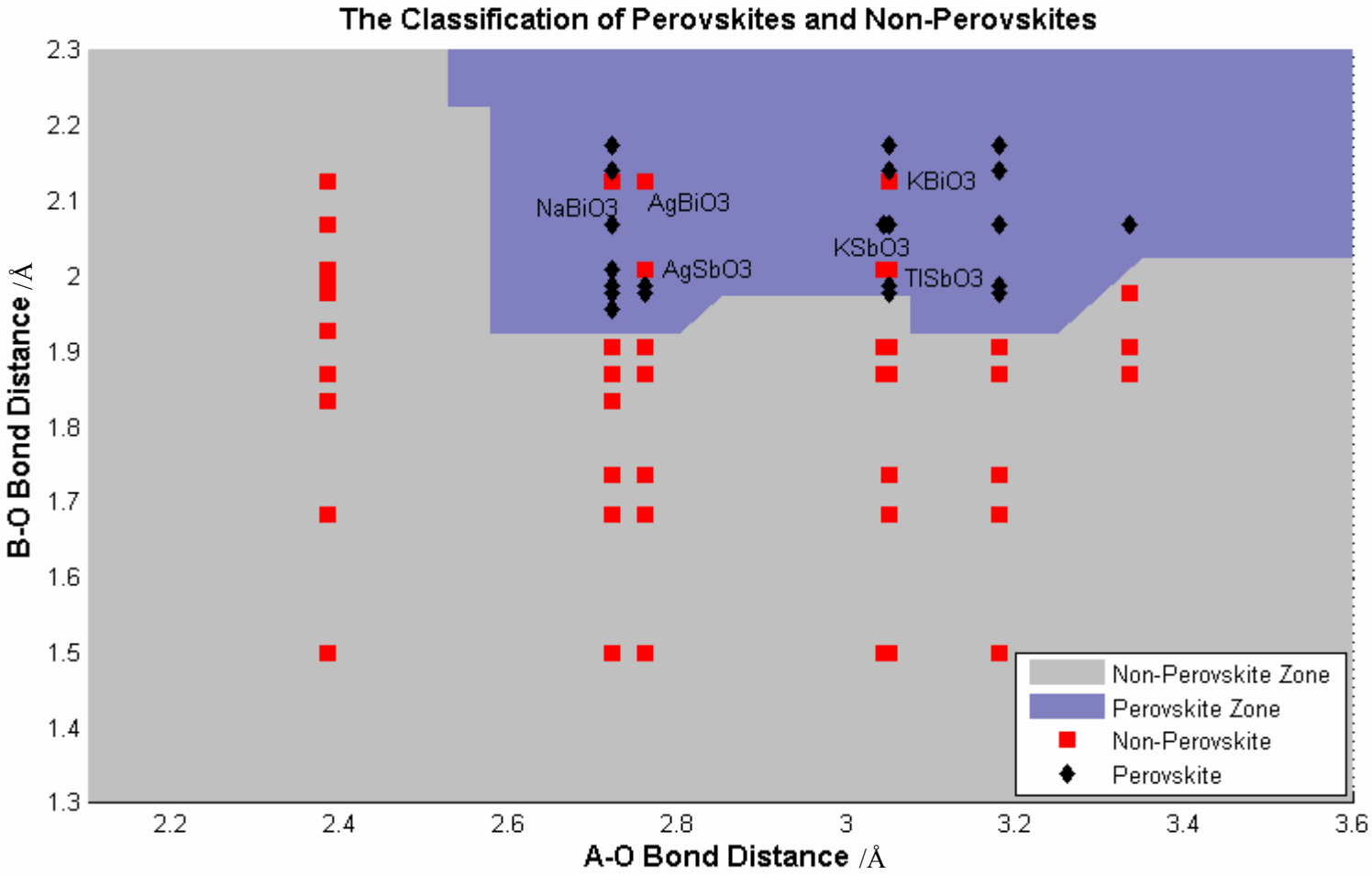

Figure 5.2.4 (a) Prediction for perovskite formability of the $A^{1+}B^{5+}O_3$ by ANN.

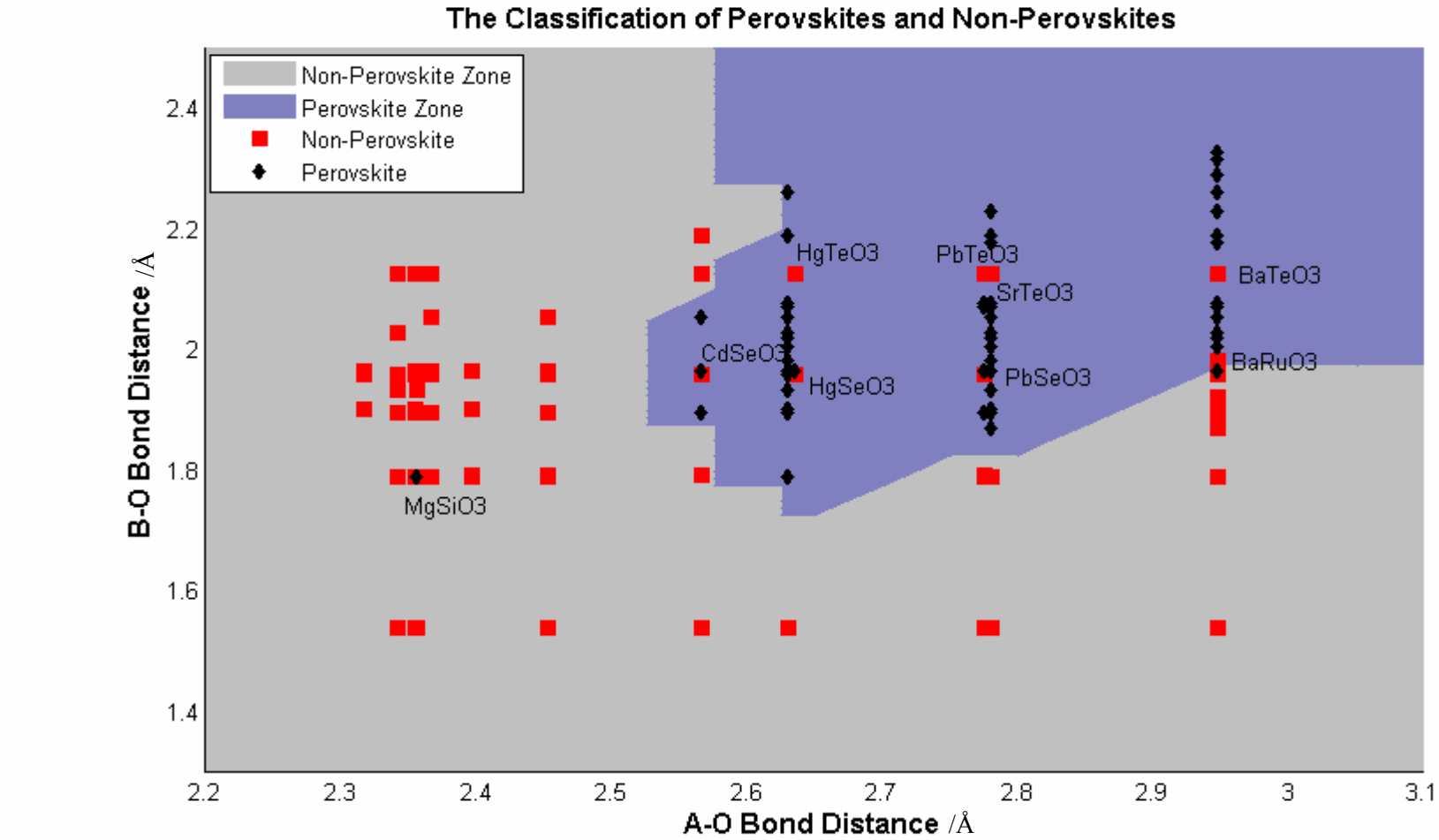

Figure 5.2.4 (b) Prediction for perovskite formability of the $A^{2+}B^{4+}O_3$ by ANN.

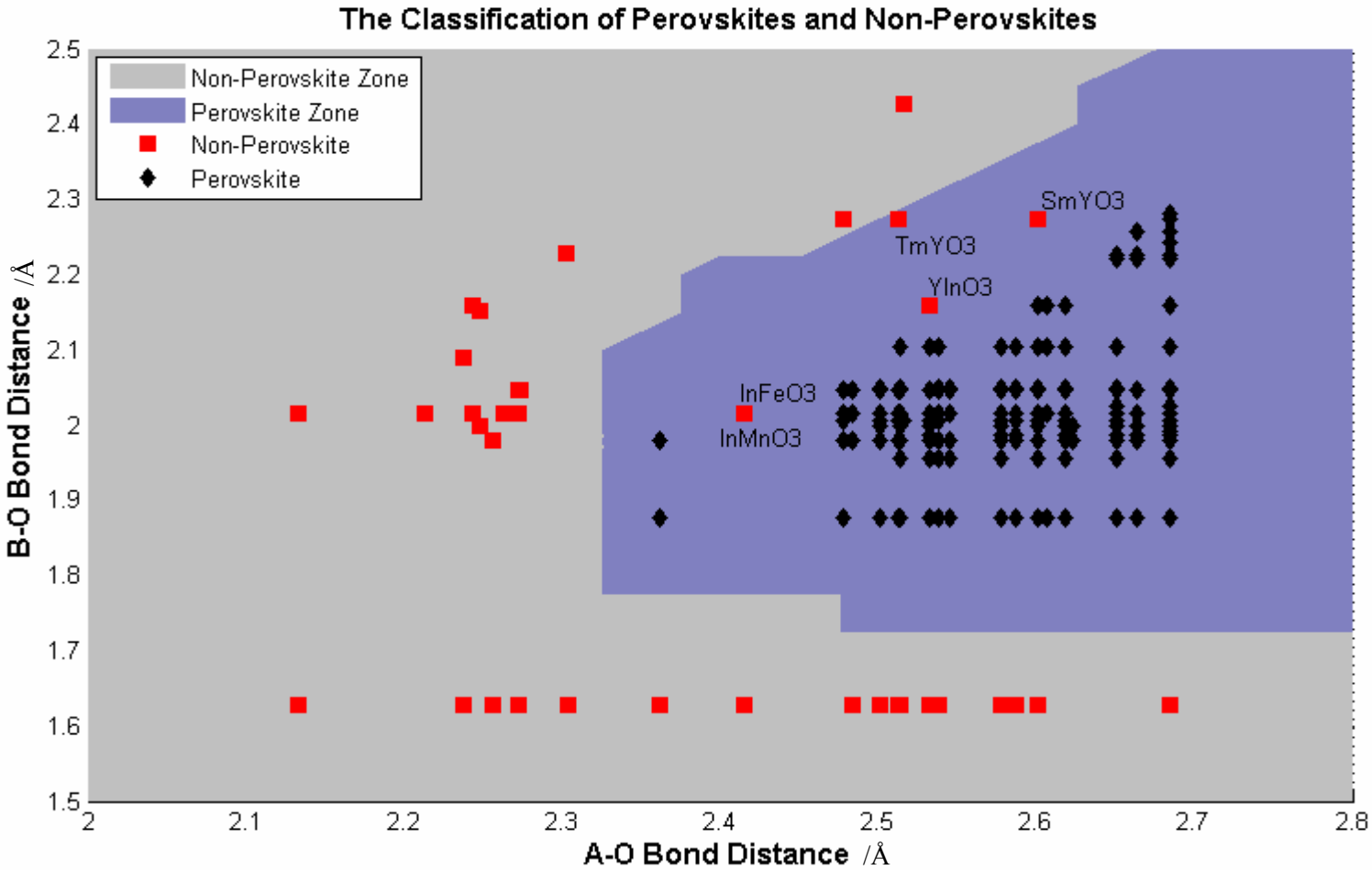

Figure 5.2.4 (c) Prediction for perovskite formability of the $A^{3+}B^{3+}O_3$ by ANN.

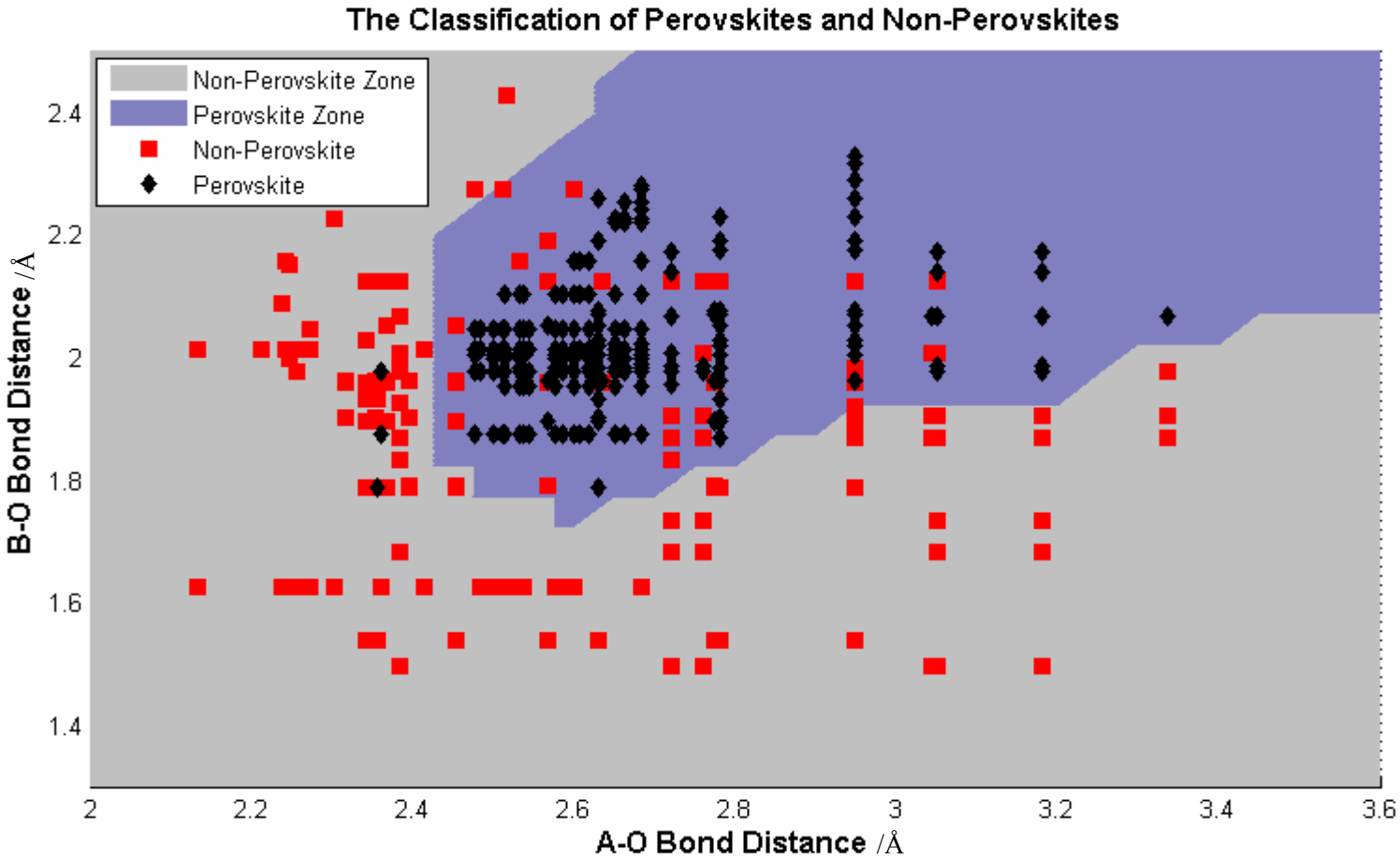

Figure 5.2.4 (d) Prediction for perovskite formability all type of ABO_3 by ANN.

6.0 Exploring unknown Cross-Properties Multiple Correlations using ANNs

6.1 Specific Experimental Details

6.1.1 Data Collection

Whole datasets of physical properties of solid elements were collected from handbooks, including Chemistry Data Handbook (CDH) (**Start and Wallace, 1982**), The Lange's Handbook of Chemistry (LHC) (**Speight, 2005**), The Elements (ELE) (**Emsley, 1998**), Table of Physical and Chemical Constants (TPC) (**Kaye and Laby, 1995**) and CRC Handbook of Chemistry and Physics (CRC) (**David, 2000**). The properties were collected for the same pressure (0.1 MPa), over a small temperature range (293~298 K) and in the solid state. The sixteen properties collected were i) normal melting point, ii) normal boiling point, iii) heat of fusion under normal melting point, iv) heat of vaporization under normal boiling point, v) molar heat capacity, vi) specific heat capacity, vii) thermal conductivity, viii) electrical conductivity, ix) photoelectric work function, x) linear thermal expansion coefficient, xi) atomic weight, xii) density, xiii) electronegativity (Pauling), xiv) first ionization potential, xv) polarizability and xvi) atomic volume. The minor exceptions are mentioned in Tables A1 to A16 (**Appendix 3**). The elements for which data was collected satisfied two criteria: 1) they are in solid state under 293~298 K and 0.1 MPa pressure; 2) they have a full record of all sixteen properties from above five handbooks. The reason for those criteria is: phase present, temperature and pressure are factors that would affect some kinds of properties. However, introducing these three parameters would weaken the generality of correlation between different properties due to the common response of composition, structure and bonding. In total, 75 elements are included.

From section 4, it has been found that there are always incorrect data in handbooks. As a result, it is necessary to have an idea about the uncertainty of the correctness for the data that is used and hence the uncertainty in the correlation explored from using these data.

The details of the data recorded from five different handbooks are listed in Tables A1-A16 and are sorted with ascending levels of variability of property P; $(P_{max}-P_{min})/P_{min}$. The data used for exploring property correlations are marked in bold and were converted to SI units before being input. Most of the elements have consistent values across the five handbooks and these values can be treated as reliable. Data clustered in a narrow range can be treated as correct since they are obtained from different sources. Identical data could have been copied. Outliers are treated as incorrect due to incorrect unit conversions, decimal point misplacements, different reference conditions or other reasons. Median values of each property from five different recordings were treated as correct. The neural network method developed in section 4 can be used to identify errors and select correct values.

6.1.2 Pre-treatment of the Data

It is well known that the materials properties vary over considerable ranges and are generally logarithmically distributed (**Ashby, 1998; Bassetti *et al.*, 1998; Ashby *et al.*, 2007**). Sha (**2008**) noted that the network can be misled by a few data far away from the average when training neural networks with skewed data because, unlike linear regression, neural network training does not have a definitive starting formula. For the neural network, logarithmic pre-treatment for properties that are logarithmically distributed is needed.

The pre-treatment of the data was as follows. Electrical resistivity was converted to electrical conductivity. From observation of these figures, it can be found that the distribution of 1) atomic volume, 2) polarizability, 3) linear thermal expansion coefficient, 4) electrical conductivity, 5) thermal conductivity, 6) specific heat capacity and 7) heat of fusion are skewed. So these data need logarithmic pre-treatment. However, from the data listed in Table A11 and shown in Figure A1 (xi) (**Appendix 4**), the electrical conductivity disperses over such a large range that taking logarithmic pre-treatment cannot normalize the distribution. Further, some data can be interpreted as sensitive to impurities (e.g. Si, Ge), and this introduces uncertainties for extracting a general correlation between properties. As a result, electrical conductivity was not introduced for exploration of property relationships. Figures A2 (i)-(vi) show the distribution of

these six properties after taking logarithms. From Figure A2 (i)-(vi), the values for atomic volume, polarizability, linear thermal expansion coefficient and heat of fusion become uniformly distributed; while for thermal conductivity and specific heat capacity, the distributions are enhanced.

As a result, the whole group of property values are 1) melting point (original value), 2) boiling point (original value), 3) atomic volume (logarithmic value), 4) polarizability (logarithmic value), 5) first ionization potential (original value), 6) electronegativity (original value), 7) density (original value), 8) atomic weight (original value), 9) linear thermal expansion coefficient (logarithmic value), 10) photonic work function (original value), 11) thermal conductivity (logarithmic value), 12) specific heat capacity (logarithmic value), 13) molar heat capacity (original value), 14) heat of vaporization (original value), 15) heat of fusion (logarithmic value). All or part of these property values constitute inputs for the neural network. Each of them in turn is also used as an output. When property values were used for output, the original values were adopted, because the neural network training is based on minimization of the difference between predicted values and experimental values. And small differences in logarithmic values correspond to large differences in original values.

6.1.3 Determination of Input and Output Parameters

Of all sixteen properties, one is taken as the property to be predicted (as an output of the neural network) in turn, and all other properties left constitute a whole set. Within the whole set, different numbers of properties with different combinations were chosen to form property groups used for predicting the named property (as input parameters of the neural networks). This process was repeated by taking each of sixteen properties one by one as a property to be predicted. Finally, when some properties values can be reasonably predicted from groups of other properties, then we can say that all of these properties are correlated.

When considering how to find the closest and highest performance for both training and testing sets, a distribution was selected on the basis of $\omega=\left|\varphi^2_{training}-\varphi^2_{testing}\right|$, where $\varphi = |M-1|+(1-R)$, and the smallest value of ω was chosen.

6.2 Results

In recent years, the range of applications of electric polarizabilities and hyper-polarizabilities has expanded dramatically (**Bonin and Kresin, 1997; Maroulis, 2006; Maroulis and Hohm, 2009**). As a result, in this work, examples of the predictions of polarizability from other 14 different properties are taken to show the process of using this method to explore correlations between diverse properties without employing the structure-property arrow of causation.

This starts with the prediction of polarizability from each of 14 properties in order to separate out the properties that present strong predictability for polarizability when using each of them individually. That is, to investigate if polarizability has direct correlation with each of them. The other properties are treated as properties that have weak or no direct correlation with polarizability. However, this does not exclude the possibility that for these properties a combination of them or a combination with previously separated properties can make a prediction, or even can improve the predictability compared with the cases in which they are excluded.

As the square of the correlation coefficient, R^2, is the proportion of the variation in the values of y that is explained by the least-squares regression of y on x and ignores the distinction between explanatory and response variables, the R^2 in our case, can be used to represent the proportion of the variation in the experimental values that is explained by the straight-line tie between predicted values and experimental values. When $R = 0.9$, $R^2 = 0.81$ and about 80% of the variation is accounted for by the straight-line relationship. Here, we use the criterion of $R = 0.9$, and determine the correlations with R values greater than 0.9 as being significant. Figures 6.2.1 (a)-(d) show the results of prediction of polarizability with R values greater than 0.9 and the Table 6.2.1 lists the statistical analysis for results shown in Figure 6.2.1

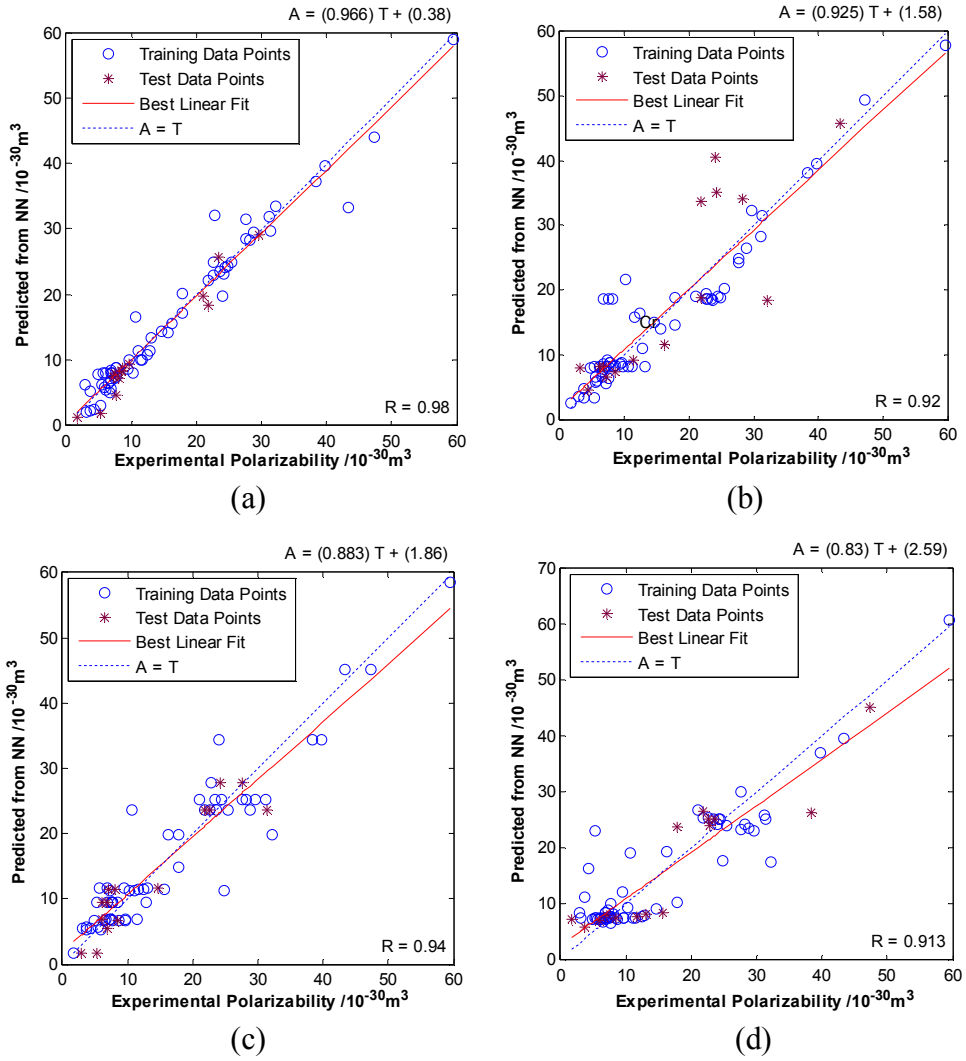

Figure 6.2.1 Results of prediction for polarizability with R values greater than 0.9, a) Prediction from atomic weight; b) Prediction from first ionization potential; c) electronegativity; d) work function.

Table 6.2.1 Statistical analysis for the results shown in Figure 6.2.1.

Conditions	Test set						Whole set					
	M	R	MME /$10^{-30}m^3$	SDME /$10^{-30}m^3$	MPME /%	SDPME /%	M	R	MME /$10^{-30}m^3$	SDME /$10^{-30}m^3$	MPME /%	SDPME /%
(a)	1.01	0.980	1.15	1.29	13.7	19.1	0.970	0.980	1.49	1.80	15.1	19.6
(b)	1.04	0.860	5.40	5.22	36.0	39.5	0.925	0.920	3.21	3.53	27.3	35.0
(c)	0.912	0.937	2.64	1.90	28.9	21.2	0.883	0.940	2.90	2.80	25.4	24.7
(d)	0.852	0.920	3.78	3.12	42.8	76.9	0.830	0.913	3.45	3.39	38.2	65.7

MME: Mean of error modulus

SDME: Standard deviation of error modulus

MPME: Mean of percentage error modulus

SDPME: Standard deviation of percentage error modulus

Table 6.2.2 Statistical analysis for the results shown in Figure 6.2.2.

Results	Test set						Whole set					
	M	R	MME /$10^{-30}m^3$	SDME /$10^{-30}m^3$	MPME /%	SDPME /%	M	R	MME /$10^{-30}m^3$	SDME /$10^{-30}m^3$	MPME /%	SDPME /%
Melting point (T_m), Heat of vaporization (ΔH_V), specific heat capacity (C_P) and first ionization potential (E_I)	1.01	0.97	1.66	1.35	15.3	15.2	0.994	0.995	0.808	0.893	6.80	8.95

Thus we have located four properties that have relatively strong correlations with polarizability and separated the other ten properties that have relative weak or even no correlations with polarizability. In the next step, based on these four properties, systematically to introduce other properties to see if continuous improvements in the prediction results, and thus to find the effect of each property on the prediction. However, the properties are obtained from different levels of structure, or even combinations of different levels of structure, and so these properties can be treated as confounding effects of different levels of structure, as shown in Figure 1.5.1(c). It needs to be clarified that the correlations between structures and properties are direct cause-effect, while those between different levels of structure and properties may be confounding. As a result, the correlations between the properties that are used for making prediction may also be confounding. As mentioned in section 1.5.2, since the effects of properties are confounded together, the influence of one property cannot be distinguished from the influence of other properties; also, it cannot be said how strong the effect of one property on polarizability is. This leads to some properties, which cannot make a prediction alone, having an effect or even a strong effect on the prediction when combined with other properties.

So, in this step, it focus on the results that show a high degree of correlation between polarizability and different combinations of other properties, and then from these results, try to find the underlying physical principles and the reasons why different combinations of properties can have similar prediction performance. The criterion used here is R^2 = 99%, which corresponding to R = 0.995 and the slope M equal to or greater than 0.99. In total, there are 665 combinations of different numbers of different kinds of properties. These different combinations are treated as having the same capability for prediction of polarizability. Due to the confounding effect mentioned before, it is still difficult to employ a systematic method. In this work, it started from the analysis of the results for the prediction using a combination of the minimum number of properties, namely the prediction of polarizability from melting point, heat of vaporization, specific heat capacity and first ionization potential. The results are shown in Figure 6.2.2, and the statistical analysis for these results are shown in Table 6.2.2.

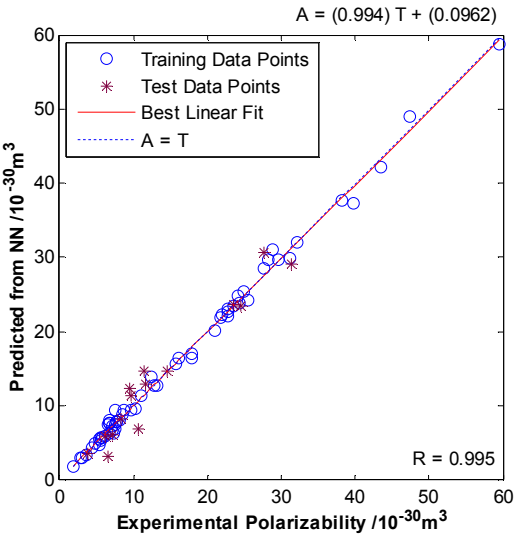

Figure 6.2.2 Result of prediction of polarizability using melting point, heat of vaporization, specific heat capacity and first ionization potential.

The following analysis for these five results (shown in Figures 6.2.1 and 6.2.2) includes the following stages: 1) Exploration of underlying physical principles for results shown in Figure 6.2.1, in order to verify the feasibility of adopting this method to explore cross-property relationships; 2) Analysis of the result shown in Figure 6.2.2, and comparison of this result with other results to explore the possible confounding effect of different properties; 3) Exploration of the possible mathematical equations that can formulate and generalize these correlations.

6.3 Discussion

6.3.1 Exploring Underlying Physical Principles

The polarizability in this work is the average static electric dipole polarizability (expressed as a polarizability volume by dividing $4\pi\varepsilon_0$, where ε_0 is the permittivity of vacuum). The polarizability of an atom or molecule is a coefficient for describing the response of the electron cloud to an external electric field having low power, which is a measure of the ease with which its electron cloud can be pulled away from the nucleus.

Correlation between polarizability and atomic weight

From the results shown in Figure 6.2.1(a), the correlation between polarizability and atomic weight is the strongest compared with other combinations, so it is interesting to find the underlying physical principles. It has been known that the polarizability increases with atomic weight for elements in the same family because the atomic size increases, which has been shown by many people's work, such as Debye (**1929**), Clark (**1934**), Denbigh (**1940**), Atoji (**1956**), Pauling (**1960**) and Ghanty and Ghosh (**1996**); and decreases with increasing atomic weight for elements in the same row of the periodic table as the outer-shell orbitals are being increasingly filled (**Yang, 2003**). From that, it is easily to think of the trends that exist in the periodic table and so it is natural to draw these two properties together and to see whether there is a trend.

Expressing these two properties on a Cartesian coordinate system, as shown in Figure 6.3.1, it can be easily found that these two properties follow a periodic trend.

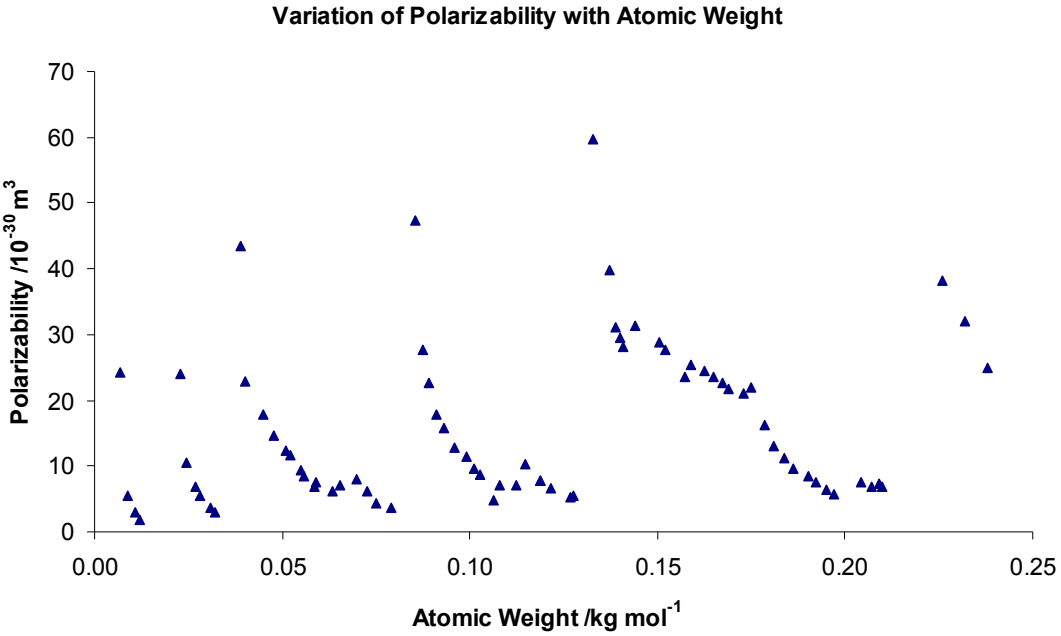

Figure 6.3.1 Variation of polarizability with atomic weight.

Correlation between polarizability and first ionization potential

Comparing the polarizability, which measures the response of an atomic system to an external electric field, the first ionization potential measures the extraction energy of the outermost electron of the atom. Dmitrieva and Plindov (**1983**) pointed out the correlation between first ionization potential (IP) and polarizability (α) follows $\alpha^{1/3}$ = 1.09/IP. Fricke (**1986**) also argued that an increasing first ionization potential implies a decreasing polarizability, and they obey direct IP ~ 1/α correlation when plotted on a double-logarithmic scale. Schwerdtfeger (**2006**) stated the relationship is in the form of $\alpha \sim 1/IP^2$. However, for all the above three cases, the trends are visible, but the two quantities are not correlated strongly in a general way for all the elements. These are explained by the fact that the structure of the valence electrons of each element is very different, and the relativistic effects that exist change the trend in polarizability within a Group of the periodic table. The result shown in Figure 6.2.1(b) is consistent to the above explanations.

Correlation between polarizability and electronegativity

The correlation between polarizability and electronegativity has also been explored. Komorowski (**1987**) applied an electrodynamical equation to the

chemical potential by analogy and got an inverse relationship between polarizability and electronegativity; Van Genechten *et al.* (**1987**) applied the electronegativity equalization method to calculate values of average electronegativity and related these values to the polarizability: large electronegativity is consistent with a low polarizability. However, in these two works, the correlations are not explored in detail. Nagle (**1990**) employed the concept of valence electron density (**Gorbunov and Kaganyuk, 1986; Gorbunov and Filippov, 1988**), and got a function of the number of valence electrons divided by polarizability, n/α. Then, the cube root of this ratio, $(n/\alpha)^{1/3}$, can be used for calculating the electronegativity χ: $\chi = 1.66\ (n/\alpha)^{1/3} + 0.37$ for s- and p-block elements, and it also can be applied to d- and f-block elements if the number of "valence" electrons for these elements can be determined from a careful analysis of their atomic spectra. Further proofs can be derived from the facts that there are correlations existing between atomic radii and polarizability, and also between atomic radii and electronegativity, such as the work done by Ghanty and Ghosh (**1996**). So, the polarizability and electronegativity can be treated as common responses from atomic radii, as shown in Figure 1.5.1(b). The discussion in the above cases describes the relationship between polarizability and electronegativity from a physical perspective, and also states there is no direct relationship between them. In order to make a comprehensive and general prediction, other parameters must be introduced.

Correlation between polarizability and work function

The electron work function ø is a measure of the minimum energy required to extract an electron from the surface of a solid, which was first pointed out by Lester (**1916**). It can be measured from thermionic, photoelectric or contact potential methods. Different methods are applied in different conditions. As mentioned by Michaelson (**1977**), the thermionic method cannot give the absolute value for polycrystalline or other patchy surfaces, while the photoelectric method does not yield the true work function for semiconductors because the emission contains contributions of both volume and surface origin. The critical review of different measurement methods and the rationale for selecting preferred values are discussed by Rivière (**1969**).

Like most of the chemical properties of the elements, the work function is a periodic function of atomic number when the values are carefully selected (**Morecroft, 1936; Klein and Lange, 1938; Scarpa, 1940 and 1941**). Michaelson (**1950, 1977**) used representative values; either the unweighted mean of the values obtained from using different measurement methods for each element, or the values for polycrystalline solids, to plot a figure of work function vs. atomic number. For both of these cases, even though the data were less reliable in 1950, the periodic trend can be observed. As a result, the work function has a correlation with atomic number, which is the same trend as the variations of polarizability.

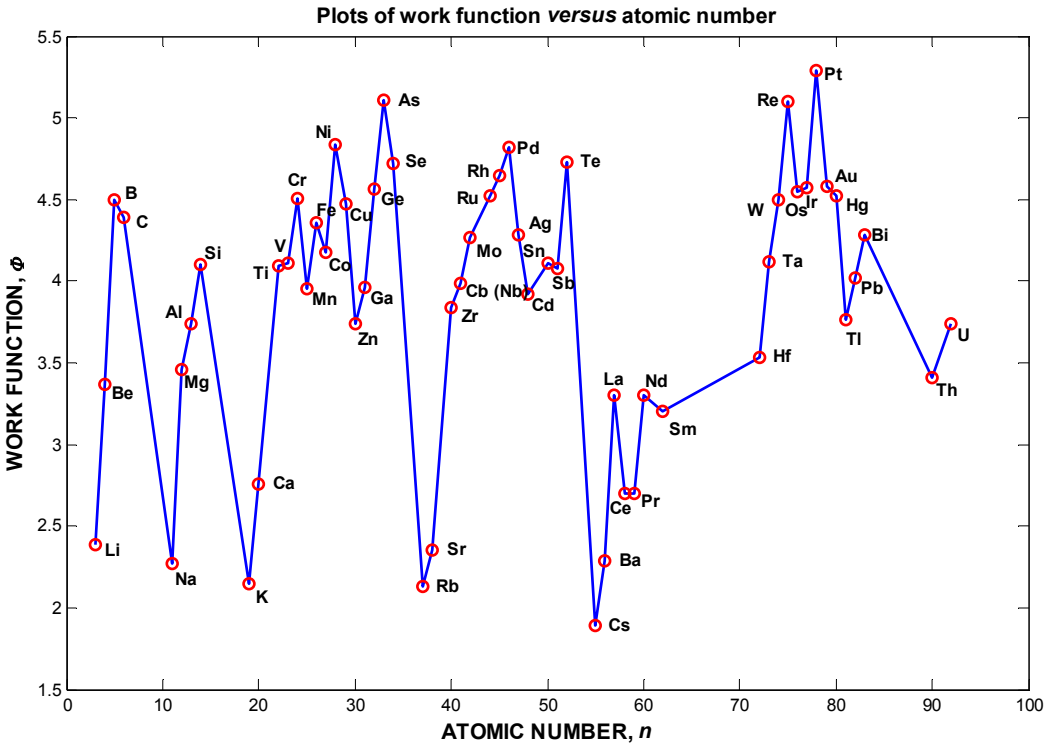

Figure 6.3.2 Plots of work function *versus* atomic number (Drawn from the values shown in **Michaelson, 1950**).

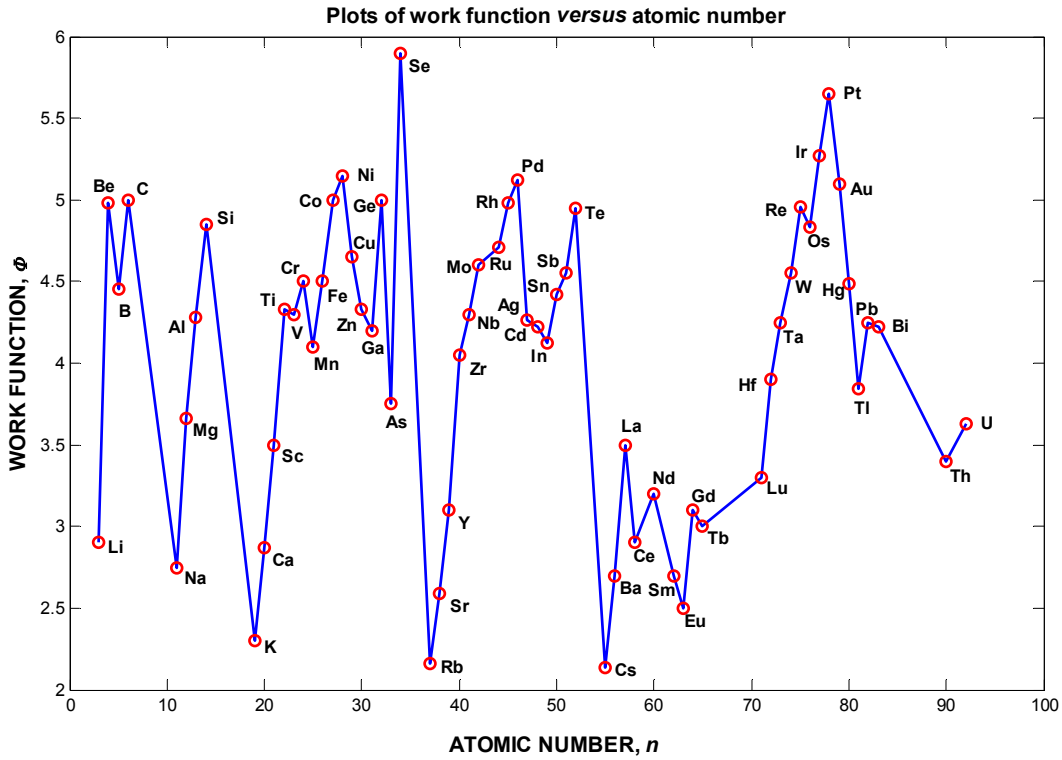

Figure 6.3.3 Relation of experimental values of the work function to the periodic system of the elements. (Drawn from the values shown in **Michaelson, 1977**).

Further proof can be found from the facts that 1) the empirical correlation between work functions and atomic weights has been derived by Rother and Bomke (**1933**); 2) Bedreag (**1946**) pointed out the correlation between work function and first ionization potential that exists within alkali metals. From before, we have got the periodic correlation between polarizability and atomic weight and so there is indeed some correlation existing between polarizability and the work function.

However, from the Figure 6.2.1(d) shown, this correlation is not very strong. The reasons are as follow:

1) The values used in this work are single values (polycrystalline, or unweighted mean values for all facets), taken from handbooks. However, the choice of preferred single values is complicated by the variations produced from the purity of the specimen, the measurement method and the surface distribution of crystal

facets (**Michaelson, 1977**). Firstly, the measurements of work function are extremely sensitive to the presence of surface impurities, such as oxides and gases (**Michaelson, 1950**). When the measurement is not carried out under ultrahigh vacua, the result is affected by trace impurities (**Michaelson, 1977**). An example is the value for Be. It has been accepted that the value is 5 eV, as employed in this work, as determined first by Dixon and Lott (**1969**) and confirmed later by Gustafsson *et al.* (**1974**). However, the previously accepted value is about 3.9 eV, as recorded in *Table of Physical and Chemical Constants* (as shown in Table A10), which is due to mercury vapour contamination. Further, the anisotropy (**Martin, 1939; Smoluchowski, 1941**), allotropy (**Goetz, 1929; Wahlin, 1942**) and temperature dependence (**Potter, 1940; Seely, 1941; Smith, 1949; Markham and Miller, 1949**) complicate the values of work functions, although the difference is not great. The data recorded in handbooks have these uncertainties.

2) For semiconductor elements, variations, although not great, exist among the values obtained from different methods of measurement (**Condon, 1938; Apker *et al.*, 1948**). Also, for the data for As (**Raisin and Pinchaux, 1975**), Te (**Williams and Polanco, 1974**) and Se (**Williams and Polanco, 1974**), which belong to semiconductors, are derived from photoelectric methods. It is stated before that the photoelectric method cannot yield the true work function for semiconductors. Actually, these values cannot be confirmed by measurements made with ultrahigh vacuum techniques. So, as suggested by Michaelson (**1977**), these values are only to be treated as possibly valid but of unknown reliability, and only can be accepted simply as being the best available and not necessarily as absolute physical quantities.

3) The periodic trend found by Michaelson (**1950, 1977**), as shown in Figures 6.3.2 and 6.3.3, is obvious, but not rigorous. As mentioned by him, in each period, the work function value tends to rise with increasing atomic number, as electron shells and subshells gradually become filled; however, the relation becomes complex in the intervals occupied by the transition metals.

6.3.2 Exploring Possible Confounding Effects of Different Properties

The results shown in Figure 6.2.2 indicate the confounding effect of melting point, heat of vaporization, specific heat capacity and first ionization potential on polarizability. It is desirable to see the relative importance of each input property on the prediction of polarizability. Before that, in order to see the effect on the prediction from different input properties separately, the correlations between each of these four properties are investigated by running the neural network to predict each of the properties from one of others; in total there are six pairs. It is found that there is a strong correlation between melting point and heat of vaporization, but there is no correlation between each other for the other five pairs (shown in Table 6.3.1, only melting point and heat of vaporization have high R and M values which indicate a strong correlation. All of the others, have very low R and M values which indicate a very weak correlation). As a result, it can be said that the predictability of polarizability comes from three distinct parts: 1) first ionization potential, 2) specific heat capacity and 3) melting point and/or heat of vaporization.

Table 6.3.1 Correlations between input properties. A strong correlation only exists between melting point and heat of vaporization.

Conditions		M	R
Predicted property	**Input property**		
Melting point	Heat of vaporization	0.886	0.912
Heat of vaporization	Melting point	0.854	0.914
Melting point	Specific heat capacity	0.48	0.472
Specific heat capacity	Melting point	0.275	0.541
Melting point	First ionization potential	0.4	0.665
First ionization potential	Melting point	0.111	0.326
Heat of vaporization	Specific heat capacity	0.0606	0.251
Specific heat capacity	Heat of vaporization	0.592	0.665
Heat of vaporization	First ionization potential	0.562	0.669
First ionization potential	Heat of vaporization	0.697	0.724
Specific heat capacity	First ionization potential	0.00108	0.132
First ionization potential	Specific heat capacity	0.463	0.638

In the following stage, the relative importance of each property is explored. Based on the result shown in Figure 6.2.2, the relative importance of each property is compared by running the network with one input property omitted at a time and the results are shown in Table 6.3.2. From observing all the parameters for these four different cases, it can easily be found that the relative importance of each property for the prediction of polarizability follows a descending order: first ionization potential, melting point, heat of vaporization and specific heat capacity. That is, the predictability of polarizability mostly comes from the first ionization potential, then smaller parts from melting point and heat of vaporization (also, melting point contributes more than heat of vaporization), and the smallest part comes from specific heat capacity.

The strong correlation between polarizability and first ionization potential has been discussed in the previous section. The correlations between polarizability and the other three properties (i.e. melting point, heat of vaporization and specific heat capacity) are compared in Table 6.3.3. From looking at these results, it can easily be found that the correlation between polarizability and these three properties are weak, following the order of degree of weakness: heat of vaporization, melting point and specific heat capacity. From this, it can be seen that although these properties have weak correlations with polarizability, the predictability can be improved when confound with the other two properties; notably, the melting point makes more contribution to the predictability of polarizability than heat of vaporization, when confound with the other two properties, although the predictability is weaker than heat of vaporization when used alone.

In the next stage, pairs of parameters are selected to predict polarizability: (1) melting point and heat of vaporization; (2) melting point and specific heat capacity; (3) heat of vaporization and specific heat capacity; (4) specific heat capacity and first ionization potential; (5) heat of vaporization and first ionization potential and (6) melting point and first ionization potential. They are shown in Table 6.3.4.

Table 6.3.2 Comparison of the criteria for predicting polarizability using different combinations of three parameters.

Conditions	Test set						Whole set					
	M	**R**	**MME /$10^{-30}m^3$**	**SDME /$10^{-30}m^3$**	**MPME /%**	**SDPME /%**	**M**	**R**	**MME /$10^{-30}m^3$**	**SDME /$10^{-30}m^3$**	**MPME /%**	**SDPME /%**
T_m, ΔH_V, and C_P	0.0674	0.314	9.80	7.17	84.6	86.2	0.0619	0.291	9.16	6.73	94.3	96.3
ΔH_V, C_P, and E_I	0.913	0.932	3.28	3.18	25.7	29.6	0.902	0.947	2.59	2.82	23.6	31.4
T_m, C_P, and E_I	0.995	0.948	2.24	1.68	24.4	23.1	0.961	0.978	1.71	1.79	15.4	20.2
T_m, ΔH_V, and E_I	1.01	0.963	2.21	2.32	17.8	25.0	0.98	0.983	1.61	1.50	16.0	18.6

Table 6.3.3 Comparison of the criteria for predicting polarizability using melting point, heat of vaporization, and specific heat capacity respectively.

Conditions	Test set						Whole set					
	M	**R**	**MME /$10^{-30}m^3$**	**SDME /$10^{-30}m^3$**	**MPME /%**	**SDPME /%**	**M**	**R**	**MME /$10^{-30}m^3$**	**SDME /$10^{-30}m^3$**	**MPME /%**	**SDPME /%**
T_m	0.210	0.482	6.80	5.31	84.6	145	0.247	0.523	7.86	6.35	90.0	132
ΔH_V	0.682	0.695	9.71	7.05	85.9	78.4	0.615	0.735	6.37	5.09	65.1	76.9
C_P	0.158	0.279	7.62	5.36	158	192	0.155	0.415	8.00	7.31	93.1	118

Table 6.3.4 Comparison of the criteria for predicting polarizability using different combinations of two parameters.

Conditions	Test set						Whole set					
	M	R	MME /$10^{-30}m^3$	SDME /$10^{-30}m^3$	MPME /%	SDPME /%	M	R	MME /$10^{-30}m^3$	SDME /$10^{-30}m^3$	MPME /%	SDPME /%
T_m, ΔH_V	0.0253	0.206	9.66	9.78	80.6	69.7	0.0304	0.203	9.56	6.57	103	113
T_m, C_P	0.0277	0.319	11.6	10.4	103	106	0.0511	0.277	9.28	6.67	94.7	91.3
ΔH_V, C_P	0.0919	0.273	8.04	4.89	102	125	0.0693	0.285	9.28	6.53	100	107
C_P, E_I	0.901	0.913	2.65	4.26	28.4	53.2	0.887	0.936	2.70	3.18	25.8	36.5
ΔH_V, E_I	0.909	0.874	3.24	3.98	32.7	55.1	0.874	0.927	3.04	3.26	28.9	42.1
T_m, E_I	0.958	0.966	2.12	2.23	25.2	39.8	0.900	0.948	2.59	2.75	24.4	34.5

From observing these results, it can be found that the combination of melting point and heat of vaporization has the weakest predictability. The reason is that, as mention before, the predictability of polarizability comes from three parts and due to the correlation that exists between melting point and heat of vaporization, the effect of melting point and heat of vaporization can be treated as the same one part and this single part cannot make the prediction better. Then from the second and third row, the role of specific heat capacity is introduced, and the performance is improved and from these two results, it is also found that when confounded with specific heat capacity, the heat of vaporization has better prediction performance than melting point, which is consistent with the trend when using melting point or heat of vaporization alone. From looking at rows 4 to 6, the first ionization potential is introduced, which has a single correlation with polarizability and the performance is improved further. Observing these three rows confirms the ascending effect of specific heat capacity, heat of vaporization and melting point on the prediction of polarizability when confound with polarizability as discussed before.

From the discussions made above, it can be concluded that: within the group of properties consisting of melting point, heat of vaporization, specific heat capacity and first ionization potential, the first ionization potential plays the most important part, the melting point and heat of vaporization play a similar role and the second most important effect while the specific heat capacity plays the least important part. For melting point and heat of vaporization, the heat of vaporization has higher predictability for polarizability when testing each of them alone, or confounding each with specific heat capacity. However, when confound with first ionization potential, the melting point has a higher performance. For all the inputs that do not adopt the property of first ionization potential, the correlations with polarizability are very weak; however, when they are confounded with first ionization potential, the performance is improved a lot (from M=0.925, R=0.92 to M=0.994, R=0.995).

6.3.3 Exploration of Possible Mathematical Equations that can Formulate Correlations

To extend these ideas, it would be more interesting to find possible mathematical functions that can describe the correlations found by the neural network. Recently this has been demonstrated by Schmidt and Lipson (**2009**), who used genetic programming to extract Hamiltonians and other laws by automatically searching motion-tracking data captured from chaotic double-pendula. So it will be possible to find mathematical equations from these correlations in the future. However, in the method proposed by Schmidt and Lipson (**2009**), researchers still need to identify mathematical building blocks such as algebraic operators, analytical functions, *etc*. So, it is reasonable to speculate some building blocks by visualizing the functional relationship which is captured by the neural network, in order to see the variance of polarizability in terms of the input properties. However, for the result shown in Figure 6.2.2, the neural network captured the correlation between polarizability and the other four different properties (i.e. melting point, heat of vaporization, specific heat capacity and first ionization potential); it is very difficult for us to visualize this kind of functional correlation, which locates within a 5-D space.

In order to visualize the functional relationship that the neural network captured, we analyzed the result for the prediction of polarizability from two other properties. Within all the results of prediction of polarizability from two properties, the prediction from atomic weight and electronegativity performs best, which has M=0.994, R=0.994, as shown in Figure 6.3.4. As a result, we analyze the variance of polarizability in terms of two input properties on this result.

Now in this case, it is possible to interpret the results visually by drawing a 3-D diagram. The interpretation is shown in Figure 6.3.5, which is constructed as follows:

1. The atomic weight A_W is placed on x-axis, electronegativity χ is placed on y-axis, and polarizability α is placed on z axis.
2. The property data for 75 elements are plotted directly. The training set and testing set are shown as red and green dots respectively. For these data, the

atomic weight values are within the range of 0.0069 kg mol^{-1} – 0.238 kg mol^{-1}; while the electronegativity values are within the range of 0.7 – 2.5.

3. The ANN, which was constructed from the training set (red dots), was fed with *artificial* atomic weights from 0.0069 to 0.238 (50 equally spaced data points) and *artificial* electronegativity from 0.7 to 2.5 (50 equally spaced data points) to predict corresponding polarizability. Those data were then used to draw the surface, which is shown in Figure 6.3.5 as a semi-transparent net.

From Figure 6.3.5, it can be found that, from the training set, the neural network has captured a functional surface and nearly all the testing set are located on this surface. This means the choice of the training set covers the problem domain, and the neural network captured the complex functional correlationships.

It is not immediately obvious what Figure 6.3.5 signifies, nor what it might signify if this methodology were applied, not to the elements, but to a class of materials with continuously varying composition.

The surface in Figure 6.3.5 is a map of property correlations upon which most of the elements repose. However the correlation is also valid for elements that do not and cannot exist. The surface predicts the polarizability of these imaginary elements in terms of their atomic weight and electronegativity. If it were possible to change the electronegativity of an element while keeping its atomic weight constant, Figure 6.3.5 predicts its new polarizability.

Designation of the elements arises from a discrete variable; atomic number. However, materials which are a mixture of 2 to n components are defined by composition which is a continuous variable and moreover, have properties which are measured in continuous variables. The derivation of such a map as Figure 6.3.5 for materials of wide-ranging composition therefore offers the possibility of enormous predictive power in which compositional space can be selected for the enhancement of properties on the basis of a map that could result from property-property correlations. Thus Figure 6.3.5 provides one of the strongest cases yet in support of the hypothesis that property correlations can be used to predict the properties of new materials.

Section 6.3.1 discusses the correlation between polarizability and atomic weight, which follows the periodic trend; and the correlation between polarizability and electronegativity, which follows the inverse correlation. From observing Figure 6.3.1, it can be speculated that the polarizability is the sum of a function of atomic weight $f(A_W)$ and a function of electronegativity $g(\chi)$. From the perspective along the electronegativity (χ) axis, the variance of polarizability in terms of atomic weight (A_W) follows the periodic trend; while from the perspective along the atomic weight (A_W) axis, the variance of polarizability in terms of electronegativity (χ) follows the inverse correlation. As a result, the mathematical function between polarizability, atomic weight and electronegativity may be a sum of two functions $\alpha = f(A_w) + g(\chi)$, where $f(A_w)$ is a kind of periodic function, and $g(\chi)$ is a kind of inverse function.

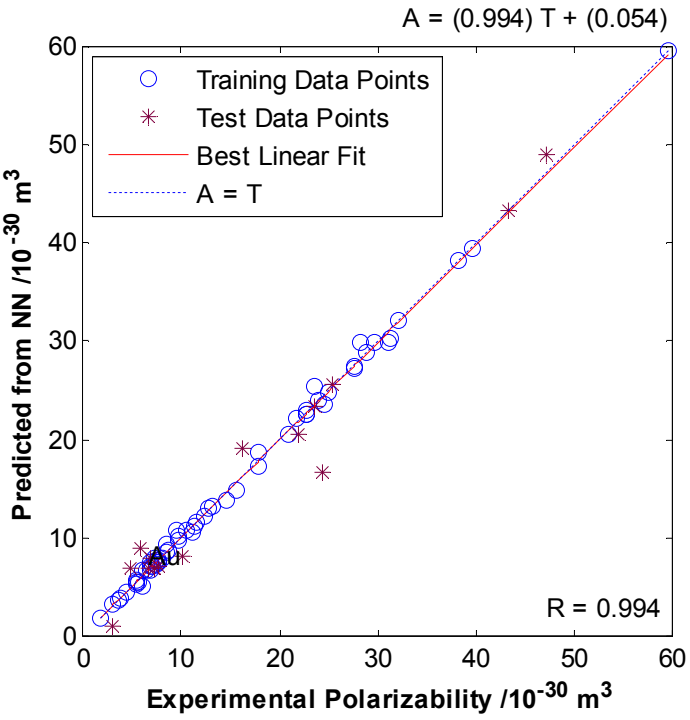

Figure 6.3.4 Result of prediction of polarizability using atomic weight and electronegativity.

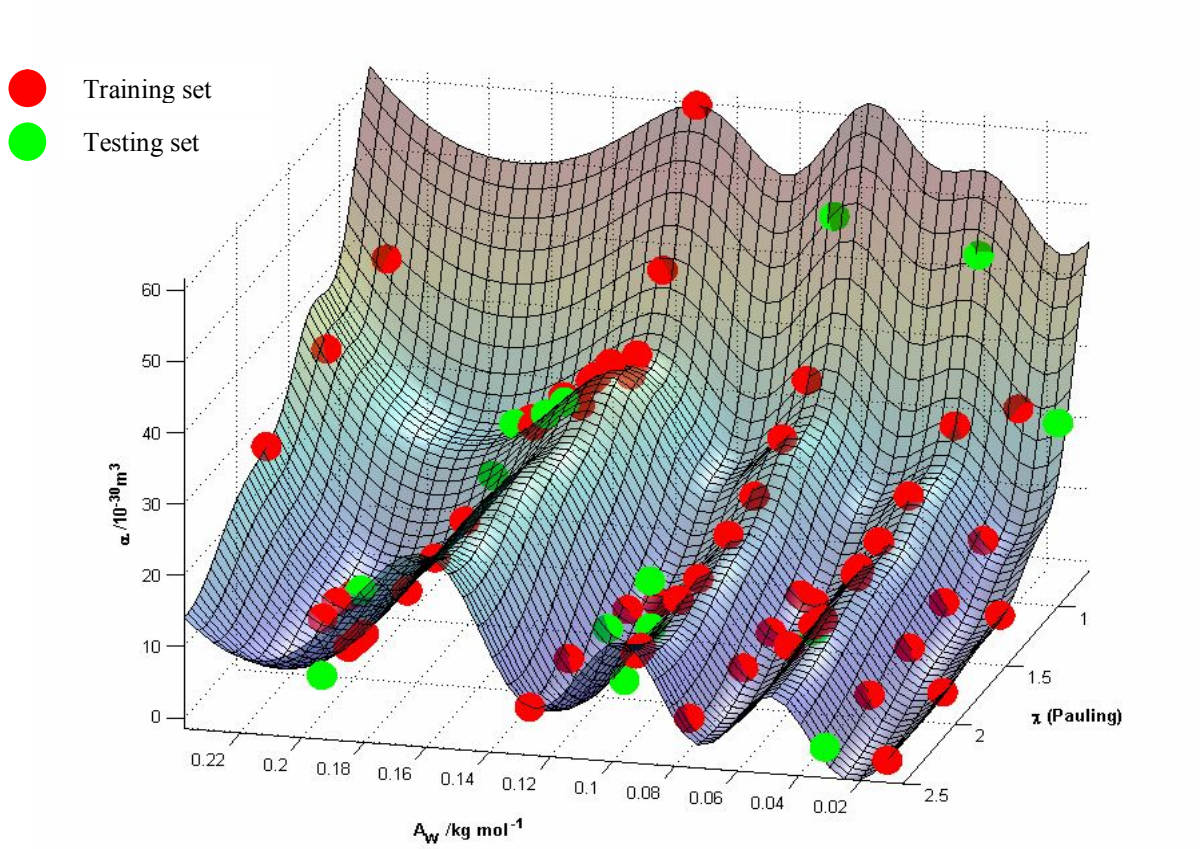

Figure 6.3.5 Variation of polarizability as a function of atomic weight and electronegativity.

Before further exploration of mathematical functions using Schmidt and Lipson's method, a function was speculated using a trial and error method. From looking at some typical functional curves, the type of periodic function may be similar to a type of curve that describes oscillation with increasing amplitude in case of resonance (**von Kármán and Biot, 1940**) plus a straight line, as shown in Figure 6.3.6, and the equation found from this approach is:

$$f(A_w) = 3.5 \times e^{5(A_W + 0.03)} \times sin(120(A_W + 0.03) + 30) + 99.85 A_W - 0.476 \quad \text{Equation 6.3.1}$$

and the type of inverse function can be stimulated from the discussion in section 6.3.1, as a type of power function with the power of -3, such as the one shown in Figure 6.3.7,

$$g(\chi) = 17 \times \chi^{-3} \quad \text{Equation 6.3.2}$$

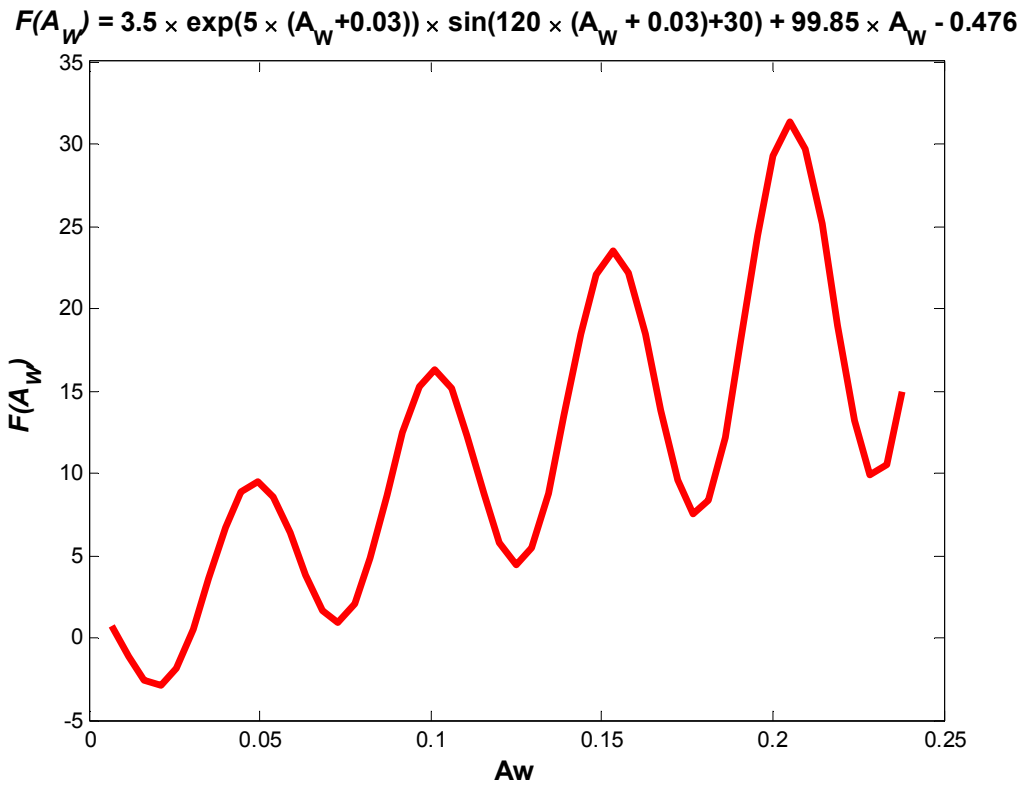

Figure 6.3.6 Free vibration with damping curve.

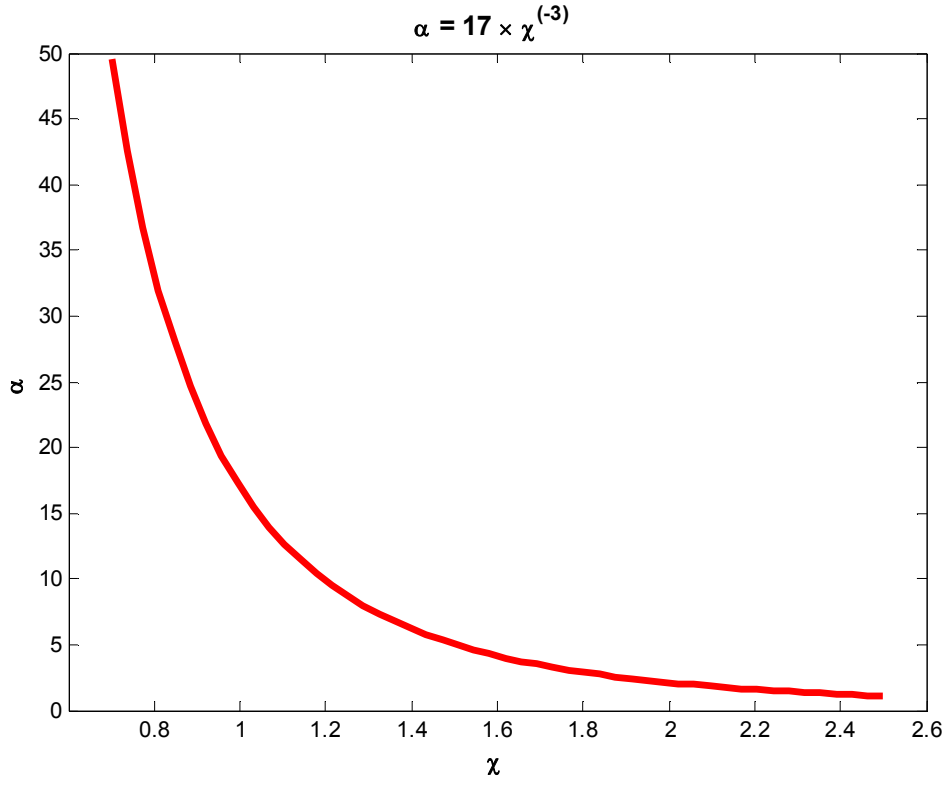

Figure 6.3.7 Inverse function curve.

The sum of functions shown in Figure 6.3.8

$$\alpha = f(A_w) + g(\chi) =$$

$$3.5 \times e^{5(A_W + 0.03)} \times sin(120(A_W + 0.03) + 30) + 99.85A_W - 0.476 + 17 \times \chi^{-3}$$

Equation 6.3.3

which is very similar to Figure 6.3.5 (redrawn in Figure 6.3.9 from the same viewpoint and with same coloured). At present, it is necessary to check whether the speculated functions can describe the functional relationship between polarizability, atomic weight and electronegativity. Substituting the values of atomic weight and electronegativity into the speculative function, which is $\alpha = f(A_w)+g(\chi) = 3.5 \times e^{5(A_W + 0.03)} \times sin(120(A_W + 0.03) + 30) + 99.85A_W - 0.476 + 17 \times \chi^{-3}$, the accuracy of prediction is not very high; it has mean error of modulus 5.25 and mean error percentage 59%. This means the coefficients of $f(A_w)$ and $g(\chi)$ still have scope for improvement, and that the real function may have a relatively more complex format of combination from $f(A_w)$ and $g(\chi)$. However, from Equation 6.3.3, it is possible to give some of the mathematical building blocks for genetic programming and use that to get a more reasonable equation.

It is arguable that this visualization method is only workable with one to one or two to one correlations. For higher dimensions, it's not possible to visualize the equation in 3D representations. However, it is possible to fix values of some properties and show only two or three properties in a series of lower dimensional pictures, which are equivalent to projections of the higher dimensions onto two or three dimensions. For example, in the case of section 6.3.2, polarizability is well predicted through the confounding effect of melting point, heat of vaporization, specific heat capacity and first ionization potential. It is not possible to visualize those five properties in three dimensions. By fixing two of the properties and varying the other two in three levels respectively, 54 figures were drawn using a similar method to that mentioned earlier in the construction of Figure 6.3.5, which are listed in Figure A3 in **Appendix 5**.

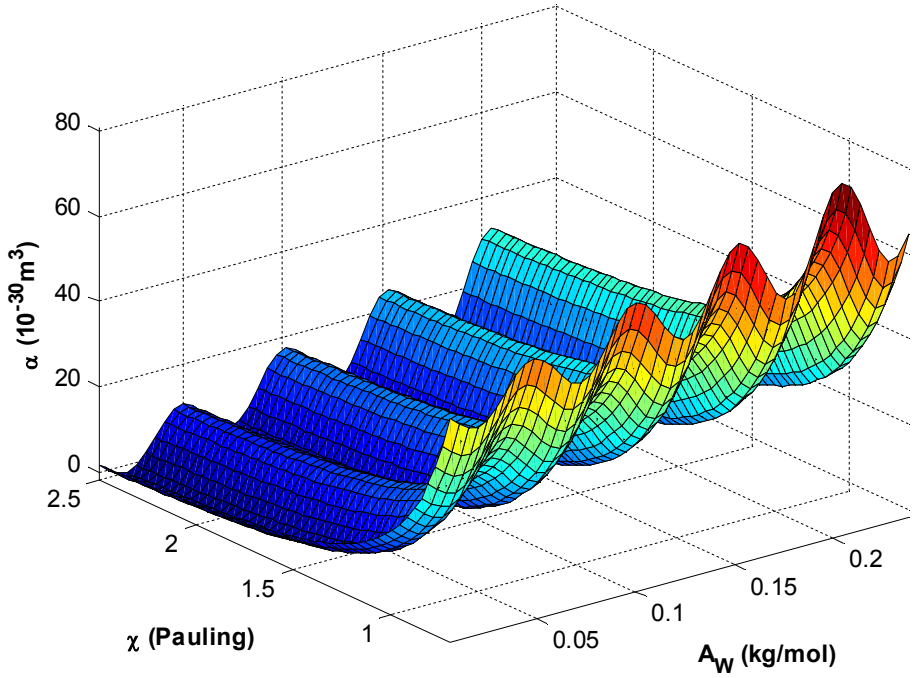

Figure 6.3.8 Plot of speculated function as shown in Equation 6.3.3.

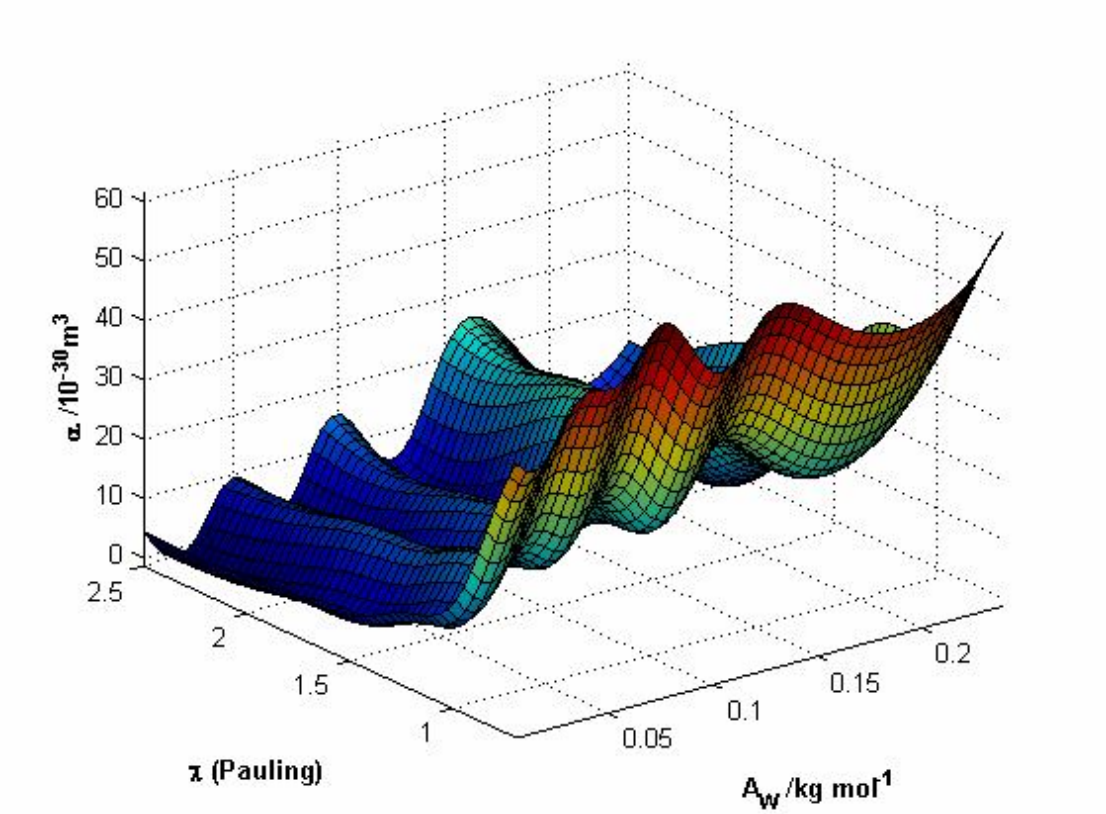

Figure 6.3.9 Redrawn of Figure 6.3.5 from the same viewpoint and with the same coloured as Figure 6.3.8.

From the discussions in section 6.3.2, specific heat c_P has smallest effect on the prediction of polarizability while first ionization potential E_I has the biggest effect on it. In Figure A3 (43), (44), (45), T_m is fixed at 4003 K and c_P is fixed at 113, 279 and 3390 J kg^{-1} K^{-1}, which correspond to minimum, mean and maximum respectively. These three figures are very similar, which confirms that the c_P has a small effect. By drawing more figures between minimum and maximum, it is possible to speculate some simple equations. In contrast, in Figure A3 (1), (2) and (3), c_P is fixed at 113 J kg^{-1} K^{-1} and E_I is fixed at 376, 691 and 1086 kJ mol^{-1}, which also correspond to minimum, mean and maximum. Those three figures are very different, which verifies the strong effect of E_I on the prediction of polarizability. In this situation, it is very difficult to speculate on a fitting equation. The other figures in Figure A3 can be examined in a similar way.

By inspection some of the pictures, for example Figure A3 (3), (6), (43), (44), (45) and (51), the surface is similar to a hyperbolic paraboloid surface, which has a function defined as

$$Z = \frac{X^2}{a^2} - \frac{Y^2}{b^2} \qquad \text{Equation 6.3.4}$$

In summary, equations in the prediction from two properties can be simply speculated through a 3D surface found by ANN. For prediction from more than two properties, part of the properties can be fixed to leave two properties only to draw 3D surfaces. Then from observing the 3D surfaces, the formats of equations can be speculated; and then the mathematical building blocks can be identified from that. By applying these building blocks, the real mathematical functions can be possibly found by using the genetic programming methodology as proposed by Schmidt and Lipson.

6.3.4 The Validity of Exploring Cross-properties relationship by using ANNs

The prediction of properties from structures are commonly used, but the interactions between different levels of structure make the problems very

complex. In this work, apply the principle that the properties of a material are determined by (or are a common response from) composition and structure, to explore correlation between different properties by using artificial neural networks. However, the interactions between input properties still exist. In neural networks, the nature of the interactions is implicit in the values of the weights. In cases like this work, there exist more than just pairwise interactions. As a result, it is difficult to visualize from the examination of the weights. As suggested by Bhadeshia (**1999**), the better method is to use the network to make predictions and to see how these depend on various combinations of inputs. In this work, it is tried to use the underlying physical principles to explain the different results and found employing neural network to explore the cross-properties relationship is reasonable.

7.0 The Feasibility of using ANN Methods

7.1 The Validity of ANN Models

From all of the works presented above, it can be concluded that: the ANN, as a method, can be treated as feasible although it cannot be relied on definitively and others also have reiterated this. It may be regarded as a useful tool for cautious use in materials science but the choice of the right ANN plays a critical role in its success especially when the dataset is restricted as is often the case in materials science.

7.2 The Effect of Number of Layers

Basheer and Hajmeer (**2000**) indicate that the choice of the number of hidden layers and the number of neurons in the hidden layers are among the most important choices in ANN design. Most of the works presented in this work are function approximation problems. It is often claimed that in most function approximation problems, one hidden layer is sufficient to approximate continuous functions (**Hecht-Nielsen, 1990; Basheer, 2000**); two hidden layers must generally be necessary for learning functions with discontinuities (**Masters, 1993**). In this work, the kind of function is not clear. Also the neural network user's guide (**Mathworks**) suggested that a two-hidden layers sigmoid/linear network can represent any function of input/output relationship. On these bases and looking at the results produced from all of the works, it can be seen that the choice of two-hidden layer network is a sensible choice.

7.3 The Effect of Size of Layer

The choice of size of the first hidden layer is critical in the ANN design. There are several rules of thumb available in the literature relating hidden layer size to the number of nodes in input (N_{INP}) and output (N_{OUT}) layers:

- Hecht-Nielsen (**1990**) used the Kolmogrov theorem to prove that $NHN \leq N_{INP} + 1$.
- Widrow and Lehr (**1990**) according to $(N_W/N_{OUT}) \leq N_{TRN} \leq (N_W/N_{OUT}) \text{Log}_2(N_W/N_{OUT})$.
- Upadhaya and Eryureka (**1992**) related NHN to N_{TRN} (via the total number of weights, N_W) according to $N_W = N_{TRN} \text{Log}_2(N_{TRN})$.

- Masters (**1994**) suggests that the ANN architecture should resemble a pyramid with $NHN \approx (N_{INP} * N_{OUT})^{1/2}$.
- Lachtermacher and Fuller (**1995**) suggest the NHN for a one-output ANN with no biases be determined from $0.11\ N_{TRN} \leq NHN(N_{INP}+1) \leq 0.30\ N_{TRN}$.
- Jadid and Fairbairn (**1996**) called for an upper bound on the number of hidden nodes (NHN) equal to $N_{TRN}/[R+(N_{INP} + N_{OUT})]$, where N_{TRN} is the number of training patterns and R=5-10.

As Basheer and Hajmeer (**2000**) suggested, the most popular way to find the optimal number of hidden nodes is by trial and error with one of those rules as a starting point. However, facing exotic problems with high nonlinearity and hysteresis such as shown in Basheer's work (**Basheer, 1998; 2000**), these 'rules of thumb' may need to be abandoned. There is some value in beginning with a small number of hidden nodes and building up iteratively to attain the accuracy required. This method is adopted in all of the works through implementation of the programs.

8.0 Conclusions

1. Revisiting Hume-Rothery's Rules

- ***Selection of Input Parameters***

In this work, the input parameters initially chosen for the network include (1) atomic size parameter, (2) valence parameter, (3) electrochemical parameter, i.e. electronegativity and (4) structure parameter of solvent and solute atoms. Three different expressions of these parameters were used to examine which gave the best performance:

1. The raw data that Hume-Rothery used.
2. The original collected values for each parameter of solvent and solute atoms.
3. The functionalized parameters.

When the raw data were used, uncertainty is the atomic size difference: some researchers believe the threshold is 14% and others believe it is 15%. The performance of ANN using the 15% criterion is slightly higher than that for 14% which implies 15% is a better threshold in the size factor. Using this same approach and including the 15% criterion, the structure parameter was introduced in terms of whether the structure of solvents and solutes are the same or not. There was no improvement in correlation. This indicates that the structure parameter employed in this way, does not play a very important role in solubility.

When the original values of input parameters are used, the training performance of the ANN is quite good but the prediction of the testing set is poor, and this clearly indicates that although the network trains satisfactorily on the actual values of input data it is unable to use these for prediction.

When the functionalized values were used as input parameters, both the training and testing set of the ANN gave good performances. Through a search of all combinations of those parameter formats, the best format of input parameters was determined as the functionalized values.

- ***Selection of Output Parameters***

From Hume-Rothery's Rules, only the possibility of whether a component is soluble or insoluble can be predicted. However, it would be more advantageous to attempt to predict the original value of solubility. The output parameters are expressed in two ways:

1) Follow a specialized criterion: if the solubility of solute metal in solvent metal exceeds 5 at. %, then it is said that this solute metal is soluble in the solvent metal; or it is not.
2) Original maximum solubility limits of each alloy system are used: the results of the prediction show the ANN can predict the solubility quantitatively with small mean modulus errors for 60 alloy systems.

- ***Testing Hume-Rothery's Rules for 60 Alloy Systems***

When the 60 alloy systems, which were used by Hume-Rothery, are tested, the rules really work well as demonstrated by the ANN correlations. These indicate the Hume-Rothery's general principles work well in several alloy systems, and can be used to estimate solid solubility.

- ***Extension of Hume-Rothery's Rules for 408 Alloy Systems***

The wider application of the same approach to a set of 408 silver, copper and gold alloys is less successful, and the predictability is poor. This is consistent with the inherent simplifications of the rules which are already documented by many people.

- ***The Effect of Melting Point***

Within a wider range of alloy systems, the introduction of melting point provides the capability for improving the predictability: it can be treated as a new parameter for solid solubility prediction. The prediction of T_{max}, under which the maximum solubility is reached, also confirms the effect of melting point.

- ***Determination of the Relative Importance of Each Rule***

In this work, the performance of the ANN, based on 60 alloy systems, was evaluated when some of the parameters were deliberately omitted. Using the

mean error of the testing set as the main criterion for accuracy of the prediction, atomic size has the strongest effect. Electronegativity has a stronger influence than valence. When pairs of parameters are omitted, the performance of the prediction became worse. Omission of the structure parameter only had small effect on the performance of the ANN, which implies that the structure parameter does not play a very important role. However, these parameters are not wholly independent of each other; their interplay makes the determination of solubility very difficult.

2. The Policing and Correction of Handbooks and Databases

In this work, it is found there were 21 elements having inconsistent boiling point recording at the 10% level or above; and 23 elements having inconsistent enthalpy of vaporization at the 10% level or above in five handbooks. These are not trivial numbers in only 82 elements inspected.

Employed both boiling points and enthalpies of vaporization that having consistent recording to train two ANNs (ANN1 and ANN2) provides a robust correlation against which the consistency of other data can be judged. Applying ANN1 to predict the enthalpies of vaporization of elements that have consistent recordings of boiling points, made the average error decrease from 231% to 8.8%. Then applying ANN2 to predict boiling points of elements that have consistent recordings of enthalpy of vaporization made the average error decrease from 18.9% to 6.43%. For the elements that have inconsistent records of both boiling point and enthalpy of vaporization, possible pairs have been found.

Compared with the statistical method adopted by Ashby *et al.*, the method developed locates more inconsistencies.

Extending the developed method to the more general situations (that is, more than two properties correlated), a systematic, intelligent and potentially automatic protocol has been developed to discover errors in handbooks. It could be imported as an immune system. It involves the collection of data and automatic exploration of indirect correlations within the data using ANNs.

3. The Prediction of Structural Stability and Formability of ABO_3-type Perovskite Compounds

In this part of work, 1) a neural network modelling method is used to make predictions of global instability index **GII** from bond-valence based tolerance factors t_{BV} for 232 ABO_3-type perovskite compounds and it is found that correlations exist between these two parameters within each subclass of ABO_3-type perovskite compounds; for the general ABO_3-type perovskite, this kind of correlation is not obeyed. However, it was found that the valence of A-site cations can be treated as another parameter to induce a unified correlation. 2) Neural networks have also been used to make predictions of formability of perovskites by using A-O and B-O bond distances in order to find the possibility of improving prediction accuracy. It was found that, in terms of the prediction accuracy, neural networks can yield better performances, although it is difficult to give simple and physically meaningful explanations.

4. Correlation between Polarizability and Other Properties

In this work, the general correlations that exist between different properties are explored by employing artificial neural network methods. The example of prediction of polarizability from combinations of other properties is analyzed in detail. Through this work, a systematic method for exploring general correlations that exist between different properties for different type of materials is provided.

1) It has been found that there are four properties that have single relatively strong correlations with polarizability. They are atomic weight, first ionization potential, electronegativity and work function. The underlying physical principles have been discussed individually.

2) The correlation between polarizability and combinations of melting point, heat of vaporization, first ionization potential and specific heat has been found, and the possible confounding effects are systematically analysed.

3) The prediction of polarizability from atomic weight and electronegativity is analysed as an example to visualize the functional relationship that neural network captured, and the surface that describes the variation of polarizability as

a function of atomic weight and electronegativity has been schematically shown. The possible mathematical equation that formulates and generalizes the correlation has been explored by a trial and error method, which could provide building blocks for generic programming.

4) For the case mentioned in 2), the neural network captured the correlation between polarizability and another four different properties. However, it is difficult for people to visualize this kind of functional correlation directly, which is located within a 5-D space. By fixing two of the properties and varying the other two in three levels respectively, a series of figures have been drawn in order to visualize this high dimensional function from its projection within a 3-D space. Also, relative impact of each parameter was verified.

9.0 Suggestions for Future Work

1. Verifying and Testing Hume-Rothery's Rules

Although Hume-Rothery's rules were tested at the beginning of this project to prove the ability of ANNs in finding known correlations in materials science, a few interesting directions have been identified from this section which can be investigated in future:

- A better way to express structures of elements for the input parameters of ANNs should be explored, for example, 1) find expressions that can reveal the similarities between FCC and HCP; 2) get some special expressions that can describe complex structures. These will help not only the proof of H-R rules but also other areas that use crystal structures as input parameters in materials science by using artificial intelligence.

- From the handbooks as mentioned in this work, such as the ASM Handbook, Alloy Phase Diagrams, Binary Phase Diagrams and Chemistry Data Book, it would be possible to draw together solubilities and physical parameters for more alloy systems for training and testing Hume-Rothery's Rules.

- It would be constructive and valuable to try to find other parameters that may affect the solid solubility of alloy systems and then to introduce them to the neural network for predicting the solid solubility limit of alloy systems. This could be done by introducing other properties such as pressure, cooling rate, and then use a combinatorial search of those properties by ANNs.

2. Policing Data with more than Two Correlating Properties

In this part of the work, a systematic method has been proposed to detect errors in handbooks. Following this trend, more properties should be progressively introduced to verify this general methodology. The method should then be applied for a wider range of databases. This forms a natural part of the project in investigating the cross property correlation method of discovery for without reliable data the correlations could not be discovered, and once the correlations is discovered, the outliers can be screened by ANNs.

3. Prediction of formability of ABO_3-type perovskite compounds by using more input parameters

Neural networks have the ability to make predictions in high dimensional spaces, *i.e.*, they can have more than two inputs to make the prediction. For the prediction of formability of ABO_3-type perovskite compounds, as mentioned by Zhang *et al.* (**2007**), besides the A-O and B-O bond distances, other factors also contribute to the formation of ABO_3-type perovskite compounds, such as i) bond-valence based tolerance factor t_{BV}, ii) temperature and iii) pressure; therefore, these parameters can be incorporated into future work in order to improve the accuracy of predictions, which can be used for practical applications.

4. Exploration of Cross Property Correlations with more data

The method applied in the exploration of cross-property correlations depends strongly on the available data. At present, the advent of e-science has meant that scientific communication can employ media not previously recognized. Data can be made accessible globally so that many geographically dispersed groups can analyze raw data according to their own skills. As a result, the sharing of data in raw form rather than through the highly processed medium of refereed journals is now possible. This means that the construction of global shared databases is a reality and it follows from that, multi-property data can be put up and shared. There are varieties of databases available, such as the ones listed by Wawrousek *et al.* (**1989**). Nowadays, more and more of these databases can be accessed via the internet (**Westbrook *et al.*, 1995; Abrate, 2000**). One recent example is the functional ceramic materials database developed by Scott *et al.* (**2008**).

After the data sharing is in place, the computational processes for mining the relationships are needed. Methods are required to develop for identifying how the measurement of properties a, b and c can be used to estimate the likely magnitude of property d. This will considerable narrow down the likely sample space for high throughput methods for d and, as the global database grows this cross-correlation may produce a new area of materials science that allows the scientific world to home in on new materials at a rate previously thought impossible. Where high throughput methods have compressed laboratory time, multi-property mapping might compress the history of science.

References

Abe T., Sundman B., Onodera H. Thermodynamic assessment of the Cu-Pt system. *Journal of Phase Equilibria and Diffusion*. 2006, **27**, 5-13.

Abrate S. World Wide Web resources for materials science. *Computer Applications in Engineering Education*. 2002, **9**, 238-247.

Ackland G. J., Vitek V. Many-body potentials and atomic-scale relaxations in noble-metal alloys. *Physical Review B*. 1990, **41**, 10324-10333.

Agren J. Calculation of phase diagrams: Calphad. *Current Opinion in Solid State and Materials Science*. 1996**, 1**, 355-360.

Agyemang M., Barker K., Alhajj R. A comprehensive survey of numeric and symbolic outlier mining techniques. *Intelligent Data Analysis*. 2006, **10**, 521-538.

Allen F. H. The development, status and scientific impact of crystallographic databases. *Acta Crystallographica*. 1998, **A54**, 758-771.

Alonso J. A., Girifalco L. A. Non-locality and the energy of alloy formation. *Journal of Physics F – Metal Physics*. 1978, **8**, 2455-2460.

Alonso J. A., Girifalco L. A. Electronegativity scale for metals. *Physical Review B*. 1979, **19**, 3889-3895.

Alonso J. A., Gonzalez D. J., Iniguez M. P. Electronegativity parameters of the theory of heats of alloy formation. *Solid State Communications*. 1979, **31**, 9-14.

Alonso J. A., Simozar S. Prediction of solid solubility in alloys. *Physical Review*. 1980, **B22**, 5583-5589.

Alonso J. A., Lopez J. M. Semi-empirical study of metastable alloys produced by ion-implantation in metals. *Philosophical Magazine A – Physics of Condensed Matter Structure Defects and Mechanical Properties*. 1982, **45**, 713-722.

Alonso J. A., Lopez J. M., Simozar S., Girifalco L. A. Prediction of solid solubility in alloys – Application to noble metal based alloys. *Acta Metallurgica*. 1982, **30**, 105-107.

Amari S. Foreword to neural networks theory. *In:* **Galushkin, A. I.** *Neural Network theory*. Springer Berlin Heidelberg New York, 2007, p. X.

American Society for Metals. *ASM handbook / Vol.3, Alloy phase diagrams.* Metals Park, Ohio: ASM International, 1992, pp.2.25-2.182.

Amis E. J., Xiang X. D., Zhao J. C. Combinatorial materials science: what's new since Edison? *MRS Bulletin*. 2002, **27**, 295-297.

Ansara I., Dinsdale A. T., Rand M. H. (Eds). *COST 507 – Thermochemical database for light metal alloys*, *Vol. 2*. European Cooperation in the Field of Scientific and Technical Research, 1998.

Apker L., Taft E., Dickey J. Photoelectric emission and contact potentials of semiconductors. *Physical Review*. 1948, **74**, 1462-1474.

Arblaster J. W. The thermodynamic properties of platinum. *Platinum Metals Review*. 2005, **49**, 141-149.

Arblaster, J. W. Vapour pressure equations for the platinum group elements. *Platinum Metals Review*. 2007, **51**, 130-135.

Arkadan A. A., Chen Y., Subramaniam S., Hoole S. R. H. NDT identification of a crack using ANNs with stochastic gradient descent. *IEEE Transactions on Magnetics*. 1995, **31,** 1984-1987.

Arroyave R., Kaufman L., Eagar T. W. Thermodynamic modelling of the Zr-O system. *CALPHAD*. 2002, **26**, 95-118.

Ashby M. F. Overview No. 80. On the engineering properties of materials. *Acta Metallurgica*. 1989, **37**, 1273-1293.

Ashby M. F. Checks and estimates for material properties I. Ranges and simple correlations. *Proceedings of the Royal Society of London A – Mathematical Physical and Engineering Sciences.* 1998, **454**, 1301-1321.

Ashby M. F. *Materials Selection in Mechanical Design*. Oxford: Butterworth-Heinemann, 1999. pp. 32-64.

Ashby M. F., Shercliff H., Cebon D. *Materials: Engineering, Science, Processing and Design*. Butterworth-Heinemann, Elsevier: 2007, pp. 22-24, 58-59.

Asta M., Ozolins V., Woodward C. A first-principles approach to modelling alloy phase equilibria. *JOM – Journal of the Minerals Metals & Materials Society*. 2001, **53**, 16-19.

Atoji M. Atomic polarizability. *The Journal of Chemical Physics*. 1956, **25**, 174.

Attoh-Okine N. O., Basheer I. A., Chen D. -H., Abu-Lebdeh G., McReynolds R., Meier R., Najjar Y. M., Penumadu D., Tutumluer E. *Use of artificial neural networks in geomechanical and pavement systems.* Transportation Research Board, National Research Council, 2101 Constitution Avenue, NW, Washington, DC 20418. Circular, Dec. 1999. 21 pages. No. E-C012, ISSN 0097-8515.

Axon H. J., Hume-Rothery W. The lattice spacings of solid solutions of different elements in aluminium. *Proceedings of the Royal Society of London, A. Mathematical and Physical Sciences*. 1948, **193**, 1-24.

Aylward G., Findlay T., ed. *SI Chemical Data, 4th edn.* New York; Chichester: Wiley, 1998, pp.6-13.

Bacalis N. C., Anagnostopoulos G. F., Papanicolaou N. I., Papaconstantopoulos D. A. Electronic structure of ordered and disordered Cu-Ag alloys. *Physical Review B*. 1997, **55**, 2144-2149.

Bacon F. (Ellis R. L., Spedding J., Robertson J. M. (**Eds.)**). Novum Organum in The Philosophical Works of Francis Bacon. Routledge Abingdon, UK 1905.

Bagnall, K. W. *The Chemistry of Selenium, Tellurium and Polonium*. Amsterdam; New York: Elsevier, 1966. pp. 37-38.

Baranyi J., Roberts T. A. Mathematics of predictive food microbiology. *International Journal of Food Microbiology*. 1995, **26**, 199-218.

Basheer I. A. *Neuromechanistic-based modeling and simulation of constitutive behavior of fine-grained soils.* PhD Dissertation, Kansas State University, Manhattan; 1998. 435p.

Basheer I. A. Selection of methodology for neural network modeling of constitutive hystereses behavior of soils. *Computer – Aided Civil and Infrastructure Engineering.* 2000**, 15,** 440-458.

Basheer I. A., Hajmeer M. Artificial neural networks: fundamentals, computing, design, and application. *Journal of Microbiological Methods*. 2000, **43,** 3-31.

Bassetti D., Brechet Y., Ashby M. F. Estimates for material properties II. The method of multiple correlations. *Proceedings of the Royal Society of London A – Mathematical Physical and Engineering Sciences.* 1998, **454**, 1323-1336.

Bedreag C. G. Electron extraction potential of alkali metals. *Comptes Rendus*. 1946, **223**, 354-354.

Ben-Gal I. Outlier detection. *In*: **Maimon O., Rokach L. (Eds.)** *Data Mining and Knowledge Discovery Handbook*. Springer: New York. 2005. pp. 131-146.

Bergerhoff G., Hundt R., Sievers R. The Inorganic Crystal Structure Database. *Journal of chemical information and computer sciences.* 1983, **23**, 66-69.

Bhadeshia H. K. D. H. A rationalisation of shear transformations in steels. *Acta Metallurgica*. 1981, **29**, 1117-1130.

Bhadeshia H. K. D. H., MacKay D. J. C., Svensson L. –E. Impact toughness of C-Mn steel arc welds – Bayesian neural network analysis. *Materials Science and Technology*. October 1995, **11**, 1046-1051.

Bhadeshia H. K. D. H. Neural networks in materials science. *ISIJ International*. 1999, **39**, 966-979.

Bhadeshia H. K. D. H. Mathematical models in materials science. *Materials Science and Technology*. 2008, **24**, 128-136.

Bhadeshia H. K. D. H. Neural networks and information in materials science. *Statistical Analysis and Data Mining*. 2009, **1**, 296-305.

Bhadeshia H. K. D. H., Dimitriu R. C., Forsik S., Pak J. H., Ryu J. H. Performance of neural networks in materials science. *Materials Science and Technology*. 2009, **25**, 504-510.

Bishop C. M. Novelty detection and neural network validation. *IEE Proceedings – Vision Image and Signal Processing*. 1994, **141**, 217-222.

Blum V., Zunger A. Structural complexity in binary bcc ground states: The case of bcc Mo-Ta. *Physical Review B*. 2004, **69**, 020103(1)-020103(4).

Bonin K. D., Kresin V. V. *Electric-Dipole Polarizabilities of Atoms, Molecules and Clusters*. Singapore: World Scientific Publishing Co. Pte. Ltd. 1997.pp. vii-viii.

Boozarjomehry R. B., Abdolahi F., Moosavian M. A. Characterization of basic properties for pure substances and petroleum fractions by neural network. *Fluid Phase Equilibria*. 2005, **231**, 188-196.

Borie B. S. X-ray diffraction effects of atomic size in alloys. *Acta Crystallographica*. 1957, **10**, 89-96.

Borie B. S. X-ray diffraction effects of atomic size in alloys II. *Acta Crystallographica*. 1959, **12**, 280-282.

Bork U., Challis R. E. Non-destructive evaluation of the adhesive fillet size in a T-peel joint using ultrasonic Lamb waves and a linear network for data discrimination. *Measurement Science and Technology*. 1995, **6**, 72-84.

Borman S. Combinatorial chemistry: researchers continue to refine techniques for identifying potential drugs in "libraries" of small organic molecules. *Chemical & Engineering News*. 1997, **February 24**, 43-62.

Borzone G., Parodi N., Cacciamani G., Watson A. Phase equilibria in the Au-In-Sn ternary system. *CALPHAD*. 2009, **33**, 17-22.

Bouwstra J. A., Geels G., Kaufman L., Oonk H. A. J. Binary common-ion alkali halide mixtures thermodynamic analysis of solid-liquid phase diagrams IV. Three systems showing isodimorphism application of the liqfit method. *CALPHAD*. 1986, **10**, 163-174.

Bozzolo G., Ferrante J. Heats of formation of bcc binary alloys. *Physical Review B*. 1992, **45**, 12191-12197.

Bozzolo G., Ferrante J., Smith J. R. Method for calculating alloy energetics. *Physical Review B*. 1992, **45**, 493-496.

Bozzolo G., Noebe R. D., Ferrante J., Amador C. An introduction to the BFS method and its use to model binary NiAl alloys. *Journal of Computer-Aided Materials Design*. 1999, **6**, 1-32.

Bragg W. L. The structure of some crystals as indicated by their diffraction of X-rays. *Proceedings of the Royal Society of London, Series A*. 1913, **89**, 248-277.

Bratchell N., Mcclure P. J., Kelly T. M., Roberts T. A. Predicting microbial-growth – graphical methods for comparing models. *International Journal of Food Microbiology*. 1990, **11**, 279-287.

Brooks H. Binding in metals. *Transactions of the Metallurgical Society of AIME*. 1963, **227**, 546-560.

Brooks L. S. The vapor pressure of tellurium and selenium. *Journal of the American Chemical Society*. 1952, **74**, 227-229.

Brugger P. From haunted brain to haunted science: a cognitive neuroscience view of paranormal and pseudoscientific thought. ***In***: **Houran J., Lange R. (Eds.)** *Hauntings and Poltergeists: Multidisciplinary Perspectives*. North Carolina: McFarland & Company, Inc. 2001. pp. 195-213.

Buckley R. A., Hume-Rothery W. The liquid → solid and δ → γ equilibria in iron-rich alloys. *Journal of the Iron and Steel Institute*. 1963, **201**, 227-232.

Burdett J. K., Rodgers J. R. Structure & property maps for inorganic solids. *In:* King R. B. (ed.), *Encyclopedia of Inorganic Chemistry*, Vol. 7, John Wiley & Sons, New York, 1994. pp. 1-19.

Cachadiña I., Mulero A. Vaporization enthalpy: corresponding-states correlations versus DIPPR database. *Journal of Physical and Chemical Reference Data*. 2007, **36**, 1133-1139.

Cai K., Xia J., Li L., Gui Z. Analysis of the electrical properties of PZT by a BP artificial neural network. *Computational Materials Science.* 2005, **34,** 166-172.

Callister W. D., Jr. *Materials Science and Engineering: An Introduction*. 6th edn. John Wiley & Sons, Inc., New York, 2003. pp. 2-3, 658-659.

Cao Z. M., Takaku Y., Ohnuma I., Kainuma R., Zhu H. M., Ishida K. Thermodynamic assessment of the Ni-Sb binary system. *Rare Metals*. 2008, **27**, 384-392.

Cargnoni F., Gatti C., Colombo L. Formation and annihilation of a bond defect in silicon: an *ab initio* quantum-mechanical characterization. *Physical Review B*. 1998, **57**, 170-177.

Cawse J. N. The Combinatorial Challenge. *In:* **Cawse J. N. (Eds).** *Experimental design for combinatorial and high throughput materials development.* John Wiley & Sons, Inc., Hoboken, New Jersey, 2003. pp. 1-26.

CES EduPack 2008. *Cambridge Engineering Selector*. Granta Design Ltd., Rustat House, 62 Clifton Court, Cambridge CB1 7EG, UK. www.grantadesign.com

Chalk A. J., Beck B., Clark T. A quantum mechanical/neural net model for boiling points with error estimation. *Journal of Chemical Information and Computer Sciences*. 2001, **41**, 457-462.

Chan P. K., Fan W., Prodromidis A. L., Stolfo S. J. Distributed data mining in credit card fraud detection. *IEEE Intelligent Systems & Their Applications*. 1999, **14**, 67-74.

Chang Y. A., Chen S., Zhang F., Yan X., Xie F., Schmid-Fetzer S., Oates W. A. Phase diagram calculation: past, present and future. *Progress in Materials Science*. 2004, **49**, 313-345.

Chelikowsky J. R., Phillips J. C. Quantum-defect theory of heats of formation and structural transition energies of liquid and solid simple metal alloys and compounds. *Physical Review B*. 1978, **17**, 2453-2477.

Chelikowsky J. R. Solid solubilities in divalent alloys. *Physical Review.* 1979, **B19**, 686-701.

Chelikowsky J. R. Microscopic basis of Miedema's theory of alloy formation. *Physical Review B*. 1982, **25**, 6506-6508.

Chelikowsky J. R. Cohesive energy. *In*: Encyclopedia of Applied Physics. Weinheim: Wiley-VCH. 2004. p. 260.

Chen N. H. Generalized correlation for latent heat of vaporization. *Journal of Chemical and Engineering Data.* 1965, **10**, 207-210.

Chen S. W., Jan C. H., Lin J. C., Chang Y. A. Phase equilibria of the Al-Li binary system. *Metallurgical and Materials Transactions A*. 1989, **20**, 2247-2258.

Chen S. L., Chang Y. A. A thermodynamic analysis of the Al-Zn system and phase diagram calculation. *CALPHAD*. 1993, **17**, 113-124.

Chin J., Harting J., Jha S., Coveney P. V. Steering in computational science: mesoscale modelling and simulation. *Contemporary Physics*. 2003, **44**, 417-434.

Chrisman N. R. The error component in spatial data. In **Maguire D. J., Goodchild M.F. and Rhind D. W. (Eds.)** *Geographical Information Systems. Vol. 1: Principals*. John Wiley & Sons, New York, 1991. pp. 165-174.

Chuang Y. Y., Hsieh K. C., Chang Y. A. Thermodynamics and phase relationships of transition metal-sulfur systems: Part V. A reevaluation of the Fe-S system using an associated solution model for the liquid phase. *Metallurgical and Materials Transactions B*. 1985, **16**, 277-285.

Chuang Y. Y., Chang Y. A., Schmid R., Lin J. C. Magnetic contributions to the thermodynamic functions of alloys and the phase equilibria of Fe-Ni system below 1200 K. *Metallurgical and Materials Transactions A*. 1986, **17**, 1361-1372.

Chuang Y. Y., Chang Y. A. A thermodynamic analysis and calculation of the Fe-Ni-Cr phase diagram. *Metallurgical and Materials Transactions A*. 1987, **18**, 733-745.

Clark C. H. D. Spectroscopy and valency. II. The periodic groups of nonhydride diatomic molecules. *Proceedings of the Leeds Philosophical and Literary Society*. 1934, **2**, 502-512.

Cockayne B., Raynor G. V. The apparent metallic valencies of transition metals in solid solution. *Proceedings of the Royal Society of London. Series A, Mathematical and Physical Sciences*. 1961, **261**, 175-188.

Colinet C., Pasturel A., Manh D. N., Pettifor D. G., Miodownik P. Phase-stability study of the Al-Nb system. *Physical Review B*. 1997, **56**, 552-565.

Colinet C. Ab-initio calculation of enthalpies of formation of intermetallic compounds and enthalpies of mixing of solid solutions. *Intermetallics*. 2003, **11**, 1095-1102.

Colliez J., Dufrenois F., Hamad D. Robust regression and outlier detection with SVR: application to optic flow estimation. *The 17th British Machine Vision Conference*. 2006. Edinburgh. 10 pages. (Entry website, on 22/10/2009: http://www.macs.hw.ac.uk/bmvc2006/papers/446.pdf)

Condon E. U. Note on the external photoelectric effect of semi-conductors. *Physical Review*. 1938, **54**, 1089-1091.

Constantinou L., Gani R. New group contribution method for estimating properties of pure compounds. *AIChE Journal*. 1994, **40**, 1697-1710.

Cottrell A. *An introduction to metallurgy*. London: Edward Arnold. 1975. pp. 345-347.

Cottrell A. *Concepts in the electron theory of alloys*. London: IOM Communications; 1998. pp. 27-102.

Cui Y., Jin Z. Assessment of the Re-Ta binary system. *Journal of Alloys and Compounds*. 1999, **285**, 150-155.

Curtarolo S., Morgan D., Persson K., Rodgers J., Ceder G. Predicting crystal structures with data mining of quantum calculations. *Physical Review Letters*. 2003, **91**, 135503(1)-135503(4).

Curtarolo S., Morgan D., Ceder G. Accuracy of *ab initio* methods in predicting the crystal structures of metals: A review of 80 binary alloys. *CALPHAD*. 2005, **29**, 163-211.

Daane A. H. Physical properties of the rare-earth metals. *In:* **Spedding F. H., Daane A. H. (Eds.)** *The Rare Earths*. John Wiley & Sons, Inc.: New York and London, 1961, pp. 177-189.

Dagani R. A faster route to new materials. *Chemical & Engineering News*. 1999, **77**, 51-60.

Dainton, F. S., Kimberley, H. M. A radioactive tracer method for the determination of the variation of vapour pressure with temperature and its

application to White Phosphorus. *Transactions of the Faraday Society*. 1950, **46**, 912-918.

Dalcin E. C. *Data quality concepts and techniques applied to taxonomic databases*. Thesis for the degree of Doctor of Philosophy. University of Southampton. 2005, p.21.

Darken L. S., Gurry R. W. *Physical Chemistry of Metals*. New York: McGraw-Hill. 1953. pp. 74-109.

David R. L. (**Eds.**) CRC Handbook of Chemistry and Physics. 2000-2001. 81st edn. Boca Raton: CRC Press, c2000, p. (4)124, pp. (6)105-(6)106.

Debye P. *Polar Molecules*. New York: Chemical Catalog Company, Inc., 1929. pp. 15-35.

De Chatel P. F., Robinson G. G. Formation energy of heterovalent alloys. *Journal of Physics F – Metal Physics*. 1976, **6**, L174-L176.

De Podesta, M. *Understanding the Properties of Matter*, 2nd edn. (Taylor & Francis, London, 2001), p.344.

De Selincourt M. The boiling point of selenium. *Proceedings of the Physical Society*. 1940, **52**, 348-352.

Dean J. A. *Lange's Handbook of Chemistry, 12th edition*. New York; London: McGraw-Hill, 1979. p. (9-112).

Deibuk V. G., Dremlyuzhenko S. G., Ostapov S. E. Thermodynamic stability of bulk and epitaxial CdHgTe, ZnHgTe, and MnHgTe alloys. *Semiconductors*. 2005, **39**, 1111-1116.

Denbigh K. G. The polarisabiliuties of bonds-I. *Transactions of the Faraday Society*. 1940, **36**, 936-948.

Diaconis P., Mosteller F. Methods for studying coincidences. *Journal of the American Statistical Association*. 1989, **84**, 853-861.

Ding X. Y., Fan P., Wang W. Z. Thermodynamic calculation for alloy systems. *Metallurgical and Materials Transactions B – Process Metallurgy and Materials Processing Science*. 1999, **30**, 271-277.

Disalvo F. J. Solid-state chemistry: a rediscovered chemical frontier. *Science*. 1990, **247**, 649-655.

Dixon R. D., Lott L. A. Work function of ultrahigh-vacuum-deposited beryllium films. *Journal of Applied Physics*. 1969, **40**, 4938-4939.

Dmitrieva I. K., Plindov G. I. Dipole polarizability, radius and ionization potential for atomic systems. *Physica Scripta*. 1983, **27**, 402-406.

Dorsett H. and White A. *Overview of molecular modeling and ab initio molecular orbital methods suitable for use with energetic materials.* Aeronautical and Maritime Research Laboratory, Salisbury, Australia. Weapons Systems Division, 2000. 36 pages. Report DSTO no. **DSTO-GD-0253**.

Drude P. Zur Elektronentheorie der Metalle. *Annalen der Physik*. 1900a, **306**, 566-613.

Drude P. Zur Elektronentheorie der Metalle; II. Teil. Galvanomagnetische und thermomagnetische Effecte. *Annalen der Physik*. 1900b, **308**, 369-402.

Du Y., Clavaguera N. Thermodynamic assessment of the Al-Ni system. *Journal of Alloys and Compounds*. 1996, **237**, 20-32.

Du Z., Xu Y., Zhang W. Thermodynamic assessment of the Cu-La system. *Journal of Alloys and Compounds***.** 1999, **289,** 89-95.

Du Z., Yang H., Li C. Thermodynamic modeling of the Pd-Y system. *Journal of Alloys and Compounds*. 2000, **297**, 185-191.

Du Z., Yang H. Thermodynamic assessment of the Gd-Pd system. *Journal of Alloys and Compounds*. 2000, **312**, 181-188.

Duhem P. *Medieval Cosmology: Theories of Infinity, Place, Time, Void, and the Plurality of Worlds.* Chicago: University of Chicago, 1985. pp. 431-439.

Duschanek H., Rogl P., Lukas H. L. A critical assessment and thermodynamic calculation of the boron-carbon-titanium [B-C-Ti] ternary system. *Journal of Phase Equilibria*. 1995, **16**, 46-60.

Eddington A. S. *The Philosophy of Physical Science.* Cambridge: University Press, 1949, pp. 1-15.

Egolf L. M., Jurs P. C. Prediction of boiling points of organic heterocyclic compounds using regression and neural network techniques. *Journal of Chemical Information and Computer Sciences*. 1993, **33**, 616-625.

Elsässer Ch., Fisher C. A. J., Howe A., Parrinello M., Scheffler M., and Gao H. Introduction to Materials Theory and Modelling. *In: European White Book on Fundamental Research in Materials Science.* Max-Planck-Institut für Metallforschung Stuttgart, 2001. Chapter 4, Materials Theory and Modelling. pp. 126-128.

Emsley J. The Elements, 3rd edn. Oxford: Oxford University Press, 1998.

Eshelby J. D. The continuum theory of lattice defects. *Solid State Physics*. 1956, **3**, 79-144.

European White Book on Fundamental Research in Materials Science. Max – Planck – Institut für Metallforschung Stuttgart, 2001. p. 10.

Evans J. R. G., Edirisinghe M. J., Coveney P. V., Eames J. Combinatorial searches of inorganic materials using the ink-jet printers: science, philosophy and technology. *Journal of the European Ceramic Society*. 2001, **21**, 2291-2299.

Falk R., Konold C. Making sense of randomness: implicit encoding as a basis for judgment. *Psychological Review*. 1997, **104**, 301-318.

Fan W. F., Geerts F., Jia X. B., Kementsietsidis A. Conditional functional dependencies for capturing data inconsistencies. *ACM Transactions on Database Systems*. 2008, **33**, Article No. 6.

Fang F., Zeng M. Q., Che X. Z., Zhu M. Embedded atom potential calculation of the Al-Pb immiscible alloy system. *Journal of Alloys and Compounds*. 2002a, **34**, 252-255.

Fang S. S., Lin G. W., Zhang J. L., Zhou Z. Q. The maximum solid solubility of the transition metals in palladium. *International Journal of Hydrogen Energy*. 2002a, **27**, 329-332.

Fang F., Zeng M. Q., Che X. Z., Zhu M. Embedded atom potential calculation of the Al-Pb immiscible alloy system. *Journal of Alloys and Compounds*. 2002b, **34**, 252-255.

Fayyad U. M., Piatetsky-Shapiro G., Uthurusamy R. Summary from the KDD-03 panel: data mining: the next 10 years. *ACM SIGKDD Explorations Newsletter*. 2003, **5**, 191-196.

Fedors R. F. A method for estimating both the solubility parameters and molar volumes of liquids. *Polymer Engineering and Science*. 1974, **14**, 147-154.

Feng L. M., Jiang L. Q., Zhu M., Liu H. B., Zhou X., Li C. H. Formability of ABO_3 cubic perovskites. *Journal of Physics and Chemistry of Solids*. 2008, **69**, 967-974.

Fey N. Review organometallic molecular modeling – the computational chemistry of metallocenes: a review. *Journal of Chemical Technology and Biotechnology*. 1999, **74**, 852-862.

Feynman R. P. What is science? *In: The Physics Teacher, Vol 9*. American Association of Physics Teachers, 1969. pp. 313-320.

Fischer C. C., Tibbetts K. J., Morgan D., Ceder G. Predicting crystal structure by merging data mining with quantum mechanics. *Nature Materials*. 2006, **5**, 641-646.

Fish L. W., Lielmezs J. General method for predicting the latent heat of vaporization. *Industrial & Engineering Chemistry Fundamentals*. 1975, **14**, 248-256.

Flandorfer H., Grobner J., Stamou A., Hassiotis N., Saccone A., Rogl P., Wouters R., Seifert H., Maccio D., Ferro R., Haidemenopoulos G., Delaey L., Effenberg G. Experimental investigation and thermodynamic calculation of the ternary system Mn-Y-Zr. *Zeitschrift Fur Metallkunde*. 1997, **88**, 529-538.

Flemings M. C. What next for departments of materials science and engineering? *Annual Review of Materials Research*. 1999, **29**, 1-23.

Fourier J. *Théorie Analytique de la Chaleur, Par M. Fourier*. A Paris, Chez Firmin Didot, Père et Fils, Libraires Pour Les Mathématiques, L'architecture Hydraulique et la Marine, Rue Jacob, N^{o} 24. 1822.

Franz R., Wiedemann G. Ueber die Wärme-Leitungsfähigkeit der Metalle. *Annalen der Physik und Chemie*. 1853, **165**, 497-531.

Fricke B. On the correlation between electric polarizabilities and the ionization potential of atoms. *The Journal of Chemical Physics*. 1986, **84**, 862-866.

Friedel J. Electronic structure of primary solid solutions in metals. *Advances in Physics*. 1954, **3**, 446-507.

Friedrich W., Knipping P., Laue M. Interferenz-erscheinungen bei rontgenstrahlen (Interference appearances in X-rays). *Proceedings of the Bavarian Academy of Sciences*. 1912, 303-322; reprinted in *Annalen der Physik*. 1913, **41**, 971-988.

Fries S. G., Jantzen T. Compilation of 'CALPHAD' formation enthalpy data binary intermetallic compounds in the COST 507 Gibbsian database. *Thermochimica Acta*. 1998, **314**, 23-33.

Fries S. G., Ansara I., Lukas H. L. Thermodynamic optimization of the Pb-Tl binary system. *Journal of Alloys and Compounds*. 2001, **320**, 228-233.

Fuks D. L., Panin V. E., Zhorovkov M. F. Calculation of solubility limits in solid-state by pseudopotential method. *Fizika Metallov I Metallovedenie*. 1975, **39**, 884-887.

Fyfe S., Williams C., Mason O. J., Pickup G. J. Apophenia, theory of mind and schizotypy: Perceiving meaning and intentionality in randomness. *CORTEX*. 2008, **44**, 1316-1325.

Gabriel A., Gustafson P., Ansara I. A thermodynamic evaluation of the C-Fe-Ni system. *CALPHAD*. 1987, **11**, 203-218.

Galushkin, A. I. *Neural Network Theory*. Springer, Berlin Heidelberg New York, 2007. p. 1.

Gavard L., Bhadeshia H. K. D. H., Mackay D. J. C. and Suzuki S. Bayesian neural network model for austenite formation in steels. *Materials Science and Technology*. 1996, **12**, 453-463.

Geysen H. M., Meloen R. H., Barteling S. J. Use of peptide-synthesis to probe viral-antigens for epitopes to a resolution of a single amino-acid. *Proceedings of the National Academy of Sciences of the United States of America-Biological Sciences*. 1984, **81**, 3998-4002.

Ghanty T. K., Ghosh S. K. New scale of atomic orbital radii and its relationship with polarizability, electronegativity, other atomic properties, and bond energies of diatomic molecules. *Journal of Physical Chemistry*. 1996, **100**, 17429-17433.

Ghosh G., Van de Walle A., Asta M. Olson G. B. Phase stability of the Hf-Nb system: From first-principles to CALPHAD. *CALPHAD*. 2002, **26**, 491-511.

Ghosh G., Asta M. First-principles calculation of structural energetics of Al-TM (TM=Ti, Zr, Hf) intermetallics. *Acta Materialia*. 2005, **53**, 3225-3252.

Giaquinta D. M., Loye H. C. Structural predictions in the ABO_3 phase diagram. *Chemistry of Materials*. 1994, **6**, 365-372.

Gillies D. *Artificial Intelligence and Scientific Method*. Oxford: Oxford University Press, 1996, pp. 1-16, 69.

Giordani D. S., Oliveira P. C., Guimarães A., Guimarães R. C. O. Correlation of modified natural rubber properties by artificial neural networks. *Polymer Engineering and Science*. 2009, **49**, 499-505.

Goetz A. The photoelectric effect of molten tin and two of its allotropic modifications. *Physical Review*. 1929, **33**, 373-385.

Gokcen N. A., Tanaka T., Morita Z. Atomic theories on energetics of alloy formation. *Journal de Chimie Physique et de Physico-Chimie Biologique*. 1993, **90**, 233-248.

Gomez-A T. Thermodynamic assessment of the Ag-Zn system. *Calphad* 1998, **22,** 203-220.

Gonzalez D. J., Alonso J. A. Charge-transfer in simple metallic alloys. *Journal de Physique*. 1983, **44**, 229-234.

Gorbunov A. I., Kaganyuk D. S. New technique for the calculation of atomic electronegativity. *Zhurnal Fizicheskoi Khimii*. 1986, **60**, 2336-2338. (*Russian Journal of Physical Chemistry (English Translation)*. 1986, **60**, 1406-1407).

Gorbunov A. I., Filippov G. G. New approximation of electrostatic scale of atomic electronegativity. *Zhurnal Fizicheskoi Khimii*. 1988, **62**, 1909-1912.

(*Russian Journal of Physical Chemistry (English Translation)*. 1988, **62**, 974-976).

Graham R. L., Spencer J. H. Ramsey theory. *Scientific American*. 1990, **263**, 112-117.

Griffiths T. L., Tenenbaum J. B. Randomness and coincidences: reconciling intuition and probability theory. *23rd Annual Conference of the Cognitive Science Society*. 2001, 370-375. (http://web.mit.edu/cocosci/Papers/random.pdf)

Grobner J., Schmid-Fetzer R., Pisch A., Cacciamani G., Riani P., Parodi N., Borzone G., Saccone A., Ferro R. Experimental investigations and thermodynamic calculation in the Al-Mg-Sc system. *Zeitschrift Fur Metallkunde*. 1999, **90**, 872-880.

Gschneider K. A. L. S. Darken's contributions to the theory of alloy formation and where we are today. *In*: **Bennett L. H. (Ed.)**. *Theory of alloy phase formation*. Warrendale: The Metallurgical Society of AIME. 1980, pp. 1-39.

Gschneidner K. A., Verkade M. Electronic and crystal structures, size (ECS^2) model for predicting binary solid solutions. *Progress in Materials Science*. 2004, **49**, 411-428.

Guessasma S., Montavon G., Coddet C. Neural networks, design of experiments and other optimization methodologies to quantity parameter dependence of atmospheric plasma spraying. ***In***: **Marple R., Moreau C. (Eds.)** *Proceedings of the Thermal Spray 2003: Advancing the Science & Applying the Technology, Vol. 2*. Materials Park (OH): ASM International; 2003, pp. 939-948.

Guessasma S., Coddet C. Microstructure of APS alumina-titania coatings analysed using artificial neural network. *Acta Materialia.* 2004, **52**, 5157-5164.

Gui X. C., Liao S. Z., Xie H. W., Zhang B. W. Parabola model of formation law of quasicrystal based on the fourth transition metals. *Rare Metal Materials and Engineering*. 2006, **35**, 1080-1084.

Guo C., Du Z., Li C., Zhang B., Tao M. Thermodynamic description of the Al-Fe-Zr system. *CALPHAD*. 2008, **32**, 637-708.

Guo D., Wang Y., Nan C., Li L., Xia J. Application of artificial neural networks technique to the formulation design of dielectric ceramics. *Sensors and Actuators A*. 2002, **102,** 93-98.

Gustafsson T., Brodén G., Nilsson P-O. Photoelectric properties of evaporated Be films. *Journal of Physics F: Metal Physics*. 1974, **4**, 2351-2358.

Guthrie J. P., Taylor K. F. Additivity methods for estimating heats of vaporization of organic compounds. *Canadian Journal of Chemistry*. 1983, **61**, 602-607.

Habermann C. E., Daane, A. H. Vapour pressures of the rare-earth metals *The Journal of Chemical Physics.* 1964, **41**, 2818-2827.

Hallemans B., Wollants P., Roos J. R. Thermodynamic reassessment and calculation of the Fe-B phase-diagram. *Zeitschrift Fur Metallkunde*. 1994, 85, 676-682.

Hallstedt B., Kim O. Thermodynamic assessment of the Al-Li system. International *Journal of materials Research*. 2007, **98**, 961-969.

Han J., Kamber M. *Data Mining: Concepts and Techniques*. Amsterdam; Boston: Elsevier; San Francisco, CA: Morgan Kaufmann. 2006. pp. 451-459.

Hanak J. J., Gittleman J. I., Pellicane J. P., Bozowski S. The effect of grain size on the superconducting transition temperature of the transition metals. *Physics Letters A*. 1969, **30**, 201-202.

Hanak J. J. The "multiple-sample concept" in materials research: synthesis, compositional analysis and testing of entire multicomponent systems. *Journal of Materials Science*. 1970, **5**, 964-971.

Hand D. J., Mannila H., Smyth P. *Principles of Data Mining*. The MIT Press, Cambridge, USA. 2001. p. 22.

Harrison N. M., Saunders V. R., Dovesi R., Mackrodt W. C. Transition metal materials: a first principles approach to the electronic structure of the insulating phase. *Philosophical Transactions of the Royal Society A – Mathematical Physical and Engineering Sciences.* 1998, **356**, 75-88.

Hassoun M. H. (Ed.) *Fundamentals of artificial neural networks.* Cambridge, MA: MIT Press, 1995.

Hatano K., Nakamura K., Akiyama T., Ito T. Theoretical study of alloy phase stabilities in zincblende $Ga_{1-x}Mn_xAs$. *Journal of Crystal Growth*. 2007, **301**, 631-633.

Hayes T. M., Brooks H., Bienenstock A. Ordering energy and effective pairwise interactions in a binary alloy of simple metals. *Physical Review*. 1968, **175**, 699-710.

Hayes T. M., Young W. H. Solubility of alkalis in alkalis. *Philosophical Magazine*. 1970, **21**, 583-590.

He X. C., Wang H., Liu H. S., Jin Z. P. Thermodynamic description of the Cu-Ag-Zr system. *CALPHAD*. 2006, **30**, 367-374.

He Z., Deng S., Xu X. Outlier detection integrating semantic knowledge. *In*: **Meng X., Su J., Wang Y. (Eds.)** *Advances in Web-Age Information Management. Third International Conference, WAIM 2002*. pp. 126-131.

Hecht-Nielsen R. Applications of counterpropagation networks. *Neural Networks*. 1988, **1**, 131-139.

Hecht-Nielsen R. (Ed.) *Neurocomputing*. Reading, MA: Addison-Wesley, 1990.

Herbstein F. H., Borie B. S., Averbach B. L. Local atomic displacements in solid solutions. *Acta Crystallographica*. 1956, **9**, 466-471.

Hernández M. A., Stolfo S. J. Real-world data is dirty: Data cleansing and the merge/purge problem. *Data Mining and Knowledge Discovery*. 1998, **2**, 9-37.

Hillert M. *Calculations of phase equilibria*. *American Society for Metals Seminar on Phase Transformations*. Metals Park, Ohio: American Society for Metal; 1968: pp. 181-218.

Hillert M. Some viewpoints on the use of a computer for calculating phase diagrams. *Physica B*. 1981, **103B**, 31-40.

Hodges C. H. Interpretation of alloying tendencies of nontransition metals. *Journal of Physics F – Metal Physics*. 1977, **7**, L247-L254.

Hodges C. H. Interpretation of alloying tendencies and impurity heats of solution. *Philosophical Magazine B – Physics of Condensed Matter Statistical Mechanics Electronic Optical and Magnetic Properties*. 1978, **38**, 205-220.

Hodge V. J., Austin J. A survey of outlier detection methodologies. *Artificial Intelligence Review*. 2004, **22**, 85-126.

Homer J., Generalis S. C. and Robson J. H. Artificial neural networks for the prediction of liquid viscosity, density, heat of vaporization, boiling point and Pitzer's acentric factor: Part I. Hydrocarbons. *Physical Chemistry Chemical Physics.* 1999, **1,** 4075-4081.

Hopfield J. J. Neurons with graded response have collective computational properties like those of two-state neurons. *Proceedings of the National Academy of Sciences of the United States of America*. 1984, **81**, 3088-3092.

Hopfield J. J., Tank D. W. Computing with neural circuits: a model. *Science*. 1986, **233**, 625-633.

Hornbeck J. W. Thermal and electrical conductivities of the alkali metals. *Physical Review*. 1913, **2**, 217-240.

Hoshino D, Nagahama K., Hirata M. Prediction of the entropy of vaporization at the normal boiling point by the group contribution method. *Industrial & Engineering Chemistry Fundamentals*. 1983, **22**, 430-433.

Huang C. Z., Zhang L., He L., Sun J., Fang B., Zou B., Li Z. Q., Ai X. A study on the prediction of the mechanical properties of a ceramic tool based on an artificial neural network. *Journal of Materials Processing Technology.* 2002, **129,** 399-402.

Huang K. X-ray reflexions from dilute solid solutions. *Proceedings of the Royal Society of London. A, Mathematical and Physical Sciences*. 1947, **190**, 102-117.

Hultgren R., Desal P. D., Hawkins D. T., Gleiser M., Kelley K. K., Wagman D. D. (Eds.) *Selected Values of the Thermodynamic Properties of the Elements.* Metals Park, Ohio: American Society for Metals. 1973.

Hume D. Of the inference from the impression to the idea. ***In****: A Treatise of Human Nature*. (Reprinted from the original edition in three volumes and edited,

with an analytical index, by Selby-Bigge L. A.) Oxford: Clarendon Press, 1896. pp. 86-94.

Hume-Rothery W. Research on the nature, properties and conditions of formation of intermetallic compounds, with special reference to certain compounds of tin. *The Journal of the Institute of Metals*. 1926, **35**, (295, 307).

Hume-Rothery W. The lattice constants of the elements. *The London, Edinburgh, and Dublin Philosophical Magazine and Journal of Science*. 1930, **10**, 217-244.

Hume-Rothery W., Mabbott G. W., and Channel-Evans K. M. The freezing points, melting points, and solid solubility limits of the alloys of silver and copper with the elements of the B Sub-Groups. *Philosophical Transactions of The Royal Society [A]*. 1934, **233**, 1-97.

Hume-Rothery W. *The Structure of Metals and Alloys*. *1st edn*. London, UK: Institute of Metals. 1936.

Hume-Rothery W., Reynolds P. W., Raynor J. V. Factors affecting the formation of 3/2 electron compounds in alloys of copper, silver and gold. *The Journal of the Institute of Metals*. 1940, **66**, 191-207.

Hume-Rothery W., Irving H. M., Williams R. J. P. The valencies of the transition elements in the metallic state. *Proceedings of the Royal Society of London. Series A, Mathematical and Physical Sciences*. 1951, **208**, 431-443.

Hume-Rothery W. *Elements of Structural Metallurgy*. London, UK: Institute of Metals. 1961. pp. 105-133.

Hume-Rothery W., Raynor G. V. *The Structure of Metals and Alloys, 4th edn.* London, UK: Institute of Metals. 1962, pp. 109-112.

Hume-Rothery W. Intermetallic chemistry of iron. *Journal of the Iron and Steel Institute*. 1965, **203**, 1181-1193.

Hume-Rothery W. Atomic diameters, atomic volumes and solid solubility relations in alloys. *Acta Metallurgica*. 1966, **14**, 17-20.

Hume-Rothery W. Factors affecting the stability of metallic phases. *In*: **Rudman P. S., Stringer J., Jaffee R. I. (Eds.)** *Phase Stability in Metals and Alloys*. New York: McGraw-Hill, 1967. pp. 3-23.

Hume-Rothery W., Smallman R. E., Haworth C. W. *The Structure of Metals and Alloys, 5th edn.* London, UK: Institute of Metals. 1969. pp. 111-202.

Inglesfield J. E. Perturbation theory and alloying behaviour I. Formalism. *Journal of Physics C: Solid State Physics*. 1969a, **2**, 1285-1292.

Inglesfield J. E. Perturbation theory and alloying behaviour II. The mercury-magnesium system. *Journal of Physics C: Solid State Physics*. 1969b, **2**, 1293-1298.

Inglesfield J. E. The electrochemical effect in alloys of cadmium, magnesium and mercury. *Acta Metallurgica*. 1969c, **17**, 1395-1402.

Ito T., Ohno T., Shiraishi K., Yamaguchi E. Computer-aided materials design for semiconductors. *Advanced Materials*. 1993, **5**, 198-206.

Jadid M. N., Fairbairn D. R. Neural-network applications in predicting moment-curvature parameters from experimental data. *Engineering Applications of Artificial Intelligence.* 1996, **9,** 309-319.

Jain A. K., Mao J., Mohiuddin K. M. Artificial neural networks: a tutorial. *Computer.* 1996, **29**, 31-34.

Jandeleit B., Schaefer D. J., Powers T. S., Turner H. W., Weinberg W. H. Combinatorial materials science and catalysis. *Angewandte Chemie (International Edn.)*. 1999, **38**, 2495-2532.

Jiang L. Q., Guo J. K., Liu H. B., Zhu M., Zhou X., Wu P., Li C. H. Prediction of lattice constant in cubic perovskite. *Journal of Physics and Chemistry of Solids*. 2006, **67**, 1531-1536.

Johnson R. A. Alloy models with the embedded-atom method. *Physical Review B*. 1989, **39**, 12554-12559.

Johnson R. A. Phase-stability of FCC alloys with the embedded-atom method. *Physical Review B*. 1990, **41**, 9717-9720.

Jones H. Extent of solid solubility in magnesium and aluminium. *Materials Science and Engineering*. 1983, **57**, L5-L8.

Jung J. J., Jo G. Semantic outlier analysis for sessionizing web logs. *Proceedings of the 14th European Conference on Machine Learning/7th European Conference on Principles and Practice of Knowledge Discovery in Databases*. 2004, 13-25. (Entry website, on 22/10/2009: http://km.aifb.uni-karlsruhe.de/ws/ewmf03/papers/Jung.pdf)

Karabulut E. Ö., Koyuncu M. Neural network-based correlations for the thermal conductivity of propane. *Fluid Phase Equilibria*. 2007, **257**, 6-17.

Kattner U. R., Lin J. C., Chang Y. A. Thermodynamic assessment and calculation of the Ti-Al system. *Metallurgical and Materials Transactions A*. 1992, **23**, 2081-2090.

Kaufman L., Cohen M. Thermodynamics and kinetics of martensitic transformations. *Progress in Metal Physics*. 1958, **7**, 165-246.

Kaufman L. The lattice stability of metals – I. Titanium and zirconium. *Acta Metallurgica*. 1959, **7**, 575-587.

Kaufman L., Clougherty E. V., Weiss R. J. The lattice stability of metals – III. Iron. *Acta Metallurgica*. 1963, **11**, 323-335.

Kaufman L. The stability of metallic phases. *Progress in Materials Science*. 1969, **14**, 57-96.

Kaufman L., Bernstein H. *Computer Calculation of Phase Diagrams.* New York: Academic Press, 1970.

Kaufman L., Nesor H. Application of computer techniques to prediction of metastable transitions in metallic systems. *Materials Science and Engineering*. 1976, **23**, 119-123.

Kaufman L. Coupled phase diagrams and thermochemical data for transition metal binary systems – III. *CALPHAD*. 1978, **2**, 117-146.

Kaufman L., Nesor H. Coupled phase diagrams and thermochemical data for transition metal binary systems – I. *CALPHAD*. 1978a, **2**, 55-80.

Kaufman L., Nesor H. Coupled phase diagrams and thermochemical data for transition metal binary systems – II. *CALPHAD*. 1978b, **2**, 81-108.

Kaufman L., Nesor H. Coupled phase diagrams and thermochemical data for transition metal binary systems – IV. *CALPHAD*. 1978c, **2**, 295-318.

Kaufman L., Nesor H. Coupled phase diagrams and thermochemical data for transition metal binary systems –V. *CALPHAD*. 1978d, **2**, 325-348.

Kaufman L. Coupled phase diagrams and thermochemical data for transition metal binary systems – VI. *CALPHAD*. 1979a, **3**, 45-76.

Kaufman L. Calculation of quasi binary and quasi ternary oxynitride systems – III. *CALPHAD*. 1979b, **3**, 275-291.

Kaufman L., Tanner L. E. Coupled phase diagrams and thermochemical descriptions of the titanium-beryllium, zirconium-beryllium and hafnium-beryllium systems. *CALPHAD*. 1979, **3**, 91-107.

Kaufman L., Hayes F., Birnie D. Calculation of quasi binary and quasi ternary oxyntiride systems – IV. *CALPHAD*. 1981, **5**, 163-184.

Kaufman L., Tanner L. E. C Coupled phase diagrams and thermochemical descriptions of the iron-beryllium, cobalt-beryllium, nickel-beryllium and copper-beryllium systems. *CALPHAD*. 1984, **8**, 121-133.

Kaufman L., Uhrenius B., Birnie D., Taylor K. Coupled pair potential, thermochemical and phase diagram data for transition metal binary systems – VII. *CALPHAD*. 1984, **8**, 25-66.

Kaufman L. Calculation of multicomponent tantalum based phase diagrams. *CALPHAD*. 1991, **15**, 261-282.

Kaufman L. Forward to **Saunders N., Miodownik A. P.** *CALPHAD: Calculation of Phase Diagrams, A Comprehensive Guide*. Oxford: Pergamon. 1998, p. xvi.

Kaufman L., Turchi P. E. A., Huang W., Liu Z. K. Thermodynamics of the Cr-Ta-W system by combining the *Ab initio* and CALPHAD methods. *CALPHAD*. 2001, **25**, 419-433.

Kaufmann E. N. Lattice location of zinc implanted into beryllium. *Physics Letters A*. 1977, **61**, 479-480.

Kaufmann E. N., Vianden R. Anomalous displacement in osmium-substituted beryllium. *Physical Review Letters*. 1977, 38, 1290-1292.

Kaufmann E. N., Vianden R., Chelikowsky J. R., Phillips J. C. Extension of equilibrium formation criteria to metastable microalloys. *Physical Review Letters*. 1977, **39**, 1671-1675.

Kawazoe Y. How *ab initio* computer simulation can predict materials properties before experiment. *Intelligent Processing and Manufacturing of Materials, 1999. IPMM '99. Proceedings of the Second International Conference on.* July 1999, **1**, 355-359.

Kaye G. W. C., Laby T. H. *Tables of Physical and Chemical Constants, 16th edn.* Harlow: Longman, 1995, pp. 212-214, pp. 338-342.

Kazius J., Nijssen S., Kok J., Bäck T., IJzerman A. P. Substructure mining using elaborate chemical representation. *Journal of Chemical Information and Modelling*. 2006, **46**, 597-605.

Kennedy K, Stefansky T., Davy G., Zackay V. F., Parker E. R. Rapid method for determining ternary-alloy phase diagrams. *Journal of Applied Physics*. 1965, **36**, 3808-3810.

Kishimoto A., Koumoto K., Yanagida H., Nameki M. Microstructure dependence of mechanical and dielectric strengths – i. porosity. *Engineering Fracture Mechanics*. 1991, **40**, 927-930.

Kittel C. *Introduction to Solid State, 8th edition*. Physics. John Wiely & Sons, 2005. pp. 156-157.

Klein O., Lange E. Work of electron emission in metals. *Zeitschrift für Elektrochemie*. 1938, **44**, 542-562.

Klein M. L., Shinoda W. Large-scale molecular dynamics simulations of self-assembling systems. *Science*. 2008, **321**, 798-800.

Kohonen T. (Ed.) *Self-organization and Associative Memory. 3rd edn.* New York: Springer, 1989.

Komorowski L. Electronegativity and hardness in the chemical approximation. *Chemical Physics*. 1987, **114**, 55-71.

Kou Y., Lu C-T., Sirwongwattana S., Huang Y-P. Survey of fraud detection techniques networking. *IEEE International Conference on Sensing and Control*. 2004, **2**, 749-754.

Lachtermacher G., Fuller J. D. Backpropagation in time-series forecasting. *Journal of Forecasting*. 1995, **14**, 381-393.

Lannoo M. Nanotechnology and semiconducing materials. *In: European White Book on Fundamental Research in Materials Science*. Max-Planck-Institut für Metallforschung Stuttgart, 2001. Chapter 1, Materials: Science and Engineering. pp. 63-66.

Larkiola J., Myllykoski P., Nylander J. and Korhonen A. S. Prediction of rolling force in cold rolling by using physical models and neural computing. *Journal of Materials Processing Technology*. 1996, **60**, 381-386.

Lawson D. D. Methods of calculating engineering parameters for gas separations. *Applied Energy*. 1980, **6**, 241-255.

Lester H. H. The determination of the work function when an electron escapes from the surface of a hot body. *Philosophical Magazine*. 1916, **31**, 197-221.

Li C., Soh K. C. K., Wu P. Formability of ABO_3 perovskites. *Journal of Alloys and Compounds*. 2004, **372**, 40-48.

Li K. Y., Xue D. F. Estimation of electronegativity values of elements in different valence states. *Journal of Physical Chemistry A*. 2006, **110**, 11332-11337.

Li Z. Properties of Novel Materials from First Principles. *Ph.D Dissertation*. 2004. University of Science and Technology of China. 146 pages.

Liang Y-Z., Kvalheim O. M. Robust methods for multivariate analysis – a tutorial review. *Chemometrics and Intelligent Laboratory Systems*. 1996, **32**, 1-10.

Lim S. S., Rossiter P. L., Tibballs J. E. Assessment of the Al-Ag binary phase diagram. *Calphad*. 1995, **19**, 131-141.

Liu B., Ma Y., Yu P. S. Discovering unexpected information from your competitors' web sites. *Proceedings of the 7th ACM SIGKDD International Conference on Knowledge Discovery and Data Mining*. San Francisco, California, 2001, pp. 144-153.

Liu Z., Zhong Y. and Schlom D. G. Computational thermodynamic modeling of the Mg-B system. *Calphad*. 2001, **25**, 299-303.

Liu J. Z., Zunger A. Thermodynamic states and phase diagrams for bulk-incoherent, bulk-coherent, and epitaxially-coherent semiconductor alloys: Application to cubic (Ga, In)N. *Physical Review B*. 2008, **77**, (205201)1-(205201)12.

Lopez J. M., Alonso J. A. Semi-empirical study of metastable alloys obtained by ion-implantation in metals and semiconductors. *Physica Status Solidi A – Applied Research.* 1982a, **72**, 777-781.

Lopez J. M., Alonso J. A. A comparison of two parametrizations of solid solubility in alloys: thermochemical coordinates versus orbital radii coordinates. *Physica B*. 1982b, **113**, 103-112.

Lopez J. M., Alonso J. A. Semi-empirical theory of solid solubility in metallic alloys. *Physica Status Solidi A – Applied Research*. 1983, **76**, 675-682.

Lopez J. M., Alonso J. A. Semi-empirical theory of solid solubility in transition-metal alloys. *Zeitschrift fur Naturforschung Section A – A Journal of Physical Sciences*. 1985, **40**, 1199-1205.

Lorenz L. Bestimmung der Wärmegrade in absolutem Maasse. *Annalen der Physik*. 1872, **223**, 429-452.

Lorenz L. Ueber das Leitungsvermögen der Metalle für Wärme und Electricität. *Annalen der Physik*. 1881a, **249**, 422-447.

Lorenz L. Ueber das Leitungsvermögen der Metalle für Wärme und Electricität. *Annalen der Physik*. 1881b, **249**, 582-606.

Lu Z. W., Wei S. H., Zunger A., Frota-Pessoa S., Ferreira L. G. First-principles statistical mechanics of structural stability of intermetallic compounds. *Physical Review B*. 1991, **44**, 512-544.

Lu Z. W., Klein B. M., Zunger A. Atomic short-range order and alloy ordering tendency in the Ag-Au system. *Modelling and Simulation in Materials Science and Engineering*. 1995, **3**, 753-770.

Lufaso M. W., Woodward P. M. Prediction of the crystal structures of perovskites using the software program *SPuDs*. *Acta Crystallographica Section B*. 2001, **B57**, 725-738.

Lukas H. L., Weiss J., Henig E.-Th. Strategies for the calculation of phase diagrams. *CALPHAD*. 1982, **6**, 229-251.

Luo W. Z., Schlesinger M. E. Thermodynamics of the iron-carbon-zinc system. *Metallurgical and Materials Transactions B – Process Metallurgy and Materials Processing Science*. 1994, **25**, 569-578.

Luo W., Jin Z., Liu H. and Wang T. Thermodynamic assessment of the Au-Ti system. *Calphad*. 2001, **25,** 19-26.

Ma P., Zhao X. Modified group contribution method for predicting the entropy of vaporization at the normal boiling point. *Industrial & Engineering Chemistry Research.* 1993, **32**, 3180-3183.

Maarleveld P. R., Kaars P. B., Weeber A. W., Bakker H. Application of the embedded atom method to the calculation of formation enthalpies and lattice-parameters of Pd-Ni alloys. *Physica B & C*. 1986, **142**, 328-331.

Mackay D. J. C. Bayesian interpolation. *Neural Computation*. 1992a, **4**, 415-447.

Mackay D. J. C. A practical Bayesian framework for backpropagation networks. *Neural Computation*. 1992b, **4**, 448-472.

Magnaterra A., Mezzetti F. Charge transfer in binary alloys. *Nuovo Cimento B*. 1971, **B6**, 206-213.

Magnaterra A., Mezzetti F. Atomic-size effect in binary-alloys. *Nuovo Cimento B*. 1974, **B24**, 135-140.

Malagoni R. A., Andrade R. M., Alves É. J., Franco Jr. M. R. Behavior of the empirical methods for prediction of vaporization enthalpy. *Fluid Phase Equilibria*. 2005, **236**, 256-260.

Maletic J. I., Marcus A. Data cleansing: A preclude to knowledge discovery. *In*: **Maimon O., Rokach L.** ***ed.*** *Data Mining and Knowledge Discovery Handbook*. Springer: New York. 2005. pp. 21-36.

Malinov S., Sha W., Guo Z. Application of artificial neural network for prediction of time-temperature-transformation diagrams in titanium alloys. *Materials Science and Engineering A*. 2000, **283**, 1-10.

Malinov S., Sha W. Software products for modelling and simulation in materials science. *Computational Materials Science.* 2003, **28,** 179-198.

Malinov S., Sha W. Application of artificial neural networks for modeling correlations in titanium alloys. *Materials Science and Engineering A*. 2004, **365,** 202-211.

Mangonon P. L. *The Principles of Materials Selection for Engineering Design.* Upper Saddle River, New Jersey: Prentice Hall. 1999, pp. 10 – 12.

Markham J. J., Jr. Miller P. H. The effect of surface states on the temperature variation of the work function of semiconductors. *Physical Review.* 1949, **75**, 959-967.

Markou M., Singh S. Novelty detection: a review – part 1: statistical approaches. *Signal Processing*. 2003a, **83**, 2481-2497.

Markou M., Singh S. Novelty detection: a review – part 2: neural network based approaches. *Signal Processing*. 2003b, **83**, 2499-2521.

Maroulis G. (Ed.) *Atoms, Molecules and Clusters in Electric Fields: Theoretical Approaches to the Calculation of Electric Polarizability*. London: Imperial College Press. 2006. pp. v-viii.

Maroulis G., Hohm U. (Eds) *Electric Polarizability and Hyperpolarizability: Theory and Experiment. A User's Handbook*. Dordrecht, Netherlands: Springer. 2009.

Martin S. T. On the thermionic and adsorptive properties of the surfaces of a tungsten single crystal. *Physical Review*. 1939, **56**, 947-959.

Martin A., Carstensen J. Extended solubility approach: Solubility parameters for crystalline solid compounds. *Journal of Pharmaceutical Sciences*. 1981, **70**, 170-172.

Martin B. Coincidences: remarkable or random? *Skeptical Inquirer*. 1998, **22**, 23-28.

Martinez S. E., Smith A. E., Bidanda B. Reducing waste in casting with a predictive neural model. *Journal of Intelligent Manufacturing*. 1994, **5**, 277-286.

Massalski T. B., King H. W. Alloy phases of the noble metals. *Progress in Materials Science*. 1963, **10**, 3-78.

Massalski T. B., Mizutani U. Electronic structure of Hume-Rothery phases. *Progress in Materials Science*. 1978, **22**, 151-262.

Massalski T. B., Murray J. L., Bennett L. H., and Baker H. ed. *Binary alloy Phase Diagrams, Vol. 1.* American Society for Metals, 1987 (copyright 1986), pp.1-87, pp. 235-341, pp.908-982.

Massalski T. B. Structure and stability of alloys. *In*: **Cahn R. W., Haasen P. (Eds.)** *Physical Metallurgy*. 4th edition. North Holland: Amsterdam – Lausanne – New York – Oxford – Shannon – Tokyo, 1996. pp. 135-204.

Massalski T. B. Hume-Rothery rules re-visited. *In:* **Turchi E. A., Shull R. D., Gonis A. (Eds.)** *Science of Alloys for the 21st Century: A Hume-Rothery Symposium Celebration*. Warrendale: TMS (The Minerals, Metals & Materials Society), 2000, pp. 55-70.

Masters T. (Ed.) *Practical Neural Network Recipes in C++*. Boston, MA: Academic Press, 1994, pp. 174-176.

Mathworks

http://www.mathworks.com/access/helpdesk/help/pdf_doc/nnet/nnet.pdf.

Access on 09/03/2009, pp. 16-188.

McCurdy K. G., Laidler K. J. Heats of vaporization of a series of aliphatic alcohols. *Canadian Journal of Chemistry*. 1963, **41**, 1867-1871.

Megaw H. D. Crystal structure of double oxides of the perovskite type. *The Proceedings of the Physical Society*. 1946, **58**, 133-152.

Meijering J. L. Segregation in regular ternary solutions, part I. *Philips Research Report*. 1950, **5**, 333-356.

Meijering J. L. Segregation in regular ternary solutions, part II. *Philips Research Report*. 1951, **6**, 183-210.

Meijering J. L., Hardy H. K. Closed miscibility in ternary and quaternary regular alloy solutions. *Acta Metallurgica*. 1956, **4**, 249-256.

Meijering J. L. Calculation of the nickel-chromium-copper phase diagram from binary data. *Acta Metallurgica*. 1957, **5**, 257-264.

Meijering J. L. Thermodynamical calculation of phase diagrams. ***In***: *The Physical Chemistry of Metallic Solutions and Intermetallic Compounds: Proceedings of a Symposium held at the National Physical Laboratory on 4th, 5th, and 6th June, 1958*. New York: Chemical Publishing Company, Inc.; 1960, pp. 124-142.

Meyer A., Young W. H. Thermoelectricity and energy-dependent pseudopotentials. *Physical Review*. 1969, **184**, 1003-1006.

Meyer A., Umar I. H., Young W. H. Lattice spacings and compressibilities vs. Pauling radii and valencies. *Physical Review B*. 1971a, **4**, 3287-3291.

Meyer A., Young W. H., Terence M. H. Pseudopotentials and residual resistivities in silver and gold. *Philosophical Magazine*. 1971b, **23**, 977-986.

Meyra A. G., Kuz V. A., Zarragoicoechea G. J. Universal behavior of the enthalpy of vaporization: an empirical equation. *Fluid Phase Equilibria*. 2004, **218**, 205-207.

Michaelson H. B. Work functions of the elements. *Journal of Applied Physics*. 1950, **21**, 536-540.

Michaelson H. B. The work function of the elements and its periodicity. *Journal of Applied Physics*. 1977, **48**, 4729-4733.

Michon L., Hanquet B. Asphalt study by neural networks. Correlation between chemical and rheological properties. *Energy & Fuels*. 1997, **11**, 1188-1193.

Miedema A. R. The electronegativity parameter for transition metals: heat of formation and charge transfer in alloys. *Journal of the Less-Common Metals*. 1973, **32**, 117-136.

Miedema A. R., De Boer F. R., De Chatel P. F. Empirical description of the role of electronegativity in alloy formation. *Journal of Physics F – Metal Physics*. 1973, **3**, 1558-1576.

Miedema A. R., Boom R., De Boer F. R. On the heat of formation of solid alloys. *Journal of the Less-Common Metals*. 1975, **41**, 283-298.

Miedema A. R. On the heat of formation of solid alloys II. *Journal of the Less-Common Metals*. 1976a, **46**, 67-83.

Miedema A. R. Heat of formation of alloys. *Philips Technical Review.* 1976b, **36**, 217-231.

Miedema A. R., De Boer F. R., Boom R. Model predictions for the enthalpy of formation of transition metal alloys. *CALPHAD*. 1977, **1**, 341-359.

Miedema A. R., De Chatel P. F. A semi-empirical approach to the heat of formation problem. In: **Bennett L. H. (Ed.)** *Theory of Alloy Phase Formation*. The Metallurgical Society of AIME: New York, 1980. pp. 344-387.

Milman V., Winkler B., White J. A., Pickard C. J., Payne M. C., Akhmatskaya E. V., Nobes R. H. Electronic structure, properties, and phase stability of inorganic crystals: A pseudopotential plane-wave study. *International Journal of Quantum Chemistry*. 2000, **77**, 895-910.

Miller N.C., Shirn G. A. Co-sputtered Au-SiO_2 cermet films. *Applied Physics Letters.* 1967, **10**, 86-88.

Miller J. N. Tutorial review: Outliers in experimental data and their treatment. *Analyst*. 1993, **118**, 455-461.

Moffatt W. G. (Ed.) *The Handbook of Binary Phase Diagrams. Vol.1*. Schenectady, N.Y.; General Electric Co., 1977 (Updated by 11/08/1994), Section Ag-Al to Ag-Zr.

Moghtased-Azar K., Zaletnyik P. Crustal velocity field modelling with neural network and polynomials. *Observing Our Changing Earth*. 2009, **133**, 809-816.

Mohammadi A. H., Richon D. New predictive methods for estimating the vaporization enthalpies of hydrocarbons and petroleum fractions. *Industrial & Engineering Chemistry Research*. 2007, **46**, 2665-2671.

Mohri T., Terakura K., Takizawa S., Sanchez J. M. First-principles study of short-range order and instabilities in Au-Cu, Au-Ag and Au-Pd alloys. *Acta Metallurgica et Materialia*. 1991, **39**, 493-501.

Moore D. S., McCabe G. P. *Introduction to the Practice of Statistics, 3rd edition.* New York: W. H. Freeman and Company. 1999. pp. 166, 207 – 212.

Moore D. S., Notz W. I. *Statistics: Concepts and Controversies*. New York: W. H. Freeman and Company. 2006. pp. 289-303.

Moore W. J. *Physical Chemistry, 5th edition.* London: London Group Limited, 1972. pp. 1-2.

Mooser E., Pearson W. B. On the crystal chemistry of normal valence compounds. *Acta crystallographica*. 1959, **12**, 1015-1022.

Morecroft J. H. *Electron Tubes and Their Applications*. New York: Wiley and Sons, Inc., 1936. p. 39.

Morgan D., Rodgers J., Ceder G. Automatic construction, implementation and assessment of Pettifor maps. *Journal of Physics: Condensed Matter*. 2003, **15**, 4361-4369.

Morgan D., Ceder G. Data mining in materials development. *In*: **Yip S.** Ed. *Handbook of Materials Modelling*. Berlin: Springer. 2005. pp. 395-421.

Moroney M. J. Correlation, Cause and Effect. *In:* **Facts from Figures**, **3rd edition**. Reprinted 1967. pp. 271 – 320.

Mott N. F. The cohesive forces in metals and alloys. *Reports on Progress in Physics*. 1962, **25**, 218-243.

Murakami M., Matsumoto Y., Nagano M., Hasegawa T., Kawasaki M., Koinuma H. Combinatorial fabrication and characterization of ferromagnetic Ti-Co-O system. *Applied Surface Science*. 2004, **223**, 245-248.

Murray J., Peruzzi A., Abriata J. P. The Al-Zr (aluminum-zirconium) system. *Journal of Phase Equilibria*. 1992, **13**, 277-291.

Music D., Takahashi T., Vitos L., Asker C., Abrikosov I. A., Schneider J. M. Elastic properties of Fe-Mn random alloys studied by *ab initio* calculations. *Applied Physics Letters*. 2007, **91**, (191904)1-(191904)3.

Nagle J. K. Atomic polarizability and electronegativity. *Journal of the American Chemical Society*. 1990, **112**, 4741-4747.

Nam S-H, Oh S-Y. Real-time dynamic visual tracking using PSD sensors and extended trapezoidal motion planning. *Applied Intelligence.* 1999, **10**, 53-70.

Nath J. Acentric factor and the heats of vaporization for unassociated polar and nonpolar organic liquids. *Industrial & Engineering Chemistry Fundamentals.* 1979, **18**, 297-298.

National Academy of Sciences. *Materials and Man's Needs: Materials Science and Engineering: Summary Report of the Committee on the Survey of Materials Science and Engineering*. 1974. p. 1.

Ohm G. S. *Die Galvanische Kette, Mathematisch Bearbeitet*. Bei T. H. Riemann, Berlin, 1827.

Ohnuma I., Fujita Y., Mitsui H., Ishikawa K., Kainuma R. and Ishida K. Phase equilibria in the Ti-Al binary system. *Acta Materialia*. 2000, **48**, 3113-3123.

Ohtani H., Ishida K. Application of CALPHAD method to material design. *Thermochimica Acta*. 1998, **314**, 69-77.

Olesinski R. W., Abbaschian G. J. The Cu-Si (Copper-Silicon) system. *Journal of Phase Equilibria*. 1986, **7**, 170-178.

Ordejón P. Linear scaling *ab initio* calculations in nanoscale materials with SIESTA. *Physica Status Solidi (b)*. 2000, **217**, 335-356.

Orr K. Data quality and systems theory. *Communications of the ACM*. 1998, **41**, 66-71.

Ortiz M. C., Sarabia L. A., Herrero A. Robust regression techniques: A useful alternative for the detection of outlier data in chemical analysis. *Talanta*. 2006, **70**, 499-512.

Ouyang Y. F., Chen H. M., Zhong X. P. Enthalpies of formation of noble metal binary alloys bearing Rh or Ir. *Journal of Materials Science and Technology*. 2003, **19**, 243-246.

Ozolins V., Wolverton C., Zunger A. Cu-Au, Ag-Au, Cu-Ag, and Ni-Au intermetallics: First-principles study of temperature-composition phase diagrams and structures. *Physical Review B*. 1998, **57**, 6427-6443.

Pal S. K., Srimani P. K. Neurocomputing: motivation, models, and hybridization. *Computer*. 1996, **29,** 24-28.

Parthé E. From Hume-Rothery's 8-N rule to valence electron rules for zintl phase and their extensions. *In:* **Turchi E. A., Shull R. D., Gonis A. (Eds.)** *Science of Alloys for the 21st Century: A Hume-Rothery Symposium Celebration*. Warrendale: TMS (The Minerals, Metals & Materials Society), 2000, pp. 71-103.

Pasturel A., Colinet C., Manh D. N., Paxton A. T., vanSchilfgaarde M. Electronic structure and phase stability study in the Ni-Ti system. *Physical Review B*. 1995, **21**, 15176-15190.

Pauling L. *The Nature of the Chemical Bond and the Structure of Molecules and Crystals: An Introduction to Modern Structural Chemistry*. Cornell University Press; Oxford University Press, 1960. pp. 505-562.

Pearl J. *Causality: Models, Reasoning, and Inference*. Cambridge: Cambridge University Press, 2000. Preface, pp. 331-358.

Pearson K. Contingency and correlation – the insufficiency of causation. ***In:*** *The Grammar of Science, Part 1 – Physical*. 3rd Edition. London: Adam and Charles Black, 1911. pp. 152-178.

Pearson W. B. *The Crystal Chemistry and Physics of Metals and Alloys*. New York: Wiley-Interscience. 1972. p. 68.

Pelton A. D., Schmalzried H. On the geometrical representation of phase equilibria. *Metallurgical and Materials Transactions B*. 1973, **4**, 1395-1404.

Petrovskiy M. I. Outlier detection algorithms in data mining systems. *Programming and Computer Software*. 2003, **29**, 228-237.

Pettifor D. G. Theory of the heats of formation of transition-metal alloys. *Physical Review Letters*. 1979, **42**, 846-850.

Pettifor D. G. A chemical scale for crystal-structure maps. *Solid State Communications*. 1984, **51**, 31-34.

Pettifor D. G. The structures of binary compounds: I. Phenomenological structure maps. *Journal of Physics C: Solid State Physics*. 1986, **19**, 285-313.

Pettifor D. G. William Hume-Rothery: his life and science. *In:* **Turchi E. A., Shull R. D., Gonis A. (Eds.)** *Science of Alloys for the 21st Century: A Hume-Rothery Symposium Celebration*. Warrendale: TMS (The Minerals, Metals & Materials Society), 2000a, pp. 9-32.

Pettifor D. G. Structure mapping. *In*: **Westbrook J. H., Fleischer R. L. (Eds.)**, *Crystal structures of intermetallic compounds.* John Wiley & Sons, New York, 2000b. pp. 195-214.

Pettifor D. G. Electron theory in materials modeling. *Acta Materialia.* 2003, **51**, 5649-5673.

Pfeifer U., Poersch T., Fuhr N. Retrieval effectiveness of proper name search methods. *Information Processing & Management*. 1996, **32**, 667-679.

Pitzer K. S., Lippmann D. Z., Curl R. F., Huggins C. M., Petersen D. E. The volumetric and thermodynamic properties of fluids. II. Compressibility factor, vapour pressure and entropy of vaporization. *Journal of the American Chemical Society*. 1955, **77**, 3433-3440.

Poincaré H. *Science and Hypothesis.* New York: Dover Publications, Inc., 1952, pp. 140-159.

Poling B. E., Prausnitz J. M., O'connell J. P. *The Properties of Gases and Liquids. 5th Edn*. McGraw-Hill Professional. 2000. pp. 7.13 – 7.25.

Pollock J. J., Zamora A. Automatic spelling correction in scientific and scholarly text. *Communications of the ACM*. 1984, **27**, 358-368.

Popper K. R. *Conjectures and Refutations, the Growth of Scientific Knowledge.* London: Routledge & Kegan Paul, 1963, pp. 33-65.

Popper K. R. *The Logic of Scientific Discovery.* New York: Harper Torchbooks, 1965, p. 59.

Potter J. G. Temperature dependence of the work function of tungsten from measurement of contact potentials by the Kelvin method. *Physical Review*. 1940, **58**, 623-632.

Provost F., Aronis J. Scaling up inductive learning with massive parallelism. *Machine Learning*. 1996, **23**, 33-46.

Pullar R. C., Zhang Y., Chen L., Yang S., Evans J. R. G., Alford N. M. Manufacture and measurement of combinatorial libraries of dielectric ceramics, part I: physical characterization of $Ba_{1-x}Sr_xTiO_3$ libraries. *Journal of European Ceramic Society.* 2007a, **27**, 3861-3865.

Pullar R. C., Zhang Y., Chen L., Yang S., Evans J. R. G., Petrov P. K., Salak A. N., Kiselev D. A., Kholkin A. L., Ferreira V. M., Alford N. M. Manufacture and measurement of combinatorial libraries of dielectric ceramics, part II: dielectric measurements of $Ba_{1-x}Sr_xTiO_3$ libraries. *Journal of European Ceramic Society.* 2007b, **27**, 4437-4443.

Raisin C., Pinchaux R. Properties photoelectriques de l'arsenic cristallise entre 7et 11,4 ev. *Solid State Communications*. 1975, **16**, 941-944.

Raj K. H., Sharma R. S., Srivastava S., Patvardhan C. Modeling of manufacturing processes with ANNs for intelligent manufacturing. *International Journal of Machine Tools & Manufacture.* 2000, **40**, 851-868.

Rajan K. Combinatorial materials sciences: experimental strategies for accelerated knowledge discovery. *Annual Review of Materials Research.* 2008, **38**, 299-322.

Rao C. R. Randomness and creativity. ***In:*** *Statistics and Truth: Putting Chance to Work*. World Scientific Publishing Co. Pte. Ltd. 1997. pp. 21-25.

Reaney I. M., Ubic R. Dielectric and structural characteristics of perovskites and related materials as a function of tolerance factor. *Ferroelectrics*. 1999, **228**, 23-38.

Redman T. C. *Data Quality for the Information Age*. Norwood, MA, USA: Artech House, Inc. 1997. pp. 5, 14.

Redman T. C. The impact of poor data quality on the typical enterprise. *Communications of the ACM*. 1998, **41**, 79-82.

Reichenbach H. *The Rise of Scientific Philosophy.* Berkeley: University of California Press, 1963, pp. 74-94.

Reid R. C., Sherwood T. K. *The Properties of Gases and Liquids: Their Estimation and Correlation*. New York, McGraw-Hill, 1958. p.2.

Reid R. C., Prausnitz J. M., Poling B. E. *The Properties of Gases and Liquids. 4th Edition*. McGraw-Hill Professional. 1987. p. 219.

Reynolds P. W., Hume-Rothery W. The constitution of silver-rich antimony-silver alloys. *The Journal of the Institute of Metals*. 1937, **60**, 365-374.

Richard A. H. General method for the rapid solid-phase synthesis of large numbers of peptides: specificity of antigen – antibody interaction at the level of individual amino acids. *Proceedings of the National Academy of Sciences.* 1985, **82**, 5131-5135.

Riedel L. Kritischer koeffizient, dichte des gesättigten dampfes und verdampfungswärme. untersuchungen über eine erweiterung des theorems der übereinstimmenden zustände. Teil III. Chemie – Ingenieur – Technik. 1954, **26**, 679-683.

Rivière J. C. Work function: measurements and results. ***In:*** **Green M. (Eds.)** *Solid State Surface Science*. New York: Marcel Dekker, 1969. pp. 179-289.

Roberts B. W. X-ray measurement of order in CuAu. *Acta Metallurgica*. 1954, **2**, 597-603.

Rosenberg H. M. *The Solid State*. Oxford University Press, 1988. p. 129.

Rother F., Bomke H. Über die Berechnung der Austrittsarbeit aus einfachen Materialkonstanten. *Zeitschrift für Physik A. Hadrons and Nuclei.* 1933, **86**, 231-240.

Rousseeuw P. J., Leroy A. M. *Robust regression and outlier detection*. Hoboken: John Wiley & Sons. 2003. pp. 1-18.

Rumelhart D. E., Hinton G. E., Williams R. J. Learning internal representation by error propagation. *In*: **RUMELHART, D.E., MCCLLELAND, J.L. (Eds.)** *Parallel distributed processing: exploration in the microstructure of cognition*. Vol. 1. MIT Press, Cambridge, MA, 1986, Chapter 8.

Russell B. *Human Knowledge, Its Scope and Limits.* New York: Simon and Schuster, Inc., 1948, pp. 451-455.

Russell B. *History of Western Philosophy, and its Connection with Political and Social Circumstances from the Earliest Times to the Present Day.* London: Routledge, 1996, p. 639.

Salinas-Sanchez A., Garcia-Munoz J.L., Rodriguez-Carvajal J., Saez-Puche R., Martinez J.L. Structural characterization of R_2BaCuO_5 (R = Y, Lu, Yb, Tm, Er, Ho, Dy, Gd, Eu and Sm) oxides by X-ray and neutron diffraction. *Journal of Solid State Chemistry.* 1992, **100**, 201-211.

Saunders N., Miodownik A. P. *CALPHAD: Calculation of Phase Diagrams. A Comprehensive Guide*. Oxford: Pergamon, 1998. Chapter 2. pp. 7-29.

Sawatzky E., Kay E. Cation deficiencies in RF sputtered gadolinium iron garnet films. *IBM Journal of Research and Development.* 1969, **13**, 696-702.

Scarpa O. Volta effect and electrochemical potentials. *Nuovo Cimento*. 1940, **17**, 54-68.

Scarpa O. Electrochemical potential and voltaic effect. VI. The electrochemical potentials of metals and their electron arrangement. *Atti (Rendiconti) della Reale Accademia Nazionale deiLincei. Classediscienze fisiche, matematiche e naturali, Roma*. 1941, **2**, 1062-1069.

Schalkoff, R. J. *Artificial Neural Networks.* London: McGraw-Hill, 1997, pp.1-35.

Schmid R. A thermodynamic analysis of the Cu-O system with an associated solution model. *Metallurgical and Materials Transactions B*. 1983, **14**, 473-481.

Schmidt M., Lipson H. Distilling free-form natural laws from experimental data. *Science*. 2009, **324**, 81-85.

Schultz P. G., Xiang X. D. Combinatorial approaches to materials science. *Current Opinion in Solid State & Materials Science*. 1998, **3**, 153-158.

Schwerdtfeger P. Atomic static dipole polarizabilities. *In:* **Maroulis G. (Eds.)** *Atoms, Molecules and Clusters in Electric Fields*. Imperial College Press. 2006. pp. 1-32.

Scott D. J., Manos S., Coveney P. V., Rossiny J. C. H., Fearn S., Kilner J. A., Pullar R. C., Alford N. Mc N., Axelsson A. -K., Zhang Y., Chen L., Yang S., Evans J. R. G., Sebastian M. T. Functional ceramic materials database: an outline resource for materials research. *Journal of Chemical Information and Modelling*. 2008, **48**, 449-455.

Seely S. Work function and temperature. *Physical Review*. 1941, **59**, 75-78.

Senkan S. M. High-throughput screening of solid-state catalyst libraries. *Nature*. 1998, **394**, 350-353.

Sha W. Private communication on 27th May 2008 *via* email.

Sharma R. C., Chang Y. A. Thermodynamics and phase relationships of transition metal-sulfur systems: Part III. Thermodynamic properties of the Fe-S liquid phase and the calculation of the Fe-S phase diagram. *Metallurgical and Materials Transactions B*. 1979, **10**, 103-108.

Shaul K. Electricity and Heat: The Connections between Two Invisible Forces. *In:* **Jürgen Renn (Ed.)** *Albert Einstein : chief engineer of the universe : one hundred authors for Einstein*. Weinheim: Wiley-VCH; Berlin: Max-Plank Institute for the History of Science. 2005, pp. 64-67.

Shekhar S., Lu C-T., Zhang P. Detection graph-based spatial outliers: Algorithms and applications. *Proceedings of the 7th ACM SIGKDD International Conference on Knowledge Discovery and Data Mining*. 2001, 371-376.

Shi T., Zheng L., Chen N. Conditions fort the formation of binary amorphous alloys. *Acta Metallurgica Sinica*. 1979, **15**, 94-97.

Shin D., Saal J. E., Liu Z. K. Thermodynamic modelling of the Cu-Si system. *CALPHAD*. 2008, **32**, 520-526.

Singh S., Young W. H. Heats of solution for simple binary alloys. *Journal of Physics F: Metal Physics*. 1972, **2**, 672-682.

Singh P. P., Gonis A., Turchi P. E. A. Toward a unified approach to the study of metallic alloys – application to the phase-stability of Ni-Pt. *Physical Review Letters*. 1993, **71**, 1605-1608.

Sivaraman A., Magee J. W., Kobayashi R. Generalized correlation of latent heats of vaporization of coal-liquid model compounds between their freezing points and critical points. *Industrial & Engineering Chemistry Fundamentals.* 1984, **23**, 97-100.

Sluiter M. H. F., Watanabe Y., deFontaine D., Kawazoe Y. First-principles calculation of the pressure dependence of phase equilibria in the Al-Li system. *Physical Review B*. 1996, **53**, 6137-6151.

Sluiter M. H. F., Kawazoe Y. Prediction of the mixing enthalpy of alloys. *Europhysics Letters*. 2002, **57**, 526-532.

Sluiter M. H. F., Colinet C., Pasturel A. Ab initio calculation of the phase stability in Au-Pd and Ag-Pt alloys. *Physical Review B*. 2006, **73**, 174204(1)-174204(17).

Smith A. H. Temperature dependence of the work function of semiconductors. *Physical Review*. 1949, **75**, 953-958.

Smith L. A., Thornton T. A., Stafford C. F., Storton J. M., Holaday V. D., Kaufman L. Theoretical and experimental study of the U-Pu-Zn system. *CALPHAD*. 1980, **4**, 201-218.

Smoluchowski R. Anisotropy of the electronic work function of metals. *Physical Review*. 1941, **60**, 661-674.

Sofu A., Ekinci F. Y. Estimation of storage time of yogurt with artificial neural network modeling. *Journal of Dairy Science*. 2007, **90**, 3118-3125.

Song Y., Guo Z. X., Yang R. First principles studies of TiAl-based alloys. *Journal of Light Metals*. 2002, **2**, 115-123.

Specht D. F. Probabilistic neural networks. *Neural Networks*. 1990, **3**, 109-118.

Specht D. F. A general regression neural network. *IEEE Transactions on Neural Network*. 1991, **2**, 568-576.

Spedding F. H., Barton R. J., Daane A. H. The vapour pressure of thulium metal. *Journal of the American Chemical Society*. 1957, **79**, 5160-5163.

Speight J. G. ed. *Lange's Handbook of Chemistry, 16th edition, 70th Anniversary Edition*. New York; London: McGraw-Hill, 2005. pp. 1.18-1.62, pp. 1.124-1.127, pp. 1.280-1.298.

Stark J. G., Wallace H. G. ed. *Chemistry Data Book. 2nd edition.* London: John Murray, 1982 (1984 reprinted), pp. 8-11, 24, 27-29, 50-51.

Steurer W. Crystal structure of the metallic elements. *In*: **Cahn R. W, Haasen P. (Eds.)** *Physical Metallurgy, 4th, revised and enhanced edition, Vol. 1*. North Holland. 1996. pp. 2-46.

Steven W., Haynes A. G. The temperature of formation of martensite and bainite in low-alloy steel. *The Journal of the Iron and Steel Institute*. 1956, **183**, 349-359.

Strechan A. A., Kabo G. J., Paulechka Y. U. The correlations of the enthalpy of vaporization and the surface tension of molecular liquids. *Fluid Phase Equilibria*. 2006, **250**, 125-130.

Stringfellow G. B. Ordered structures and metastable alloys grown by OMVPE. *Journal of Crystal Growth*. 1989, **98**, 108-117.

Stroud D., Ashcroft N. W. Phase stability in binary alloys. *Journal of Physics F: Metal Physics*. 1971, **1**, 113-124.

Stuparevic L., Zivkovic D. Phase diagram investigation and thermodynamic study of Os-B system. *Journal of Thermal Analysis and Calorimetry*. 2004, **76**, 975-983.

Suter J. L., Coveney P. V., Greenwell H. C., Thyveetil M. A. Large-scale molecular dynamics study of montmorillonite clay: emergence of undulatory fluctuations and determination of material properties. *Journal of Physical Chemistry C*. 2007, **111**, 8248-8259.

Suter J. L., Anderson R. L., Greenwell H. C., Coveney P. V. Recent advances in large-scale atomistic and coarse-grained molecular dynamics simulation of clay minerals. *Journal of Materials Chemistry*. 2009, **19**, 2482-2493.

Takizawa S., Terakura K., Mohri T. Electronic theory for phase-stability of nine *AB* binary-alloys, with A=Ni, Pd, or Pt and B=Cu, Ag, or Au. *Physical Review B*. 1989, **39**, 5792-5797.

Teles L. K., Furthmuller J., Scolfaro L. M. R., Leite J. R., Bechstedt F. First-principles calculations of the thermodynamic and structural properties of strained $In_xGa_{1-x}N$ and $Al_xGa_{1-x}N$ alloys. *Physical Review B*. 2000, **62**, 2475-2485.

Terakura K., Oguchi T., Mohri T., Watanabe K. Electronic theory of the alloy phase stability of Cu-Ag, Cu-Au, and Ag-Au systems. *Physical Review B*. 1987, **35**, 2169-2173.

Teyssier J., Viennois R., Salamin J., Giannini E., Van der Marel D. Experimental and first principle calculation of $Co_xNi_{(1-x)}Si$ solid solution structural stability. *Journal of Alloys and Compounds*. 2008, **465**, 462-467.

Thyveetil M. A., Coveney P. V., Suter J. L., Greenwell H. C. Emergence of undulations and determination of materials properties in large-scale molecular dynamics simulation of layered double hydroxides. *Chemistry of Materials*. 2007, **19**, 5510-5523.

Tokunaga T., Ohtani H., Hasebe M. Thermodynamic analysis of the Zr-Be system using thermochemical properties based on ab initio calculations. *CALPHAD*. 2006, **30**, 201-208.

TOP 500. http://www.top500.org/ Access on 13 July 2009.

Trulson O. C., Hudson D. E., Spedding F. H. Cohesive energies of europium, gadolinium, holmium, and erbium. *The Journal of Chemical Physics*. 1961, **35**, 1018-1026.

Tu C.-H, Liu C.-P. Group-contribution estimation of the enthalpy of vaporization of organic compounds. *Fluid Phase Equilibria*. 1996, **121**, 45-65.

Turchi P. E. A., Reinhard L., Stocks G. M. First-principles study of stability and local order in BCC-based Fe-Cr and Fe-V alloys. *Physical Review B*. 1994, **50**, 15542-15558.

Ubic R. Revised method for the prediction of lattice constants in cubic and pseudocubic perovskites. *Journal of the American Ceramic Society*. 2007, **90**, 3326-3330.

Udovskii A. L., Ivanov O. S. Calculation of limited solubility curves and excess free-energy of silver-copper solid-solutions. *Zhurnal Fizicheskoi Khimii.* 1977, **51**, 796-799.

Uhland S., Lechtman H., Kaufman L. Assessment of the As-Cu-Ni system: an example from archaeology. *CALPHAD*. 2001, **25**, 109-124.

Upadhaya B., Eryureka E. Application of neural network for sensory validation and plant monitoring. *Neural Technology.* 1992, **97,** 170-176.

Van de Walle A., Moser Z., Gasior W. First-principles calculation of the Cu-Li phase diagram. *Archives of Metallurgy and Materials*. 2004, **49**, 535-544.

Van de Walle C. G., Neugebauer J. First-principles calculations for defects and impurities: Applications to III-nitrides. *Journal of Applied Physics*. 2004, **95**, 3851-3879.

Van Genechten K. A., Mortier W. J., Geerlings P. Intrinsic framework electronegativity: a novel concept in solid state chemistry. *Journal of Chemical Physics*. 1987, **86**, 5063-5071.

Van Laar J. J. The melting or freezing curves of binary systems I. *Zeitschrift für Physikalische Chemie, Leipzige Ausgabe*. 1908, **63**, 216-253.

Van Laar J. J. The melting or freezing curves of binary systems II. *Zeitschrift für Physikalische Chemie, Leipzige Ausgabe*. 1908, **64**, 257-297.

Van Vlack L. H. *Elements of Materials Science and Engineering*, *6th Edn*. Addison-Wesley Publisher, 1989. pp. 51-52.

Varma C. M. Quantum-theory of the heats of formation of metallic alloys. *Solid State Communications*. 1979, **31**, 295-297.

Vegard L. Gitterkonstanten von mischkristallen. *Zeitschrift für Physik.* 1921, **5**, 17-26.

Verma A.S., Kumar A., Bhardwaj S.R. Correlation between ionic charge and the lattice constant of cubic perovskite solids. *Physica Status Solidi (b)*. 2008, **245**, 1520-1526.

Vetere A. New Generalized Correlations for Enthalpy of Vaporization of Pure Compounds, Laboratori Ricerche Chimica Industriale, SNAM PROGETTI, San Donato Milanese, 1973.

Vicino F. The probabilistic neural network. *Substance Use & Misuse.* 1998, **33**, 335-352.

Villars P. A three-dimensional structural stability diagram for 998 binary AB intermetallic compounds. *Journal of the Less Common Metals*. 1983, **92**, 215-238.

Villars P. A three-dimensional structural stability diagram for 1011 binary AB2 intermetallic compounds: II. *Journal of the Less Common Metals*. 1984a, **99**, 33-43.

Villars P. Three-dimensional structural stability diagrams for 648 binary AB_3 and 389 binary A_3B_5 intermetallic compounds: III. *Journal of the Less Common Metals*. 1984b, **102**, 199-211.

Villars P., Onodera N., Iwata S. The Linus Pauling file (LPF) and its application to materials design. *Journal of Alloys and Compounds.* 1998, **279**, 1-7.

Villars P. Factors governing crystal structures. *In*: **Westbrook J. H., Fleischer R. L. (Eds.)** *Crystal structures of intermetallic compounds.* John Wiley & Sons, New York, 2000. pp. 1-49.

von Kármán T., Biot M. A. *Mathematical Methods in Engineering: An Introduction to the Mathematical Treatment of Engineering Problems*. New York and London: McGraw-Hill Book Company, Inc. 1940. p. 136.

Waber J. T., Gschneidner K. A., Larson A. C., Prince M. Y. Prediction of solid solubility in metallic alloys. *Transactions of the Metallurgical Society of AIME*. 1963, **227**, 717-723.

Wahlin H. B. Thermionic properties of the iron group. *Physical Review.* 1942, **61**, 509-512.

Wakefield G. F., Daane A. H., Spedding F. H. Vapour pressure of holmium. *The Journal of Chemical Physics*. 1967, **47**, 4994-4999.

Walczak B., Massart D. L. Multiple outlier detection revisited. *Chemometrics and Intelligent Laboratory Systems*. 1998, **41**, 1-15.

Wang L. L., Huang W. Q., Deng H. Q., Li X. F., Tang L. M., Zhao L. H. A method for predicting formation of quasicrystalline alloys. *Rare Metal Materials and Engineering*. 2003, **32**, 889-892.

Wang S. Q., Schneider M., Ye H. Q., Gottstein G. First-principles study of the formation of Guinier-Preston zones in Al-Cu alloys. *Scripta Materialia*. 2004, **51**, 665-669.

Warren B. E., Averbach B. L., Roberts B. W. Atomic size effect in the x-ray scattering by alloys. *Journal of Applied Physics*. 1951, **22**, 1493-1496.

Watson R. E., Bennett L. H. Transition metals: *d*-band hybridization, electronegativities and structural stability of intermetallic compounds. *Physical Review. B, Condensed Matter.* 1978, **18**, 6439-6449.

Watson R. E., Weinert M. The Hume-Rothery "parameters" and bonding in the Hume-Rothery and transition-metal alloys. ***In***: **Turchi E. A., Shull R. D. and Gonis A.** ed. *Science of Alloys for the 21st Century: A Hume-Rothery Symposium Celebration*. Warrendale: TMS (The Minerals, Metals & Materials Society), 2000, pp. 105-119.

Wawrousek H., Westbrook J. H., Grattidge W. *Data Sources of Mechanical and Physical Properties of Engineering Materials*. ***In:*** *Physik Daten (Physics Data)*. Fachinformationszentrum, Karlsruhe, German. 1989, No. 30-1.

Wei S. H., Mbaye A. A., Ferreira L. G., Zunger A. First-principles calculations of the phase-diagrams of noble metals – Cu-Au, Cu-Ag, and Ag-Au. *Physical Review B*. 1987, **36**, 4163-4185.

Wei S. H., Ferreira L. G., Zunger A. First-principles calculation of temperature-composition phase diagrams of semiconductor alloys. *Physical Review B*. 1990, **41**, 8240-8269.

Westbrook J. H., Kaufman J. G., Cverna F. Electronic access to factual materials information: the state of the art. *MRS Bulletin*. 1995, **20**, 40-48.

Westgren A., Phragmén G. X-ray analysis of the Cu-Zn, Ag-Zn and Au-Zn alloys. *Philosophical Magazine*. 1925, **50**, 311-341.

White D., Walsh P. N., Goldstein W., Dever D. F. Rare earths. II. A mass spectrometric determination of the heats of sublimation (or vaporization) of neodymium, praseodymium, gadolinium, terbium, dysprosium, holmium, erbium and lutetium. *The Journal of Physical Chemistry*. 1961, **65**, 1404-1409.

White P. S., Rodgers J. R., Page Y. L. CRYSTMET: a database of the structures and powder patterns of metals and intermetallics. *Acta Crystallographica*. 2002, **B58**, 343-348.

Whitehead A. N. *An Introduction to Mathematics*. New York: H. Holt and Company, 1911, p. 27.

Widrow B., Lehr M. A. 30 years of adaptive neural networks: perceptron, Madaline, and backpropagation. *Proceedings of the IEEE*. 1990, **78,** 1415-1442.

Wigner E., Seitz F. On the constitution of metallic sodium. *Physical Review*. 1933, **43**, 804-810.

Wigner E., Seitz F. On the constitution of metallic sodium II. *Physical Review*. 1934, **46**, 509-524.

Williams A. R., Gelatt C. D., Moruzzi V. L. Microscopic basis of Miedema empirical-theory of transition-metal compound formation. *Physical Review Letters*. 1980, **44**, 429-433.

Williams R. H., Polanco J. I. The electronic structure of chalcogenide solids: a photoemission study of ordered and disordered selenium and tellurium. *Journal of Physics C: Solid State Physics*. 1974, **7**, 2745-2759.

Wilson A. H. *The Theory of Metals*. Cambridge at the University Press. 1953. pp. 1-3.

Wolverton C., Yan X. –Y, Vijayaraghavan R., Ozoliņš. Incorporating first-principles energies in computational thermodynamics approaches. *Acta Materialia*. 2002, **50**, 2187-2197.

Woodley S. M., Battle P. D., Gale J. D., Catlow C. R. A. The prediction of inorganic crystal structures using a genetic algorithm and energy minimisation. *Physical Chemistry Chemical Physics.* 1999, **1**, 2535-2542.

Wyatt O. H., Dew-Hughes D. *Metals, Ceramics and Polymers: An Introduction to the Structure and Properties of Engineering Materials*. London: Cambridge University Press, 1974. p. 42.

Xiang X. D., Sun X., Briceño G., Lou Y., Wang K., Chang H., Wallace-Freedman W. G., Chen S., Schultz P. G. A combinatorial approach to materials discovery. *Science.* 1995, **268**, 1738-1740.

Xiang X. D. Combinatorial materials synthesis and screening: an integrated materials chip approach to discovery and optimization of functional materials. *Annual Review of Materials Science.* 1999, **29**, 149-171.

Xiong W., Du Y., Liu Y., Huang B. Y., Xu H. H., Chen H. L., Pan Z. Thermodynamic assessment of the Mo-Nb-Ta system. *CALPHAD*. 2004, **28**, 133-140.

Yamamoto S., Wakabayashi T., Kobayashi H. Calculation of solid solubility and compound formability of Al-alloys by extended Huckel-method. *Journal of the Japan Institute of Metals*. 1993, **57**, 1367-1373.

Yamanish K., Takeuchi J. A unifying framework for detecting outliers and change points from non-stationary time series data. *Proceedings of the 8th ACM SIGKDD International Conference on Knowledge Discovery and Data Mining*. Edmonton, Alberta, Canada. 2002, 676-681.

Yan X., Chang Y. A. A thermodynamic analysis of the Cu-Si system. *Journal of Alloys and Compounds*. 2000, **308**, 221-229.

Yang J., Silk N. J., Watson A., Bryant A. W., Chart T. G., Argent B. B. The thermodynamics and phase diagrams of the Cd-Hg and Cd-Hg-Te systems. *Calphad- Computer Coupling of Phase Diagrams and Thermochemistry*. 1995a, **19**, 415-430.

Yang J., Silk N. J., Watson A., Bryant A. W., Argent B. B. Thermodynamic and phase diagram assessment of the Cd-Te and Hg-Te systems. *Calphad-Computer Coupling of Phase Diagrams and Thermochemistry*. 1995b, **19**, 399-414.

Yang R. T. *Adsorbents: Fundamentals and Applications*. John Wiley & Sons, Inc., Hoboken, New Jersey, 2003. p. 12.

Ye C. Z., Yang J., Yao L. X., Chen N. Y. Regularities of formation and lattice distortion of perovskite-type compounds. *Chinese Science Bulletin*. 2002, **47**, 458-460.

Yip S. Introduction. *In:* **Yip S. (Ed.)** *Handbook of Materials Modelling*. Berlin: Springer, 2005. pp. 1-5.

Zakulski W., Moser Z. A calculation of the Cd-Pb (cadmium-lead) system. *Journal of Phase Equilibria*. 1995, **16**, 239-242.

Zhang B. W. The effect of size factor in the formation of amorphous alloys. *Acta Metallurgica Sinica*. 1981, **17**, 285-292.

Zhang B. W. Application of Miedema's coordinates to the formation of binary amorphous alloys. *Physica*. 1983, **121B**, 405-408.

Zhang B. W. Description of the formation of binary amorphous alloys by chemical coordinates. *Physica*. 1985a, **132B**, 319-322.

Zhang B. W. Semi-empirical theory of solid solubility in binary-alloys. *Zeitschrift fur Metallkunde*. 1985b, **76**, 264-270.

Zhang B. W. A semiempirical approach to the prediction of the amorphous-alloys formed by ion-beam mixing. *Physica Status Solidi A – A Applied Research*. 1987a, **102**, 199-206.

Zhang B. W. An approach to the solid solubilities of binary non-transition metal based alloys. *Scripta Metallurgica*. 1987b, **21**, 1207-1211.

Zhang B. W., Tan Z. S. Prediction of the formation of binary metal-metal amorphous-alloys by ion-implantation. *Journal of Materials Science Letters*. 1988, **7**, 681-682.

Zhang B. W., Liao S. Z. Progress on the theories of solid solubility of alloys (part1). *ShangHai Metals*. 1999a, **21 (2)**, 3-10.

Zhang B. W., Liao S. Z. Progress on the theories of solid solubility of alloys (part2). *ShangHai Metals*. 1999b, **21 (3)**, 3-10.

Zhang H., Li N., Li K., Xue D. Structural stability and formability of ABO_3-type perovskite compounds. *Acta Crystallographica B*. 2007, **B63**, 812-818.

Zhang J. L., Fang S. S., Zhou Z. Q., Lin G. W., Ge J. S., Feng F. Maximum solid solubility of transition metals in vanadium solvent. *Transactions of Nonferrous Metals Society of China*. 2005a, **15**, 1085-1088.

Zhang Z. H., Wang Y., Bian X. F. and Wang W. M. Orientation of nanocrystals in rapidly solidified Al-based alloys and its correlation to the compound-forming tendency of alloys. *Journal of Crystal Growth*. 2005b, **281**, 646-653.

Zhang Y. M., Yang S., Evans J. R. G. Revisiting Hume-Rothery's Rules with artificial neural networks. *Acta Materialia*. 2008, **56**, 1094-1105.

Zhao J., Lu C., Kou Y. Detecting region outliers in meteorological data. *Proceedings of the 11th ACM International Symposium on Advances in Geographical Information Systems*. 2003. pp. 49-55.

Zhao J. C. Combinatorial approaches as effective tools in the study of phase diagrams and composition-structure-property relationships. *Progress in Materials Science.* 2006, **51**, 557-631.

Zhou Z. Q., Fang S. S., Feng F. Rules for maximum solid solubility of transition metals in Ti, Zr and Hf solvents. *Transactions of Nonferrous Metals Society of China*. 2003a, **13**, 864-868.

Zhou Z. Q., Fang S. S., Feng F. Comparison between methods for predicting maximum solid solubility of transition metals in solvent metal. *Transactions of Nonferrous Metals Society of China*. 2003b, **13**, 1185-1189.

Zunger A. Structural stability of 495 binary compounds. *Physical Review Letters*. 1980, **44**, 582-586.

Zunger A., Wei S. H., Ferreira L. G., Bernard J. E. Special quasi-random structures. *Physical Review Letters*. 1990, **65**, 353-356.

Zupan J., Gasteiger J. Neural networks: a new method for solving chemical problems or just a passing phase? *Analytica Chimica Acta.* 1991, **248**, 1-30.

Zupan J., Gasteiger J. (Eds.) *Neural networks for chemists: an introduction.* Weinheim: VCH Verlagsgesellscaft mbH, 1993.

Appendix 1 General Programming Codes of Neural Networks (on which the programmes for special cases are based)

1 BPANN Program

```
[TotalDataBaseRead,TotalElements]=xlsread('Properties','A2:Q76');
% Read Property Data In
[rowofwholeproperties,columnofwholeproperties]=size(TotalDataBaseRead);
for i=1:columnofwholeproperties
% Output Property (Property to be predicted) One by One in Turn
   PropertiesOut=TotalDataBaseRead(:,i);
   if i==1
      j=(2:columnofwholeproperties);
   elseif i==columnofwholeproperties
      j=(1:(columnofwholeproperties-1));
   else
      j=[1:(i-1),(i+1):columnofwholeproperties];
   end
   PropertiesInWhole=TotalDataBaseRead(:,j); % Decide Input Property Family
   Groups=combnk(1:(columnofwholeproperties-1),7)';
   % Doing Combinatorial Calculation
   [rowofGroups,columnofGroups]=size(Groups);
   for iii=1:columnofGroups % 2 (can run part to part)
      clc
      clear TotalDataBaseN
      clear TotalDataBaseNFinal
      clear index
      clear mrand1
      clear brand1
      clear rrand1
      clear mrand2
      clear brand2
      clear rrand2
      clear PropertiesIn
      clear EvaluateFun1
      clear EvaluateFun2
      clear EvaluateFun
      clear MinEvaluateFunoftime
      clear indexoftime
      clear PropertiesInIndex

      PropertiesInIndex=Groups(:,iii);
      PropertiesIn=PropertiesInWhole(:,PropertiesInIndex);
      TotalDataBaseO=[PropertiesIn PropertiesOut];
      [row,column]=size(TotalDataBaseO);
      TrainingNumber=round(row*4/5);
      NNHLMax=fix((TrainingNumber-1)/(column+1));
      % Number of Possible Maximum Neurons in Hidden Layer
      NDistribu=30; % Number of data redistribution
      TotalDataBaseN=zeros(row,column,NDistribu,NNHLMax);
      mrand1=zeros(NDistribu,NNHLMax); brand1=zeros(NDistribu,NNHLMax);
      rrand1=zeros(NDistribu,NNHLMax);
```

```
    mrand2=zeros(NDistribu,NNHLMax); brand2=zeros(NDistribu,NNHLMax);
    rrand2=zeros(NDistribu,NNHLMax);

    OutCell=cell(76,16);

    EvaluateFun=zeros(NDistribu,NNHLMax);
    MinEvaluateFunoftime=zeros(1,NNHLMax);
    indexoftime=zeros(1,NNHLMax);
    index=zeros(row,1,NDistribu,NNHLMax);
    for k=1:NNHLMax % Search of Number of Neurons in Hidden Layer
      for kk=1:NDistribu
  % Search of Distribution of Data for the Training set to Cover Problem Domain
        if k==1
          AddNumber=rand(row,1); % Redistribute Data
          [AddNumberNew,index(:,1,kk,k)]=sort(AddNumber);
          TotalDataBaseN(:,:,kk,k)=TotalDataBaseO(index(:,1,kk,k),:);
        end
        TotalDataBaseN(:,:,kk,k)=TotalDataBaseN(:,:,kk,1);
        index(:,:,kk,k)=index(:,:,kk,1);
        PropertiesInNew=TotalDataBaseN(:,(1:(column-1)),kk,k)';
        PropertiesOutNew=TotalDataBaseN(:,column,kk,k)';

        [PropertiesInNewn,PropertiesInNews]= mapminmax(PropertiesInNew);
        [PropertiesOutNewn,PropertiesOutNews]=mapminmax(PropertiesOutNew);
        iitst=3:5:row; % Testing set
        iitr=[1:5:row 2:5:row 4:5:row 5:5:row]; % Training set
        test.P=PropertiesInNewn(:,iitst);test.T=PropertiesOutNewn(:,iitst);
        ptr=PropertiesInNewn(:,iitr);ttr=PropertiesOutNewn(:,iitr);
        net=newff(minmax(ptr),[k 1],{'tansig' 'purelin'},'trainbrs');
        net.trainParam.epochs = 800;
        net.trainParam.goal = 1e-8;
        net=init(net);
        [net,tr]=train(net,ptr,ttr,[],[],[],test);
        PropertiesOutSimulatenTr=sim(net,ptr);
        PropertiesOutSimulatents=sim(net,test.P);

        clear net

PropertiesOutSimulateTr=mapminmax('reverse',PropertiesOutSimulatenTr,PropertiesOu
tNews);

PropertiesOutSimulatets=mapminmax('reverse',PropertiesOutSimulatents,PropertiesOut
News);

[mrand1(kk,k),brand1(kk,k),rrand1(kk,k)]=postregnopic(PropertiesOutSimulateTr,Prope
rtiesOutNew(:,iitr));

[mrand2(kk,k),brand2(kk,k),rrand2(kk,k)]=postregnopic(PropertiesOutSimulatets,Proper
tiesOutNew(:,iitst));
        if isnan(rrand1(kk,k))
          rrand1(kk,k)=0;
        elseif rrand1(kk,k)==Inf
          rrand1(kk,k)=0;
        elseif rrand1(kk,k)==-Inf
          rrand1(kk,k)=0;
```

```
            end
            if isnan(rrand2(kk,k))
               rrand2(kk,k)=0;
            elseif rrand2(kk,k)==Inf
               rrand2(kk,k)=0;
            elseif rrand2(kk,k)==-Inf
               rrand2(kk,k)=0;
            end

            EvaluateFun(kk,k)=((abs(mrand1(kk,k)-1)+(1-
                                rrand1(kk,k)))+(abs(mrand2(kk,k)-1)+(1-
                                rrand2(kk,k))))/2+abs((abs(mrand1(kk,k)-1)+(1-
                                rrand1(kk,k)))-(abs(mrand2(kk,k)-1)+(1-rrand2(kk,k))));
         end
         [MinEvaluateFunoftime(k),indexoftime(k)]=min(EvaluateFun(:,k));
         % Get minimum value of criterion within Different Distributions
      end
      [MinEvaluateFunofNeurons,indexofneuron]=min(MinEvaluateFunoftime(:));
      % Get minimum value of criterion within Different Number of Neurons


TotalDataBaseNFinal=TotalDataBaseN(:,:,indexoftime(indexofneuron),indexofneuron);
 PropertiesInNewFinal=TotalDataBaseNFinal(:,(1:(column-1)))';
 PropertiesOutNewFinal=TotalDataBaseNFinal(:,column)';


[PropertiesInNewFinaln,PropertiesInNewFinals]=mapminmax(PropertiesInNewFinal);

[PropertiesOutNewFinaln,PropertiesOutNewFinals]=mapminmax(PropertiesOutNewFin
al);
      iitstFinal=3:5:row;
      iitrFinal=[1:5:row 2:5:row 4:5:row 5:5:row];
      testFinal.P=PropertiesInNewFinaln(:,iitstFinal);
       testFinal.T=PropertiesOutNewFinaln(:,iitstFinal);
      ptrFinal=PropertiesInNewFinaln(:,iitrFinal);
       ttrFinal=PropertiesOutNewFinaln(:,iitrFinal);
      netFinal=newff(minmax(ptr),[indexofneuron 1],{'tansig' 'purelin'},'trainbrs');
      netFinal.trainParam.epochs = 800;
      netFinal.trainParam.goal = 1e-8;
      netFinal=init(netFinal);
      [netFinal,trFinal]=train(netFinal,ptrFinal,ttrFinal,[],[],[],testFinal);
      PropertiesOutNewFinalSimulatenTr=sim(netFinal,ptrFinal);
      PropertiesOutNewFinalSimulatents=sim(netFinal,testFinal.P);
      clear netFinal

PropertiesOutNewFinalSimulateTr=mapminmax('reverse',PropertiesOutNewFinalSimul
atenTr,PropertiesOutNewFinals);

PropertiesOutNewFinalSimulatets=mapminmax('reverse',PropertiesOutNewFinalSimula
tents,PropertiesOutNewFinals);

      PropertiesOutNewFinalTr=PropertiesOutNewFinal(:,iitrFinal);
      PropertiesOutNewFinalts=PropertiesOutNewFinal(:,iitstFinal);
      Erroroftesting=PropertiesOutNewFinalts-PropertiesOutNewFinalSimulatets;
      ErroroftestingPercentage=Erroroftesting./PropertiesOutNewFinalts;
```

```
FinalProperty=[PropertiesOutNewFinalTr PropertiesOutNewFinalts];
FinalSimulate=[PropertiesOutNewFinalSimulateTr
                PropertiesOutNewFinalSimulatets];
Errorofwhole=FinalProperty-FinalSimulate;
ErrorofwholePercentage=Errorofwhole./FinalProperty;
% Testing
MeanErroroftesting=mean(abs(Erroroftesting));
StdvErroroftesting=std(abs(Erroroftesting));
MeanErroroftestingPercentage=mean(abs(ErroroftestingPercentage));
StdvErroroftestingPercentage=std(abs(ErroroftestingPercentage));
% Whole
MeanErrorofwhole=mean(abs(Errorofwhole));
StdvErrorofwhole=std(abs(Errorofwhole));
MeanErrorofwholePercentage=mean(abs(ErrorofwholePercentage));
StdvErrorofwholePercentage=std(abs(ErrorofwholePercentage));
% Find Names
strPI=cell(rowofGroups,1);
for jjj=1:rowofGroups
   switch j(Groups(jjj,iii))
      case 1
         strPI(jjj)={'MP'}; % Melting Point
      case 2
         strPI(jjj)={'BP'}; % Boiling Point
      case 3
         strPI(jjj)={'H of F'}; % Heat of Fusion
      case 4
         strPI(jjj)={'H of V'}; % Heat of Vaporization
      case 5
         strPI(jjj)={'MHC'}; % Molar Heat Capacity
      case 6
         strPI(jjj)={'SHC'}; % Specific Heat Capacity
      case 7
         strPI(jjj)={'TC'}; % Thermal Conductivity
      case 8
         strPI(jjj)={'EC'}; % Electrical Conductivity
      case 9
         strPI(jjj)={'WF'}; % Work Function
      case 10
         strPI(jjj)={'LTherExC'}; % Linear Thermal Expansion Coeff.
      case 11
         strPI(jjj)={'AW'}; % Atomic Weight
      case 12
         strPI(jjj)={'D'}; % Density
      case 13
         strPI(jjj)={'Electronega.'}; % Electronegativity
      case 14
         strPI(jjj)={'Fir. Ioni. En.'}; % First Ionization Energy
      case 15
         strPI(jjj)={'Polari.'}; % Polarizability
      case 16
         strPI(jjj)={'AV'}; % Atomic Volumn
   end
end
switch i
   case 1
```

```
            strPO='MP';
        case 2
            strPO='BP';
        case 3
            strPO='H of F';
        case 4
            strPO='H of V';
        case 5
            strPO='MHC';
        case 6
            strPO='SHC';
        case 7
            strPO='TC';
        case 8
            strPO='EC';
        case 9
            strPO='WF';
        case 10
            strPO='LTherExC';
        case 11
            strPO='AW';
        case 12
            strPO='D';
        case 13
            strPO='Electronega.';
        case 14
            strPO='Fir. Ioni. En.';
        case 15
            strPO='Polari.';
        case 16
            strPO='AV';
    end

[m3,b3,r3]=postregsfinal(PropertiesOutNewFinalSimulateTr,PropertiesOutNewFinalSi_
                         mulatets,PropertiesOutNewFinalTr,PropertiesOutNewFinalts);
% Draw Figure of Whole set
    FigureCrit=abs(1-m3)+(1-r3);
    ElementIndex=index(:,1,indexoftime(indexofneuron),indexofneuron);
    ElementIndexFinal=ElementIndex([iitrFinal,iitstFinal],:);
    FinalElements(:,:)=TotalElements(ElementIndexFinal,:);
    Evaluateofaway(:,:)=abs(Errorofwhole);

    dv=0.8*max([PropertiesOutNewFinalTr PropertiesOutNewFinalts])/60;
    for iiii=1:75
        if abs(Errorofwhole(iiii))/FinalProperty(iiii)>=0.3
            xposition=FinalProperty(:,iiii)+dv;
            yposition=FinalSimulate(:,iiii)-dv;
            Elementsmarker=FinalElements(iiii,:);
            text(xposition,yposition,Elementsmarker)
        end
    end

    nameoffileTr=['(',num2str(FigureCrit),')',' ','Predict',' ',strPO,' ','from',','
                  ',char(strPI(1)),',',char(strPI(2)),',',char(strPI(3)),',',char(strPI(4)),',',
                  char(strPI(5)),',',char(strPI(6)),',',char(strPI(7)),' ','(training)','.fig'];
```

```
nameoffileTs=['(',num2str(FigureCrit),')',' ','Predict',' ',strPO,' ','from','
                ',char(strPI(1)),',',char(strPI(2)),',',char(strPI(3)),',',char(strPI(4)),',',char(st
                rPI(5)),',',char(strPI(6)),',',char(strPI(7)),' ','(testing)','.fig'];

 nameoffileWhole=['(',num2str(FigureCrit),')',' ','Predict',' ',strPO,' ','from','
                    ',char(strPI(1)),',',char(strPI(2)),',',char(strPI(3)),',',char(strPI(4)),',',ch
                    ar(strPI(5)),',',char(strPI(6)),',',char(strPI(7)),' ','(whole set)','.fig'];

 nameoffile2=['(',num2str(FigureCrit),')',' ','Predict',' ',strPO,' ','from','
                ',char(strPI(1)),',',char(strPI(2)),',',char(strPI(3)),',',char(strPI(4)),',',char(st
                rPI(5)),',',char(strPI(6)),',',char(strPI(7)),'.xls'];

        h3=gcf;
        saveas(h3,nameoffileWhole,'fig')
        delete(h3)

        [m1,b1,r1]=postreglabel(PropertiesOutNewFinalSimulateTr,PropertiesOutNewFi
        _nalTr); % Draw Figure of Training set

        h1=gcf;
        saveas(h1,nameoffileTr,'fig')
        delete(h1)

        [m2,b2,r2]=postreglabel(PropertiesOutNewFinalSimulatets,PropertiesOutNewFi
                                _nalts);   % Draw Figure of Testing set
        h2=gcf;
        saveas(h2,nameoffileTs,'fig')
        delete(h2)

        OutCell(1,:)={'Predicted Error of Testing','Percentage Error of Testing','Predicted
                    Error of Whole Set','Percentage Error of Whole Set','Mean Error
                    of Testing (modul)','Error Standard Deviation of Testing
                    (modul)','Mean Percentage Error of Testing (modul)','Percentage
                    Error Standard Deviation of Testing (modul)','Mean Error of
                    Whole (modul)','Error Standard Deviation of Whole
                    (modul)','Mean Percentage Error of Whole (modul)','Percentage
                    Error Standard Deviation of Whole (modul)','Number of Neurons
                    in Hidden Layer','Real Values','Values from
                    Predictioin','Elements'};
        OutCell(2:16,1)=num2cell(Erroroftesting)';
        OutCell(2:16,2)=num2cell(ErroroftestingPercentage)';
        OutCell(2:76,3)=num2cell(Errorofwhole)';
        OutCell(2:76,4)=num2cell(ErrorofwholePercentage)';

OutCell(2,5:13)={MeanErroroftesting,StdvErroroftesting,MeanErroroftestingPercentage
,StdvErroroftestingPercentage,MeanErrorofwhole,StdvErrorofwhole,MeanErrorofwhole
Percentage,StdvErrorofwholePercentage,indexofneuron};
        OutCell(2:76,14)=num2cell(FinalProperty)';
        OutCell(2:76,15)=num2cell(FinalSimulate)';
        OutCell(2:76,16)=FinalElements(:,:);
        xlswrites(nameoffile2,OutCell,'A1:P76') % Write Results in

   end
end
```

2 PNN Program

```
[TotalDataBaseRead00,TotalCompounds00]=xlsread('Whole','A2:E377');
% Read Property Data in
TotalDataBaseRead=TotalDataBaseRead00';
TotalCompounds=TotalCompounds00';
PerovskiteJudge=TotalDataBaseRead(4,:); % Decide Output
Parameters=TotalDataBaseRead(1:2,:);  % Decide Input

TotalDataBaseO=[Parameters;PerovskiteJudge];
[row,column]=size(TotalDataBaseO);
NDistribu=100; % Number of Data Redistribution
Spread=10; % Decide maximum value of spread
TotalDataBaseN=zeros(3,column,NDistribu,10); index=zeros(1,column,NDistribu,10);
EvaluateFun=zeros(NDistribu,10);MinEvaluateFunoftime=zeros(1,10);
indexoftime=zeros(1,10);
ft=zeros(column);
for k=1: Spread
   for kk=1:NDistribu
      if k==1
         AddNumber=rand(1,column); % Redistribute Data
         [AddNumberNew,index(1,:,kk,k)]=sort(AddNumber);
         TotalDataBaseN(:,:,kk,k)=TotalDataBaseO(:,index(1,:,kk,k));
      end
      TotalDataBaseN(:,:,kk,k)=TotalDataBaseN(:,:,kk,1);
      index(:,:,kk,k)=index(:,:,kk,1);
      ParametersNew=TotalDataBaseN(1:2,:,kk,k);
      PerovskiteJudgeNew=TotalDataBaseN(3,:,kk,k);
      iitst=3:5:column;
      iitr=[1:5:column 2:5:column 4:5:column 5:5:column];
      ptr=ParametersNew(:,iitr); ttr=PerovskiteJudgeNew(:,iitr);
      pts=ParametersNew(:,iitst);
      net=newpnn(ptr,ind2vec(ttr),k/10);
      SimulatePredict=sim(net,ParametersNew);
      DeviationofPrediction=abs(PerovskiteJudgeNew-vec2ind(SimulatePredict));
      EvaluateFun(kk,k)=sum(DeviationofPrediction);
   end
   [MinEvaluateFunoftime(k),indexoftime(k)]=min(EvaluateFun(:,k));
end
[MinEvaluateFunofSpread,indexofSpread]=min(MinEvaluateFunoftime(:));
TotalDataBaseNFinal=TotalDataBaseN(:,:,indexoftime(indexofSpread),indexofSpread);
ParametersNewFinal=TotalDataBaseNFinal(1:2,:);
PerovskiteJudgeNewFinal=TotalDataBaseNFinal(3,:);
iitstFinal=3:5:column;
iitrFinal=[1:5:column 2:5:column 4:5:column 5:5:column];

ptrFinal=ParametersNewFinal(:,iitrFinal);  ttrFinal=PerovskiteJudgeNewFinal(:,iitrFinal);
ptsFinal=ParametersNewFinal(:,iitstFinal);
netFinal=newpnn(ptrFinal,ind2vec(ttrFinal),indexofSpread/10);
p1=2.0:0.05:3.6;
p2=1.3:0.05:2.5;
[P1,P2]=meshgrid(p1,p2);
pp=[P1(:) P2(:)]';
aa=sim(netFinal,pp);
```

```
aa=full(aa);
m=mesh(P1,P2,reshape(aa(1,:),length(p2),length(p1)));
set(m,'facecolor','yellow','linestyle','none'); % Non-perovskite
hold on
m=mesh(P1,P2,reshape(aa(2,:),length(p2),length(p1))); % Perovskite
set(m,'facecolor','green','linestyle','none');
plot3(TotalDataBaseRead(1,1:144),TotalDataBaseRead(2,1:144),ones(1,144)+0.1,'x','ma
        rkersize',7)
plot3(TotalDataBaseRead(1,145:376),TotalDataBaseRead(2,145:376),ones(1,232)+0.1,'
        diamond','markersize',7)
bb=sim(netFinal,TotalDataBaseRead(1:2,:));
bb=full(bb);
for i=1:column
   ft(i)=isequal(vec2ind(bb(:,i)),TotalDataBaseRead(4,i));
   if ft(i)==0

text(TotalDataBaseRead(1,i),TotalDataBaseRead(2,i)+0.01,1.1,TotalCompounds(1,i),'fo
ntsize',8);
   end
end
axis([2.0 3.6 1.3 2.5])
hold off
view(2)
title('The Classification of Perovskites and Non-Perovskites')
xlabel('A-O Bond Distance')
ylabel('B-O Bond Distance')
```

Appendix 2

1. Silver and Copper Alloy Systems

1.The valences of elements which were mentioned by Hume-Rothery in 1934 followed by him
(Cu=1, Ag=1, Au=1, Be=2, Ga=3, Sn=4, Ge=4, Sb=5, As=5, Tl=3, Pb=4, Cd=2)

2.The Ag alloy Solid Solubility Limit are recorded from "Binary Phase Diagram Vol.1 Thaddeus B. Massalski 1987 second printing (copyright 1986)"

3.The Cu alloy Solid Solubility Limit are recorded from "Binary Phase Diagram Vol.1 Thaddeus B. Massalski 1987 second printing (copyright 1986)"

4.Physical parameters are recorded from "Chemistry Data Book 2nd Edition in SI. J G Stark, H G Wallace 1984 reprinted (1982 edition)"

Binary System	Solvent	Solute	Solubility Limits (Atoms %)	Size(solvent) Radii in	Size(Solute) (Angstronms)	Valence Solvent	Valence Solute	Electrochemical Factors(Solvent)	Electrochemical Factors(Solute)	Structure[(2)] (Solvent)	Structure[(2)] (Solute)
Ag-Be	Ag	Alfa-Be	0.3	1.44	1.12	1	2	1.9	1.5	cF4	hP2
	Alfa-Be	Ag	0.048	1.12	1.44	2	1	1.5	1.9	hP2	cF4
	Ag	Beta-Be	0.3	1.44	1.12	1	2	1.9	1.5	cF4	cI2
	Beta-Be	Ag	0	1.12	1.44	2	1	1.5	1.9	cI2	cF4
Ag-Zn	Ag	Zn	40.2	1.44	1.33	1	2	1.9	1.6	cF4	hP2
	Zn	Ag	5	1.33	1.44	2	1	1.6	1.9	hP2	cF4
Ag-Cd	Ag	Cd	42.2	1.44	1.49	1	2	1.9	1.7	cF4	hP2
	Cd	Ag	7	1.49	1.44	2	1	1.7	1.9	hP2	cF4
Ag-Hg	Ag	Hg	37.3	1.44	1.52	1	2	1.9	1.9	cF4	hR1
	Hg	Ag	0	1.52	1.44	2	1	1.9	1.9	hR1	cF4
Ag-Al	Ag	Al	20.4	1.44	1.35[(4)]	1	3	1.9	1.5	cF4	cF4

	Al	Ag	23.5	1.43	1.44	3	1	1.5	1.9	cF4	cF4
Ag-Ga	Ag	Ga	18.8	1.44	1.325[4]	1	3	1.9	1.6	cF4	oC8
	Ga	Ag	3	1.22[4]	1.44	3	1	1.6	1.9	oC8	cF4
Ag-In	Ag	In	20	1.44	1.51	1	3	1.9	1.7	cF4	tI2
	In	Ag	0	1.66	1.44	3	1	1.7	1.9	tI2	cF4
Ag-Sn	Ag	Alfa-Sn	11.5	1.44	1.62	1	4	1.9	1.8	cF4	cF8
	Alfa-Sn	Ag	0	1.62	1.44	4	1	1.8	1.9	cF8	cF4
	Ag	Beta-Sn	11.5	1.44	1.47	1	4	1.9	1.8	cF4	tI4
	Beta-Sn	Ag	0.088034[2]	1.62	1.44	4	1	1.8	1.9	tI4	cF4
Ag-Pb	Ag	Pb	2.8	1.44	1.6	1	4	1.9	1.8	cF4	cF4
	Pb	Ag	0.19	1.75	1.44	4	1	1.8	1.9	cF4	cF4
Ag-Cu	Ag	Cu	14.07[2]	1.44	1.28	1	1	1.9	1.9	cF4	cF4
	Cu	Ag	4.87[2]	1.28	1.44	1	1	1.9	1.9	cF4	cF4
Ag-Sb	Ag	Sb	7.2	1.44	1.45[3]	1	5	1.9	1.9	cF4	hR2
	Sb	Ag	0	1.45[3]	1.44	5	1	1.9	1.9	hR2	cF4
Ag-Bi	Ag	Bi	2.615[2]	1.44	1.7	1	5	1.9	1.9	cF4	hR2
	Bi	Ag	0	1.7	1.44	5	1	1.9	1.9	hR2	cF4
Ag-As	Ag	As	7.8	1.44	1.25[3]	1	5	1.9	2	cF4	hR2
	As	Ag	0	1.25[3]	1.44	5	1	2	1.9	hR2	cF4
Cu-Au	Cu	Au	100	1.28	1.44	1	1	1.9	2.4	cF4	cF4
	Au	Cu	100	1.44	1.28	1	1	2.4	1.9	cF4	cF4
Cu-Be	Cu	Alfa-Be	16.5	1.28	1.12	1	2	1.9	1.5	cF4	hP2
	Alfa-Be	Cu	9.5	1.12	1.28	2	1	1.5	1.9	hP2	cF4

	Cu	Beta-Be	16.5	1.28	1.12	1	2	1.9	1.5	cF4	cI2
	Beta-Be	Cu	17.3	1.12	1.28	2	1	1.5	1.9	cI2	cF4
Cu-Mg	Cu	Mg	6.93	1.28	1.6	1	2	1.9	1.2	cF4	hP2
	Mg	Cu	0.013	1.6	1.28	2	1	1.2	1.9	hP2	cF4
Cu-Zn	Cu	Zn	38.3	1.28	1.33	1	2	1.9	1.6	cF4	hP2
	Zn	Cu	2.8	1.33	1.28	2	1	1.6	1.9	hP2	cF4
Cu-Cd	Cu	Cd	2.14	1.28	1.49	1	2	1.9	1.7	cF4	hP2
	Cd	Cu	0	1.49	1.28	2	1	1.7	1.9	hP2	cF4
Cu-Al	Cu	Al	19.7	1.28	1.35[4]	1	3	1.9	1.5	cF4	cF4
	Al	Cu	2.48	1.43	1.28	3	1	1.5	1.9	cF4	cF4
Cu-Ga	Cu	Ga	20	1.28	1.325[4]	1	3	1.9	1.6	cF4	oC8
	Ga	Cu	0	1.22[4]	1.28	3	1	1.6	1.9	oC8	cF4
Cu-Si	Cu	Si	11.25	1.28	1.17*	1	4	1.9	1.8	cF4	cF8
	Si	Cu	0	1.17*	1.28	4	1	1.8	1.9	cF8	cF4
Cu-Ge	Cu	Ge	12	1.28	1.23[3]	1	4	1.9	1.8	cF4	cF8
	Ge	Cu	0	1.23[3]	1.28	4	1	1.8	1.9	cF8	cF4
Cu-Sn	Cu	Alfa-Sn	9.1	1.28	1.62	1	4	1.9	1.8	cF4	cF8
	Alfa-Sn	Cu	0	1.62	1.28	4	1	1.8	1.9	cF8	cF4
	Cu	Beta-Sn	9.1	1.28	1.47	1	4	1.9	1.8	cF4	tI4
	Beta-Sn	Cu	0	1.62	1.28	4	1	1.8	1.9	tI4	cF4
Cu-Pb	Cu	Pb	0.09	1.28	1.6	1	4	1.9	1.8	cF4	cF4
	Pb	Cu	0.023	1.75	1.28	4	1	1.8	1.9	cF4	cF4
Cu-Sb	Cu	Sb	6.1	1.28	1.45[3]	1	5	1.9	1.9	cF4	hR2

	Sb	Cu	0	1.45[3]	1.28	5	1	1.9	1.9	hR2	cF4
Cu-Bi	Cu	Bi	0.003	1.28	1.7	1	5	1.9	1.9	cF4	hR2
	Bi	Cu	0	1.7	1.28	5	1	1.9	1.9	hR2	cF4
Cu-Hg	Cu	Hg	5	1.28	1.52	1	2	1.9	1.9	cF4	hR1
	Hg	Cu	0	1.52	1.28	2	1	1.9	1.9	hR1	cF4
Ag-Au	Ag	Au	100	1.44	1.44	1	1	1.9	2.4	cF4	cF4
	Au	Ag	100	1.44	1.44	1	1	2.4	1.9	cF4	cF4
Ag-B	Ag	B	0[1]	1.44	0.8*	1	3	1.9	2	cF4	hR105
	B	Ag	0[1]	0.8*	1.44	3	1	2	1.9	hR105	cF4
Ag-Ba	Ag	Ba	0	1.44	2.17	1	2	1.9	0.9	cF4	cI2
	Ba	Ag	0	2.17	1.44	2	1	0.9	1.9	cI2	cF4
Ag-Ca	Ag	Alfa-Ca	0	1.44	1.97	1	2	1.9	1	cF4	cF4
	Alfa-Ca	Ag	0	1.97	1.44	2	1	1	1.9	cF4	cF4
	Ag	Beta-Ca	0	1.44	1.97	1	2	1.9	1	cF4	cI2
	Beta-Ca	Ag	0	1.97	1.44	2	1	1	1.9	cI2	cF4
Ag-Ce	Ag	Alfa-Ce	0.05	1.44	1.83[3]	1	3**	1.9	1.1	cF4	cF4
	Alfa-Ce	Ag	0	1.83[3]	1.44	3**	1	1.1	1.9	cF4	cF4
	Ag	Beta-Ce	0.05	1.44	1.83[3]	1	3**	1.9	1.1	cF4	hP4
	Beta-Ce	Ag	0	1.83[3]	1.44	3**	1	1.1	1.9	hP4	cF4
	Ag	Gama-Ce	0.05	1.44	1.83[3]	1	3**	1.9	1.1	cF4	cF4
	Gama-Ce	Ag	2	1.83[3]	1.44	3**	1	1.1	1.9	cF4	cF4
	Ag	Delta-Ce	0.05	1.44	1.83[3]	1	3**	1.9	1.1	cF4	cI2
	Delta-Ce	Ag	2	1.83[3]	1.44	3**	1	1.1	1.9	cI2	cF4

Ag-Co	Ag	Epsilon-Co	0.81	1.44	1.25	1	2**	1.9	1.8	cF4	hP2
	Epsilon-Co	Ag	0	1.25	1.44	2**	1	1.8	1.9	hP2	cF4
	Ag	Alfa-Co	0.81	1.44	1.25	1	2**	1.9	1.8	cF4	cF4
	Alfa-Co	Ag	0	1.25	1.44	2**	1	1.8	1.9	cF4	cF4
Ag-Cr	Ag	Cr	0	1.44	1.25	1	3**	1.9	1.6	cF4	cI2
	Cr	Ag	0	1.25	1.44	3**	1	1.6	1.9	cI2	cF4
Ag-Cs	Ag	Cs	0	1.44	2.62	1	1	1.9	0.7	cF4	cI2
	Cs	Ag	0	2.62	1.44	1	1	0.7	1.9	cI2	cF4
Ag-Dy	Ag	Alfa'-Dy	1.3	1.44	1.75(3)	1	3	1.9	1.1	cF4	oC4
	Alfa'-Dy	Ag	0	1.75(3)	1.44	3	1	1.1	1.9	oC4	cF4
	Ag	Alfa-Dy	1.3	1.44	1.75(3)	1	3	1.9	1.1	cF4	hP2
	Alfa-Dy	Ag	0	1.75(3)	1.44	3	1	1.1	1.9	hP2	cF4
	Ag	Beta-Dy	1.3	1.44	1.75(3)	1	3	1.9	1.1	cF4	cI2
	Bety-Dy	Ag	0	1.75(3)	1.44	3	1	1.1	1.9	cI2	cF4
Ag-Er	Ag	Er	3.6	1.44	1.73(3)	1	3	1.9	1.2	cF4	hP2
	Er	Ag	0	1.73(3)	1.44	3	1	1.2	1.9	hP2	cF4
Ag-Eu	Ag	Eu	0	1.44	1.99(3)	1	2	1.9	1.1	cF4	cI2
	Eu	Ag	0	1.99(3)	1.44	2	1	1.1	1.9	cI2	cF4
Ag-Fe	Ag	Delta-Fe	0.0065	1.44	1.26	1	2**	1.9	1.8	cF4	cI2
	Delta-Fe	Ag	0.017	1.26	1.44	2**	1	1.8	1.9	cI2	cF4
	Ag	Gama-Fe	0.0065	1.44	1.26	1	2**	1.9	1.8	cF4	cF4
	Gama-Fe	Ag	0.022	1.26	1.44	2**	1	1.8	1.9	cF4	cF4
	Ag	Alfa-Fe	0.0065	1.44	1.24(4)	1	2**	1.9	1.8	cF4	cI2

	Alfa-Fe	Ag	0.0002	1.24[4]	1.44	2**	1	1.8	1.9	cI2	cF4
Ag-Gd	Ag	Alfa-Gd	0.95	1.44	1.79[3]	1	3	1.9	1.1	cF4	hP2
	Alfa-Gd	Ag	0	1.79[3]	1.44	3	1	1.1	1.9	hP2	cF4
	Ag	Beta-Gd	0.95	1.44	1.79[3]	1	3	1.9	1.1	cF4	cI2
	Beta-Gd	Ag	0	1.79[3]	1.44	3	1	1.1	1.9	cI2	cF4
Ag-Ge	Ag	Ge	9.6	1.44	1.23[3]	1	4	1.9	1.8	cF4	cF8
	Ge	Ag	0	1.23[3]	1.44	4	1	1.8	1.9	cF8	cF4
Ag-Ho	Ag	Ho	1.6	1.44	1.74[3]	1	3	1.9	1.2	cF4	hP2
	Ho	Ag	0	1.74[3]	1.44	3	1	1.2	1.9	hP2	cF4
Ag-Ir	Ag	Ir	0	1.44	1.35	1	4	1.9	2.2	cF4	cF4
	Ir	Ag	0	1.35	1.44	4	1	2.2	1.9	cF4	cF4
Ag-K	Ag	K	0	1.44	2.31	1	1	1.9	0.8	cF4	cI2
	K	Ag	0	2.31	1.44	1	1	0.8	1.9	cI2	cF4
Ag-La	Ag	Alfa-La	0	1.44	1.88	1	3	1.9	1.1	cF4	hP4
	Alfa-La	Ag	0	1.88	1.44	3	1	1.1	1.9	hP4	cF4
	Ag	Beta-La	0	1.44	1.88	1	3	1.9	1.1	cF4	cF4
	Beta-La	Ag	0	1.88	1.44	3	1	1.1	1.9	cF4	cF4
	Ag	Gama-La	0	1.44	1.88	1	3	1.9	1.1	cF4	cI2
	Gama-La	Ag	0	1.88	1.44	3	1	1.1	1.9	cI2	cF4
Ag-Li	Ag	Alfa-Li	60.87[2]	1.44	1.52	1	1	1.9	1	cF4	hP2
	Alfa-Li	Ag	0[2]	1.52	1.44	1	1	1	1.9	hP2	cF4
	Ag	Beta-Li	60.87[2]	1.44	1.52	1	1	1.9	1	cF4	cI2
	Beta-Li	Ag	9.14[2]	1.52	1.44	1	1	1	1.9	cI2	cF4

Ag-Lu	Ag	Lu	5.8	1.44	1.72[3]	1	3	1.9	1.2	cF4	hP2
	Lu	Ag	0	1.72[3]	1.44	3	1	1.2	1.9	hP2	cF4
Ag-Mg	Ag	Mg	29.3	1.44	1.6	1	2	1.9	1.2	cF4	hP2
	Mg	Ag	3.83	1.6	1.44	2	1	1.2	1.9	hP2	cF4
Ag-Mn	Ag	Alfa-Mn	47	1.44	1.29	1	2**	1.9	1.5	cF4	cI58
	Alfa-Mn	Ag	0	1.29	1.44	2**	1	1.5	1.9	cI58	cF4
	Ag	Beta-Mn	47	1.44	1.29	1	2**	1.9	1.5	cF4	cP20
	Beta-Mn	Ag	1	1.29	1.44	2**	1	1.5	1.9	cP20	cF4
	Ag	Gama-Mn	47	1.44	1.29	1	2**	1.9	1.5	cF4	cF4
	Gama-Mn	Ag	3.4	1.29	1.44	2**	1	1.5	1.9	cF4	cF4
	Ag	Delta-Mn	47	1.44	1.29	1	2**	1.9	1.5	cF4	cI2
	Delta-Mn	Ag	1.5	1.29	1.44	2**	1	1.5	1.9	cI2	cF4
Ag-Mo	Ag	Mo	0.15[2]	1.44	1.36	1	4**	1.9	1.8	cF4	cI2
	Mo	Ag	0	1.36	1.44	4**	1	1.8	1.9	cI2	cF4
Ag-Na	Ag	Na	0	1.44	1.86	1	1	1.9	0.9	cF4	cI2
	Na	Ag	0	1.86	1.44	1	1	0.9	1.9	cI2	cF4
Ag-Nd	Ag	Alfa-Nd	0.2	1.44	1.81[3]	1	3	1.9	1.2	cF4	hP4
	Alfa-Nd	Ag	1.3	1.81[3]	1.44	3	1	1.2	1.9	hP4	cF4
	Ag	Beta-Nd	0.2	1.44	1.81[3]	1	3	1.9	1.2	cF4	cI2
	Beta-Nd	Ag	3.5	1.81[3]	1.44	3	1	1.2	1.9	cI2	cF4
Ag-Ni	Ag	Ni	1.28[2]	1.44	1.24	1	2**	1.9	1.8	cF4	cF4
	Ni	Ag	0.99[2]	1.24	1.44	2**	1	1.8	1.9	cF4	cF4
Ag-Os	Ag	Os	0	1.44	1.34	1	4	1.9	2.2	cF4	hP2

	Os	Ag	0	1.34	1.44	4	1	2.2	1.9	hP2	cF4
Ag-Pd	Ag	Pd	100	1.44	1.38	1	2	1.9	2.2	cF4	cF4
	Pd	Ag	100	1.38	1.44	2	1	2.2	1.9	cF4	cF4
Ag-Pr	Ag	Alfa-Pr	0.05	1.44	1.32[3]	1	3**	1.9	1.1	cF4	hP4
	Alfa-Pr	Ag	1.3	1.32[3]	1.44	3**	1	1.1	1.9	hP4	cF4
	Ag	Beta-Pr	0.05	1.44	1.32[3]	1	3**	1.9	1.1	cF4	cI2
	Beta-Pr	Ag	3.5	1.32[3]	1.44	3**	1	1.1	1.9	cI2	cF4
Ag-Pt	Ag	Pt	40.62[2]	1.44	1.38	1	2	1.9	2.2	cF4	cF4
	Pt	Ag	22.16[2]	1.38	1.44	2	1	2.2	1.9	cF4	cF4
Ag-Pu	Ag	Alfa-Pu	0	1.44	1.51[3]	1	3**	1.9	1.3	cF4	mP16
	Alfa-Pu	Ag	0	1.51[3]	1.44	3**	1	1.3	1.9	mP16	cF4
	Ag	Beta-Pu	0	1.44	1.51[3]	1	3**	1.9	1.3	cF4	mC34
	Beta-Pu	Ag	0	1.51[3]	1.44	3**	1	1.3	1.9	mC34	cF4
	Ag	Gama-Pu	0	1.44	1.51[3]	1	3**	1.9	1.3	cF4	oF8
	Gama-Pu	Ag	0	1.51[3]	1.44	3**	1	1.3	1.9	oF8	cF4
	Ag	Delta-Pu	0	1.44	1.51[3]	1	3**	1.9	1.3	cF4	cF4
	Delta-Pu	Ag	0	1.51[3]	1.44	3**	1	1.3	1.9	cF4	cF4
	Ag	Delta'-Pu	0	1.44	1.51[3]	1	3**	1.9	1.3	cF4	tI2
	Delta'-Pu	Ag	0	1.51[3]	1.44	3**	1	1.3	1.9	tI2	cF4
	Ag	Epsilon-Pu	0	1.44	1.51[3]	1	3**	1.9	1.3	cF4	cI2
	Epsilon-Pu	Ag	5	1.51[3]	1.44	3**	1	1.3	1.9	cI2	cF4
Ag-Rb	Ag	Rb	0	1.44	2.44	1	1	1.9	0.8	cF4	cI2
	Rb	Ag	0	2.44	1.44	1	1	0.8	1.9	cI2	cF4

Ag-Rh	Ag	Rh	0.4[(1)]	1.44	1.34	1	2	1.9	2.2	cF4	cF4
	Rh	Ag	17.2[(1)]	1.34	1.33	2	1	2.2	1.9	cF4	cF4
Ag-Ru	Ag	Ru	0[(1)]	1.44	1.33	1	3[**]	1.9	2.2	cF4	hP2
	Ru	Ag	0[(1)]	1.33	1.44	3[**]	1	2.2	1.9	hP2	cF4
Ag-S	Ag	Alfa-S	0.14	1.44	1.04[*]	1	-2	1.9	2.5	cF4	oF128
	Alfa-S	Ag	0	1.04[*]	1.44	-2	1	2.5	1.9	oF128	cF4
	Ag	Beta-S	0.14	1.44	1.04[*]	1	-2	1.9	2.5	cF4	mP48
	Beta-S	Ag	0	1.04[*]	1.44	-2	1	2.5	1.9	mP48	cF4
Ag-Sc	Ag	Alfa-Sc	10.4	1.44	1.6	1	3	1.9	1.3	cF4	hP2
	Alfa-Sc	Ag	0	1.6	1.44	3	1	1.3	1.9	hP2	cF4
	Ag	Beta-Sc	10.4	1.44	1.6	1	3	1.9	1.3	cF4	cI2
	Beta-Sc	Ag	0	1.6	1.44	3	1	1.3	1.9	cI2	cF4
Ag-Se	Ag	Se	0	1.44	1.16[(3)]	1	-2	1.9	2.4	cF4	hP3
	Se	Ag	0	1.16[(3)]	1.44	-2	1	2.4	1.9	hP3	cF4
Ag-Si	Ag	Si	0	1.44	1.17[*]	1	4	1.9	1.8	cF4	cF8
	Si	Ag	0	1.17[*]	1.44	4	1	1.8	1.9	cF8	cF4
Ag-Sm	Ag	Alfa-Sm	1	1.44	1.79[(3)]	1	3	1.9	1.2	cF4	hR3
	Alfa-Sm	Ag	0	1.79[(3)]	1.44	3	1	1.2	1.9	hR3	cF4
	Ag	Beta-Sm	1	1.44	1.79[(3)]	1	3	1.9	1.2	cF4	hP2
	Beta-Sm	Ag	0	1.79[(3)]	1.44	3	1	1.2	1.9	hP2	cF4
	Ag	Gama-Sm	1	1.44	1.79[(3)]	1	3	1.9	1.2	cF4	cI2
	Gama-Sm	Ag	0	1.79[(3)]	1.44	3	1	1.2	1.9	cI2	cF4
Ag-Sr	Ag	Alfa-Sr	0	1.44	2.15	1	2	1.9	1	cF4	cF4

	Alfa-Sr	Ag	0	2.15	1.44	2	1	1	1.9	cF4	cF4
	Ag	Beta-Sr	0	1.44	2.15	1	2	1.9	1	cF4	cI2
	Beta-Sr	Ag	0	2.15	1.44	2	1	1	1.9	cI2	cF4
Ag-Tb	Ag	Alfa-Tb	1.1	1.44	1.76(3)	1	3	1.9	1.2	cF4	oC4
	Alfa-Tb	Ag	0	1.76(3)	1.44	3	1	1.2	1.9	oC4	cF4
	Ag	Alfa'-Tb	1.1	1.44	1.76(3)	1	3	1.9	1.2	cF4	hP2
	Alfa'-Tb	Ag	0	1.76(3)	1.44	3	1	1.2	1.9	hP2	cF4
	Ag	Beta-Tb	1.1	1.44	1.76(3)	1	3	1.9	1.2	cF4	cI2
	Beta-Tb	Ag	0	1.76(3)	1.44	3	1	1.2	1.9	cI2	cF4
Ag-Te	Ag	Te	0	1.44	1.43(3)	1	-2	1.9	2.1	cF4	hP3
	Te	Ag	0	1.43(3)	1.44	-2	1	2.1	1.9	hP3	cF4
Ag-Th	Ag	Alfa-Th	0	1.44	1.8(3)	1	3**	1.9	1.3	cF4	cF4
	Alfa-Th	Ag	0	1.8(3)	1.44	3**	1	1.3	1.9	cF4	cF4
	Ag	Beta-Th	0	1.44	1.8(3)	1	3**	1.9	1.3	cF4	cI2
	Beta-Th	Ag	0	1.8(3)	1.44	3**	1	1.3	1.9	cI2	cF4
Ag-Ti	Ag	Alfa-Ti	5	1.44	1.46	1	2**	1.9	1.5	cF4	hP2
	Alfa-Ti	Ag	4.7	1.46	1.44	2**	1	1.5	1.9	hP2	cF4
	Ag	Beta-Ti	5	1.44	1.46	1	2**	1.9	1.5	cF4	cI2
	Beta-Ti	Ag	15.5	1.46	1.44	2**	1	1.5	1.9	cI2	cF4
Ag-Tl	Ag	Alfa-Tl	7.5	1.44	1.56	1	3	1.9	1.8	cF4	hP2
	Alfa-Tl	Ag	0	1.71	1.44	3	1	1.8	1.9	hP2	cF4
	Ag	Beta-Tl	7.5	1.44	1.56	1	3	1.9	1.8	cF4	cI2
	Beta-Tl	Ag	0	1.71	1.44	3	1	1.8	1.9	cI2	cF4

Ag-Tm	Ag	Tm	4.57	1.44	1.72[3]	1	3	1.9	1.2	cF4	hP2
	Tm	Ag	0	1.72[3]	1.44	3	1	1.2	1.9	hP2	cF4
Ag-U	Ag	Alfa-U	2.3	1.44	1.39[3]	1	3**	1.9	1.7	cF4	oC4
	Alfa-U	Ag	0	1.39[3]	1.44	3**	1	1.7	1.9	oC4	cF4
	Ag	Beta-U	2.3	1.44	1.39[3]	1	3**	1.9	1.7	cF4	tP30
	Beta-U	Ag	0	1.39[3]	1.44	3**	1	1.7	1.9	tP30	cF4
	Ag	Gama-U	2.3	1.44	1.39[3]	1	3**	1.9	1.7	cF4	cI2
	Gama-U	Ag	0	1.39[3]	1.44	3**	1	1.7	1.9	cI2	cF4
Ag-V	Ag	V	0[1]	1.44	1.31	1	3**	1.9	1.6	cF4	cI2
	V	Ag	0[1]	1.31	1.44	3**	1	1.6	1.9	cI2	cF4
Ag-Y	Ag	Alfa-Y	1.31	1.44	1.8	1	3	1.9	1.2	cF4	hP2
	Alfa-Y	Ag	0	1.8	1.44	3	1	1.2	1.9	hP2	cF4
	Ag	Beta-Y	1.31	1.44	1.8	1	3	1.9	1.2	cF4	cI2
	Beta-Y	Ag	0	1.8	1.44	3	1	1.2	1.9	cI2	cF4
Ag-Yb	Ag	Alfa-Yb	1.92	1.44	1.94[3]	1	2	1.9	1.1	cF4	hP2
	Alfa-Yb	Ag	0	1.94[3]	1.44	2	1	1.1	1.9	hP2	cF4
	Ag	Beta-Yb	1.92	1.44	1.94[3]	1	2	1.9	1.1	cF4	cF4
	Beta-Yb	Ag	0	1.94[3]	1.44	2	1	1.1	1.9	cF4	cF4
	Ag	Gama-Yb	1.92	1.44	1.94[3]	1	2	1.9	1.1	cF4	cI2
	Gama-Yb	Ag	0	1.94[3]	1.44	2	1	1.1	1.9	cI2	cF4
Ag-Zr	Ag	Alfa-Zr	0.11	1.44	1.57	1	4	1.9	1.4	cF4	hP2
	Alfa-Zr	Ag	1.1	1.57	1.44	4	1	1.4	1.9	hP2	cF4
	Ag	Beta-Zr	0.11	1.44	1.57	1	4	1.9	1.4	cF4	cI2

	Beta-Zr	Ag	20	1.57	1.44	4	1	1.4	1.9	cI2	cF4
Cu-As	Cu	As	6.7	1.28	1.25[3]	1	5	1.9	2	cF4	hR2
	As	Cu	0	1.25[3]	1.28	5	1	2	1.9	hR2	cF4
Cu-B	Cu	Alfa-B	0	1.28	0.8*	1	3	1.9	2	cF4	hR12
	Alfa-B	Cu	0	0.8*	1.28	3	1	2	1.9	hR12	cF4
	Cu	Beta-B	0	1.28	0.8*	1	3	1.9	2	cF4	hR105
	Beta-B	Cu	0	0.8*	1.28	3	1	2	1.9	hR105	cF4
Cu-Ba	Cu	Ba	0	1.28	2.17	1	2	1.9	0.9	cF4	cI2
	Ba	Cu	0	2.17	1.28	2	1	0.9	1.9	cI2	cF4
Cu-C	Cu	C	0.052884[2]	1.28	0.77*	1	4**	1.9	2.5	cF4	hP4
	C	Cu	0[2]	0.77*	1.28	4**	1	2.5	1.9	hP4	cF4
Cu-Ca	Cu	Alfa-Ca	0	1.28	1.97	1	2	1.9	1	cF4	cF4
	Alfa-Ca	Cu	0	1.97	1.28	2	1	1	1.9	cF4	cF4
	Cu	Beta-Ca	0	1.28	1.97	1	2	1.9	1	cF4	cI2
	Beta-Ca	Cu	0	1.97	1.28	2	1	1	1.9	cI2	cF4
Cu-Ce	Cu	Alfa-Ce	0	1.28	1.83[3]	1	3**	1.9	1.1	cF4	cF4
	Alfa-Ce	Cu	0	1.83[3]	1.28	3**	1	1.1	1.9	cF4	cF4
	Cu	Beta-Ce	0	1.28	1.83[3]	1	3**	1.9	1.1	cF4	hP4
	Beta-Ce	Cu	0	1.83[3]	1.28	3**	1	1.1	1.9	hP4	cF4
	Cu	Gama-Ce	0	1.28	1.83[3]	1	3**	1.9	1.1	cF4	cF4
	Gama-Ce	Cu	0	1.83[3]	1.23	3**	1	1.1	1.9	cF4	cF4
	Cu	Delta-Ce	0	1.28	1.83[3]	1	3**	1.9	1.1	cF4	cI2
	Delta-Ce	Cu	0	1.83[3]	1.28	3**	1	1.1	1.9	cI2	cF4

Cu-Co	Cu	Alfa-Co	8	1.28	1.25	1	2**	1.9	1.8	cF4	cF4
	Alfa-Co	Cu	20	1.25	1.28	2**	1	1.8	1.9	cF4	cF4
	Cu	Epsilon-Co	8	1.28	1.25	1	2**	1.9	1.8	cF4	hP2
	Epsilon-Co	Cu	0.4	1.25	1.28	2**	1	1.8	1.9	hP2	cF4
Cu-Cr	Cu	Cr	0.89	1.28	1.25	1	3**	1.9	1.6	cF4	cI2
	Cr	Cu	0.2	1.25	1.28	3**	1	1.6	1.9	cI2	cF4
Cu-Cs	Cu	Cs	0	1.28	2.62	1	1	1.9	0.7	cF4	cI2
	Cs	Cu	0	2.62	1.28	1	1	0.7	1.9	cI2	cF4
Cu-Dy	Cu	Alfa'-Dy	0	1.28	1.75(3)	1	3	1.9	1.1	cF4	oC4
	Alfa'-Dy	Cu	0	1.75(3)	1.28	3	1	1.1	1.9	oC4	cF4
	Cu	Alfa-Dy	0	1.28	1.75(3)	1	3	1.9	1.1	cF4	hP2
	Alfa-Dy	Cu	0	1.75(3)	1.28	3	1	1.1	1.9	hP2	cF4
	Cu	Beta-Dy	0	1.28	1.75(3)	1	3	1.9	1.1	cF4	cI2
	Beta-Dy	Cu	0	1.75(3)	1.28	3	1	1.1	1.9	cI2	cF4
Cu-Er	Cu	Er	0	1.28	1.73(3)	1	3	1.9	1.2	cF4	hP2
	Er	Cu	0	1.73(3)	1.28	3	1	1.2	1.9	hP2	cF4
Cu-Eu	Cu	Eu	0	1.28	1.99(3)	1	2	1.9	1.1	cF4	cI2
	Eu	Cu	0	1.99(3)	1.28	2	1	1.1	1.9	cI2	cF4
Cu-Fe	Cu	Alfa-Fe	4.64	1.28	1.24(4)	1	2**	1.9	1.8	cF4	cI2
	Alfa-Fe	Cu	1.94	1.24(4)	1.28	2**	1	1.8	1.9	cI2	cF4
	Cu	Gama-Fe	4.64	1.28	1.26	1	2**	1.9	1.8	cF4	cF4
	Gama-Fe	Cu	11.61	1.26	1.28	2**	1	1.8	1.9	cF4	cF4
	Cu	Delta-Fe	4.64	1.28	1.26	1	2**	1.9	1.8	cF4	cI2

	Delta-Fe	Cu	6.74	1.26	1.28	2**	1	1.8	1.9	cI2	cF4
Cu-Gd	Cu	Alfa-Gd	0	1.28	1.79(3)	1	3	1.9	1.1	cF4	hP2
	Alfa-Gd	Cu	1.8	1.79(3)	1.28	3	1	1.1	1.9	hP2	cF4
	Cu	Beta-Gd	0	1.28	1.79(3)	1	3	1.9	1.1	cF4	cI2
	Beta-Gd	Cu	0	1.79(3)	1.28	3	1	1.1	1.9	cI2	cF4
Cu-Hf	Cu	Alfa-Hf	0.39442(2)	1.28	1.57	1	4	1.9	1.3	cF4	hP2
	Alfa-Hf	Cu	0.8381(2)	1.57	1.28	4	1	1.3	1.9	hP2	cF4
	Cu	Beta-Hf	0.39442(2)	1.28	1.57	1	4	1.9	1.3	cF4	cI2
	Beta-Hf	Cu	4.37(2)	1.57	1.28	4	1	1.3	1.9	cI2	cF4
Cu-In	Cu	In	11	1.28	1.51	1	3	1.9	1.7	cF4	tI2
	In	Cu	0	1.66	1.28	3	1	1.7	1.9	tI2	cF4
Cu-Ir	Cu	Ir	8	1.28	1.35	1	4	1.9	2.2	cF4	cF4
	Ir	Cu	1.3	1.35	1.28	4	1	2.2	1.9	cF4	cF4
Cu-K	Cu	K	0	1.28	2.31	1	1	1.9	0.8	cF4	cI2
	K	Cu	0	2.31	1.28	1	1	0.8	1.9	cI2	cF4
Cu-La	Cu	Alfa-La	0	1.28	1.88	1	3	1.9	1.1	cF4	hP4
	Alfa-La	Cu	0	1.88	1.28	3	1	1.1	1.9	hP4	cF4
	Cu	Beta-La	0	1.28	1.88	1	3	1.9	1.1	cF4	cF4
	Beta-La	Cu	0	1.88	1.28	3	1	1.1	1.9	cF4	cF4
	Cu	Gama-La	0	1.28	1.88	1	3	1.9	1.1	cF4	cI2
	Gama-La	Cu	0	1.88	1.28	3	1	1.1	1.9	cI2	cF4
Cu-Li	Cu	Alfa-Li	22	1.28	1.52	1	1	1.9	1	cF4	hP2
	Alfa-Li	Cu	0	1.52	1.28	1	1	1	1.9	hP2	cF4

	Cu	Beta-Li	22	1.28	1.52	1	1	1.9	1	cF4	cI2
	Beta-Li	Cu	0	1.52	1.28	1	1	1	1.9	cI2	cF4
Cu-Mn	Cu	Alfa-Mn	100[(2)]	1.28	1.29	1	2[**]	1.9	1.5	cF4	cI58
	Alfa-Mn	Cu	0.26[(2)]	1.29	1.28	2[**]	1	1.5	1.9	cI58	cF4
	Cu	Beta-Mn	100[(2)]	1.28	1.29	1	2[**]	1.9	1.5	cF4	cP20
	Beta-Mn	Cu	0.43[(2)]	1.29	1.28	2[**]	1	1.5	1.9	cP20	cF4
	Cu	Delta-Mn	100[(2)]	1.28	1.29	1	2[**]	1.9	1.5	cF4	cI2
	Delta-Mn	Cu	12.52[(2)]	1.29	1.28	2[**]	1	1.5	1.9	cI2	cF4
	Cu	Gama-Mn	100[(2)]	1.28	1.29	1	2[**]	1.9	1.5	cF4	cF4
	Gama-Mn	Cu	100[(2)]	1.29	1.28	2[**]	1	1.5	1.9	cF4	cF4
Cu-Mo	Cu	Mo	0	1.28	1.36	1	4[**]	1.9	1.8	cF4	cI2
	Mo	Cu	0	1.36	1.28	4[**]	1	1.8	1.9	cI2	cF4
Cu-Na	Cu	Alfa-Na	0	1.28	1.86	1	1	1.9	0.9	cF4	hP2
	Alfa-Na	Cu	0	1.86	1.28	1	1	0.9	1.9	hP2	cF4
	Cu	Beta-Na	0	1.28	1.86	1	1	1.9	0.9	cF4	cI2
	Beta-Na	Cu	0	1.86	1.28	1	1	0.9	1.9	cI2	cF4
Cu-Nb	Cu	Nb	0	1.28	1.41	1	5	1.9	1.6	cF4	cI2
	Nb	Cu	1.2	1.41	1.28	5	1	1.6	1.9	cI2	cF4
Cu-Nd	Cu	Alfa-Nd	0	1.28	1.81[(3)]	1	3	1.9	1.2	cF4	hP4
	Alfa-Nd	Cu	0	1.81[(3)]	1.28	3	1	1.2	1.9	hP4	cF4
	Cu	Beta-Nd	0	1.28	1.81[(3)]	1	3	1.9	1.2	cF4	cI2
	Beta-Nd	Cu	0	1.81[(3)]	1.28	3	1	1.2	1.9	cI2	cF4
Cu-Ni	Cu	Ni	100	1.28	1.24	1	2[**]	1.9	1.8	cF4	cF4

	Ni	Cu	100	1.24	1.28	2**	1	1.8	1.9	cF4	cF4
Cu-Pd	Cu	Pd	100	1.28	1.38	1	2	1.9	2.2	cF4	cF4
	Pd	Cu	100	1.38	1.28	2	1	2.2	1.9	cF4	cF4
Cu-Pr	Cu	Alfa-Pr	0	1.28	1.32(3)	1	3**	1.9	1.1	cF4	hP4
	Alfa-Pr	Cu	0	1.32(3)	1.28	3**	1	1.1	1.9	hP4	cF4
	Cu	Beta-Pr	0	1.28	1.32(3)	1	3**	1.9	1.1	cF4	cI2
	Beta-Pr	Cu	0	1.32(3)	1.28	3**	1	1.1	1.9	cI2	cF4
Cu-Pt	Cu	Pt	100	1.28	1.38	1	2	1.9	2.2	cF4	cF4
	Pt	Cu	100	1.38	1.28	2	1	2.2	1.9	cF4	cF4
Cu-Pu	Cu	Alfa-Pu	0(2)	1.28	1.51(3)	1	3**	1.9	1.3	cF4	mP16
	Alfa-Pu	Cu	0(2)	1.51(3)	1.28	3**	1	1.3	1.9	mP16	cF4
	Cu	Beta-Pu	0(2)	1.28	1.51(3)	1	3**	1.9	1.3	cF4	mC34
	Beta-Pu	Cu	0(2)	1.51(3)	1.28	3**	1	1.3	1.9	mC34	cF4
	Cu	Gama-Pu	0(2)	1.28	1.51(3)	1	3**	1.9	1.3	cF4	oF8
	Gama-Pu	Cu	0(2)	1.51(3)	1.28	3**	1	1.3	1.9	oF8	cF4
	Cu	Delta-Pu	0(2)	1.28	1.51(3)	1	3**	1.9	1.3	cF4	cF4
	Delta-Pu	Cu	0(2)	1.51(3)	1.28	3**	1	1.3	1.9	cF4	cF4
	Cu	Delta'-Pu	0(2)	1.28	1.51(3)	1	3**	1.9	1.3	cF4	tI2
	Delta'-Pu	Cu	0(2)	1.51(3)	1.28	3**	1	1.3	1.9	tI2	cF4
	Cu	Epsilon-Pu	0(2)	1.28	1.51(3)	1	3**	1.9	1.3	cF4	cI2
	Epsilon-Pu	Cu	4.5**	1.51(3)	1.28	3**	1	1.3	1.9	cI2	cF4
Cu-Rb	Cu	Rb	0	1.28	2.44	1	1	1.9	0.8	cF4	cI2
	Rb	Cu	0	2.44	1.28	1	1	0.8	1.9	cI2	cF4

Cu-Rh	Cu	Rh	100	1.28	1.34	1	2	1.9	2.2	cF4	cF4
	Rh	Cu	100	1.34	1.28	2	1	2.2	1.9	cF4	cF4
Cu-S	Cu	S	0	1.28	1.04*	1	-2	1.9	2.5	cF4	oF128
	S	Cu	0	1.04*	1.28	-2	1	2.5	1.9	oF128	cF4
Cu-Se	Cu	Se	0	1.28	1.16(3)	1	-2	1.9	2.4	cF4	hP3
	Se	Cu	0	1.16(3)	1.28	-2	1	2.4	1.9	hP3	cF4
Cu-Sm	Cu	Alfa-Sm	0	1.28	1.79(3)	1	3	1.9	1.2	cF4	hR3
	Alfa-Sm	Cu	0	1.79(3)	1.28	3	1	1.2	1.9	hR3	cF4
	Cu	Beta-Sm	0	1.28	1.79(3)	1	3	1.9	1.2	cF4	hP2
	Beta-Sm	Cu	0	1.79(3)	1.28	3	1	1.2	1.9	hP2	cF4
	Cu	Gama-Sm	0	1.28	1.79(3)	1	3	1.9	1.2	cF4	cI2
	Gama-Sm	Cu	0	1.79(3)	1.28	3	1	1.2	1.9	cI2	cF4
Cu-Sr	Cu	Alfa-Sr	0	1.28	2.15(3)	1	2	1.9	1	cF4	cF4
	Alfa-Sr	Cu	0	2.15(3)	1.28	2	1	1	1.9	cF4	cF4
	Cu	Beta-Sr	0	1.28	2.15(3)	1	2	1.9	1	cF4	cI2
	Beta-Sr	Cu	0	2.15(3)	1.28	2	1	1	1.9	cI2	cF4
Cu-Te	Cu	Te	0	1.28	1.43(3)	1	-2	1.9	2.1	cF4	hP3
	Te	Cu	0	1.43(3)	1.28	-2	1	2.1	1.9	hP3	cF4
Cu-Th	Cu	Alfa-Th	0	1.28	1.8(3)	1	3**	1.9	1.3	cF4	cF4
	Alfa-Th	Cu	0	1.8(3)	1.28	3**	1	1.3	1.9	cF4	cF4
	Cu	Beta-Th	0	1.28	1.8(3)	1	3**	1.9	1.3	cF4	cI2
	Beta-Th	Cu	0	1.8(3)	1.28	3**	1	1.3	1.9	cI2	cF4
Cu-Ti	Cu	Alfa-Ti	8	1.28	1.46	1	2**	1.9	1.5	cF4	hP2

	Alfa-Ti	Cu	1.6	1.46	1.28	2**	1	1.5	1.9	hP2	cF4
	Cu	Beta-Ti	8	1.28	1.46	1	2**	1.9	1.5	cF4	cI2
	Beta-Ti	Cu	13.5	1.46	1.28	2**	1	1.5	1.9	cI2	cF4
Cu-Tl	Cu	Alfa-Tl	0.275	1.28	1.56	1	3	1.9	1.8	cF4	hP2
	Alfa-Tl	Cu	0	1.71	1.28	3	1	1.8	1.9	hP2	cF4
	Cu	Beta-Tl	0.275	1.28	1.56	1	3	1.9	1.8	cF4	cI2
	Beta-Tl	Cu	0	1.71	1.28	3	1	1.8	1.9	cI2	cF4
Cu-U	Cu	Alfa-U	0	1.28	1.39(3)	1	3**	1.9	1.7	cF4	oC4
	Alfa-u	Cu	0	1.39(3)	1.28	3**	1	1.7	1.9	oC4	cF4
	Cu	Beta-U	0	1.28	1.39(3)	1	3**	1.9	1.7	cF4	tP30
	Beta-U	Cu	0	1.39(3)	1.28	3**	1	1.7	1.9	tP30	cF4
	Cu	Gama-U	0	1.28	1.39(3)	1	3**	1.9	1.7	cF4	cI2
	Gama-U	Cu	0	1.39(3)	1.28	3**	1	1.7	1.9	cI2	cF4
Cu-V	Cu	V	0.1	1.28	1.31	1	3**	1.9	1.6	cF4	cI2
	V	Cu	7.5	1.31	1.28	3**	1	1.6	1.9	cI2	cF4
Cu-Y	Cu	Alfa-Y	0.04	1.28	1.8	1	3	1.9	1.2	cF4	hP2
	Alfa-Y	Cu	0.14	1.8	1.28	3	1	1.2	1.9	hP2	cF4
	Cu	Beta-Y	0.04	1.28	1.8	1	3	1.9	1.2	cF4	cI2
	Beta-Y	Cu	0	1.8	1.28	3	1	1.2	1.9	cI2	cF4
Cu-Yb	Cu	Alfa-Yb	0	1.28	1.94(3)	1	2	1.9	1.1	cF4	hP2
	Alfa-Yb	Cu	0	1.94(3)	1.28	2	1	1.1	1.9	hP2	cF4
	Cu	Beta-Yb	0	1.28	1.94(3)	1	2	1.9	1.1	cF4	cF4
	Beta-Yb	Cu	0.03	1.94(3)	1.28	2	1	1.1	1.9	cF4	cF4

	Cu	Gama-Yb	0	1.28	1.94[3]	1	2	1.9	1.1	cF4	cI2
	Gama-Yb	Cu	0	1.94[3]	1.28	2	1	1.1	1.9	cI2	cF4
Cu-Zr	Cu	Alfa-Zr	0.12[2]	1.28	1.57	1	4	1.9	1.4	cF4	hP2
	Alfa-Zr	Cu	0.2[2]	1.57	1.28	4	1	1.4	1.9	hP2	cF4
	Cu	Beta-Zr	0.12[2]	1.28	1.57	1	4	1.9	1.4	cF4	cI2
	Beta-Zr	Cu	3.13[2]	1.57	1.28	4	1	1.4	1.9	cI2	cF4

Resource: Binary Phase Diagram Vol.1 Thaddeus B. Massalski 1987 second printing (copyright 1986)

The Handbook of Bianary Phases Diagrams Vol. 1. Moffatt, W. G. 11/8/1994.

ASM Handbook Vol.3, Alloy Phase Diagrams, 1992

SI Chemical Data 4th Edition, Gordon Aylward & Tristan Findlay. 1998(4th edition)

Chemistry Data Book 2nd Edition in SI. J G Stark, H G Wallace 1984 reprinted (1982 edition)

* Use Covalent Radius from "Chemistry Data Book 2nd Edition in SI."

** Unsure Values

(1) The Handbook of Binary Phases Diagrams Vol.1 Moffatt,W.G.11/8/1994

(2) ASM Handbook Vol.3, Alloy Phase Diagrams, 1992

(3) SI Chemical Data 4th Edition, Gordon Aylward & Tristan Findlay. 1998(4th edition)

(4) W.Hume-Rothery. *Elements of Structural Metallurgy*.
London: Institute of Metals Monograph and Report Series No. 26, The Institute of Metals 1961

2. Introducing Temperature Parameters

Solvent	Solute	Tm (Solvent)	Tm (Solute)	Solvent	Solute	Tm (Solvent)	Tm (Solute)	Solvent	Solute	Tm (Solvent)	Tm (Solute)	Solvent	Solute	Tm (Solvent)	Tm (Solute)
Ag	Alfa-Be	961.93	1289	Ag	Alfa-Ca	961.93	842	Ag	Delta-Mn	961.93	1246	Ag	Te	961.93	449.57
Alfa-Be	Ag	1289	961.93	Alfa-Ca	Ag	842	961.93	Delta-Mn	Ag	1246	961.93	Te	Ag	449.57	961.93
Ag	Beta-Be	961.93	1289	Ag	Beta-Ca	961.93	842	Ag	Mo	961.93	2623	Ag	Alfa-Th	961.93	1755
Beta-Be	Ag	1289	961.93	Beta-Ca	Ag	842	961.93	Mo	Ag	2623	961.93	Alfa-Th	Ag	1755	961.93
Ag	Zn	961.93	419.58	Ag	Alfa-Ce	961.93	798	Ag	Na	961.93	97.8	Ag	Beta-Th	961.93	1755
Zn	Ag	419.58	961.93	Alfa-Ce	Ag	798	961.93	Na	Ag	97.8	961.93	Beta-Th	Ag	1755	961.93
Ag	Cd	961.93	321.108	Ag	Beta-Ce	961.93	798	Ag	Alfa-Nd	961.93	1021	Ag	Alfa-Ti	961.93	1670
Cd	Ag	321.108	961.93	Beta-Ce	Ag	798	961.93	Alfa-Nd	Ag	1021	961.93	Alfa-Ti	Ag	1670	961.93
Ag	Hg	961.93	-38.84	Ag	Gama-Ce	961.93	798	Ag	Beta-Nd	961.93	1021	Ag	Beta-Ti	961.93	1670
Hg	Ag	-38.84	961.93	Gama-Ce	Ag	798	961.93	Beta-Nd	Ag	1021	961.93	Beta-Ti	Ag	1670	961.93
Ag	Al	961.93	660.452	Ag	Delta-Ce	961.93	798	Ag	Ni	961.93	1455	Ag	Alfa-Tl	961.93	304
Al	Ag	660.452	961.93	Delta-Ce	Ag	798	961.93	Ni	Ag	1455	961.93	Alfa-Tl	Ag	304	961.93
Ag	Ga	961.93	29.7741	Ag	Epsilon-Co	961.93	1495	Ag	Os	961.93	3033	Ag	Beta-Tl	961.93	304
Ga	Ag	29.7741	961.93	Epsilon-Co	Ag	1495	961.93	Os	Ag	3033	961.93	Beta-Tl	Ag	304	961.93
Ag	In	961.93	156.634	Ag	Alfa-Co	961.93	1495	Ag	Pd	961.93	1555	Ag	Tm	961.93	1545
In	Ag	156.634	961.93	Alfa-Co	Ag	1495	961.93	Pd	Ag	1555	961.93	Tm	Ag	1545	961.93
Ag	Alfa-Sn	961.93	231.968	Ag	Cr	961.93	1863	Ag	Alfa-Pr	961.93	931	Ag	Alfa-U	961.93	1135
Alfa-Sn	Ag	231.968	961.93	Cr	Ag	1863	961.93	Alfa-Pr	Ag	931	961.93	Alfa-U	Ag	1135	961.93
Ag	Beta-Sn	961.93	231.968	Ag	Cs	961.93	28.39	Ag	Beta-Pr	961.93	931	Ag	Beta-U	961.93	1135

Beta-Sn	Ag	231.968	961.93	Cs	Ag	28.39	961.93	Beta-Pr	Ag	931	961.93	Beta-U	Ag	1135	961.93
Ag	Pb	961.93	327.502	Ag	Alfa'-Dy	961.93	1412	Ag	Pt	961.93	1769	Ag	Gama-U	961.93	1135
Pb	Ag	327.502	961.93	Alfa'-Dy	Ag	1412	961.93	Pt	Ag	1769	961.93	Gama-U	Ag	1135	961.93
Ag	Cu	961.93	1084.87	Ag	Alfa-Dy	961.93	1412	Ag	Alfa-Pu	961.93	640	Ag	V	961.93	1910
Cu	Ag	1084.87	961.93	Alfa-Dy	Ag	1412	961.93	Alfa-Pu	Ag	640	961.93	V	Ag	1910	961.93
Ag	Sb	961.93	630.755	Ag	Beta-Dy	961.93	1412	Ag	Beta-Pu	961.93	640	Ag	Alfa-Y	961.93	1522
Sb	Ag	630.755	961.93	Bety-Dy	Ag	1412	961.93	Beta-Pu	Ag	640	961.93	Alfa-Y	Ag	1522	961.93
Ag	Bi	961.93	271.442	Ag	Er	961.93	1529	Ag	Gama-Pu	961.93	640	Ag	Beta-Y	961.93	1522
Bi	Ag	271.442	961.93	Er	Ag	1529	961.93	Gama-Pu	Ag	640	961.93	Beta-Y	Ag	1522	961.93
Ag	As	961.93	808	Ag	Eu	961.93	822	Ag	Delta-Pu	961.93	640	Ag	Alfa-Yb	961.93	819
As	Ag	808	961.93	Eu	Ag	822	961.93	Delta-Pu	Ag	640	961.93	Alfa-Yb	Ag	819	961.93
Cu	Au	1084.87	1064.43	Ag	Delta-Fe	961.93	1538	Ag	Delta'-Pu	961.93	640	Ag	Beta-Yb	961.93	819
Au	Cu	1064.43	1084.87	Delta-Fe	Ag	1538	961.93	Delta'-Pu	Ag	640	961.93	Beta-Yb	Ag	819	961.93
Cu	Alfa-Be	1084.87	1289	Ag	Gama-Fe	961.93	1538	Ag	Epsilon-Pu	961.93	640	Ag	Gama-Yb	961.93	819
Alfa-Be	Cu	1289	1084.87	Gama-Fe	Ag	1538	961.93	Epsilon-Pu	Ag	640	961.93	Gama-Yb	Ag	819	961.93
Cu	Beta-Be	1084.87	1289	Ag	Alfa-Fe	961.93	1538	Ag	Rb	961.93	39.48	Ag	Alfa-Zr	961.93	1855
Beta-Be	Cu	1289	1084.87	Alfa-Fe	Ag	1538	961.93	Rb	Ag	39.48	961.93	Alfa-Zr	Ag	1855	961.93
Cu	Mg	1084.87	650	Ag	Alfa-Gd	961.93	1313	Ag	Rh	961.93	1963	Ag	Beta-Zr	961.93	1855
Mg	Cu	650	1084.87	Alfa-Gd	Ag	1313	961.93	Rh	Ag	1963	961.93	Beta-Zr	Ag	1855	961.93
Cu	Zn	1084.87	419.58	Ag	Beta-Gd	961.93	1313	Ag	Ru	961.93	2334	Cu	As	1084.87	603
Zn	Cu	419.58	1084.87	Beta-Gd	Ag	1313	961.93	Ru	Ag	2334	961.93	As	Cu	603	1084.87
Cu	Cd	1084.87	321.108	Ag	Ge	961.93	938.3	Ag	Alfa-S	961.93	115.22	Cu	Alfa-B	1084.87	2092
Cd	Cu	321.108	1084.87	Ge	Ag	938.3	961.93	Alfa-S	Ag	115.22	961.93	Alfa-B	Cu	2092	1084.87

Cu	Al	1084.87	660.452	Ag	Ho	961.93	1474	Ag	Beta-S	961.93	115.22	Cu	Beta-B	1084.87	2092
Al	Cu	660.452	1084.87	Ho	Ag	1474	961.93	Beta-S	Ag	115.22	961.93	Beta-B	Cu	2092	1084.87
Cu	Ga	1084.87	29.7741	Ag	Ir	961.93	2447	Ag	Alfa-Sc	961.93	1541	Cu	Ba	1084.87	729
Ga	Cu	29.7741	1084.87	Ir	Ag	2447	961.93	Alfa-Sc	Ag	1541	961.93	Ba	Cu	729	1084.87
Cu	Si	1084.87	1414	Ag	K	961.93	63.71	Ag	Beta-Sc	961.93	1541	Cu	C	1084.87	3826
Si	Cu	1414	1084.87	K	Ag	63.71	961.93	Beta-Sc	Ag	1541	961.93	C	Cu	3826	1084.87
Cu	Ge	1084.87	938.3	Ag	Alfa-La	961.93	918	Ag	Se	961.93	221	Cu	Alfa-Ca	1084.87	842
Ge	Cu	938.3	1084.87	Alfa-La	Ag	918	961.93	Se	Ag	221	961.93	Alfa-Ca	Cu	842	1084.87
Cu	Alfa-Sn	1084.87	231.968	Ag	Beta-La	961.93	918	Ag	Si	961.93	1414	Cu	Beta-Ca	1084.87	842
Alfa-Sn	Cu	231.968	1084.87	Beta-La	Ag	918	961.93	Si	Ag	1414	961.93	Beta-Ca	Cu	842	1084.87
Cu	Beta-Sn	1084.87	231.968	Ag	Gama-La	961.93	918	Ag	Alfa-Sm	961.93	1074	Cu	Alfa-Ce	1084.87	798
Beta-Sn	Cu	231.968	1084.87	Gama-La	Ag	918	961.93	Alfa-Sm	Ag	1074	961.93	Alfa-Ce	Cu	798	1084.87
Cu	Pb	1084.87	327.502	Ag	Alfa-Li	961.93	180.6	Ag	Beta-Sm	961.93	1074	Cu	Beta-Ce	1084.87	798
Pb	Cu	327.502	1084.87	Alfa-Li	Ag	180.6	961.93	Beta-Sm	Ag	1074	961.93	Beta-Ce	Cu	798	1084.87
Cu	Sb	1084.87	630.755	Ag	Beta-Li	961.93	180.6	Ag	Gama-Sm	961.93	1074	Cu	Gama-Ce	1084.87	798
Sb	Cu	630.755	1084.87	Beta-Li	Ag	180.6	961.93	Gama-Sm	Ag	1074	961.93	Gama-Ce	Cu	798	1084.87
Cu	Bi	1084.87	271.442	Ag	Lu	961.93	1663	Ag	Alfa-Sr	961.93	769	Cu	Delta-Ce	1084.87	798
Bi	Cu	271.442	1084.87	Lu	Ag	1663	961.93	Alfa-Sr	Ag	769	961.93	Delta-Ce	Cu	798	1084.87
Cu	Hg	1084.87	-38.84	Ag	Mg	961.93	650	Ag	Beta-Sr	961.93	769	Cu	Alfa-Co	1084.87	1495
Hg	Cu	-38.84	1084.87	Mg	Ag	650	961.93	Beta-Sr	Ag	769	961.93	Alfa-Co	Cu	1495	1084.87
Ag	Au	961.93	1064.43	Ag	Alfa-Mn	961.93	1246	Ag	Alfa-Tb	961.93	1356	Cu	Epsilon-Co	1084.87	1495
Au	Ag	1064.43	961.93	Alfa-Mn	Ag	1246	961.93	Alfa-Tb	Ag	1356	961.93	Epsilon-Co	Cu	1495	1084.87
Ag	B	961.93	2092	Ag	Beta-Mn	961.93	1246	Ag	Alfa'-Tb	961.93	1356	Cu	Cr	1084.87	1863

B	Ag	2092	961.93	Beta-Mn	Ag	1246	961.93	Alfa'-Tb	Ag	1356	961.93	Cr	Cu	1863	1084.87
Ag	Ba	961.93	729	Ag	Gama-Mn	961.93	1246	Ag	Beta-Tb	961.93	1356	Cu	Cs	1084.87	28.39
Ba	Ag	729	961.93	Gama-Mn	Ag	1246	961.93	Beta-Tb	Ag	1356	961.93	Cs	Cu	28.39	1084.87
Cu	Alfa'-Dy	1084.87	1412	Cu	Pt	1084.87	1769	Cu	Gama-La	1084.9	918	Cu	Alfa-Th	1084.87	1755
Alfa'-Dy	Cu	1412	1084.87	Pt	Cu	1769	1084.87	Gama-La	Cu	918	1084.9	Alfa-Th	Cu	1755	1084.87
Cu	Alfa-Dy	1084.87	1412	Cu	Alfa-Pu	1084.87	640	Cu	Alfa-Li	1084.9	180.6	Cu	Beta-Th	1084.87	1755
Alfa-Dy	Cu	1412	1084.87	Alfa-Pu	Cu	640	1084.87	Alfa-Li	Cu	180.6	1084.9	Beta-Th	Cu	1755	1084.87
Cu	Beta-Dy	1084.87	1412	Cu	Beta-Pu	1084.87	640	Cu	Beta-Li	1084.9	180.6	Cu	Alfa-Ti	1084.87	1670
Beta-Dy	Cu	1412	1084.87	Beta-Pu	Cu	640	1084.87	Beta-Li	Cu	180.6	1084.9	Alfa-Ti	Cu	1670	1084.87
Cu	Er	1084.87	1529	Cu	Gama-Pu	1084.87	640	Cu	Alfa-Mn	1084.9	1246	Cu	Beta-Ti	1084.87	1670
Er	Cu	1529	1084.87	Gama-Pu	Cu	640	1084.87	Alfa-Mn	Cu	1246	1084.9	Beta-Ti	Cu	1670	1084.87
Cu	Eu	1084.87	822	Cu	Delta-Pu	1084.87	640	Cu	Beta-Mn	1084.9	1246	Cu	Alfa-Tl	1084.87	304
Eu	Cu	822	1084.87	Delta-Pu	Cu	640	1084.87	Beta-Mn	Cu	1246	1084.9	Alfa-Tl	Cu	304	1084.87
Cu	Alfa-Fe	1084.87	1538	Cu	Delta'-Pu	1084.87	640	Cu	Delta-Mn	1084.9	1246	Cu	Beta-Tl	1084.87	304
Alfa-Fe	Cu	1538	1084.87	Delta'-Pu	Cu	640	1084.87	Delta-Mn	Cu	1246	1084.9	Beta-Tl	Cu	304	1084.87
Cu	Gama-Fe	1084.87	1538	Cu	Epsilon-Pu	1084.87	640	Cu	Gama-Mn	1084.9	1246	Cu	Alfa-U	1084.87	1135
Gama-Fe	Cu	1538	1084.87	Epsilon-Pu	Cu	640	1084.87	Gama-Mn	Cu	1246	1084.9	Alfa-u	Cu	1135	1084.87
Cu	Delta-Fe	1084.87	1538	Cu	Rb	1084.87	39.48	Cu	Mo	1084.9	2623	Cu	Beta-U	1084.87	1135
Delta-Fe	Cu	1538	1084.87	Rb	Cu	39.48	1084.87	Mo	Cu	2623	1084.9	Beta-U	Cu	1135	1084.87
Cu	Alfa-Gd	1084.87	1313	Cu	Rh	1084.87	1963	Cu	Alfa-Na	1084.9	97.8	Cu	Gama-U	1084.87	1135
Alfa-Gd	Cu	1313	1084.87	Rh	Cu	1963	1084.87	Alfa-Na	Cu	97.8	1084.9	Gama-U	Cu	1135	1084.87
Cu	Beta-Gd	1084.87	1313	Cu	S	1084.87	115.22	Cu	Beta-Na	1084.9	97.8	Cu	V	1084.87	1910
Beta-Gd	Cu	1313	1084.87	S	Cu	115.22	1084.87	Beta-Na	Cu	97.8	1084.9	V	Cu	1910	1084.87

Cu	Alfa-Hf	1084.87	2231	Cu	Se	1084.87	221	Cu	Nb	1084.9	2469	Cu	Alfa-Y	1084.87	1522
Alfa-Hf	Cu	2231	1084.87	Se	Cu	221	1084.87	Nb	Cu	2469	1084.9	Alfa-Y	Cu	1522	1084.87
Cu	Beta-Hf	1084.87	2231	Cu	Alfa-Sm	1084.87	1074	Cu	Alfa-Nd	1084.9	1021	Cu	Beta-Y	1084.87	1522
Beta-Hf	Cu	2231	1084.87	Alfa-Sm	Cu	1074	1084.87	Alfa-Nd	Cu	1021	1084.9	Beta-Y	Cu	1522	1084.87
Cu	In	1084.87	156.634	Cu	Beta-Sm	1084.87	1074	Cu	Beta-Nd	1084.9	1021	Cu	Alfa-Yb	1084.87	819
In	Cu	156.634	1084.87	Beta-Sm	Cu	1074	1084.87	Beta-Nd	Cu	1021	1084.9	Alfa-Yb	Cu	819	1084.87
Cu	Ir	1084.87	2447	Cu	Gama-Sm	1084.87	1074	Cu	Ni	1084.9	1455	Cu	Beta-Yb	1084.87	819
Ir	Cu	2447	1084.87	Gama-Sm	Cu	1074	1084.87	Ni	Cu	1455	1084.9	Beta-Yb	Cu	819	1084.87
Cu	K	1084.87	63.71	Cu	Alfa-Sr	1084.87	7769	Cu	Pd	1084.9	1555	Cu	Gama-Yb	1084.87	819
K	Cu	63.71	1084.87	Alfa-Sr	Cu	769	1084.87	Pd	Cu	1555	1084.9	Gama-Yb	Cu	819	1084.87
Cu	Alfa-La	1084.87	918	Cu	Beta-Sr	1084.87	769	Cu	Alfa-Pr	1084.9	931	Cu	Alfa-Zr	1084.87	1855
Alfa-La	Cu	918	1084.87	Beta-Sr	Cu	769	1084.87	Alfa-Pr	Cu	931	1084.9	Alfa-Zr	Cu	1855	1084.87
Cu	Beta-La	1084.87	918	Cu	Te	1084.87	449.57	Cu	Beta-Pr	1084.9	931	Cu	Beta-Zr	1084.87	1855
Beta-La	Cu	918	1084.87	Te	Cu	449.57	1084.87	Beta-Pr	Cu	931	1084.9	Beta-Zr	Cu	1855	1084.87

3. Gold Alloy Systems

Solvent	Solute	Solubility Limits (Atoms %)	Size(solvent) Radii in	Size(Solute) (Angstronms)	Valence Solvent	Valence Solute	Electrochemical Factors(Solvent)	Electrochemical Factors(Solute)	Tm (Solvent)	Tm (Solute)
Au	B	5	1.44	0.8	1	3	2.4	2	1064.43	2092
Au	Alfa-Be	0.2	1.44	1.12	1	2	2.4	1.5	1064.43	1289
Alfa-Be	Au	0.25	1.12	1.44	2	1	1.5	2.4	1289	1064.43
Au	Beta-Be	0.2	1.44	1.12	1	2	2.4	1.5	1064.43	1289
Au	Zn	33.5	1.44	1.33	1	2	2.4	1.6	1064.43	419.58
Zn	Au	7.5	1.33	1.44	2	1	1.6	2.4	419.58	1064.43
Au	Cd	32.5	1.44	1.49	1	2	2.4	1.7	1064.43	321.108
Cd	Au	3.5	1.49	1.44	2	1	1.7	2.4	321.108	1064.43
Au	Hg	19.8	1.44	1.52	1	2	2.4	1.9	1064.43	38.836
Au	Al	84	1.44	1.43	1	3	2.4	1.5	1064.43	660.452
Al	Au	0.048	1.43	1.44	3	1	1.5	2.4	660.452	1064.43
Au	Ga	12.4	1.44	1.22	1	3	2.4	1.6	1064.43	29.7741
Au	In	12.7	1.44	1.51	1	3	2.4	1.7	1064.43	156.634
Au	Alfa-Sn	6.8	1.44	1.62	1	4	2.4	1.8	1064.43	13.05
Au	Beta-Sn	6.8	1.44	1.47	1	4	2.4	1.8	1064.43	231.9681
Beta-Sn	Au	0.2	1.62	1.44	4	1	1.8	2.4	231.9681	1064.43
Au	Sb	1.2	1.44	1.45	1	5	2.4	1.9	1064.43	630.755
Au	Alfa-Ca	1.8	1.44	1.97	1	2	2.4	1	1064.43	842
Au	Beta-Ca	1.8	1.44	1.97	1	2	2.4	1	1064.43	842

Beta-Ca	Au	4.5	1.97	1.44	2	1	1	2.4	842	1064.43
Au	Epsilon-Co	23	1.44	1.25	1	2	2.4	1.8	1064.43	1495
Au	Alfa-Co	23	1.44	1.25	1	2	2.4	1.8	1064.43	1495
Alfa-Co	Au	2.5	1.25	1.44	2	1	1.8	2.4	1495	1064.43
Au	Cr	47	1.44	1.25	1	3	2.4	1.6	1064.43	1863
Cr	Au	3	1.25	1.44	3	1	1.6	2.4	1863	1064.43
Au	Alfa-Dy	2.3	1.44	1.75	1	3	2.4	1.1	1064.43	1412
Au	Beta-Dy	2.3	1.44	1.75	1	3	2.4	1.1	1064.43	1412
Au	Er	5.7	1.44	1.73	1	3	2.4	1.2	1064.43	1529
Au	Alfa-Fe	74.1	1.44	1.26	1	2	2.4	1.8	1064.43	1538
Alfa-Fe	Au	3.2	1.24	1.44	2	1	1.8	2.4	1538	1064.43
Au	Gama-Fe	74.1	1.44	1.26	1	2	2.4	1.8	1064.43	1538
Game-Fe	Au	8.1	1.26	1.44	2	1	1.8	2.4	1538	1064.43
Au	Delta-Fe	74.1	1.44	1.24	1	2	2.4	1.8	1064.43	1538
Delta-Fe	Au	2.4	1.24	1.44	2	1	1.8	2.4	1538	1064.43
Au	Alfa-Gd	0.7	1.44	1.79	1	3	2.4	1.1	1064.43	1313
Au	Beta-Gd	0.7	1.44	1.79	1	3	2.4	1.1	1064.43	1313
Au	Ge	3	1.44	1.23	1	4	2.4	1.8	1064.43	938.8
Au	Ho	3.92	1.44	1.74	1	3	2.4	1.2	1064.43	1474
Au	Li	40	1.44	1.52	1	1	2.4	1	1064.43	180.6
Li	Au	0.7	1.52	1.44	1	1	1	2.4	180.6	1064.43
Au	Lu	7.7	1.44	1.72	1	3	2.4	1.2	1064.43	1663
Mg	Au	0.1	1.6	1.44	2	1	1.2	2.4	650	1064.43

Au	Alfa-Mn	31	1.44	1.29	1	2	2.4	1.5	1064.43	1246
Au	Beta-Mn	31	1.44	1.29	1	2	2.4	1.5	1064.43	1246
Au	Gama-Mn	31	1.44	1.29	1	2	2.4	1.5	1064.43	1246
Gama-Mn	Au	25	1.29	1.44	2	1	1.5	2.4	1246	1064.43
Au	Delta-Mn	31	1.44	1.29	1	2	2.4	1.5	1064.43	1246
Au	Mo	1.25	1.44	1.36	1	4	2.4	1.8	1064.43	2623
Mo	Au	0.4	1.36	1.44	4	1	1.8	2.4	2623	1064.43
Alfa-Pr	Au	0.12	1.32	1.44	3	1	1.1	2.4	931	1064.43
Beta-Pr	Au	1.56	1.32	1.44	3	1	1.1	2.4	931	1064.43
Au	Rh	1.6	1.44	1.34	1	2	2.4	2.2	1064.43	1963
Rh	Au	0.5	1.34	1.33	2	1	2.2	2.4	1963	1064.43
Au	Ru	1.9	1.44	1.33	1	3	2.4	2.2	1064.43	2334
Au	Beta-Sm	0.3	1.44	1.79	1	3	2.4	1.2	1064.43	1074
Beta-Sm	Au	0.3	1.79	1.44	3	1	1.2	2.4	1074	1064.43
Au	Gama-Sm	0.3	1.44	1.79	1	3	2.4	1.2	1064.43	1074
Au	Te	0.15	1.44	1.43	1	-2	2.4	2.1	1064.43	449.57
Beta-Th	Au	10	1.8	1.44	3	1	1.3	2.4	1755	1064.43
Au	Alfa-Ti	12	1.44	1.46	1	2	2.4	1.5	1064.43	882
Alfa-Ti	Au	1.7	1.46	1.44	2	1	1.5	2.4	882	1064.43
Au	Beta-Ti	12	1.44	1.46	1	2	2.4	1.5	1064.43	1670
Beta-Ti	Au	15	1.46	1.44	2	1	1.5	2.4	1670	1064.43
Au	Alfa-Tl	1	1.44	1.56	1	3	2.4	1.8	1064.43	304
Au	Beta-Tl	1	1.44	1.56	1	3	2.4	1.8	1064.43	304

Au	Alfa-U	0.6	1.44	1.39	1	3	2.4	1.7	1064.43	1135
Alfa-U	Au	1	1.39	1.44	3	1	1.7	2.4	1135	1064.43
Au	Beta-U	0.6	1.44	1.39	1	3	2.4	1.7	1064.43	1135
Beta-U	Au	1.15	1.39	1.44	3	1	1.7	2.4	1135	1064.43
Au	Gama-U	0.6	1.44	1.39	1	3	2.4	1.7	1064.43	1135
Gama-U	Au	3.2	1.39	1.44	3	1	1.7	2.4	1135	1064.43
V	Au	33	1.31	1.44	3	1	1.6	2.4	1910	1064.43
Au	Alfa-Yb	6.9	1.44	1.94	1	2	2.4	1.1	1064.43	819
Au	Beta-Yb	6.9	1.44	1.94	1	2	2.4	1.1	1064.43	819
Au	Gama-Yb	6.9	1.44	1.94	1	2	2.4	1.1	1064.43	819

Appendix 3

Table A1 List of melting points from five handbooks (acronyms as in text). The elements are sorted in ascending (Max.-Min.)/Min.

Elements	CDH	LNG	ELE	TPC	CRC	(Unit: °C)	(Max-Min)/Min	Median
As (grey)	-	-	**816.85****	-	-		0.00%	816.85
Th	**1750**	1750	1749.85	1750	1750		0.01%	1750
Yb	**824**	824	823.85	824	824		0.02%	824
Sn (white)	**232**	232	231.97	231.93	231.93		0.03%	231.97
Sn (Grey)	**232**	232	231.97	231.93	231.93		0.03%	231.97
Cd	**321**	321	320.95	321.08	321.07		0.04%	321
Al	**660**	660	660.37	660.32	660.32		0.06%	660.32
Po	**254**	254	253.85	254	254		0.06%	254
Sc	**1540**	1540	1540.85	1540	1541		0.06%	1540
La	**920**	920	920.85	920	920		0.09%	920
Ag	**961**	961	961.93	961.78	961.78		0.10%	961.78
Te	**450**	450	449.55	450	449.51		0.11%	450
Na	**97.8**	97.8	97.81	97.7	97.79		0.11%	97.8
Zn	**420**	420	419.58	419.53	419.53		0.11%	419.58
P (White)	**44.2**	44.2	44.15	44.2	44.15		0.11%	44.2
Sb	**630**	630	630.74	630.63	630.63		0.12%	630.63
Ge	**937**	937	937.45	938	938.25		0.13%	937.45
Ga	**29.8**	29.8	29.78	29.76	29.77		0.13%	29.78
Au	**1063**	1063	1064.43	1064.18	1064.18		0.13%	1064.18
Dy	**1410**	1410	1411.85	1410	1412		0.14%	1410
Ni	**1453**	1453	1452.85	1455	1455		0.15%	1453
Tl	**304**	304	303.55	304	304		0.15%	304
Cu	**1083**	1083	1083.45	1084.62	1084.62		0.15%	1083.45
Pb	**327**	327	327.50	327.50	327.46		0.15%	327.46
Bi	**271**	271	271.35	271.44	271.41		0.16%	271.35
Mg	**650**	650	648.85	650	650		0.18%	650
Re	**3180**	3180	3179.85	3186	3185		0.19%	3180
Co	**1492**	1492	1494.85	1495	1495		0.20%	1494.85
Pt	**1769**	1769	1771.85	1768	1768.2		0.22%	1769
Zr	**1850**	1850	1851.85	1850	1854.7		0.25%	1850
Si	**1410**	1410	1409.85	1410	1414		0.29%	1410
Li	**180**	180	180.54	180.5	180.5		0.30%	180.50

Gd	**1310**	1310	1312.85	1314	1313	0.31%	1312.85
Tb	**1360**	1360	1355.85	1360	1359	0.31%	1360
Pd	**1550**	1550	1551.85	1555	1554.8	0.32%	1551.85
Fe	**1535**	1535	1534.85	1540	1538	0.34%	1535
Rh	**1970**	1970	1965.85	1963	1964	0.36%	1965.85
Nb	**2470**	2470	2467.85	2477	2477	0.37%	2470
I (I_2)	**114**	114	113.55	113.6	113.7	0.40%	113.7
U	**1130**	1130	1132.35	1135	1135	0.44%	1132.35
W	**3410**	3410	3406.85	3422	3422	0.44%	3410
Pr	**935**	935	930.85	931	931	0.45%	931
K	**63.7**	63.7	63.65	63.4	63.5	0.47%	63.65
Nd	**1020**	1020	1020.85	1016	1016	0.48%	1020
Mo	**2610**	2610	2616.85	2623	2623	0.50%	2616.85
Eu	**826**	826	821.85	822	822	0.50%	822
In	**157**	157	156.17	156.6	156.6	0.53%	156.6
Ra	**700**	700	699.85	700	696	0.57%	700
Hf	**2220**	2220	2229.85	2230	2233	0.59%	2229.85
Ce	**795**	795	798.85	800	799	0.63%	798.85
Tm	**1540**	1540	1544.85	1550	1545	0.65%	1544.85
Be	**1280**	1280	1277.85	1287	1287	0.72%	1280
Lu	**1650**	1650	1662.85	1660	1663	0.79%	1660
Ta	**3000**	3000	2995.85	3020	3017	0.81%	3000
Mn	**1240**	1240	1243.85	1250	1246	0.81%	1243.85
Ti	**1675**	1675	1659.85	1670	1668	0.91%	1670
Ho	**1460**	1460	1473.85	1470	1472	0.95%	1470
Rb	**38.9**	38.9	39.05	39.3	39.3	1.03%	39.05
Cs	**28.7**	28.7	28.4	28.4	28.5	1.06%	28.5
Sr	**768**	768	768.85	777	777	1.17%	768.85
Ca	**850**	850	838.85	840	842	1.33%	842
Ir	**2440**	2440	2409.85	2447	2446	1.54%	2440
Y	**1500**	1500	1521.85	1525	1522	1.67%	1521.85
V	**1900**	1900	1886.85	1920	1910	1.76%	1900
Os	**3000**	3000	3053.85	3030	3033	1.79%	3030
Se	**217**	217	216.85	220	220.8	1.82%	217
Tc	**2200**	2200	2171.85	2160	2157	1.99%	2171.85
Er	**1500**	1500	1528.85	1530	1529	2.00%	1528.85
Ba	**714**	714	728.85	728	727	2.08%	727

Cr	**1890**	1890	1856.85	1907	1907	2.70%	1890
S (monoclinic)	**119**	119	119.05	115.32	115.21	3.33%	119
Sm	**1070**	1070	1076.85	1170	1072	9.35%	1072
B	**2300**	2300	2299.85	2075	2075	10.84%	2299.85
Ru	**2500**	2500	2309.85	2330	2034	22.91%	2330
Graphite	**3730**[*]	3730[*]	3526.85	4490	4489[**]	27.31%	3730

* Sublimation temperature

** Measure under pressure

Table A2 List of boiling points from five handbooks (acronyms as in text). The elements are sorted in ascending (Max.-Min.)/Min.

Elements	CDH	LNG	ELE	TPC	CRC	(Unit: ºC)	(Max-Min)/Min	Median
Se	**685**	685	684.95	685	685		0.01%	685
S (monoclinic)	**445**	445	444.67	444.67	444.61		0.09%	444.67
Ge	**2830**	2830	2829.85	2830	2833		0.11%	2830
Te	**990**	990	989.85	990	988		0.20%	990
Po	**960**	960	961.85	960	962		0.21%	960
Ca	**1487**	1487	1483.85	1484	1484		0.21%	1484
I (I_2)	**184**	184	184.35	184	184.4		0.22%	184
Sr	**1380**	1380	1383.85	1380	1382		0.28%	1380
Rb	**688**	688	687.85	690	688		0.31%	688
Zn	**907**	907	906.85	910	907		0.35%	907
La	**3470**	3470	3456.85	3460	3464		0.38%	3464
Os	**5000**	5000	5026.85	5000	5012		0.54%	5000
Pb	**1744**	1744	1739.85	1750	1749		0.58%	1744
Re	**5630**	5630	5626.85	5600	5596		0.61%	5626.85
Cd	**765**	765	764.85	770	767		0.67%	765
Ti	**3260**	3260	3286.85	3290	3287		0.92%	3286.85
As (grey)	**613**[*]	613[*]	615.85[*]	610[*]	616[*]		0.98%	613
Tl	**1460**	1460	1456.85	1470	1473		1.11%	1460
Na	**890**	890	882.95	880	882.94		1.14%	882.95
P (White)	**280**	280	279.85	277	280.5		1.26%	280
Li	**1330**	1330	1346.85	1340	1342		1.27%	1340
Cu	**2595**	2595	2566.85	2560	2562		1.37%	2566.85
Er	**2900**	2900	2862.85	2860	2868		1.40%	2868
Nd	**3030**	3030	3067.85	3070	3074		1.45%	3067.85
Ce	**3470**	3470	3425.85	3420	3443		1.46%	3443

Dy	**2600**	2600	2561.85	2560	2567	1.56%	2567
Mg	**1110**	1110	1089.85	1090	1090	1.85%	1090
K	**774**	774	773.85	760	759	1.98%	773.85
Co	**2900**	2900	2869.85	2930	2927	2.10%	2900
Al	**2470**	2470	2466.85	2520	2519	2.15%	2470
Lu	**3330**	3330	3394.85	3390	3402	2.16%	3390
Ag	**2210**	2210	2211.85	2160	2162	2.40%	2210
Ta	**5420**	5420	5424.85	5560	5458	2.58%	5424.85
Cs	**690**	690	678.45	670	671	2.99%	678.45
Bi	**1560**	1560	1609.85	1560	1564	3.20%	1560
Ho	**2600**	2600	2694.85	2700	2700	3.85%	2694.85
Sc	**2730**	2730	2830.85	2830	2836	3.88%	2830
In	**2000**	2000	2079.85	2070	2072	3.99%	2070
Au	**2970**	2970	2806.85	2850	2856	5.81%	2856
Sm	**1900**	1900	1790.85	1790	1794	6.15%	1794
W	**5930**	5930	5656.85	5550	5555	6.85%	5656.85
Mn	**2100**	2100	1961.85	2060	2061	7.04%	2061
Cr	**2482**	2482	2671.85	2670	2671	7.65%	2670
Fe	**3000**	3000	2749.85	2860	2861	9.10%	2861
Gd	**3000**	3000	3265.85	3260	3273	9.10%	3260
Ga	**2400**	2400	2402.85	2200	2204	9.22%	2400
B	**3930**	3930	3657.85	4000	4000	9.35%	3930
Ni	**2730**	2730	2731.85	2990	2931	9.52%	2731.85
U	**3820**	3820	3744.85	4130	4131	10.31%	3820
Eu	**1440**	1440	1596.85	1600	1529	11.11%	1529
Pr	**3130**	3130	3511.85	3510	3520	12.46%	3510
Tm	**1730**	1730	1946.85	1950	1950	12.72%	1946.85
V	**3000**	3000	3376.85	3400	3407	13.57%	3376.85
Y	**2930**	2930	3337.85	3340	3345	14.16%	3337.85
Tb	**2800**	2800	3122.85	3220	3230	15.36%	3122.85
Sn (white)	**2270**	2270	2269.85	2620	2602	15.43%	2270
Sn (Grey)	**2270**	2270	2269.85	2620	2602	15.43%	2270
Ba	**1640**	1640	1636.85	1900	1897	16.08%	1640
Hf	**5400**	5400	5196.85	4600	4603	17.39%	5196.85
Sb	**1380**	1380	1634.85	1587	1587	18.47%	1587
Pt	**4530**	4530	3826.85	3820	3825	18.59%	3826.85
Yb	**1430**	1430	1192.85	1200	1196	19.88%	1200

Be	**2477**	2477	2969.85**	2470	2471	20.24%	2477
Mo	**5560**	5560	4611.85	4640	4639	20.56%	4640
Rh	**4500**	4500	3726.85	3700	3695	21.79%	3726.85
Zr	**3580**	3580	4376.85	4400	4409	23.16%	4376.85
Th	**3850**	3850	4786.85	4790	4788	24.42%	4786.85
Ru	**4900**	4900	3899.85	4150	4150	25.65%	4150
Graphite	**4830**	4830	4826.85*	-	3825*	26.27%	4828.43
Ir	**5300**	5300	4129.85	4430	4428	28.33%	4430
Ra	**1140**	1140	1139.85	1500	-	31.60%	1140
Pd	**3980**	3980	3139.85	2960	2963	34.46%	3139.85
Si	**2360**	2360	2354.85	3260	3265	38.65%	2360
Tc	**3500**	3500	4876.85	4260	4265	39.34%	4260
Nb	**3300**	3300	4741.85	4700	4744	43.76%	4700

* Sublimation temperature

** Measure under pressure

Table A3 List of atomic volume from five handbooks (acronyms as in text). The elements are sorted in ascending (Max.-Min.)/Min.

Elements	**CDH**	**LNG**	**ELE**	**TPC**	**CRC**	**(Unit: cm^{-3} mol^{-1})**	**(Max-Min)/Min**	**Median**
P (White)	**17.02**	17.02	17.02	17.02	-		0.01%	17.02
Ra	**45.2**	45.21	45.2	45.21	45.21		0.01%	45.21
Sn (Grey)	**20.64**	20.65	-	-	-		0.02%	20.64
Lu	**17.78**	17.78	17.78	17.78	17.78		0.02%	17.78
Ag	**10.27**	10.27	10.27	10.27	10.27		0.03%	10.27
Ho	**18.74**	18.74	18.75	18.75	18.74		0.04%	18.74
Al	**9.99**	9.99	10	10	9.99		0.07%	9.99
Nb	**10.84**	10.84	10.84	10.83	10.84		0.09%	10.84
Sc	**15.04**	15.04	15.04	15.03	15.04		0.10%	15.04
Ni	**6.60**	6.59	6.59	6.59	6.59		0.11%	6.59
Tm	**18.11**	18.11	18.12	18.12	18.13		0.11%	18.12
Ga	**11.8**	11.8	11.81	11.81	11.8		0.11%	11.8
Mg	**13.97**	13.97	13.98	13.98	13.97		0.12%	13.97
Nd	**20.61**	20.61	20.59	20.61	20.58		0.14%	20.61
Pr	**20.78**	20.78	20.8	20.79	20.81		0.15%	20.79
Eu	**29**	29	28.98	28.96	29		0.15%	29
Zn	**9.16**	9.16	9.17	9.16	9.16		0.16%	9.16
Rh	**8.3**	8.3	8.29	8.29	8.3		0.16%	8.3

Rb	**55.86**	55.86	55.79	55.75	55.86	0.20%	55.86
Th	**19.83**	19.83	19.8	19.79	19.83	0.21%	19.83
Fe	**7.11**	7.11	7.09	7.09	7.1	0.21%	7.1
Be	**4.87**	4.87	4.88	4.88	4.87	0.22%	4.87
Mo	**9.41**	9.41	9.39	9.39	9.41	0.24%	9.41
Pd	**8.87**	8.87	8.85	8.87	8.87	0.25%	8.87
Au	**10.21**	10.21	10.19	10.22	10.21	0.25%	10.21
Hf	**13.42**	13.42	13.41	13.44	13.42	0.26%	13.42
In	**15.73**	15.73	15.71	15.75	15.71	0.27%	15.73
Sm	**19.95**	19.94	20	19.95	19.99	0.29%	19.95
Dy	**18.98**	18.98	19	19.05	19.01	0.34%	19
Os	**8.45**	8.45	8.43	8.42	8.42	0.38%	8.43
Pb	**18.34**	18.34	18.26	18.27	18.34	0.42%	18.34
Zr	**14.06**	14.06	14.02	14.02	13.99	0.46%	14.02
I (I_2)	**25.74**	25.74	25.74	25.62	-	0.47%	25.74
Pt	**9.12**	9.12	9.10	9.09	9.07	0.47%	9.10
Cu	**7.12**	7.12	7.09	7.11	7.09	0.48%	7.11
Tb	**19.22**	19.22	19.31	19.22	19.31	0.49%	19.22
Na	**23.7**	23.7	23.68	23.8	23.7	0.50%	23.7
Ir	**8.54**	8.54	8.57	8.52	8.54	0.54%	8.54
Bi	**21.32**	21.32	21.44	21.32	21.35	0.57%	21.32
Cd	**13.01**	13.01	13	13	12.94	0.58%	13
Tl	**17.32**	17.32	17.24	17.22	17.32	0.60%	17.32
Cr	**7.23**	7.23	7.23	7.23	7.27	0.62%	7.23
Sn (white)	**16.30**	16.31	16.24	16.3	16.35	0.68%	16.3
Ti	**10.55**	10.55	10.55	10.62	10.61	0.71%	10.55
Graphite	**5.34**	5.34	-	5.3	-	0.71%	5.34
La	**22.44**	22.44	22.6	22.5	22.59	0.71%	22.5
W	**9.48**	9.48	9.53	9.55	9.53	0.75%	9.53
Li	**13.1**	13.1	13	13.02	13	0.75%	13.02
U	**12.46**	12.46	12.56	12.49	12.46	0.78%	12.46
Gd	**19.78**	19.78	19.9	19.98	19.91	1.02%	19.9
Sb	**18.39**	18.39	18.20	18.19	18.23	1.08%	18.23
Co	**6.62**	6.62	6.62	6.7	6.65	1.16%	6.62
Yb	**24.79**	24.79	24.84	24.84	25.08	1.17%	24.84
Er	**18.26**	18.26	18.44	18.49	18.44	1.28%	18.44
Ca	**26.03**	26.03	25.86	26.19	26.02	1.29%	26.03

Ta	**10.9**	10.9	10.87	10.85	11.03	1.65%	10.9
Po	**22.34**	22.23	22.4	22.23	22.72	2.17%	22.34
V	**8.55**	8.55	8.34	8.36	8.49	2.48%	8.49
Re	**9.08**	9.08	8.86	8.86	8.95	2.55%	8.95
Ru	**8.22**	8.22	8.14	8.18	8.35	2.62%	8.22
Cs	**69.95**	69.95	70.96	69.95	68.86	3.05%	69.95
Y	**20.49**	20.49	19.89	19.87	19.89	3.11%	19.89
Ba	**39.13**	39.13	38.21	38.21	37.94	3.14%	38.21
K	**45.47**	45.46	45.36	45.36	43.93	3.50%	45.36
Mn	**7.63**	7.63	7.38	7.35	7.53	3.79%	7.53
Sr	**33.44**	33.44	34.50	33.92	33.19	3.95%	33.44
Tc	**8.61**	8.52	8.6	8.52	8.9	4.51%	8.6
Ge	**13.57**	13.57	13.64	13.64	12.97	5.16%	13.57
Te	**20.42**	20.42	20.45	20.43	22.39	9.65%	20.43
Si	**12.05**	12.05	12.06	12.06	10.93	10.36%	12.05
As (grey)	**13.1**	13.1	12.95	12.97	14.35	10.83%	13.1
S (monoclinic)	**16.36**	16.36	15.49	-	17.63	13.80%	16.36
B	**4.62**	4.62	4.62	4.38	5.20	18.56%	4.62
Se	**16.42**	16.42	16.48	16.42	19.79	20.55%	16.42
Ce	**20.67**	20.67	17	20.88	20.7	22.81%	20.67

Table A4 List of polarizability from five handbooks (acronyms as in text). The elements are sorted in ascending (Max.-Min.)/Min.

Elements	**CDH**	**LNG**	**ELE**	**TPC**	**CRC**	**(Unit: $10^{-24}cm^3$)**
Li	-	-	-	-	**24.3**	
Be	-	-	-	-	**5.6**	
B	-	-	-	-	**3.03**	
Na	-	-	-	-	**24.08**	
Mg	-	-	-	-	**10.6**	
Al	-	-	-	-	**6.8**	
Si	-	-	-	-	**5.38**	
K	-	-	-	-	**43.4**	
Ca	-	-	-	-	**22.8**	
Sc	-	-	-	-	**17.8**	
Ti	-	-	-	-	**14.6**	
V	-	-	-	-	**12.4**	
Cr	-	-	-	-	**11.6**	

Mn	-	-	-	-	**9.4**
Fe	-	-	-	-	**8.4**
Co	-	-	-	-	**7.5**
Ni	-	-	-	-	**6.8**
Cu	-	-	-	-	**6.1**
Zn	-	-	-	-	**5.75**
Ge	-	-	-	-	**6.07**
As (grey)	-	-	-	-	**4.31**
Se	-	-	-	-	**3.77**
Sr	-	-	-	-	**27.6**
Y	-	-	-	-	**22.7**
Zr	-	-	-	-	**17.9**
Nb	-	-	-	-	**15.7**
Mo	-	-	-	-	**12.8**
Ru	-	-	-	-	**9.6**
Rh	-	-	-	-	**8.6**
Pd	-	-	-	-	**4.8**
Ag	-	-	-	-	**7.2**
Cd	-	-	-	-	**7.36**
In	-	-	-	-	**10.2**
Sn (white)	-	-	-	-	**7.7**
Sb	-	-	-	-	**6.6**
Te	-	-	-	-	**5.5**
I (I_2)	-	-	-	-	**5.35**
Ba	-	-	-	-	**39.7**
La	-	-	-	-	**31.1**
Hf	-	-	-	-	**16.2**
Ta	-	-	-	-	**13.1**
W	-	-	-	-	**11.1**
Re	-	-	-	-	**9.7**
Os	-	-	-	-	**8.5**
Ir	-	-	-	-	**7.6**
Pt	-	-	-	-	**6.5**
Au	-	-	-	-	**5.8**
Tl	-	-	-	-	**7.6**
Pb	-	-	-	-	**6.8**
Bi	-	-	-	-	**7.4**

Ra	-	-	-	-	**38.3**
Ce	-	-	-	-	**29.6**
Pr	-	-	-	-	**28.2**
Nd	-	-	-	-	**31.4**
Sm	-	-	-	-	**28.8**
Eu	-	-	-	-	**27.7**
Gd	-	-	-	-	**23.5**
Tb	-	-	-	-	**25.5**
Dy	-	-	-	-	**24.5**
Ho	-	-	-	-	**23.6**
Er	-	-	-	-	**22.7**
Tm	-	-	-	-	**21.8**
Yb	-	-	-	-	**21**
Lu	-	-	-	-	**21.9**
Th	-	-	-	-	**32.1**
U	-	-	-	-	**24.9**
Graphite	-	-	-	-	**1.76**
Cs	-	-	-	-	**59.42**
Ga	-	-	-	-	**8.12**
P (White)	-	-	-	-	**3.63**
Po	-	-	-	-	**6.8**
Rb	-	-	-	-	**47.3**
Tc	-	-	-	-	**11.4**
S (monoclinic)	-	-	-	-	**2.9**
Sn (Grey)	-	-	-	-	**7.7**

Table A5 List of first ionization potential from five handbooks (acronyms as in text). The elements are sorted in ascending (Max.-Min.)/Min.

						(Unit: kJ mol^{-1})		
Elements	**CDH**	**LNG**	**ELE**	**TPC**	**CRC**	**at 298K**	**(Max-Min)/Min**	**Median**
S (monoclinic)	1006	**1000**	1005.6	999.74	999.59		0.64%	1000
Se	947	**941**	946.9	940.88	940.96		0.65%	941
Cd	872	**868**	873.6	867.54	867.77		0.70%	868
B	805	**801**	806.6	800.95	800.64		0.74%	801
Po	818	**812**	818	-	811.83		0.76%	815
Ni	742	**737**	742.7	737.26	737.13		0.77%	737.26
Be	906	**899**	905.4	899.38	899.5		0.78%	899.5

I (I_2)	1016	**1008**	1014.4	1008.43	1008.39	0.79%	1008.43
Te	876	**869**	875.2	869.47	869.29	0.81%	869.47
Mg	742	**738**	743.7	738.23	737.75	0.81%	738.23
Au	897	**890**	896	889.73	890.13	0.82%	890.13
Si	792	**786**	792.5	786.48	786.52	0.83%	786.52
Tc	705	**702**	708	702.52	702.41	0.85%	702.52
Cu	751	**745**	751.4	744.98	745.48	0.86%	745.48
Zn	914	**906**	912.4	906.14	906.4	0.88%	906.4
Sn (white)	713	**709**	714.6	708.31	708.58	0.89%	709
Sn (Grey)	713	**709**	714.6	708.31	708.58	0.89%	709
Bi	709	**703**	709.2	-	702.94	0.89%	706
Pd	809	**805**	811	803.85	804.39	0.89%	805
Mn	722	**717**	723.4	717	717.27	0.89%	717.27
Pb	722	**716**	721.5	716.03	715.6	0.89%	716.03
Graphite	1096	**1086**	1092.2	1086.59	1086.45	0.92%	1086.59
V	654	**650**	656	650.41	650.91	0.92%	650.91
Cr	659	**653**	658.7	653.31	652.87	0.94%	653.31
Er	-	**589**	594.7	-	589.3	0.97%	589.3
Ho	-	**581**	586.7	-	580.99	0.98%	581
Ge	768	**762**	768.1	760.42	762.18	1.01%	762.18
Al	583	**578**	583.4	578.04	577.54	1.01%	578.04
Ag	738	**731**	737	730.51	731	1.03%	731
Ga	583	**579**	584.80	579	578.84	1.03%	579
Co	763	**758**	766	758.49	760.4	1.06%	760.4
Yb	604	**603**	609.4	-	603.44	1.06%	603.72
Ca	596	**590**	595.7	589.62	589.83	1.08%	590
Sb	839	**834**	839.7	833.76	830.58	1.10%	834
Li	525	**520**	519.3	520.14	520.22	1.10%	520.14
Sc	638	**631**	637	631.11	633.09	1.11%	633.09
Tm	-	**596**	602.7	-	596.7	1.12%	596.7
In	562	**558**	564.3	558.74	558.3	1.13%	558.74
Sm	546	**543**	549.3	-	544.53	1.16%	545.27
Sr	554	**549**	555.50	549.09	549.47	1.18%	549.47
Fe	768	**759**	765.3	759.46	762.47	1.19%	762.47
Tl	596	**589**	595.3	589.62	589.35	1.19%	589.62
Ba	508	**503**	508.8	502.77	502.85	1.20%	503
Na	500	**496**	501.8	496.01	495.85	1.20%	496.01

Eu	554	**547**	552.7	-	547.11	1.28%	549.9
Pt	872	**870**	876	868.50	864.39	1.34%	870
Gd	600	**592**	598.5	-	593.37	1.35%	595.93
Ti	667	**658**	664	658.13	658.81	1.37%	658.81
Ra	516	**509**	515.3	509.52	509.29	1.38%	509.52
K	424	**419**	424.8	418.81	418.81	1.43%	419
La	546	**538**	544.1	541.37	538.09	1.49%	541.37
Rb	408	**403**	409	403.37	403.03	1.49%	403.37
Re	768	**760**	766	759.46	755.82	1.61%	760
Cs	382	**376**	381.7	375.39	375.7	1.76%	376
W	776	**770**	776	770.07	758.76	2.27%	770.07
Nb	659	**664**	670	653.31	652.13	2.74%	659
Mo	700	**685**	691	681.29	684.32	2.75%	685
Ru	730	**711**	717	710.24	710.18	2.79%	711
As (grey)	972	**947**	953	946.67	944.46	2.92%	947
Ir	893	**880**	886	-	865.19	3.21%	883
Os	847	**840**	846	839.55	814.17	4.03%	840
Rh	751	**720**	726	719.89	719.67	4.35%	720
Ta	766	**761**	767	760.42	728.42	5.30%	761
P (White)	1066	**1012**	1017.7	1012.29	1011.81	5.36%	1012.29
Zr	675	**660**	666	670.68	640.07	5.46%	666
Y	642	**616**	622	603.13	599.88	7.02%	616
Pr	562	**523**	529.1	-	528.06	7.46%	528.58
Lu	487	**524**	529.5	-	523.52	8.73%	523.76
Nd	613	**530**	535.6	-	533.08	15.66%	534.34
Dy	663	**572**	577.9	-	573.02	15.91%	575.46
Tb	654	**564**	570.6	-	565.77	15.96%	568.19
Th	680	**587**	593	723.75	608.5	23.30%	608.5
Hf	537	**680**	648	-	658.52	26.63%	653.26
Ce	671	**528**	533.4	-	534.4	27.08%	533.9
U	391	**598**	590	597.34	597.64	52.94%	597.34

Table A6 List of electronegativity from five handbooks (acronyms as in text). The elements are sorted in ascending (Max.-Min.)/Min.

Elements	**CDH**	**LNG**	**ELE**	**TPC**	**CRC**	**(Unit: Pauling)**	**(Max-Min)/Min**	**Median**
Ca	**1**	1	1	-	1		0%	1
Cu	**1.9**	1.9	1.9	-	1.9		0%	1.9

Nb	**1.6**	1.6	1.6	-	1.6	0%	1.6
Ru	**2.2**	2.2	2.2	-	2.2	0%	2.2
Pd	**2.2**	2.2	2.2	-	2.2	0%	2.2
Te	**2.10**	2.1	2.1	-	2.1	0%	2.1
La	**1.10**	1.1	1.1	-	1.1	0%	1.1
Hf	**1.30**	1.3	1.3	-	1.3	0%	1.3
Ta	**1.5**	1.5	1.5	-	1.5	0%	1.5
Re	**1.9**	1.9	1.9	-	1.9	0%	1.9
Os	**2.2**	2.2	2.2	-	2.2	0%	2.2
Ir	**2.2**	2.2	2.2	-	2.2	0%	2.2
Eu	**1.1**	-	-	-	-	0%	1.1
Tb	**1.2**	-	-	-	-	0%	1.2
Yb	**1.1**	-	-	-	-	0%	1.1
Th	**1.3**	1.3	1.3	-	1.3	0%	1.3
Po	**2**	2	2	-	2	0%	2
Cd	**1.7**	1.69	1.69	-	1.69	0.59%	1.69
Ba	**0.9**	0.89	0.89	-	0.89	1.12%	0.89
Ra	**0.9**	0.9	0.89	-	0.9	1.12%	0.9
Ag	**1.9**	1.93	1.93	-	1.93	1.58%	1.93
Fe	**1.8**	1.83	1.83	-	1.83	1.67%	1.83
Y	**1.2**	1.22	1.22	-	1.22	1.67%	1.22
Ce	**1.1**	1.12	1.12	-	1.12	1.82%	1.12
V	**1.6**	1.63	1.63	-	1.63	1.87%	1.63
B	**2**	2.04	2.04	-	2.04	2.00%	2.04
Graphite	**2.5**	2.55	2.55	-	2.55	2.00%	2.55
Li	**1**	0.98	0.98	-	0.98	2.04%	0.98
K	**0.8**	0.82	0.82	-	0.82	2.50%	0.82
Rb	**0.8**	0.82	0.82	-	0.82	2.50%	0.82
Ho	**1.2**	1.23	1.23	-	1.23	2.50%	1.23
Sm	**1.2**	1.17	1.17	-	1.17	2.56%	1.17
Ti	**1.5**	1.54	1.54	-	1.54	2.67%	1.54
Pr	**1.1**	1.13	1.13	-	1.13	2.73%	1.13
Zn	**1.6**	1.65	1.65	-	1.65	3.12%	1.65
S (monoclinic)	**2.5**	2.58	2.58	-	2.58	3.20%	2.58
Na	**0.9**	0.93	0.93	-	0.93	3.33%	0.93
Mn	**1.5**	1.55	1.55	-	1.55	3.33%	1.55
Er	**1.2**	1.24	1.24	-	1.24	3.33%	1.24

Rh	**2.2**	2.28	2.28	-	2.28	3.64%	2.28
Pt	**2.2**	2.2	2.28	-	2.2	3.64%	2.2
Cr	**1.6**	1.66	1.66	-	1.66	3.75%	1.66
Tm	**1.2**	1.25	1.25	-	1.25	4.17%	1.25
P (White)	**2.1**	2.19	2.19	-	2.19	4.29%	2.19
Co	**1.8**	1.88	1.88	-	1.88	4.44%	1.88
Sc	**1.3**	1.36	1.36	-	1.36	4.62%	1.36
Be	**1.5**	1.57	1.57	-	1.57	4.67%	1.57
In	**1.7**	1.78	1.78	-	1.78	4.71%	1.78
Sr	**1**	0.95	0.95	-	0.95	5.26%	0.95
Zr	**1.4**	1.33	1.33	-	1.33	5.26%	1.33
Nd	**1.2**	1.14	1.14	-	1.14	5.26%	1.14
Si	**1.8**	1.9	1.9	-	1.9	5.56%	1.9
Au	**2.4**	2.4	2.54	-	2.4	5.83%	2.4
Ni	**1.8**	1.91	1.91	-	1.91	6.11%	1.91
Se	**2.4**	2.55	2.55	-	2.55	6.25%	2.55
Bi	**1.9**	1.9	2.02	-	1.9	6.32%	1.9
I (I_2)	**2.5**	2.66	2.66	-	2.66	6.40%	2.66
Al	**1.5**	1.61	1.61	-	1.61	7.33%	1.61
Sb	**1.9**	2.05	2.05	-	2.05	7.89%	2.05
Sn (white)	**1.8**	1.96	1.96	-	1.96	8.89%	1.96
Sn (Grey)	**1.8**	1.96	1.96	-	1.96	8.89%	1.96
As (grey)	**2**	2.18	2.18	-	2.18	9%	2.18
Gd	**1.1**	1.2	1.2	-	1.2	9.09%	1.2
Mg	**1.2**	1.31	1.31	-	1.31	9.17%	1.31
Tc	**1.9**	2.1	1.9	-	2.1	10.53%	2
Dy	**1.1**	1.22	1.22	-	1.22	10.91%	1.22
Tl	**1.8**	1.8	1.62*	-	1.8	11.11%	1.8
Ge	**1.80**	2.01	2.01	-	2.01	11.67%	2.01
Cs	**0.7**	0.79	0.79	-	0.79	12.86%	0.79
Ga	**1.6**	1.81	1.81	-	1.81	13.13%	1.81
Mo	**1.8**	2.16	2.16	-	2.16	20%	2.16
U	**1.7**	1.7	1.38	-	1.7	23.19%	1.7
Lu	**1.2**	1	1.27	-	1	27%	1.1
Pb	**1.8**	1.8	2.33	-	1.8	29.44%	1.8
W	**1.7**	1.7	2.36	-	1.7	38.82%	1.7

* Tl: 1.62 (valence: I), 2.04 (valence: II)

Table A7 List of density from five handbooks (acronyms as in text). The elements are sorted in ascending (Max.-Min.)/Min.

Elements	CDH	LNG	ELE	TPC	CRC	(Unit: g cm^{-3})	(Max-Min)/Min	Median
Ag	**10.5**	10.5	10.5	10.5	10.5		0.00%	10.5
Ra	**5**	5	5	5	5		0.00%	5
P (White)	**1.82**	1.82	1.82	1.82	-		0.00%	1.82
Sn (Grey)	**5.75**	5.75	5.75	-	-		0.00%	5.75
Lu	**9.84**	9.84	9.84	9.842	9.84		0.02%	9.84
Ho	**8.8**	8.8	8.795	8.797	8.8		0.06%	8.8
Al	**2.7**	2.7	2.698	2.698	2.7		0.07%	2.70
Ni	**8.9**	8.9	8.902	8.907	8.9		0.08%	8.90
Ga	**5.91**	5.91	5.907	5.905	5.91		0.08%	5.91
Nb	**8.57**	8.57	8.57	8.578	8.57		0.09%	8.57
Zn	**7.14**	7.14	7.133	7.135	7.14		0.10%	7.14
Sc	**2.99**	2.99	2.989	2.992	2.99		0.10%	2.99
Tm	**9.33**	9.33	9.321	9.325	9.32		0.11%	9.33
Mg	**1.74**	1.74	1.738	1.738	1.74		0.12%	1.74
Nd	**7**	7	7.01	7	7.01		0.14%	7
Pr	**6.78**	6.78	6.77	6.78	6.77		0.15%	6.78
Eu	**5.24**	5.24	5.24	5.25	5.24		0.15%	5.24
Rh	**12.4**	12.4	12.41	12.42	12.4		0.16%	12.4
Fe	**7.86**	7.86	7.87	7.87	7.87		0.18%	7.87
Rb	**1.53**	1.53	1.53	1.53	1.53		0.20%	1.53
Au	**19.3**	19.3	19.32	19.28	19.3		0.20%	19.3
Pd	**12**	12	12.02	12	12		0.21%	12
Th	**11.7**	11.7	11.72	11.73	11.7		0.21%	11.7
Mo	**10.2**	10.2	10.22	10.22	10.2		0.22%	10.2
Be	**1.85**	1.85	1.8477	1.846	1.85		0.22%	1.85
Hf	**13.3**	13.3	13.31	13.28	13.3		0.26%	13.3
Sm	**7.54**	7.54	7.52	7.54	7.52		0.27%	7.54
Ir	**22.5**	22.5	22.56	22.55	22.5		0.27%	22.5
In	**7.3**	7.3	7.31	7.29	7.31		0.27%	7.3
Dy	**8.56**	8.56	8.55	8.53	8.55		0.34%	8.55
Os	**22.5**	22.5	22.59	22.58	22.59		0.40%	22.58
Pb	**11.3**	11.3	11.35	11.34	11.3		0.44%	11.3
Cu	**8.92**	8.92	8.96	8.93	8.96		0.45%	8.93
Zr	**6.49**	6.49	6.51	6.51	6.52		0.46%	6.51

I (I_2)	**4.93**	4.93	4.93	4.95	-	0.47%	4.93
Pt	**21.4**	21.4	21.45	21.45	21.5	0.47%	21.45
Tb	**8.27**	8.27	8.23	8.27	8.23	0.50%	8.27
Na	**0.97**	0.97	0.971	0.966	0.97	0.52%	0.97
Bi	**9.8**	9.8	9.75	9.8	9.79	0.57%	9.8
Cd	**8.64**	8.64	8.65	8.65	8.69	0.58%	8.65
Tl	**11.8**	11.8	11.85	11.87	11.8	0.60%	11.8
Cr	**7.19**	7.19	7.19	7.19	7.15	0.62%	7.19
Sn (white)	**7.28**	7.28	7.31	7.29	7.26	0.69%	7.28
Ti	**4.54**	4.54	4.54	4.51	4.51	0.71%	4.54
Graphite	**2.25**	2.25	2.26	2.27	-	0.71%	2.26
La	**6.19**	6.19	6.15	6.17	6.15	0.73%	6.17
Li	**0.53**	0.53	0.53	0.53	0.53	0.75%	0.53
W	**19.4**	19.4	19.3	19.25	19.3	0.76%	19.3
U	**19.1**	19.1	18.95	19.05	19.1	0.79%	19.1
Gd	**7.95**	7.95	7.9	7.87	7.9	1.02%	7.9
Ce	**6.78**	6.78	6.77*	6.71	6.77	1.03%	6.77
Sb	**6.62**	6.62	6.69	6.69	6.68	1.09%	6.68
Co	**8.9**	8.9	8.9	8.8	8.86	1.14%	8.9
Yb	**6.98**	6.98	6.97	6.97	6.9	1.16%	6.97
Er	**9.16**	9.16	9.07	9.04	9.07	1.28%	9.07
Ca	**1.54**	1.54	1.55	1.53	1.54	1.31%	1.54
Ta	**16.6**	16.6	16.65	16.67	16.4	1.65%	16.6
Po	**9.4**	9.4	9.32	9.4	9.2	2.17%	9.4
Ru	**12.3**	12.3	12.37	12.36	12.1	2.23%	12.3
V	**5.96**	5.96	6.11	6.09	6	2.52%	6
Re	**20.5**	20.5	21.02	21.02	20.8	2.55%	20.8
Cs	**1.9**	1.9	1.87	1.9	1.93	3.04%	1.9
Y	**4.34**	4.34	4.47	4.48	4.47	3.11%	4.47
Ba	**3.51**	3.51	3.59	3.59	3.62	3.13%	3.59
K	**0.86**	0.86	0.86	0.86	0.89	3.49%	0.86
Mn	**7.2**	7.2	7.44	7.47	7.3	3.79%	7.3
Sr	**2.62**	2.62	2.54	2.58	2.64	3.94%	2.62
Tc	**11.5**	11.5	11.5	11.5	11	4.55%	11.5
Ge	**5.35**	5.35	5.32	5.32	5.6**	5.20%	5.35
S (monoclinic)	**1.96**	1.96	1.96	-	1.82**	7.75%	1.96
Te	**6.25**	6.25	6.24	6.25	5.7**	9.65%	6.25

Si	**2.33**	2.33	2.33	2.33	2.57**	10.35%	2.33
As (grey)	**5.72**	5.72	5.78	5.78	5.22**	10.73%	5.72
B	**2.34**	2.34	2.34	2.47	2.08**	18.56%	2.34
Se	**4.81**	4.81	4.79	4.81	3.99**	20.55%	4.81

* Ce: 8.24 (α), 6.749 (β), 6.773 (γ), 6.7 (δ)

** At melting point

Table A8 List of atomic weight from five handbooks (acronyms as in text). The elements are sorted in ascending (Max.-Min.)/Min.

Elements	CDH	LNG	ELE	TPC	CRC	(Unit: g mol^{-1})	(Max-Min)/Min	Median
Hf	**178.49**	178.49	178.49	178.49	178.49		0.00%	178.49
Cs	**132.91**	132.91	132.91	132.91	132.91		0.00%	132.91
Bi	**208.98**	208.98	208.98	208.98	208.98		0.00%	208.98
Graphite	**12.01**	12.01	-	12.01	12.01		0.00%	12.01
Rb	**85.47**	85.47	85.47	85.47	85.47		0.00%	85.47
Sc	**44.96**	44.96	44.95	44.96	44.96		0.00%	44.96
I (I_2)	**126.9**	126.91	126.9	126.9	126.9		0.01%	126.9
Al	**26.98**	26.98	26.98	26.98	26.98		0.01%	26.98
Te	**127.6**	127.6	127.61	127.6	127.6		0.01%	127.6
U	**238.03**	238.03	238.01	238.03	238.03		0.01%	238.03
Th	**232.04**	232.04	232.06	232.04	232.04		0.01%	232.04
Si	**28.09**	28.09	28.09	28.09	28.09		0.01%	28.09
Nb	**92.91**	92.91	92.90	92.91	92.91		0.01%	92.91
Lu	**174.97**	174.97	174.96	174.97	174.97		0.01%	174.97
P (White)	**30.97**	30.97	30.98	30.97	30.97		0.01%	30.97
B	**10.81**	10.81	10.81	10.81	10.81		0.01%	10.81
K	**39.102**	39.098	39.1	39.098	39.098		0.01%	39.1
Ba	**137.34**	137.33	137.33	137.33	137.33		0.01%	137.33
Zr	**91.22**	91.22	91.21	91.22	91.22		0.01%	91.22
Ra	**226***	226.03	226	226.03*	226.03*		0.01%	226.03
Sr	**87.62**	87.62	87.63	87.62	87.62		0.01%	87.62
Ca	**40.08**	40.08	40.08	40.08	40.08		0.01%	40.08
Li	**6.941**	6.941	6.942	6.941	6.941		0.01%	6.941
Ho	**164.93**	164.93	164.91	164.93	164.93		0.01%	164.93
Tb	**158.93**	158.93	158.9	158.93	158.93		0.01%	158.93
Eu	**151.96**	151.96	151.94	151.97	151.96		0.02%	151.96
Na	**22.9898**	22.9898	22.99	22.9898	22.9898		0.02%	22.99

Sn (Grey)	**118.69***	118.71	-	118.71	118.71	0.02%	118.71
In	**114.82**	114.82	114.84	114.82	114.82	0.02%	114.82
Y	**88.91**	88.91	88.89	88.91	88.91	0.02%	88.91
Re	**186.2**	186.21	186.24	186.21	186.21	0.02%	186.21
Gd	**157.25**	157.25	157.22	157.25	157.25	0.02%	157.25
Sn (white)	**118.69**	118.71	118.71	118.71	118.71	0.02%	118.71
La	**138.91**	138.91	138.88	138.91	138.91	0.02%	138.91
Pr	**140.91**	140.91	140.88	140.91	140.91	0.02%	140.91
Sb	**121.75**	121.75	121.78	121.76	121.76	0.02%	121.76
Tm	**168.93**	168.93	168.9	168.93	168.93	0.02%	168.93
Nd	**144.24**	144.24	144.27	144.24	144.24	0.02%	144.24
Cr	**52**	52	51.98	52	52	0.02%	52
Pb	**207.2**	207.2	207.25	207.2	207.2	0.02%	207.2
Yb	**173.04**	173.04	173.01	173.04	173.05	0.03%	173.04
Co	**58.93**	58.93	58.92	58.93	58.93	0.03%	58.93
Rh	**102.91**	102.91	102.88	102.91	102.91	0.03%	102.91
Se	**78.96**	78.96	78.94	78.96	78.96	0.03%	78.96
Sm	**150.4**	150.36	150.4	150.36	150.36	0.03%	150.36
Mo	**95.94**	95.94	95.97	95.94	95.96	0.03%	95.94
Dy	**162.5**	162.5	162.45	162.5	162.5	0.03%	162.5
Ag	**107.87**	107.87	107.84	107.87	107.87	0.03%	107.87
Cu	**63.55**	63.55	63.53	63.55	63.55	0.03%	63.55
V	**50.94**	50.94	50.96	50.94	50.94	0.03%	50.94
Mg	**24.31**	24.31	24.30	24.31	24.31	0.03%	24.31
Fe	**55.85**	55.85	55.83	55.85	55.85	0.04%	55.85
Pd	**106.4**	106.42	106.38	106.42	106.42	0.04%	106.42
Tl	**204.37**	204.38	204.29	204.38	204.38	0.04%	204.38
Cd	**112.4**	112.41	112.45	112.41	112.41	0.04%	112.41
Ta	**180.95**	180.95	181.03	180.95	180.95	0.04%	180.95
W	**183.85**	183.85	183.93	183.84	183.84	0.05%	183.85
Au	**196.97**	196.97	196.87	196.97	196.97	0.05%	196.97
Er	**167.26**	167.26	167.18	167.26	167.26	0.05%	167.26
Be	**9.01**	9.01	9.02	9.01	9.01	0.05%	9.01
Mn	**54.94**	54.94	54.91	54.94	54.94	0.06%	54.94
Pt	**195.09**	195.08	195.20	195.08	195.08	0.06%	195.08
Ga	**69.72**	69.72	69.76	69.72	69.72	0.06%	69.72
Zn	**65.37**	65.39	65.41	65.39	65.38	0.06%	65.39

Ge	**72.59**	72.59	72.61	72.61	72.64		0.07%	72.61
Ti	**47.90**	47.88	47.90	47.88	47.87		0.07%	47.88
Ni	**58.71**	58.69	58.66	58.69	58.69		0.08%	58.69
As (grey)	**74.92**	74.92	74.85	74.92	74.92		0.09%	74.92
Os	**190.2**	190.2	190.43	190.23	190.23		0.12%	190.23
Ru	**101.07**	101.07	100.69	101.07	101.07		0.38%	101.07
Ir	**192.22**	192.22	193.34	192.22	192.22		0.58%	192.22
Po	**210***	209*	208.77	208.98	208.98*		0.59%	208.98
Tc	**99***	98*	98.90	97.91	97.91*		1.12%	98
S (monoclinic)	**32.06**	32.06	30.31	32.07	32.07		5.78%	32.06
Ce	**140.12**	140.12	115.09	140.12	140.12		21.75%	140.12

* For most stable isotrope

Table A9 List of linear thermal expansion coefficient from five handbooks (acronyms as in text). The elements are sorted in ascending (Max.-Min.)/Min.

Elements	**CDH**	**LNG**	**ELE**	**TPC**	**CRC**	**(Unit: 10^6*K^{-1})**	**(Max-Min)/Min**	**Median**
Cu	-	16.5	16.5	16.5	**16.5**		0.00%	16.5
As (grey)	-	-	**4.7**	-	-		0.00%	4.7
Y	-	10.6	10.6	-	**10.6**		0.00%	10.6
						29.41		
Te	-	-	16.75	-	-	(From Journal)	0.00%	16.75
I (I_2)	-	-	-	**32.10**	-		0.00%	32.1
Hf	-	5.9	5.9	-	**5.9**		0.00%	5.9
Ir	-	6.4	6.4	6.4	**6.4**		0.00%	6.4
Bi	-	13.4	13.4	13.4	**13.4**		0.00%	13.4
Ra	-	-	**20.2**	-	-		0.00%	20.2
Tm	-	13.3	13.3	-	**13.3**		0.00%	13.3
Graphite	-	-	-	**7.1**	-		0.00%	7.1
Cs	-	-	97	-	**97**		0.00%	97
P (White)	-	-	**124.5**	-	-		0.00%	124.5
Rb	-	-	**90**	-	-		0.00%	90
Tc	-	-	**8.06**	-	-		0.00%	8.06
S (monoclinic)	-	-	**74.33**	-	-		0.00%	74.33
Se	-	**37**	36.9	-	-		0.27%	36.95
Au	-	14.2	14.16	14.2	**14.2**		0.28%	14.2
Al	-	23.1	23.03	23.1	**23.1**		0.30%	23.1

K	-	-	83	-	**83.3**	0.36%	83.15
Na	-	71	70.6	-	**71**	0.57%	71
Pb	-	28.9	29.1	28.9	**28.9**	0.69%	28.9
Ni	-	13.4	13.3	13.4	**13.4**	0.75%	13.4
Dy	-	9.9	10	-	**9.9**	1.01%	9.9
V	-	8.4	8.3	8.4	**8.4**	1.20%	8.4
Pr	-	6.7	6.79	-	**6.7**	1.34%	6.7
Ca	-	22.3	22	-	**22.3**	1.36%	22.3
Mn	-	21.7	22	-	**21.7**	1.38%	21.7
Zr	-	5.7	5.78	-	**5.7**	1.40%	5.7
Ag	-	18.9	19.2	18.9	**18.9**	1.59%	18.9
Be	-	11.3	11.5	11.3	**11.3**	1.77%	11.3
Sc	-	10.2	10	-	**10.2**	2.00%	10.2
W	-	4.5	4.59	4.5	**4.5**	2.00%	4.5
Po	-	-	23	-	**23.5**	2.17%	23.25
Sr	-	22.5	23	-	**22.5**	2.22%	22.5
Pt	-	8.8	9	8.8	**8.8**	2.27%	8.8
Rh	-	8.2	8.4	8.2	**8.2**	2.44%	8.2
Co	-	13	13.36	13	**13**	2.77%	13
In	-	32.1	33	-	**32.1**	2.80%	32.1
Ti	-	8.6	8.35	8.6	**8.6**	2.99%	8.6
Nb	-	7.3	7.07	7.3	**7.3**	3.25%	7.3
Cd	-	30.8	29.8	30.8	**30.8**	3.36%	30.8
Sn (white)	-	22	21.2	22	**22**	3.77%	22
Fe	-	11.8	12.3	11.8	**11.8**	4.24%	11.8
Ta	-	6.3	6.6	6.3	**6.3**	4.76%	6.3
Yb	-	26.3	25	-	**26.3**	5.20%	26.3
Pd	-	11.8	11.2	11.8	**11.8**	5.36%	11.8
Ba	-	20.6	19.55	-	**20.6**	5.37%	20.6
B	-	**5**[**]	5	4.7	-	6.38%	5
Tl	-	29.9	28	29.9	**29.9**	6.79%	29.9
Re	-	6.2	6.63	-	**6.2**	6.94%	6.2
Ge	-	**6**	5.57	5.7	-	7.72%	5.7
Gd	-	9.4[†]	8.6	-	**9.4**[†]	9.30%	9.4
Eu	-	35	32	-	**35**	9.38%	35
U	-	13.9	12.6	13.9	**13.9**	10.32%	13.9
Mo	-	4.8	5.43	4.8	**4.8**	13.13%	4.8

Th	-	11.1	12.5	-	**11**	13.64%	11.1
Ho	-	11.2	9.5	-	**11.2**	17.89%	11.2
Os	-	5.1	4.3*	-	**5.1**	18.60%	5.1
Zn	-	30.2	25	30.2	**30.2**	20.80%	30.2
Li	-	46	56	-	**46**	21.74%	46
Lu	-	9.9	8.12	-	**9.9**	21.92%	9.9
Sm	-	12.7	10.4	-	**12.7**	22.12%	12.7
Cr	-	4.9	6.2	4.9	**4.9**	26.53%	4.9
Sb	-	11	8.5	11	**11**	29.41%	11
Er	-	12.2	9.2	-	**12.2**	32.61%	12.2
Ce	-	6.3	8.5	-	**6.3**	34.92%	6.3
Ru	-	6.4	9.1	-	**6.4**	42.19%	6.4
Nd	-	9.6	6.7	-	**9.6**	43.28%	9.6
Tb	-	10.3	7	-	**10.3**	47.14%	10.3
Si	-	-	4.2	**2.6**	-	61.54%	3.4
La	-	12.1	4.9	-	**12.1**	146.94%	12.1
Mg	-	24.8	26.1	8.2	**24.8**	218.29%	24.8
Sn (Grey)	-	22	5.3	22	**22**	315.09%	22
Ga	-	120	11.5*	-	**18**	943.48%	18

* Os: 4.3 (a axis), 6.1 (b axis), 6.8 (c axis); Ga: 11.5 (a axis), 31.5 (b axis), 16.5 (c axis)

** B: range of 5~7

↑ Gd: recorded at 100 ºC

Table A10 List of work function from five handbooks (acronyms as in text). The elements are sorted in ascending (Max.-Min.)/Min.

						Ptable	**(Unit: eV)**		
Elements	**CDH**	**LNG**	**ELE**	**TPC**	**CRC****	**Software**	**Polycr.**	**(Max-Min)/Min**	**Median**
Sc	-	**3.5**	-	-	3.5			0.00%	3.5
Se	-	**5.9**	-	-	5.9			0.00%	5.9
Y	-	**3.1**	-	-	3.1			0.00%	3.1
I (I_2)	-	**-**	-	-	-	**2.8**		0.00%	2.8
W	-	**4.55**	-	4.55	4.55			0.00%	4.55
Ra	-	**-**	-	-	-	**3.2**		0.00%	3.2
Pr	-	**2.7**	-	-	-			0.00%	2.7
Eu	-	**2.5**	-	-	2.5			0.00%	2.5
Tb	-	**3**	-	-	3			0.00%	3
Dy	-	-	-	-	-	**3.09**		0.00%	3.09

Ho	-	-	-	-	-	**3.09**	0.00%	3.09
Er	-	-	-	-	-	**3.12**	0.00%	3.12
Tm	-	-	-	-	-	**3.12**	0.00%	3.12
Yb	-	-	-	-	-	**2.59**	0.00%	2.59
Lu	-	-	-	-	**3.3***		0.00%	3.3
Graphite	-	**5***	-	5	5*		0.00%	5
P (White)	-	-	-	-	-	**3.96**	0.00%	3.96
Po	-	**4.6**	-	-	-		0.00%	4.6
Tc	-	-	-	-	-	**4.6**	0.00%	4.6
S (monoclinic)	-	-	-	-	-	**4.2**	0.00%	4.2
Sb	-	**4.56**	-	4.56	4.55		0.22%	4.56
In	-	**4.08**	-	4.08	4.09		0.25%	4.08
K	-	**2.3**	-	2.3	2.29		0.44%	2.3
Bi	-	**4.36**	-	4.34	4.34		0.46%	4.34
Ta	-	**4.22**	-	4.22	4.25		0.71%	4.22
Au	-	**5.32**	-	5.28	5.31		0.76%	5.31
Zr	-	**4**	-	4	4.05		1.25%	4
Mg	-	**3.66**	-	3.61	3.66		1.39%	3.66
Al	-	**4.19**	-	4.19	4.26		1.67%	4.19
Pb	-	**4.18**	-	4.25	4.25		1.67%	4.25
Ru	-	**4.8**	-	4.73	4.71		1.91%	4.73
U	-	**3.7**	-	3.63	3.63		1.93%	3.63
Si	-	**4.85**	-	4.95	4.85		2.06%	4.85
Cr	-	**4.4**	-	4.44	4.5		2.27%	4.44
Ga	-	**4.25**	-	4.35	4.32		2.35%	4.32
Cs	-	**1.9**	-	1.95	1.95		2.63%	1.95
La	-	**3.4**	-	-	3.5		2.94%	3.45
Ge	-	**5**	-	5.15	5		3.00%	5
Nd	-	**3.1**	-	-	3.2		3.23%	3.15
V	-	**4.44**	-	-	4.3		3.26%	4.37
Sn (white)	-	**4.35**	-	4.28	4.42		3.27%	4.35
Sn (Grey)	-	**4.35**	-	4.28	4.42		3.27%	4.35
Cd	-	**4.12**	-	4.22	4.08		3.43%	4.12
Ce	-	**2.8**	-	-	2.9		3.57%	2.85
Nb	-	**4.2**	-	4.3	4.36		3.81%	4.3

Ni	-	**5.15**	-	5.15	5.35	3.88%	5.15
Fe	-	**4.65**	-	4.6	4.81	4.57%	4.65
Tl	-	**4.02**	-	-	3.84*	4.69%	3.93
Re	-	**4.95**	-	4.72	4.72	4.87%	4.72
Mn	-	**3.9**	-	4.08	4.1	5.13%	4.08
Pt	-	**5.4**	-	5.36	5.64	5.22%	5.4
Te	-	**4.7**	-	-	4.95	5.32%	4.83
Rh	-	**4.98**	-	4.72	4.98	5.51%	4.98
Ti	-	**4.1**	-	4.1	4.33	5.61%	4.1
Mo	-	**4.3**	-	4.33	4.55	5.81%	4.33
Ca	-	**2.71**	-	2.87	2.87	5.90%	2.87
Cu	-	**4.7**	-	4.65	4.94	6.24%	4.7
Co	-	**4.7**	-	4.97	5	6.38%	4.97
Sr	-	**2.76**	-	-	2.59*	6.56%	2.68
B	-	**4.75***	-	-	4.45*	6.74%	4.6
Hf	-	**3.65**	-	3.65	3.9	6.85%	3.65
Gd	-	**3.1**	-	-	2.9	6.90%	3
Ba	-	**2.35**	-	2.35	2.52	7.23%	2.35
Pd	-	**5**	-	5.4	5.22	8%	5.22
Th	-	**3.71**	-	3.71	3.4	9.12%	3.71
Sm	-	**2.95**	-	-	2.7	9.26%	2.83
Rb	-	**2.2**	-	2.05	2.26	10.29%	2.2
Ag	-	**4.64**	-	4.29	4.74	10.49%	4.64
Na	-	**2.7**	-	2.46	2.36	14.41%	2.46
Zn	-	**4.3**	-	4.11	3.63	18.46%	4.11
Os	-	**4.83**	-	-	5.93	22.77%	5.38
Ir	-	**5.6**	-	4.57	5.76	26.04%	5.6
As (grey)	-	**3.75***	-	4.79	3.75*	27.73%	3.75
Be	-	**5.08**	-	3.91	4.98	29.92%	4.98
Li	-	**3.1**	-	2.32	2.93	33.62%	2.93

* Approximation value

** For single crystals, values are recorded for (111) plane

Table A11 List of electrical resistivity from five handbooks (acronyms as in text). The elements are sorted in ascending (Max.-Min.)/Min.

						(Unit: *10^8 ohm m)		
Elements	**CDH**	**LNG**	**ELE**	**TPC**	**CRC**	**at 293K**	**(Max-Min)/Min**	**Median**
Ra	-	**100**	100	-	-		0.00%	100
Sn (white)	**11.36**	11.5	-	11.5*	11.5*		1.20%	11.5
Cr	**12.82**	12.5	12.7	12.7*	12.5		2.56%	12.7
Sm	**90.91**	94	94	91.40*	94		3.40%	94
Tb	**111.11**	115	114	113*	115		3.50%	114
Sn (Grey)	**11.36**	11.5*	11	11.5*	11.5*		4.55%	11.5
Rh	**4.55**	4.33*	4.51	4.3*	4.3*		5.71%	4.33
Cd	**6.85**	7.27	6.83	6.8*	6.8*		6.91%	6.83
Er	**83.33**	86	87	81*	86		7.41%	86
Ti	**41.67**	42	42	39*	39*		7.69%	41.67
Pr	**66.67**	70	68	65*	70		7.69%	68
Y	**55.56**	59.6	57	55*	59.6		8.36%	57
Sb	**38.46**	41.7	39	39*	39*		8.42%	39
Pt	**10.64**	10.6	10.6	9.81*	10.5		8.44%	10.6
Zr	**41.67**	42.1	42.1	38.8*	42.1		8.51%	42.1
Li	**9.26**	9.28	8.55	8.53*	9.28		8.79%	9.26
Cs	**18.87**	20.5	20	18.8*	20.5		9.04%	20
Zn	**5.99**	5.9	5.92	5.48*	5.9		9.27%	5.9
Cu	**1.69**	1.68	1.67	1.54*	1.68		9.50%	1.68
Al	**2.62**	2.65	2.65	2.42*	2.65		9.70%	2.65
Ag	**1.61**	1.59	1.59	1.47*	1.59		9.72%	1.59
U	**30.3**	28*	30.8	28*	28*		10.00%	28
Mo	**5.26**	5.34	5.2	4.85*	5.34		10.10%	5.26
Pd	**10.75**	10.54	10.8	9.8*	10.54		10.20%	10.54
Mg	**4.46**	4.39	4.38	4.05*	4.39		10.23%	4.39
Ta	**12.35**	13.5	12.45	12.2*	13.1		10.66%	12.45
Rb	**12.5**	12.8	12.5	11.5*	12.8		11.30%	12.5
Co	**6.25**	6.24	6.24	5.6*	5.6*		11.61%	6.24
Ho	**90.91**	81.4	87	90*	81.4		11.68%	87
Os	**9.09**	8.12*	8.12	8.1*	8.1*		12.23%	8.12
Ni	**6.9**	6.93	6.84	6.16*	6.93		12.50%	6.9
In	**9.01**	8.37	8.37	8*	8*		12.61%	8.37
Ir	**5.26**	4.71	5.30	4.70*	4.70*		12.77%	4.71

Pb	**21.74**	20.8	20.65	19.2*	20.8	13.22%	20.8
Gd	**142.86**	131	134	126*	131	13.38%	131
Ce	**76.92**	82.8↓	73	73*	74.4↓	13.42%	74.4
Na	**4.59**	4.77	4.2	4.33*	4.77	13.57%	4.59
La	**58.82**	61.5	57	54*	61.5	13.89%	58.82
Re	**19.61**	19.3	19.3	17.2*	17.2*	14.00%	19.3
Au	**2.38**	2.21	2.35	2.05*	2.21	16.14%	2.21
Fe	**10**	9.61	9.71	8.57*	9.61	16.69%	9.61
K	**6.99**	7.2	6.15	6.49*	7.2	17.07%	6.99
W	**5.56**	5.28	5.65	4.82*	5.28	17.22%	5.28
Hf	**35.71**	33.1	35.1	30.4*	33.1	17.48%	33.1
Yb	**29.41**	25	29	27.7*	25	17.65%	27.7
Bi	**111.11**	129	106.8	107*	107*	20.79%	107
Tl	**18.18**	18	18	15*	15*	21.21%	18
Nb	**12.5**	15.2*	12.5	15.2*	15.2*	21.6%	15.2
Po	**50**	40*	-	40*	40*	25.00%	40
Nd	**76.92**	64.3	64	61*	64.3	26.10%	64.3
Sc	**66.67**	56.2	61	50.5*	56.2	32.01%	56.2
Be	**4**	3.56	4	3.02*	3.56	32.45%	3.56
As (grey)	**34.48**	33.3	26	26*	-	32.63%	29.65
Tm	**90.91**	67.6	79	67*	67.6	35.69%	67.6
I (I_2)	**1E+15**	1.30E+15*	1.37E+15	-	-	37.00%	1.30E+15
V	**25**	19.7	24.8	18.1*	19.7	38.12%	19.7
Th	**18.18**	15.4	13	14.7*	14.7*	39.86%	14.7
Ru	**10**	7.1*	7.6	7.1*	7.1*	40.85%	7.1
Lu	**76.92**	58.2	79	54*	58.2	46.30%	58.2
Ca	**4.59**	3.36	3.43	3.11*	3.36	47.50%	3.36
Dy	**90.91**	92.6	57	89*	92.6	62.46%	90.91
B	**1E+12**	1.50E+12	1.80E+12	-	-	80.00%	1.50E+12
Sr	**23.26**	13.2	23	12.3*	13.2	89.07%	13.2
Ga	**17.24**	25.8**	27↑	13.6*	13.6*	98.53%	17.24
S (monoclinic)	**1E+23**	2E+23	2E+23	-	-	100.00%	2E+23
Ba	**62.5**	33.2	50	30.2*	33.2	106.95%	33.2
Graphite	**1428.57**	1375	1375	300↕	-	376.19%	1375
Mn	**18.52**	144	185	143*	144	899.00%	144

Eu	**90.91**	90	990	89*	90	1.01E+01	90
Te	**1E+06**	3.30E+4$	4.36E+5	3E+5$	-	2.93E+01	3.68E+05
Ge	**4.6E+7**	5.30E+4	4.60E+7	1E+5↕	-	8.67E+02	2.28E+07
Tc	**1E+05**	22.6§	22.6	-	-	4.42E+03	22.6
Si	**10**	1E+05	1E+05	1E+7↕	-	1E+06	1E+05
Se	**12.5**	1.2*	1E+06	0.1	-	1E+07	6.85
P (White)	**1E+17**	10	1E+17	-	-	1E+16	1E+17

* At 0 ºC

** Ga: at 30 ºC

↑ Ga: varies with axis

↕ C: 300-6000; Ge: 100000-50000000; Si: 10000000-6000000000

$ Te: 5800-33000

§ At 100 ºC

¦ Ce: 82.8 (β, hex), 74.4 (γ, Cub.)

Table A12 List of thermal conductivity from five handbooks (acronyms as in text). The elements are sorted in ascending (Max.-Min.)/Min.

						(Unit: $Wm^{-1}K^{-1}$)		
Elements	**CDH**	**LNG**	**ELE**	**TPC**	**CRC**	**at 300K**	**(Max-Min)/Min**	**Median**
Ru	-	**117**	117	117↕	117		0.00%	117
Ba	-	**18.4**	18.4	-	18.4		0.00%	18.4
Hf	-	**23**	23	23↕	23		0.00%	23
Ir	-	**147**	147	147↕	147		0.00%	147
Ra	-	**18.6**	18.6	-	-		0.00%	18.6
Nd	-	**16.5**	16.5	-	16.5		0.00%	16.5
Eu	-	**13.9**	13.9	-	13.9$		0.00%	13.9
Th	-	**54**	54	54↕	54		0.00%	54
Ag	-	**429**	429	428↕	429		0.23%	429
Pd	-	**71.8**	71.8	72↕	71.8		0.28%	71.8
Cs	-	**35.9**	35.9	36↕	35.9		0.28%	35.9
Sr	-	**35.4**	35.3	-	35.3		0.28%	35.3
Rb	-	**58.2**	58.2	58↕	58.2		0.34%	58.2
As (grey)	-	**50.2**	50	-	-		0.40%	50.1
Cd	-	**96.6**	96.8	97↕	96.8		0.41%	96.8
Al	-	**237**	237	236↕	237		0.42%	237
Ti	-	**21.9**	21.9	22↕	21.9		0.46%	21.9
Os	-	**87.6**	87.6	88↕	87.6		0.46%	87.6
Cu	-	**401**	401	403↕	401		0.50%	401

Ca	-	**201**	200	-	200	0.50%	200
Pt	-	**71.6**	71.6	72‡	71.6	0.56%	71.6
Au	-	**318**	317	319‡	317	0.63%	317.5
Mg	-	**156**	156	157‡	156	0.64%	156
Rh	-	**150**	150	151‡	150	0.67%	150
Na	-	**142**	141	142‡	141	0.71%	141.5
Mo	-	**138**	138	139‡	138	0.72%	138
Tc	-	**50.6**	50.6	51‡	50.6	0.79%	50.6
Zn	-	**116**	116	117‡	116	0.86%	116
Ta	-	**57.5**	57.5	57‡	57.5	0.88%	57.5
V	-	**30.7**	30.7	31‡	30.7	0.98%	30.7
Ga	-	**40.6**	40.6	41‡	40.6	0.99%	40.6
Y	-	**17.2**	17.2	17‡	17.2	1.18%	17.2
Tm	-	**16.9**	16.8	17‡	16.9	1.19%	16.9
Ho	-	**16.2**	16.2	16‡	16.2	1.25%	16.2
Sc	-	**15.8**	15.8	16‡	15.8	1.27%	15.8
Nb	-	**53.7**	53.7	53‡	53.7	1.32%	53.7
Li	-	**84.8**	84.7	86‡	84.7	1.53%	84.75
K	-	**102.5**	102.4	104‡	102.4	1.56%	102.45
Zr	-	**22.6**	22.7	23‡	22.7	1.77%	22.7
Dy	-	**10.7**	10.7	10.5‡	10.7	1.90%	10.7
Tl	-	**46.1**	46.1	47‡	46.1	1.95%	46.1
Pb	-	**35.3**	35.3	36‡	35.3	1.98%	35.3
Sn (white)	-	**66.8**	-	68‡	66.6	2.10%	66.8
Sn (Grey)	-	**66.8**	66.6	68‡	66.6	2.10%	66.7
U	-	**27.5**	27.6	27‡	27.6	2.22%	27.55
Re	-	**48**	47.9	49‡	47.9	2.30%	47.95
Sm	-	**13.3**	13.3	13‡	13.3	2.31%	13.3
W	-	**173**	174	177‡	174	2.31%	174
Mn	-	**7.81**	7.82	8‡	7.82	2.43%	7.82
S (monoclinic)	-	**0.21**	-	0.2‡	-	2.50%	0.2
In	-	**81.8**	81.6	84‡	81.6	2.94%	81.7
Cr	-	**93.9**	93.7	96.5‡	93.7	2.99%	93.8
Ce	-	**11.3**	11.4	11‡	11.3	3.64%	11.3
Ni	-	**90.9**	90.7	94‡	90.7	3.64%	90.8
Lu	-	**16.4**	16.4	17‡	16.4	3.66%	16.4
La	-	**13.4**	13.5	13‡	13.4	3.85%	13.4

Fe	-	**80.4**	80.2	83.5[‡]	80.2		4.11%	80.3
Pr	-	**12.5**	12.5	12[‡]	12.5		4.17%	12.5
Bi	-	**7.97**	7.87	8.20[‡]	7.87		4.19%	7.92
Er	-	**14.5**	14.3	15[‡]	14.5		4.90%	14.5
Sb	-	**24.4**	24.3	25.5[‡]	24.3		4.94%	24.35
Co	-	**100**	100	105[‡]	100		5%	100
Tb	-	**11.1**	11.1	10.5[‡]	11.1		5.71%	11.1
Gd	-	**10.5**	10.6	10[‡]	10.5		6%	10.5
P (White)	-	**0.24**	0.24	0.25[‡]	-		6.38%	0.24
Be	-	**200**	200	218[‡]	200		9%	200
Yb	-	**38.5**	34.9	-	38.5		10.32%	38.5
Ge	-	**60.2**	59.9	67[‡]	-		11.85%	60.2
Si	-	**149**	148	168[‡]	-		13.51%	149
B	-	**27.4**	27	32[‡]	-		18.52%	27.4
Te	-	**2.68**[↑]	2.35	2.85[‡]	-		21.28%	2.68
Se	-	**0.52**	2.04	0.43[‡]	-		374.42%	0.52
Graphite	-	**119**[**]	5.7[*]	80[‡]	-		1987.72%	80
Po	-	**0.2**	20	-	20		9900%	20
I (I_2)	-	**449**	0.45	0.5[‡]	-		99900%	0.5

* Graphite: 5.7 (perpendicular), 1960 (parallel)

** Graphite: 119-165

↑ Te: 1.97-3.38

‡ At 273.2 K, and Graphite: 80-230

$ Eu: estimated value

Table A13 List of specific heat capacity from five handbooks (acronyms as in text). The elements are sorted in ascending (Max.-Min.)/Min.

Elements	**CDH**	**LNG**	**ELE**	**TPC**	**CRC**	**(Unit: J Kg^{-1} K^{-1})**	**(Max-Min)/Min**	**Median**
S (monoclinic)	**732**	732	-	-	-		0.00%	732
Si	**711**	711	712.05	-	712		0.15%	711.5
Os	**130**	130	129.7	130[*]	130		0.23%	130
Graphite	**711**	711	-	-	709		0.28%	711
Se	**322**	322	321.3	-	321		0.31%	321.65
Nb	**264**	264	264.8	265[*]	265		0.38%	264.8
B	**1030**	1030	1025.83	-	1026		0.41%	1028
Ag	**234**	234	235.09	235[*]	235		0.47%	235
Te	**201**	201	201.63	-	202		0.50%	201.32

Ge	**322**	322	321.56	-	320	0.63%	321.78
Tm	**159**	159	160.04	159*	160	0.65%	159
Dy	**172**	172	173.35	-	173	0.78%	172.5
Po	**126**	126	125.02	-	-	0.78%	126
Zn	**385**	385	388.32	385*	388	0.86%	385
Re	**138**	138	136.81	138*	137	0.87%	138
Ra	**121**	121	119.91	-	-	0.91%	121
Bi	**121**	121	122.12	122*	122	0.93%	122
As (grey)	**326**	326	329.19	-	329	0.98%	327.5
Nd	**188**	188	190.26	-	190	1.20%	189
Ho	**163**	163	164.64	164*	165	1.23%	164
Cd	**230**	230	231.04	229*	232	1.31%	230
Er	**167**	167	168.20	166*	168	1.33%	167
Sn (Grey)	**218**	218	-	221*	-	1.38%	218
Sb	**209**	209	207.18	206*	207	1.46%	207.18
Ta	**138**	138	140.09	139*	140	1.51%	139
Pt	**134**	134	132.48	132*	133	1.52%	133
Y	**297**	297	298.46	294*	298	1.52%	297
W	**134**	134	131.95	133*	132	1.55%	133
Au	**130**	130	129.11	128*	129	1.56%	129.11
Cu	**385**	385	384.64	379*	385	1.58%	385
V	**481**	481	488.45	489*	489	1.66%	488.45
P (White)	**757**	757	769.62	-	769	1.67%	763
Ru	**238**	238	238.95	235*	238	1.68%	238
Tl	**130**	130	128.83	131*	129	1.68%	130
Fe	**448**	448	449.61	442*	449	1.72%	448
Zr	**276**	276	278.03	273*	278	1.84%	276
Mo	**251**	251	250.71	246*	251	2.03%	251
Pr	**192**	192	193.07	196*	193	2.08%	193
Hf	**146**	146	144.16	143*	144	2.10%	144.16
Rh	**243**	243	242.81	238*	243	2.10%	243
Sc	**556**	556	567.68	557*	568	2.16%	557
Tb	**184**	184	181.94	186*	182	2.23%	184
Ti	**523**	523	522.37	511*	523	2.35%	523
Pb	**130**	130	127.57	127*	130	2.36%	130
Na	**1230**	1230	1228.18	1200*	1228	2.50%	1228.18
Pd	**243**	243	244.23	240*	246	2.50%	243

Cr	**448**	448	449.18	438*	449	2.55%	448
Al	**900**	900	902.52	880*	897	2.56%	900
Sm	**197**	197	196.41	192*	197	2.60%	197
U	**117**	117	116.23	114*	116	2.63%	116.23
Mn	**477**	477	479.35	467*	479	2.65%	477
Ga	**381**	381	370.69	-	373	2.78%	377
Mg	**1030**	1030	1024.4	1000*	1023	3.00%	1024.4
In	**238**	238	232.85	231*	233	3.03%	233
La	**201**	201	195.21	-	195	3.08%	198.1
Ir	**134**	134	129.82	-	131	3.22%	132.5
Ca	**653**	653	631.44	-	647	3.41%	650
K	**753**	753	756.52	732*	757	3.42%	753
Cs	**234**	234	242.05	-	242	3.44%	238
Ni	**439**	439	444.39	429*	444	3.59%	439
Tc	**243**	243	252.78	-	-	4.02%	243
Be	**1820**	1820	1823.27	1750*	1825	4.29%	1820
Th	**113**	113	117.73	117*	118	4.42%	117
Sn (white)	**218**	218	217.08	221*	227	4.57%	218
Rb	**360**	360	363.42	346*	363	5.04%	360
Co	**435**	435	421.09	414*	421	5.07%	421.09
Li	**3390**	3390	3568.14	3480*	3582	5.66%	3480
Yb	**146**	146	154.56	-	155	6.16%	150.28
Ba	**192**	192	204.4	-	204	6.46%	198
Sr	**284**	284	301.27	-	306	7.75%	292.63
Ce	**184**	184	234.08	190*	192	27.22%	190
Gd	**234**	234	235.53	300*	236	28.21%	235.53
Eu	**138**	138	182.04	-	182	31.92%	160
I (I_2)	**218**	218	428.99	-	214	100.46%	218
Lu	**155**	155	153.53	640*	154	316.87%	155

* At 273 K

Table A14 List of molar heat capacity from five handbooks (acronyms as in text). The elements are sorted in ascending (Max.-Min.)/Min.

Elements	CDH	LNG	ELE	TPC	CRC	(Unit: J K^{-1} Mol^{-1})	(Max-Min)/Min	Median
S (monoclinic)	**23.47**	23.47	-	-	-		0.00%	23.47
Os	**24.73**	24.73	24.7	24.73*	24.7		0.12%	24.73
Si	**19.97**	19.97	20	-	19.99		0.16%	19.98
Se	**25.43**	25.43	25.36	-	25.36		0.24%	25.39
Graphite	**8.54**	8.54	8.53	-	8.52		0.27%	8.53
Te	**25.65**	25.65	25.73	-	25.73		0.32%	25.69
Nb	**24.53**	24.53	24.6	24.62*	24.6		0.38%	24.6
B	**11.13**	11.13	11.09	-	11.09		0.43%	11.11
Ag	**25.24**	25.24	25.35	25.35*	25.35		0.44%	25.35
Tm	**26.86**	26.86	27.03	26.86*	27.03		0.63%	26.86
Ge	**23.37**	23.37	23.35	-	23.22		0.65%	23.36
Dy	**27.95**	27.95	28.16	-	28.16		0.75%	28.06
Re	**25.7**	25.7	25.48	25.7*	25.48		0.85%	25.7
As (grey)	**24.42**	24.42	24.64	-	24.64		0.88%	24.53
Ra	**27.35**	27.35	27.1	-	-		0.92%	27.35
Bi	**25.29**	25.29	25.52	25.5*	25.52		0.92%	25.5
Zn	**25.17**	25.18	25.4	25.18*	25.39		0.92%	25.18
Ho	**26.88**	26.88	27.15	27.05*	27.15		0.99%	27.05
Cd	**25.85**	25.85	25.98	25.74*	26.02		1.08%	25.85
Nd	**27.12**	27.12	27.45	-	27.45		1.23%	27.28
Er	**27.93**	27.93	28.12	27.77*	28.12		1.28%	27.93
Ru	**24.05**	24.05	24.06	23.75*	24.06		1.30%	24.05
Po	**26.46**	26.33	26.1	-	-		1.38%	26.33
Sb	**25.45**	25.45	25.23	25.08*	25.23		1.45%	25.23
Y	**26.41**	26.41	26.53	26.14*	26.53		1.50%	26.41
W	**24.64**	24.64	24.27	24.45*	24.27		1.51%	24.45
Pt	**26.14**	26.14	25.86	25.75*	25.86		1.52%	25.86
Ta	**24.97**	24.97	25.36	25.15*	25.36		1.56%	25.15
Au	**25.61**	25.61	25.42	25.21*	25.42		1.56%	25.42
Cu	**24.47**	24.47	24.44	24.08*	24.44		1.58%	24.44
V	**24.50**	24.50	24.89	24.91*	24.89		1.66%	24.89
P (White)	**23.45**	23.45	23.84	-	23.82		1.68%	23.64
Fe	**25.02**	25.02	25.1	24.68*	25.1		1.68%	25.02
Pd	**25.86**	25.86	25.98	25.54*	25.98		1.72%	25.86

Tl	**26.57**	26.57	26.32	26.77*	26.32	1.73%	26.57
Sn (Grey)	**25.87**	25.88	25.77	26.23*	-	1.80%	25.88
Zr	**25.18**	25.18	25.36	24.90*	25.36	1.83%	25.18
Mo	**24.08**	24.08	24.06	23.60*	24.06	2.03%	24.06
Pr	**27.05**	27.05	27.2	27.62*	27.2	2.08%	27.2
Hf	**26.06**	26.06	25.73	25.52*	25.73	2.10%	25.73
Sc	**25**	25	25.52	25.04*	25.52	2.10%	25.04
Rh	**25.01**	25.01	24.98	24.49*	24.98	2.10%	24.98
Tb	**29.24**	29.24	28.91	29.56*	28.91	2.25%	29.24
Pb	**26.94**	26.94	26.44	26.31*	26.84	2.36%	26.84
Ti	**25.05**	25.04	25.02	24.47*	25.06	2.43%	25.04
Na	**28.28**	28.28	28.24	27.59*	28.23	2.50%	28.24
Cr	**23.29**	23.29	23.35	22.77*	23.35	2.53%	23.29
Al	**24.28**	24.28	24.35	23.74*	24.20	2.55%	24.28
Mn	**26.21**	26.21	26.32	25.66*	26.32	2.59%	26.21
Ir	**25.76**	25.76	25.1	-	25.1	2.62%	25.43
Sm	**29.63**	29.62	29.54	28.87*	29.54	2.63%	29.54
U	**27.85**	27.85	27.67	27.14*	27.67	2.63%	27.67
Ga	**26.56**	26.56	25.86	-	26.03	2.72%	26.30
La	**27.92**	27.92	27.11	-	27.11	2.99%	27.52
Mg	**25.03**	25.03	24.89	24.31*	24.87	3%	24.89
In	**27.33**	27.33	26.74	26.52*	26.74	3.03%	26.74
Ca	**26.17**	26.17	25.31	-	25.93	3.41%	26.05
K	**29.44**	29.44	29.58	28.62*	29.6	3.42%	29.44
Ni	**25.77**	25.76	26.07	25.18*	26.07	3.54%	25.77
Cs	**31.1**	31.1	32.17	-	32.21	3.57%	31.63
Th	**26.22**	26.22	27.32	27.15*	27.32	4.19%	27.15
Be	**16.4**	16.4	16.44	15.77*	16.44	4.26%	16.4
Ce	**25.78**	25.78	26.94	26.62*	26.94	4.49%	26.62
Sn (white)	**25.87**	25.88	25.77	26.23*	26.99	4.73%	25.88
Tc	**24.06**	23.81	25	-	-	4.98%	24.06
Rb	**30.77**	30.77	31.06	29.57*	31.06	5.04%	30.77
Co	**25.64**	25.64	24.81	24.4*	24.81	5.07%	24.81
Li	**23.53**	23.53	24.77	24.15*	24.86	5.65%	24.15
Yb	**25.26**	25.26	26.74	-	26.74	5.84%	26
Ba	**26.37**	26.37	28.07	-	28.07	6.46%	27.22
Sr	**24.88**	24.88	26.4	-	26.79	7.66%	25.64

Gd	**36.80**	36.80	37.03	47.18*	37.03		28.21%	37.03
Eu	**20.97**	20.97	27.66	-	27.66		31.90%	24.32
I (I_2)	**27.67**	27.67	54.44	-	54.43		96.77%	41.05
Lu	**27.12**	27.12	26.86	111.98*	26.86		316.90%	27.12

* At 273 K

Table A15 List of heat of vaporization from five handbooks (acronyms as in text). The elements are sorted in ascending (Max.-Min.)/Min.

Elements	**CDH**	**LNG**	**ELE**	**TPC**	**CRC**	**(Unit: kJ mol^{-1})**	**(Max-Min)/Min**	**Median**
Tm	-	**247**	247	-	-		0.00%	247
Yb	-	**159**	159	-	-		0.00%	159
Cd	**100**	99.9	99.87	99.87	99.9		0.13%	99.9
Eu	-	**176**	175.7	175.73	-		0.17%	175.73
Pr	-	**331**	332.6	332.63	-		0.49%	332.6
Graphite	**715***	-	710.9	-	-		0.58%	712.95
La	**400**	402.1	399.6	399.57	-		0.63%	399.8
Ga	**256**	254	256.1	256.06	254		0.83%	256
Ti	**427**	425	428.9	425.2	-		0.92%	426.1
Nb	**694**	689.9	696.6	690.1	-		0.97%	692.05
Ge	**330**	334	334.3	334.3	334		1.30%	334
U	-	**417.1**	422.6	422.58	-		1.32%	422.58
Cu	**305**	300.4	304.6	300.49	-		1.53%	302.54
As (grey)	**32.4***	-	31.9	-	-		1.57%	32.15
Pb	**177**	179.5	179.4	177.93	180		1.69%	179.4
Tl	**162**	165	162.1	162.09	-		1.85%	162.1
Nd	-	**289**	283.7	283.68	-		1.87%	283.7
Ni	**379**	377.5	371.8	377.48	-		1.94%	377.49
Sn (white)	**290**	296.1	290.4	290.37	-		2.10%	290.38
Sn (Grey)	**290**	296.1	290.4	290.37	-		2.10%	290.38
Mn	**225**	221	219.7	219.74	-		2.41%	220.37
Cr	**347**	339.5	348.78	339.48	-		2.74%	343.25
Ta	**753**	732.8	753.1	737	-		2.77%	745
K	**79.1**	76.9	77.53	76.91	-		2.86%	77.22
Sr	**141**	136.9	138.91	136.94	-		2.99%	137.92
In	**225**	231.8	226.4	226.35	-		3.02%	226.37
Ca	**153**	154.7	149.95	154.67	-		3.17%	153.83

V	**444**	459	458.6	446.74	-	3.38%	452.67
Lu	-	**414**	428	-	-	3.38%	421
Mg	**132**	128	128.7	127.63	-	3.43%	128.35
Gd	-	**301.3**	311.7	311.71	-	3.46%	311.7
Be	**309**	297	308.8	297.58	-	4.04%	303.19
Fe	**354**	340	351	349.5	-	4.12%	350.25
W	**774**	806.7	799.1	805.93	-	4.22%	802.51
Co	**390**	377	382.4	373.32	-	4.47%	379.7
Er	-	**280**	292.9	292.88	-	4.61%	292.88
Dy	-	**280**	293	-	-	4.64%	286.5
Au	**342**	324	324.4	324.43	324	5.56%	324.4
Th	-	**514**	543.9	543.92	-	5.82%	543.9
Cs	**66.1**	63.9	65.9	67.77	-	6.06%	66
Zn	**115**	123.6	115.3	115.31	-	7.48%	115.31
Rh	**531**	494	495.4	495.39	-	7.49%	495.39
Y	**390**	365	393.3	393.3	-	7.75%	391.65
Ba	**149**	140.3	150.9	140.18	140	7.79%	140.3
Pd	**380**	362	393.3	393.3	-	8.65%	386.65
Pt	**510**	469	510.5	510.45	-	8.85%	510.23
Ru	**619**	591.6	567.8	567.77	-	9.02%	579.7
Sc	**310**	332.7	304.8	304.8	-	9.15%	307.4
Li	**136**	147.1	134.7	147.08	-	9.21%	141.54
Rb	**69**	75.77	69.2	69.2	-	9.81%	69.2
Re	**636**	704	707.1	707.1	-	11.18%	705.55
B	**540**	480	538.9	507.77	480	12.50%	507.77
Na	**101**	97.42	89.04	97.36	-	13.43%	97.39
Mo	**536**	617	594.1	590.41	-	15.11%	592.26
Hf	**648**	571	661.1	661.07	-	15.78%	654.54
Sm	-	**165**	191.6	191.63	-	16.14%	191.6
Tc	**502**	585.20	585.22	-	-	16.58%	585.2
Os	**678**	738	627.6	627.6	-	17.59%	652.8
Zr	**502**	573	581.6	590.5	-	17.63%	577.3
Po	**120**	102.91	100.8	-	-	19.05%	102.91
Ra	**115**	113	136.8	136.82	-	21.08%	125.9
Bi	**179**	151	179.1	187.29	151	24.03%	179
Ce	-	**398**	313.8	313.8	-	26.83%	313.8
Si	**300**	359	383.3	359.02	-	27.77%	359.01

Tb	-	**293**	391	-	-	33.45%	342
I (I_2)	**22**	41.6	41.67	41.94	41.6	90.63%	41.6
Te	49.8	**114.1**	50.63	50.63	114	129.12%	50.63
Ir	**636**	231.80	563.6	563.58	-	174.37%	563.59
Sb	**195**	193.43	67.91	67.91	-	187.14%	130.67
Ho	-	71	**251**	251.04	-	253.58%	251
P (White)	**12.4**	12.4	51.9	-	12.4	318.55%	12.4
S (monoclinic)	**10**	45	9.62	-	45	367.78%	27.5
Se	14	95.48	**26.32**	26.32	95.5	582.14%	26.32
Al	**284**	294	293.72	29.08	294	910.86%	293.72
Ag	**254**	258	255.1	25.51	-	911.54%	254.55

* Sublimation

Table A16 List of heat of fusion from five handbooks (acronyms as in text). The elements are sorted in ascending (Max.-Min.)/Min.

Elements	**CDH**	**LNG**	**ELE**	**TPC**	**CRC**	**(Unit: kJ mol^{-1})**	**(Max-Min)/Min**	**Median**
Cs	**2.09**	2.09	2.09	2.09	2.09		0.15%	2.09
Al	**10.7**	10.71	10.67	10.7	10.71		0.37%	10.7
Ga	**5.61**	5.59	5.59	5.59	5.59		0.45%	5.59
In	**3.26**	3.28	3.27	3.26	3.29		0.97%	3.27
Na	**2.6**	2.6	2.64	2.6	2.6		1.54%	2.6
Cu	**13**	13.26	13	13.14	13.26		2.00%	13.14
Ni	**17.6**	17.48	17.6	17.21	17.48		2.26%	17.48
Cd	**6.11**	6.19	6.11	6.07	6.21		2.31%	6.11
Sn (white)	**7.2**	7.03	7.2	7.2	7.15		2.42%	7.2
Sn (Grey)	**7.2**	7.03	7.2	7.2	-		2.42%	7.2
Au	**12.7**	12.55	12.7	12.36	12.55		2.72%	12.55
Pd	**17**	16.74	17.2	16.74	16.74		2.77%	16.74
Tl	**4.27**	4.14	4.31	4.27	4.14		4.11%	4.27
K	**2.3**	2.32	2.4	2.33	2.34		4.35%	2.33
Sb	**19.8**	19.87	20.9	19.83	19.79		5.61%	19.83
Ag	**11.3**	11.95	11.3	11.3	11.3		5.76%	11.3
Mg	**8.95**	8.48	9.04	8.95	8.48		6.60%	8.95
Co	**15.2**	16.2	15.2	16.21	16.2		6.67%	16.2
Rb	**2.3**	2.19	2.2	2.34	2.19		6.68%	2.2
Pb	**5.1**	4.77	5.12	4.77	4.77		7.36%	4.77

Bi	**11**	11.3	10.48	11.3	11.11	7.82%	11.11
Tm	-	**16.84**	18.4	-	16.84	9.26%	16.84
Ca	**9.2**	8.54	9.33	8.53	8.54	9.37%	8.54
Zn	**7.36**	7.32	6.67	7.38	7.07	10.69%	7.32
Nb	**27**	30	27.2	26.94	30	11.36%	27.2
Fe	**15.4**	13.81	14.9	13.8	13.81	11.58%	13.81
Graphite	-	**117**	105.1	-	117.4	11.70%	117
Ba	**7.66**	7.12	7.66	8.01	7.12	12.46%	7.66
Pt	**22**	22.17	19.7	19.66	22.18	12.77%	22
As (grey)	**27.7**	24.44	27.7	-	24.44	13.34%	26.07
Mn	**14.6**	12.9	14.4	14.64	12.91	13.50%	14.4
Eu	-	**9.21**	10.5	10.46	9.21	14.01%	9.83
Sc	**16**	14.1	15.9	16.11	14.1	14.28%	15.9
Er	-	**19.9**	17.2	17.15	19.9	16.02%	18.55
Ge	**32**	36.94	34.7	31.8	36.94	16.15%	34.7
Lu	-	**22**[*]	19.2	-	18.65	17.96%	19.2
Yb	-	**7.66**	9.2	-	7.66	20.10%	7.66
Rh	**22**	26.59	21.55	21.76	26.59	23.39%	22
Sr	**9.2**	7.43	9.16	8.23	7.43	23.82%	8.23
Hf	**22**	27.2	25.5	21.76	27.2	25.01%	25.5
Si	**46.4**	50.21	39.6	50.22	50.21	26.82%	50.21
Sm	-	**8.62**	10.9	11.09	8.62	28.67%	9.76
V	**18**	21.5	17.6	22.78	21.5	29.44%	21.5
Po	**13**	-	10	-	10	30%	10
Ta	**28**	36.57	31.4	35.75	36.57	30.61%	35.75
Se	**5.23**	6.69	5.1	5.44	6.69	31.18%	5.44
Te	**17.9**	17.49	13.5	17.49	17.38	32.59%	17.49
Zr	**17**	21	23	20.79	21	35.29%	21
Mo	**28**	37.48	27.6	36	37.48	35.80%	36
Th	-	**13.81**	19.2[**]	15.65	13.81	39.03%	14.73
Ra	**10**	8.5	7.15	8.37	7.7	39.86%	8.37
S (monoclinic)	**1.42**	1.73	1.23	1.73	1.72	40.60%	1.72
Tc	**23**	33.29	23.81	-	33.29	44.74%	28.55
Ho	-	**16.80**	17.2	17.15	11.76	46.26%	16.98
Ti	**15**	14.15	20.9	18.62	14.15	47.70%	15
Cr	**14**	21	15.3	19.95	21	50%	19.95
Y	**17**	11.42	17.2	17.15	11.39	51.01%	17

Be	**12**	7.9	9.8	11.71	7.9	51.99%	9.8
Nd	-	**7.14**	7.11	10.88	7.14	53.01%	7.14
Li	**3**	3	4.6	3	3	53.33%	3
W	**33.7**	52.31	35.2	35.42	52.31	55.22%	35.42
Dy	-	**11.06**	17.2	-	11.35	55.52%	11.35
Ir	**28**	41.12	26.4	26.36	41.12	56.01%	28
Gd	-	**10.05**	15.5	15.48	9.67	60.29%	12.77
Tb	-	**10.15**	16.3	-	10.15	60.59%	10.15
Ru	**26**	38.59	23.7	25.52	38.59	62.83%	26
Pr	-	**6.89**	11.3	10.04	6.89	64.01%	8.47
Ce	-	**5.46**	8.87	9.2	5.46	68.42%	7.17
U	-	**9.14**	15.5	15.48	9.14	69.58%	12.31
La	**11**	6.2	10.04	11.3	6.2	82.25%	10.04
Re	**33**	60.43	33.1	33.05	34.08	83.12%	33.1
Os	**27**	57.85	29.3	29.29	57.85	114.26%	29.3
B	**22**	50.2	22.2	22.6	50.2	128.18%	22.6
P (White)	**0.63**	0.66	2.51	-	0.66	298.41%	0.66
I (I_2)	**7.87**	150.66	15.27	15.52	15.52	1814.36%	15.52

* Approximation value

** Th: <19.2

Appendix 4

Figure A1: Distribution of (i) melting point (/K); (ii) boiling point (/K); (iii) atomic volume (/m^3 mol^{-1}); (iv) polarizability (/10^{-30} m^3); (v) 1st ionization potential (/J mol^{-1}); (vi) electronegativity (Pauling); (vii) density (/kg m^{-3}); (viii) atomic weight (/kg mol^{-1}); (ix) linear thermal expansion coefficient (/10^6 K^{-1}); (x) photonic work function (/10^{-19} J); (xi) electrical conductivity (/10^8 Ω^{-1} m^{-1}); (xii) thermal conductivity (/W m^{-1} K^{-1}); (xiii) specific heat capacity (/J kg^{-1} K^{-1}); (xiv) molar heat capacity (/J mol^{-1} K^{-1}); (xv) heat of vaporization (/J mol^{-1}); (xvi) heat of fusion (/J mol^{-1}). Figure A2: Distribution of (i) atomic volume (Ln /cm^3 mol^{-1}); (ii) polarizability (Ln /10^{-30} m^3); (iii) linear thermal expansion coefficient (Ln /K^{-1}); (iv) thermal conductivity (Ln /W m^{-1} K^{-1}); (v) specific heat capacity (Ln /J kg^{-1} K^{-1}); (vi) heat of fusion (Ln /J mol^{-1}) after taking logarithms.

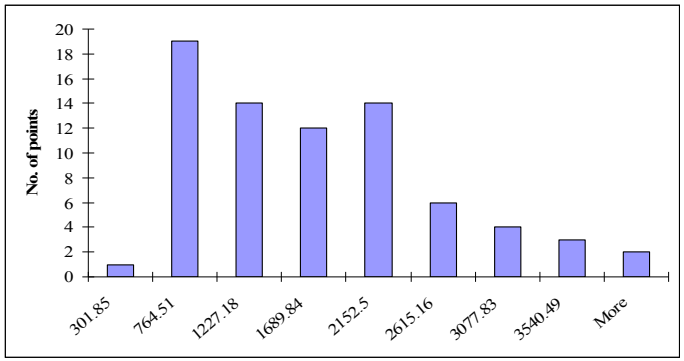

Figure A1 (i) Distribution of melting point (/K)

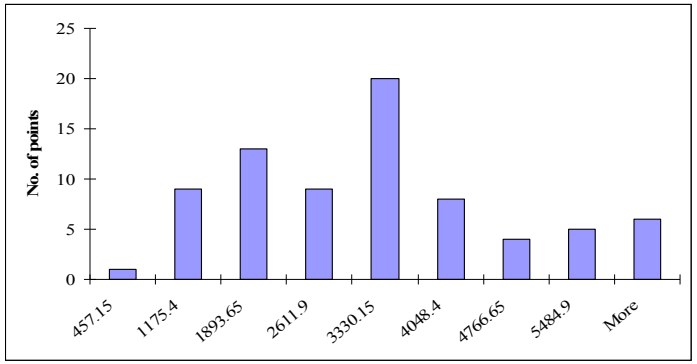

Figure A1 (ii) Distribution of boiling point (/K)

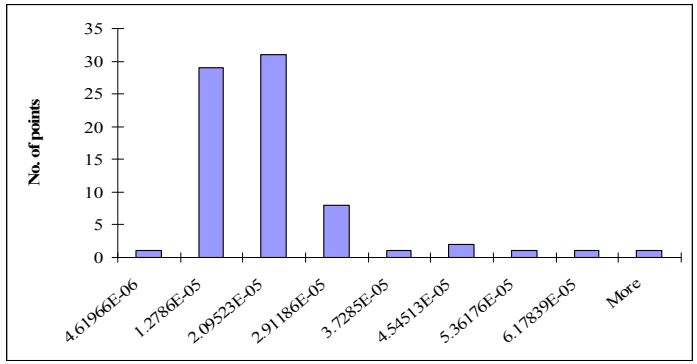

Figure A1 (iii) Distribution of atomic volume (/m^3 mol^{-1})

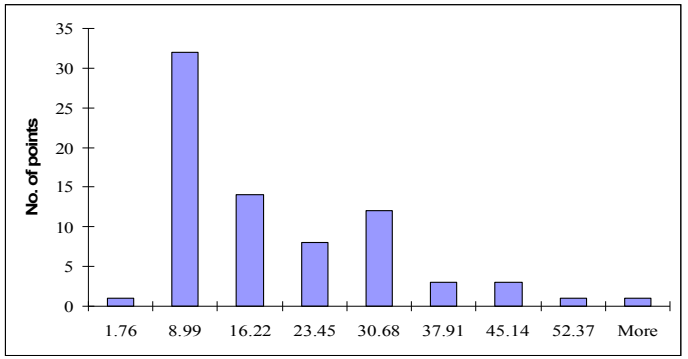

Figure A1 (iv) Distribution of polarizability (/10^{-30} m^3)

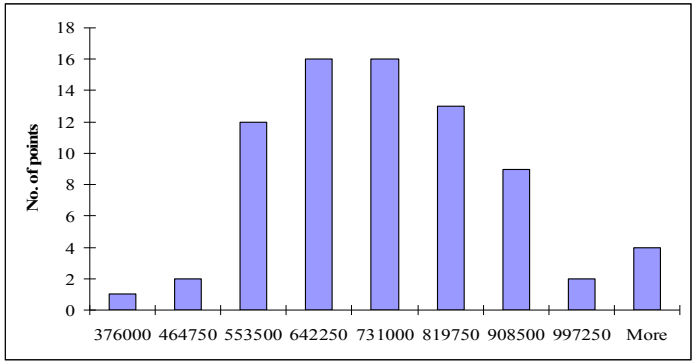

Figure A1 (v) Distribution of 1st ionization potential (/J mol^{-1})

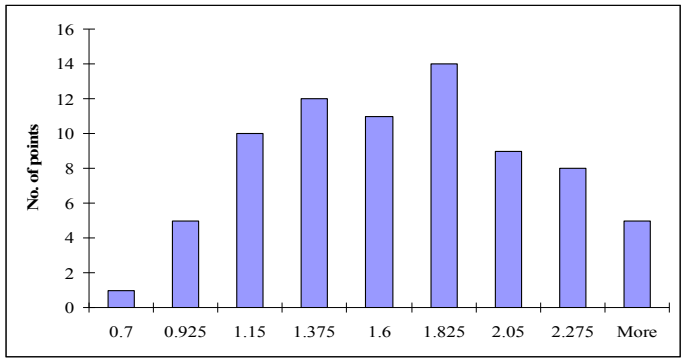

Figure A1 (vi) Distribution of electronegativity (Pauling)

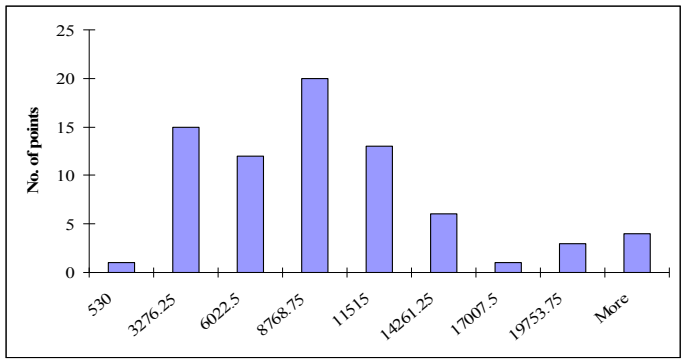

Figure A1 (vii) Distribution of density (/kg m^{-3})

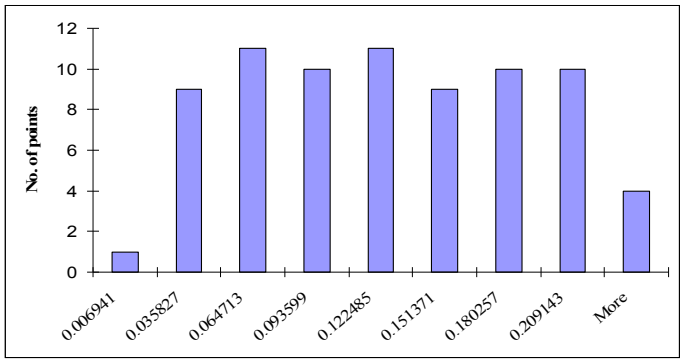

Figure A1 (viii) Distribution of atomic weight (/kg mol^{-1})

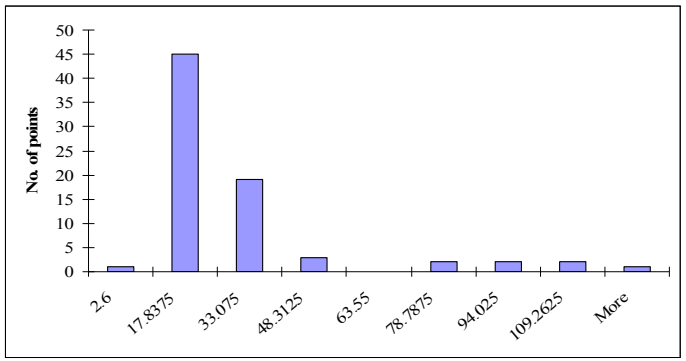

Figure A1 (ix) Distribution of linear thermal expansion coefficient (/10^{6} K^{-1})

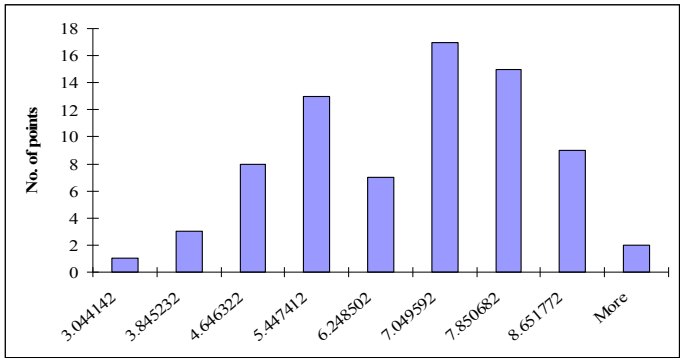

Figure A1 (x) Distribution of photonic work function (/10^{-19} J)

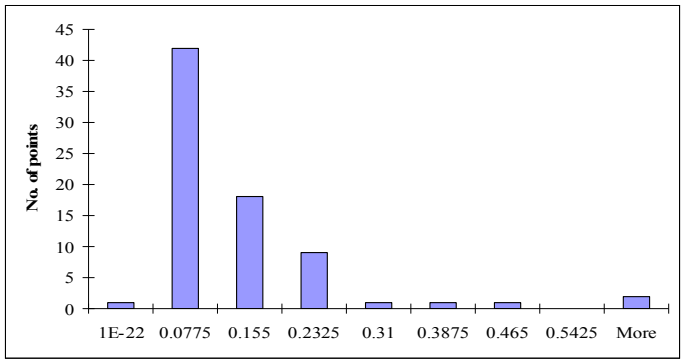

Figure A1 (xi) Distribution of electrical conductivity (/10^8 Ω^{-1} m^{-1})

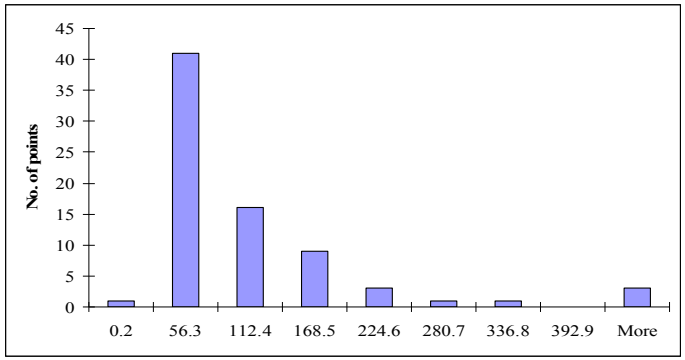

Figure A1 (xii) Distribution of thermal conductivity (/W m^{-1} K^{-1})

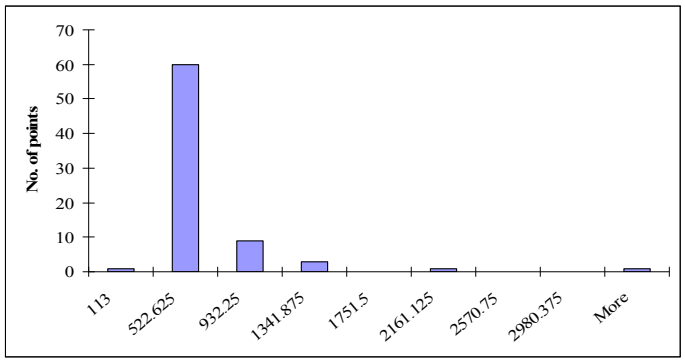

Figure A1 (xiii) Distribution of specific heat capacity (/J kg^{-1} K^{-1})

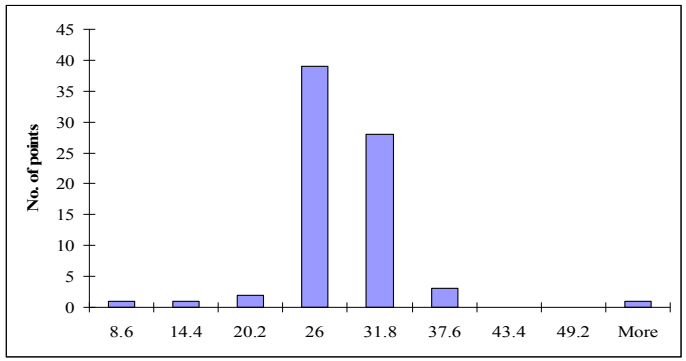

Figure A1 (xiv) Distribution of molar heat capacity (/J mol^{-1} K^{-1})

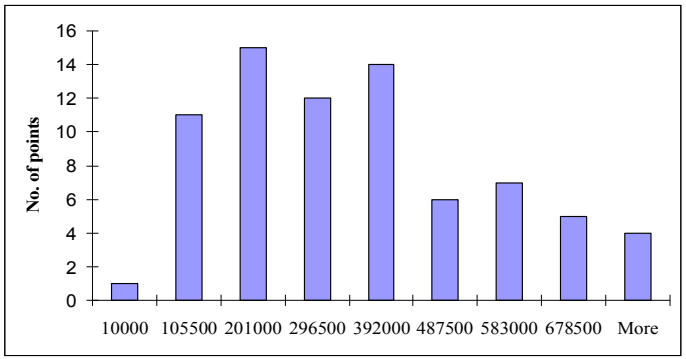

Figure A1 (xv) Distribution of heat of vaporization (/J mol^{-1})

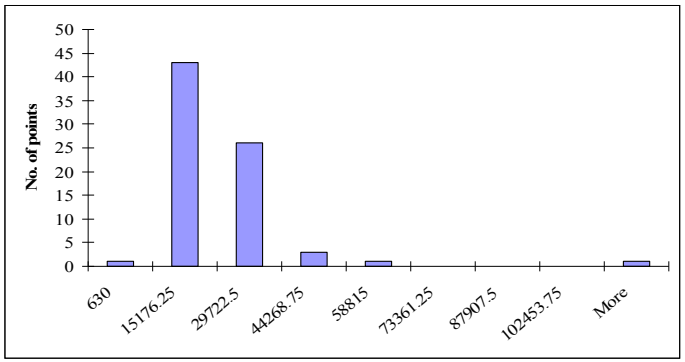

Figure A1 (xvi) Distribution of heat of fusion (/J mol^{-1})

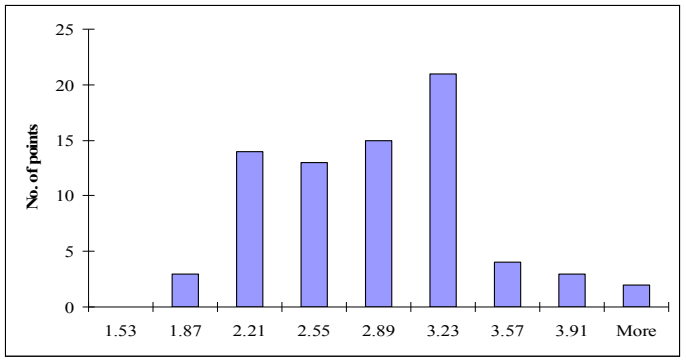

Figure A2 (i) Distribution of atomic volume (Ln /cm^3 mol^{-1})

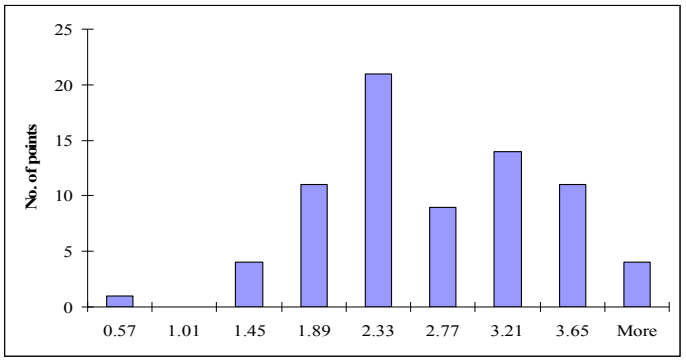

Figure A2 (ii) Distribution of polarizability (Ln /10^{-30} m^3)

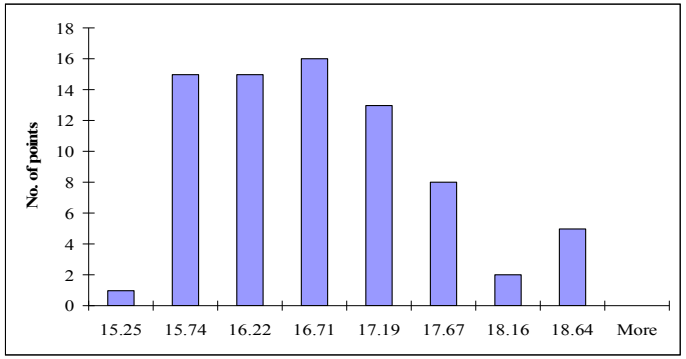

Figure A2 (iii) Distribution of linear thermal expansion coefficient (Ln /K^{-1})

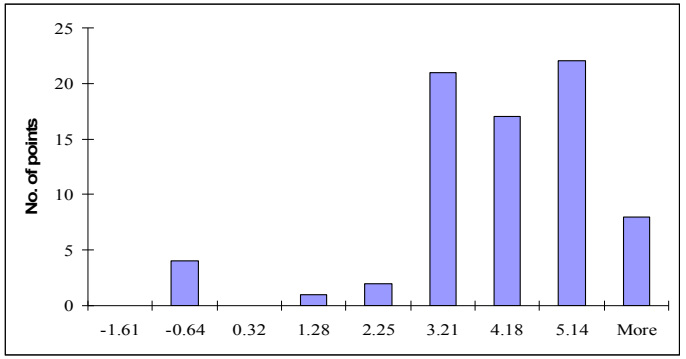

Figure A2 (iv) Distribution of thermal conductivity (Ln /W m^{-1} K^{-1})

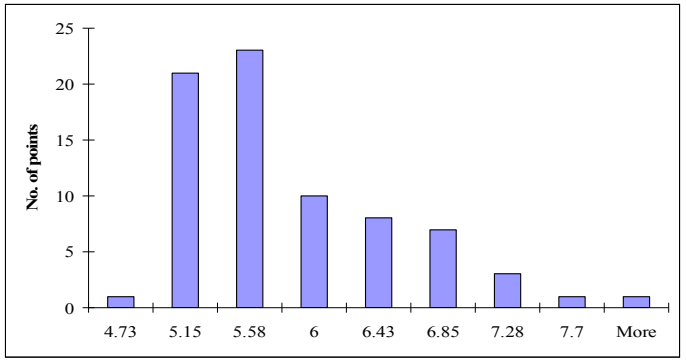

Figure A2 (v) Distribution of specific heat capacity (Ln /J kg^{-1} K^{-1})

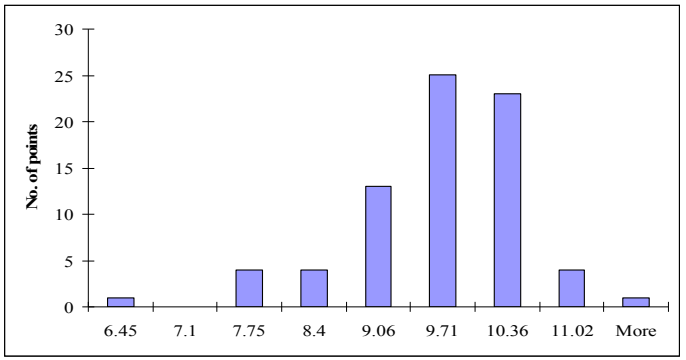

Figure A2 (vi) Distribution of heat of fusion (Ln /J mol^{-1})

Appendix 5

Figure A3 Variation of polarizability (vertical axis) as a function of two input variables (horizontal axes)

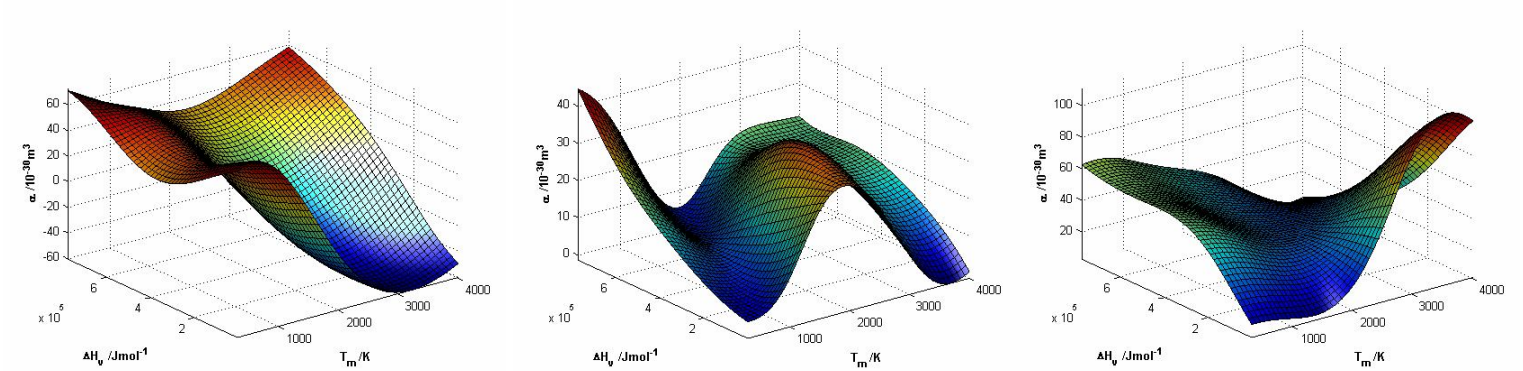

(1) $c_p = 113$ J kg^{-1} K^{-1}, $E_I = 376$ kJ mol^{-1} (2) $c_p = 113$ J kg^{-1} K^{-1}, $E_I = 691$ kJ mol^{-1} (3) $c_p = 113$ J kg^{-1} K^{-1}, $E_I = 1086$ kJ mol^{-1}

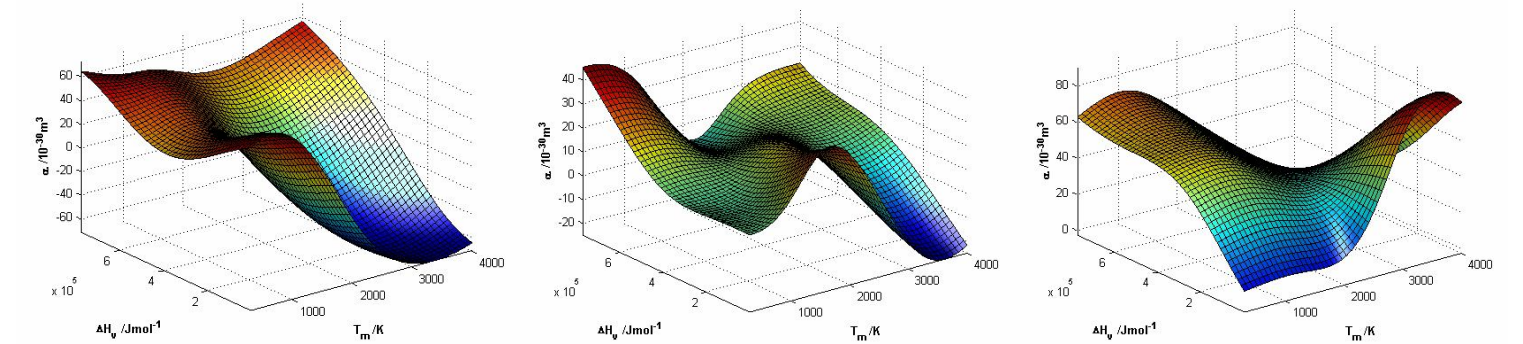

(4) $c_p = 279$ J kg^{-1} K^{-1}, $E_I = 376$ kJ mol^{-1} (5) $c_p = 279$ J kg^{-1} K^{-1}, $E_I = 691$ kJ mol^{-1} (6) $c_p = 279$ J kg^{-1} K^{-1}, $E_I = 1086$ kJ mol^{-1}

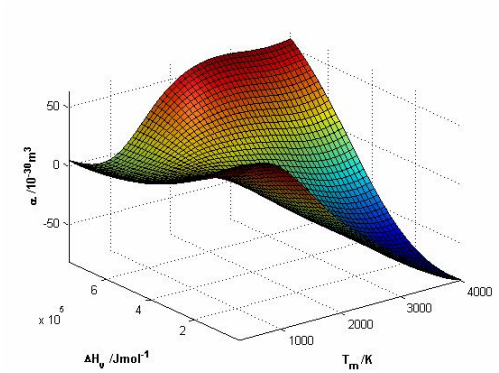

(7) $c_p = 3390$ J kg^{-1} K^{-1}, $E_I = 376$ kJ mol^{-1}

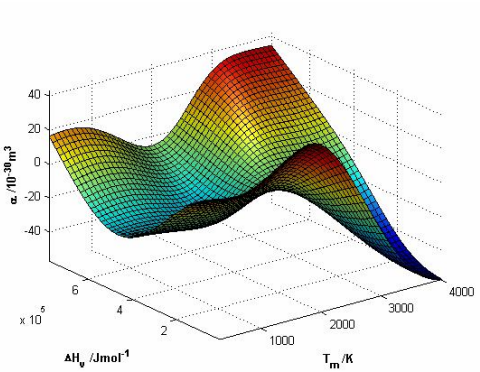

(8) $c_p = 3390$ J kg^{-1} K^{-1}, $E_I = 691$ kJ mol^{-1}

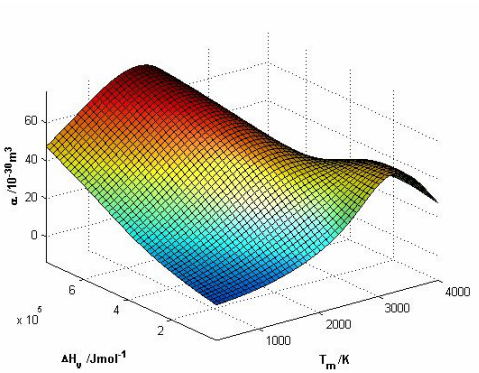

(9) $c_p = 3390$ J kg^{-1} K^{-1}, $E_I = 1086$ kJ mol^{-1}

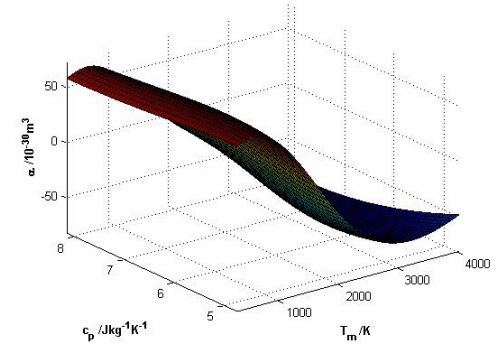

(10) $\Delta H_V = 10$ kJ mol^{-1}, $E_I = 376$ kJ mol^{-1}

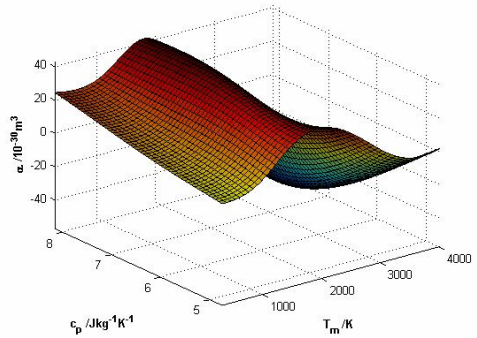

(11) $\Delta H_V = 10$ kJ mol^{-1}, $E_I = 691$ kJ mol^{-1}

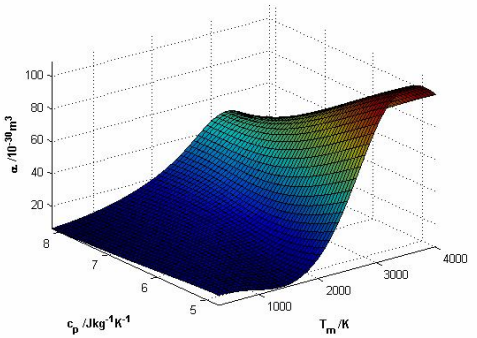

(12) $\Delta H_V = 10$ kJ mol^{-1}, $E_I = 1086$ kJ mol^{-1}

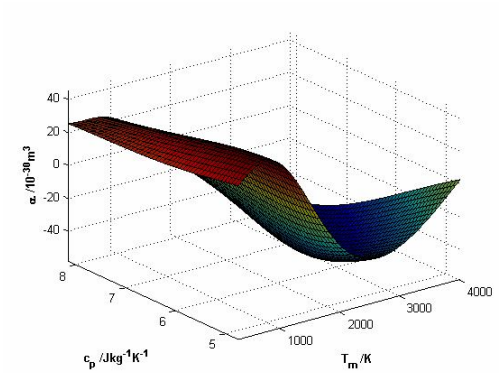

(13) $\Delta H_V = 309$ kJ mol^{-1}, $E_I = 376$ kJ mol^{-1}

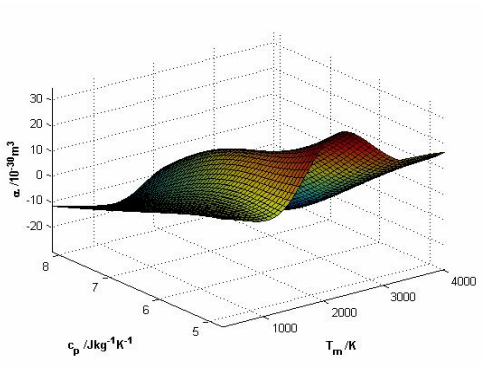

(14) $\Delta H_V = 309$ kJ mol^{-1}, $E_I = 691$ kJ mol^{-1}

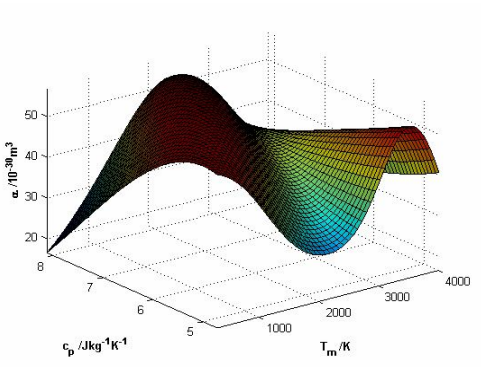

(15) $\Delta H_V = 309$ kJ mol^{-1}, $E_I = 1086$ kJ mol^{-1}

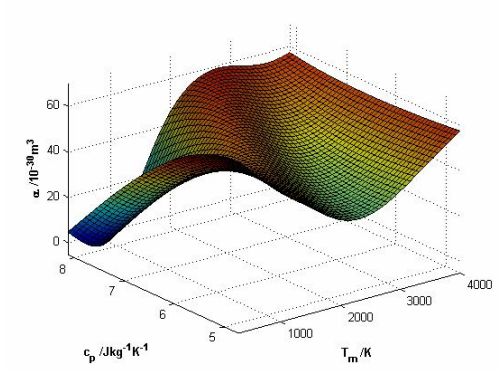

(16) $\Delta H_V = 774$ kJ mol^{-1}, $E_I = 376$ kJ mol^{-1}

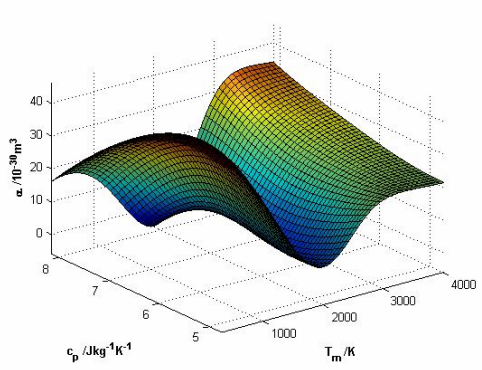

(17) $\Delta H_V = 774$ kJ mol^{-1}, $E_I = 691$ kJ mol^{-1}

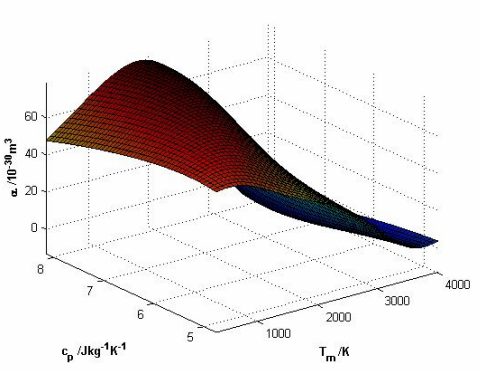

(18) $\Delta H_V = 774$ kJ mol^{-1}, $E_I = 1086$ kJ mol^{-1}

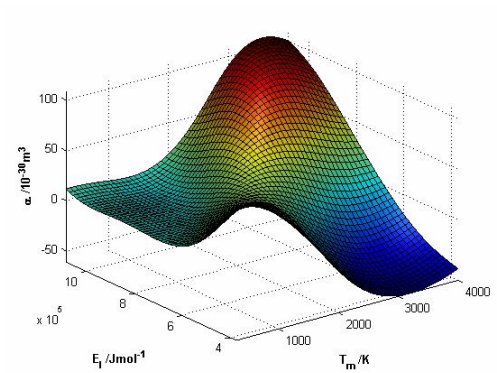

(19) $\Delta H_V = 10$ kJ mol^{-1}, $c_p = 113$ J kg^{-1} K^{-1}

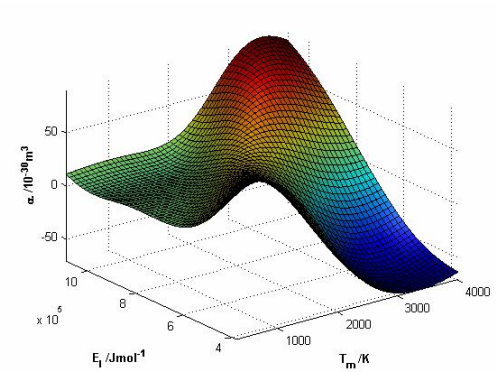

(20) $\Delta H_V = 10$ kJ mol^{-1}, $c_p = 279$ J kg^{-1} K^{-1}

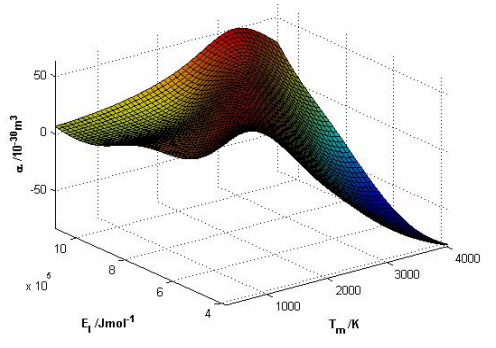

(21) $\Delta H_V = 10$ kJ mol^{-1}, $c_p = 3390$ J kg^{-1} K^{-1}

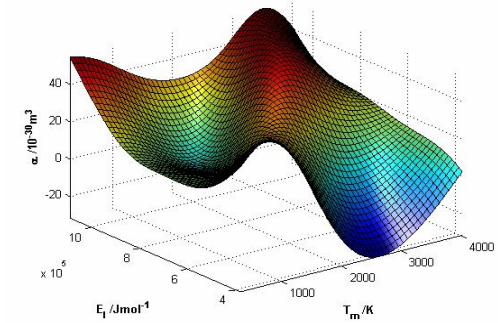

(22) $\Delta H_V = 309$ kJ mol^{-1}, $c_p = 113$ J kg^{-1} K^{-1}

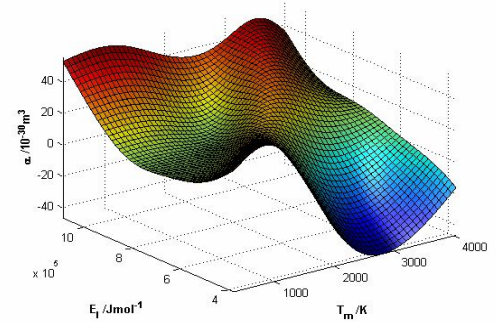

(23) $\Delta H_V = 309$ kJ mol^{-1}, $c_p = 279$ J kg^{-1} K^{-1}

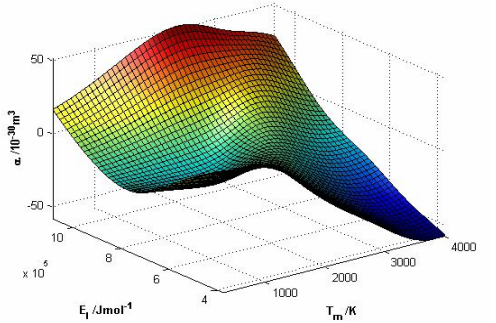

(24) $\Delta H_V = 309$ kJ mol^{-1}, $c_p = 3390$ J kg^{-1} K^{-1}

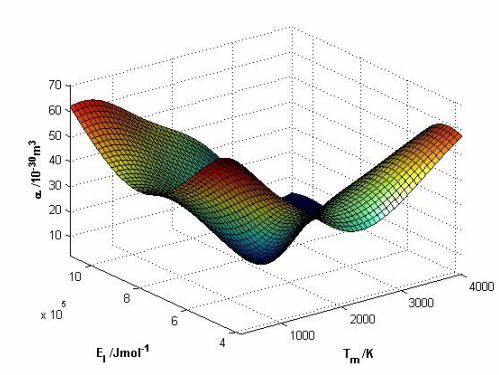

(25) $\Delta H_V = 774$ kJ mol^{-1}, $c_p = 113$ J kg^{-1} K^{-1}

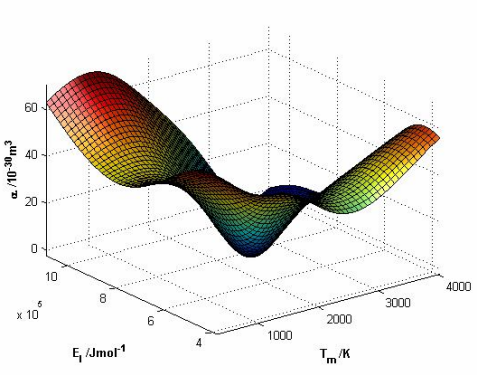

(26) $\Delta H_V = 774$ kJ mol^{-1}, $c_p = 279$ J kg^{-1} K^{-1}

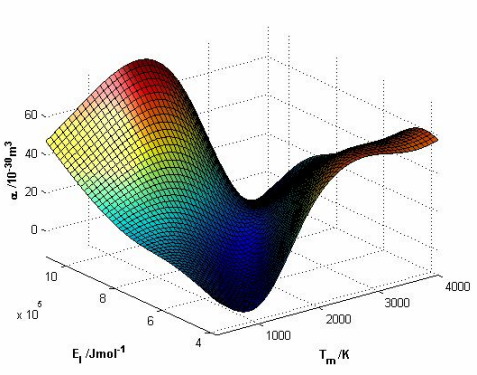

(27) $\Delta H_V = 774$ kJ mol^{-1}, $c_p = 3390$ J kg^{-1} K^{-1}

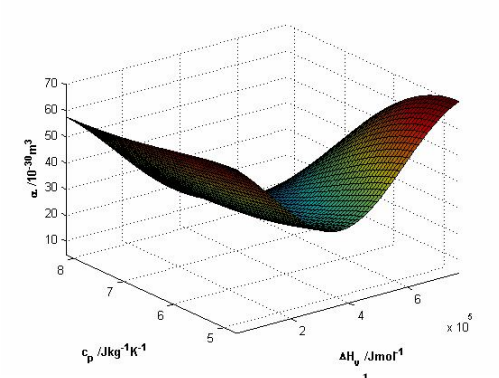

(28) $T_m = 302$ K, $E_I = 376$ kJ mol^{-1}

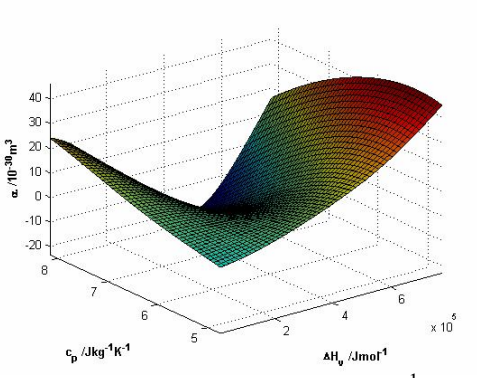

(29) $T_m = 302$ K, $E_I = 691$ kJ mol^{-1}

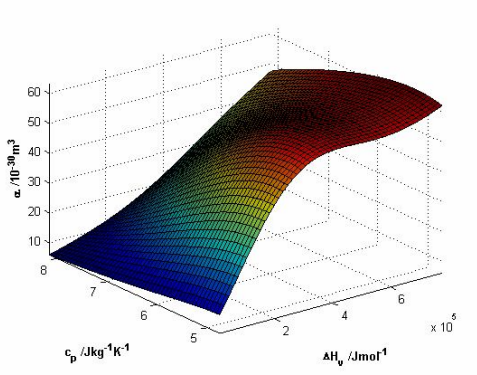

(30) $T_m = 302$ K, $E_I = 1086$ kJ mol^{-1}

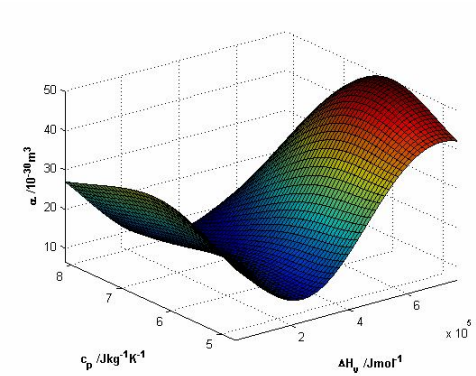

(31) T_m = 1478 K, E_I = 376 kJ mol^{-1}

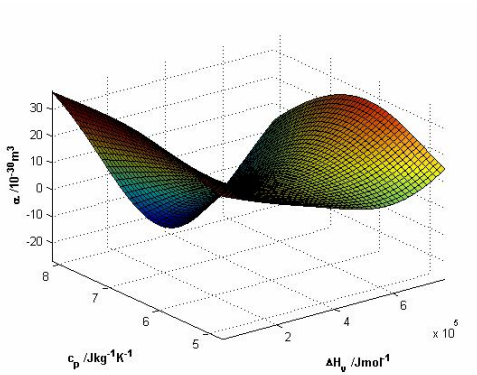

(32) T_m = 1478 K, E_I = 691 kJ mol^{-1}

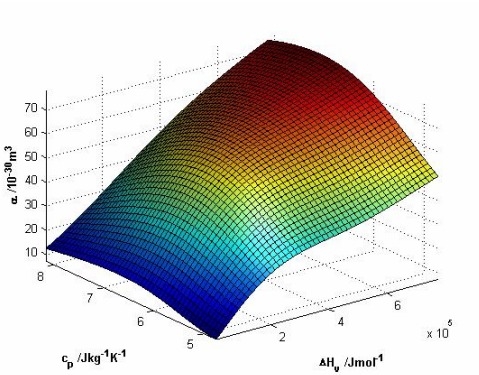

(33) T_m = 1478 K, E_I = 1086 kJ mol^{-1}

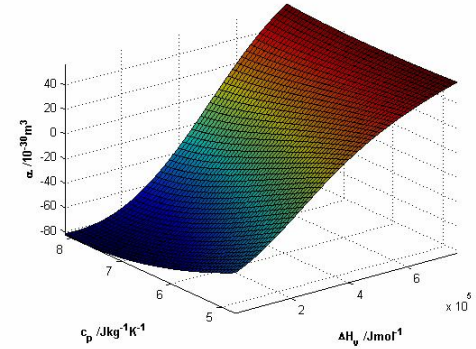

(34) T_m = 4003 K, E_I = 376 kJ mol^{-1}

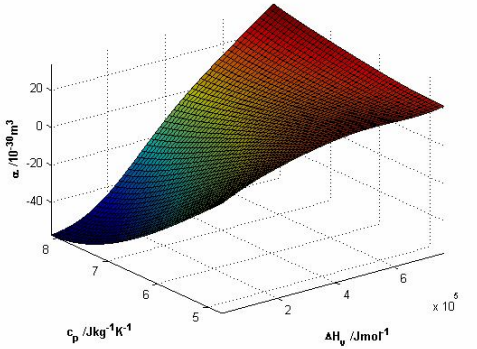

(35) T_m = 4003 K, E_I = 691 kJ mol^{-1}

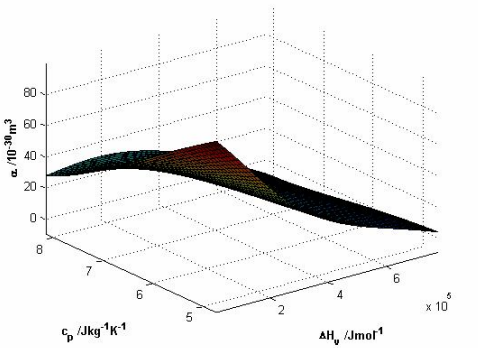

(36) T_m = 4003 K, E_I = 1086 kJ mol^{-1}

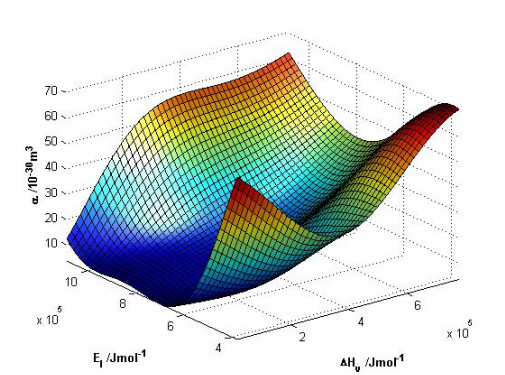

(37) $T_m = 302$ K, $c_p = 113$ J kg^{-1} K^{-1}

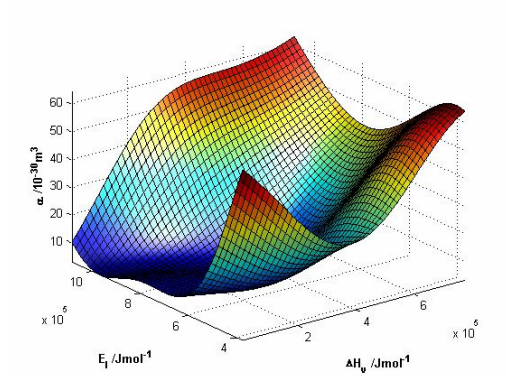

(38) $T_m = 302$ K, $c_p = 279$ J kg^{-1} K^{-1}

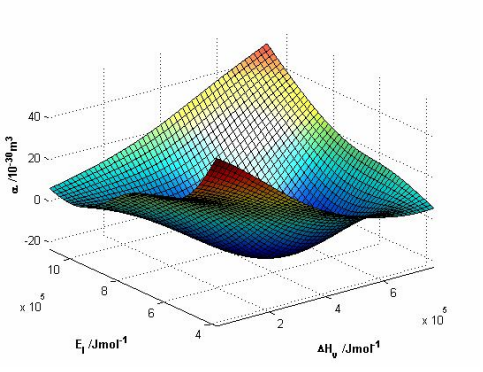

(39) $T_m = 302$ K, $c_p = 3390$ J kg^{-1} K^{-1}

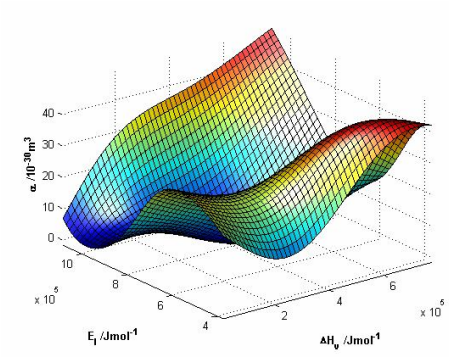

(40) $T_m = 1478$ K, $c_p = 113$ J kg^{-1} K^{-1}

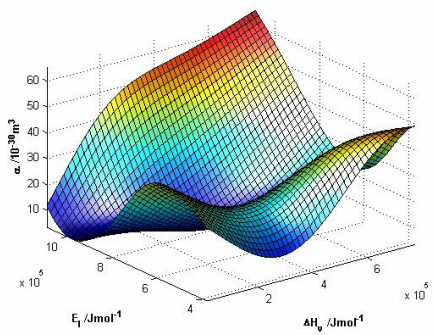

(41) $T_m = 1478$ K, $c_p = 279$ J kg^{-1} K^{-1}

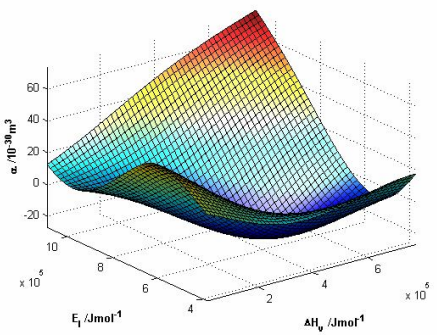

(42) $T_m = 1478$ K, $c_p = 3390$ J kg^{-1} K^{-1}

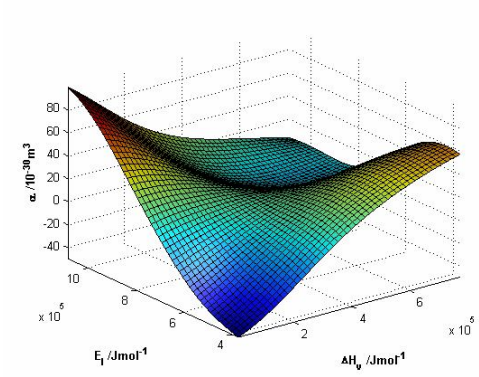

(43) $T_m = 4003$ K, $c_p = 113$ J kg^{-1} K^{-1}

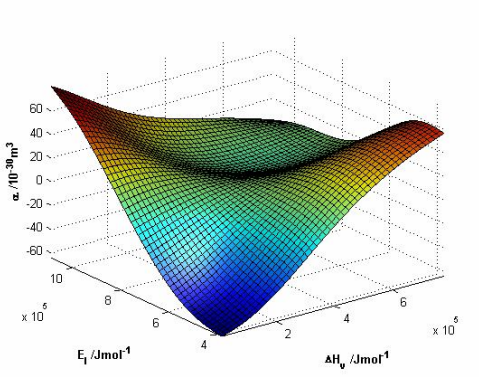

(44) $T_m = 4003$ K, $c_p = 279$ J kg^{-1} K^{-1}

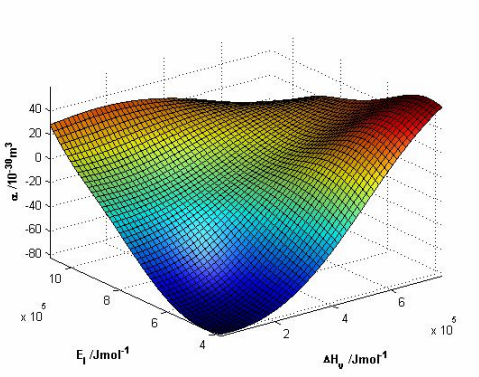

(45) $T_m = 4003$ K, $c_p = 3390$ J kg^{-1} K^{-1}

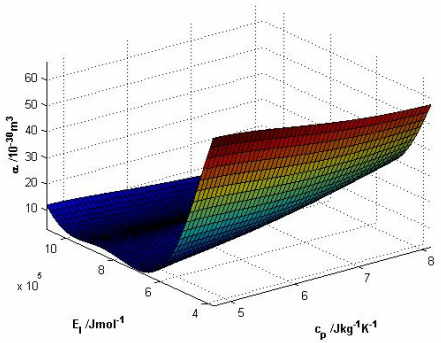

(46) $T_m = 302$ K, $\Delta H_V = 10$ kJ mol^{-1}

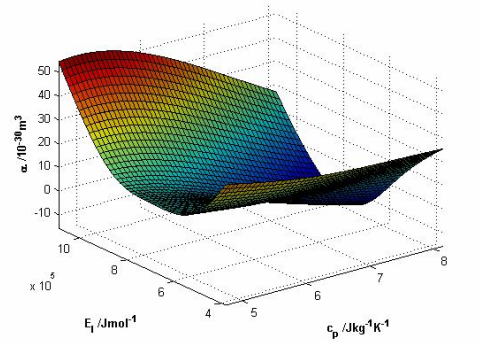

(47) $T_m = 302$ K, $\Delta H_V = 309$ kJ mol^{-1}

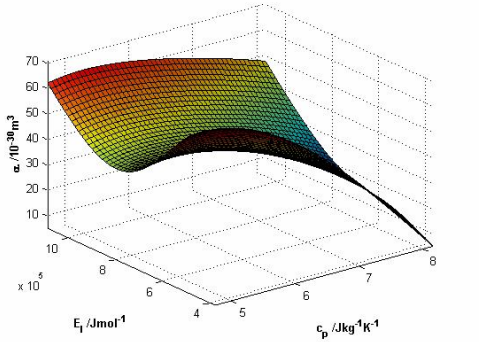

(48) $T_m = 302$ K, $\Delta H_V = 774$ kJ mol^{-1}

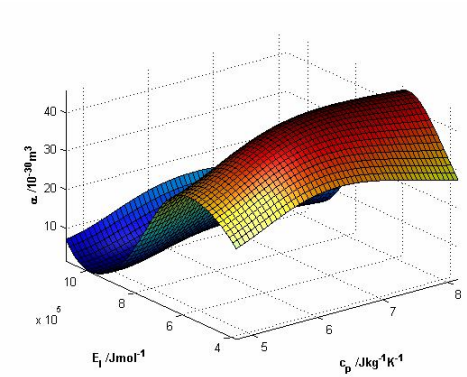

(49) $T_m = 1478$ K, $\Delta H_V = 10$ kJ mol^{-1}

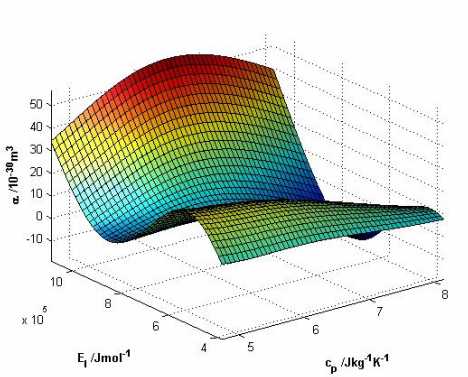

(50) $T_m = 1478$ K, $\Delta H_V = 309$ kJ mol^{-1}

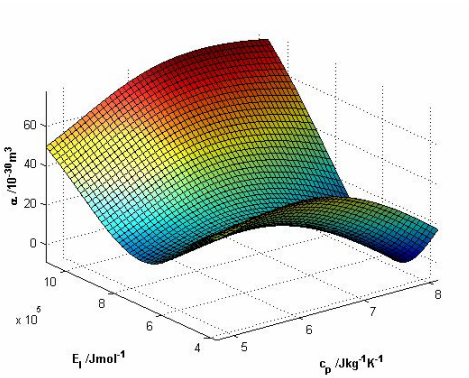

(51) $T_m = 1478$ K, $\Delta H_V = 774$ kJ mol^{-1}

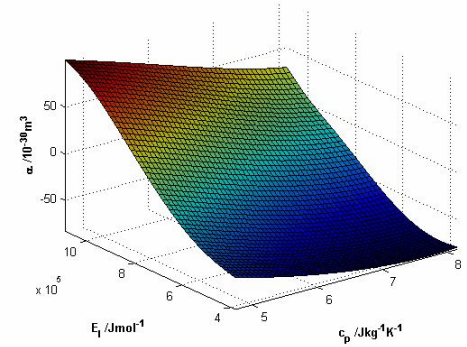

(52) $T_m = 4003$ K, $\Delta H_V = 10$ kJ mol^{-1}

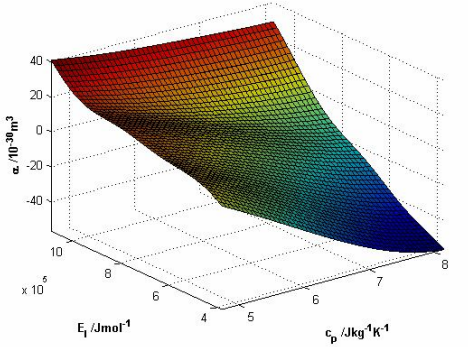

(53) $T_m = 4003$ K, $\Delta H_V = 309$ kJ mol^{-1}

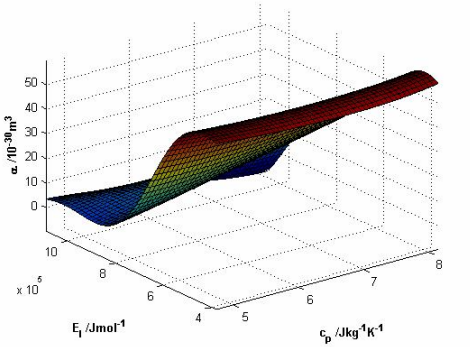

(54) $T_m = 4003$ K, $\Delta H_V = 774$ kJ mol^{-1}